AD-A194 957 PIEZOELECTRIC AND ELECTROSTRICTIVE MATERIALS FOR TRANSDUCER APPLICATIONS VOLUME 1(U) PENNSYLVANIA STATE UNIV UNIVERSITY PARK MATERIALS RESEARCH LA... 1/3

UNCLASSIFIED L E CROSS ET AL. MAR 88 N00014-82-K-0339 F/G 20/3 NL

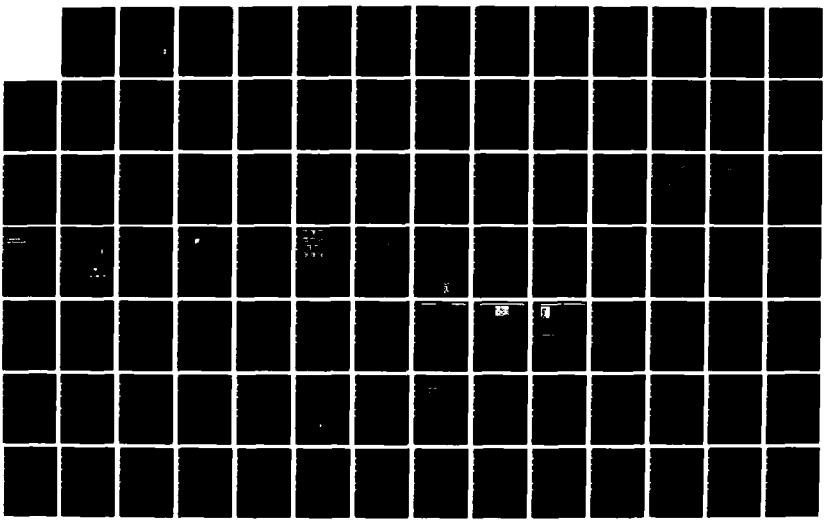

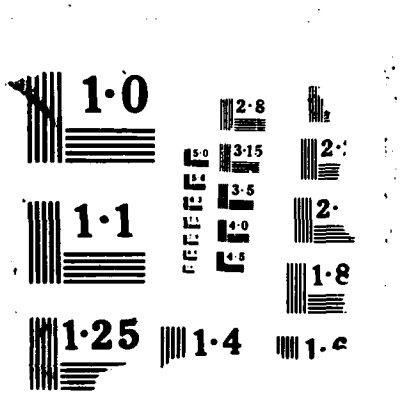
1·0
1·1
1·25
1·4
2·8
3·15
3·5
4·0
2·
2·
1·8

PIEZOELECTRIC AND ELECTROSTRICTIVE MATERIALS FOR TRANSDUCER APPLICATIONS

Period January 1 to December 31, 1987

Annual Report

OFFICE OF NAVAL RESEARCH

Contract No. N00014-82-K0339

L.E. Cross
R.E. Newnham
G.R. Barsch
J.V. Biggers

March 1988

Volume I

THE MATERIALS RESEARCH LABORATORY

THE PENNSYLVANIA STATE UNIVERSITY

UNIVERSITY PARK, PENNSYLVANIA

TABLE OF CONTENTS

REPORT DOCUMENTATION PAGE

1a. REPORT SECURITY CLASSIFICATION	1b. RESTRICTIVE MARKINGS
2a. SECURITY CLASSIFICATION AUTHORITY	3. DISTRIBUTION/AVAILABILITY OF REPORT Reproduction in whole or in part is permitted for any purpose of the United States Government.
2b. DECLASSIFICATION/DOWNGRADING SCHEDULE	
4. PERFORMING ORGANIZATION REPORT NUMBER(S) N00014-82-K0339	5. MONITORING ORGANIZATION REPORT NUMBER(S)
6a. NAME OF PERFORMING ORGANIZATION Materials Research Laboratory 6b. OFFICE SYMBOL (If applicable)	7a. NAME OF MONITORING ORGANIZATION
6c. ADDRESS (City, State and ZIP Code) The Pennsylvania State University University Park, PA 16802	7b. ADDRESS (City, State and ZIP Code)
8a. NAME OF FUNDING/SPONSORING ORGANIZATION Office of Naval Research 8b. OFFICE SYMBOL (If applicable)	9. PROCUREMENT INSTRUMENT IDENTIFICATION NUMBER
8c. ADDRESS (City, State and ZIP Code) 619 Ballston Tower 800 N. Quincy Street Arlington, VA 22217	10. SOURCE OF FUNDING NOS. PROGRAM ELEMENT NO. / PROJECT NO. / TASK NO. / WORK UNIT NO.
11. TITLE (Include Security Classification) Piezoelectric and Electrostrictive Mtls. for Transducer Appl.	
12. PERSONAL AUTHOR(S) L.E. Cross, R.E. Newnham, G.R. Barsch, J. V. Biggers	
13a. TYPE OF REPORT Annaul 13b. TIME COVERED FROM 01/01/87 TO 12/31/87	14. DATE OF REPORT (Yr., Mo., Day) 15. PAGE COUNT
16. SUPPLEMENTARY NOTATION	

17. COSATI CODES			18. SUBJECT TERMS (Continue on reverse if necessary and identify by block number)
FIELD	GROUP	SUB. GR.	

19. ABSTRACT (Continue on reverse if necessary and identify by block number)

This report covers work carried out over the period January 31, 1987 to February 1, 1988 on the second year of a three-year extension of ONR Contract N00014-82-0339 "Piezoelectric and Electrostrictive Materials for Transducer Applications." The topics covered under the program are reported under three major topic areas:

Piezoelectric and Related Composites, Electrostriction, Phenomenology and Properties of Conventional Ceramic, and Piezoelectrics.

A brief report is also given of related studies requires to support and supplement work on the three major areas, under the title Associated Programs. The year has seen major personnel changes at the Post-Doctoral and Graduate Assistant levels as befits a University based program and new personnel are now in place. The summer apprentice program under ONR sponsorship on this program has again given research oppotunity to four upward bound high school students who joined Universities in Science and Engineering programs in the fall of 1987.

20. DISTRIBUTION/AVAILABILITY OF ABSTRACT UNCLASSIFIED/UNLIMITED ☐ SAME AS RPT. ☐ DTIC USERS ☐	21. ABSTRACT SECURITY CLASSIFICATION
22a. NAME OF RESPONSIBLE INDIVIDUAL	22b. TELEPHONE NUMBER (Include Area Code) 22c. OFFICE SYMBOL

Upon the four major topics, the following highlights can be reported. Studies of the composite systems are continually mutating into more complex multicomponent systems and to cover the new requirements an update and extension of the composite nomenclature has been accomplished.

For the 3:0 type composites, a new modification of the original "Safari" design has been implemented using a very shallow cavity to modify the stress distribution and enhance the $d_h g_h$ product. The expectation is to produce a higher permittivity composite which will still have an effective $d_h g_h$ product. Analysis has continued defining the measurement of the complex coefficients for polymer ceramic composites, and the Banno simple cubes model has been extended to include cubes with complex coefficients. Following from thermistor work on associated programs, a new polymer:NTC ceramic composite has been devised which exhibits strong pressure dependence of conductivity but much reduced temperature dependence promising interesting possibility for tactile and for hydrostatic pressure measurement.

Basic studies in the theory of electrostriction are concerned with the many body forces which are a consequence of the charge transfer model. To provide experimental backup, the compressometer has been modified to permit measurement of the temperature dependence of the electrostriction constants in $KMnF_3$. New attempts are being made using the optical dilatometer to measure the direct effect and we hope to be able to report convergence of these two techniques next year.

In practical electrostrictors, the emphasis has been upon relaxor compositions such as lead zinc niobate:lead titanate and analogues. In the lead magnesium niobate:lead titanate aging studies under DC bias have given the first clear measurements of the effective defect dipole field.

The thermodynamic phenomenology for the PZT family has now been completed for all phases from pure $PbZrO_3$ to pure $PbTiO_3$. Extensive measurements on sol-gel prepared pure compositions have been required to provide data to refine the higher order stiffnesses the electrostriction and rotostriction constants and the antiferroelectric polarization coupling constants. The theory now permits a calculation of the intrinsic single domain dielectric and piezoelectric properties for any composition at any temperature in the phase field. Data from the theory has now been used to propose a mechanism for the high piezoelectric anistropy in the $PbTiO_3$ based compositions, based on the anisotropy in the electrostriction constants.

In the associated programs a wide range of preparation techniques has been exploited to provide the many compositions needed in powder, ceramic and single crystal for studies reported above.

The report appends 24 published papers, and 15 preprints of papers which have been submitted for publication.

Faculty on the program made 16 invited presentation at National and International meetings and the program contributed 32 papers at major meetings. As an example of the attempt being made to inform Industry, Academe and Government of the importance of electroceramics, the schedule of seminars presented by R.E. Newnham over the past year is included.

1. INTRODUCTION

This annual report documents the work carried out in the second year (January 31 1987 - February 1, 1988) on a three-year extension of ONR Contract N00014-82-K-0339 "Piezoelectric and Electrostrictive Materials for Transducer Applications." Following already established custom, the work is documented largely through reprints of papers published by the investigators on the program. There has been a major turnover of both post-doctoral fellows and graduate students on the program this year which delayed several of the submissions to journals and for this reason preprints of the more important papers will be included this year.

To key the rather large assembly of data a brief summary overview is given which highlights the major progress over the year. For convenience the technical appendices are divided into four major topic areas presented sequentially.

1) Piezoelectric and Related Composites
2) Electrostriction
3) Phenomenology and Properties of Conventional Ceramic Piezoelectrics
4) Associated Programs

The past year as mentioned above has been one of transition with many people leaving the program and new people taking over. The dynamic trio of T.R. Gururaja, A. Halliyal and A. Safari have left. Dr. Gururaja to join the biomedical transducer group of Hewlett-Packard, Dr. A. Halliyal to go to the Electroceramic Laboratory of E.I DuPont and Dr. Ahmad Safari to take up an Associate Professor position in Ceramics at Rutgers University. These stalwarts have been replaced by Dr. Shoko Yoshikawa who joined us from Center Engineering, Dr. T.T. Srinivasan from Baker Chemical and by Professor Q.C. Xu who is able to spend part time helping the group. In the graduate students, Drs. Steve DaVanzo took up a position at Dow Chemical, W. Carlson at Alfred University, E. Furman at Allied Signal, M.J. Haun at E.I. DuPont and Steve Pilgrim at Martin Marietta. New students joining the program are Glen Fox, T. Guo and D. Taylor.

In concert with the changing needs of the program, S. Kumar who joined last year has been spending all of his time designing and building, with help from Professor Xu, a flow testing tank.

For a number of years now, ONR has been sponsoring a summer apprentice program in MRL in association with this contract. Over time, we have accumulated experience in selected students through our Upward Bound program at PSU who will benefit most, and 1987 was probably the most successful year to date in this program. It was pleasing to note one of the early ONR apprentices participating in the Gordon Conference on Ceramics this year as a research scientist for his company.

2. PIEZOELECTRIC AND RELATED COMPOSITES

2.1 Introduction

With the increasing sophistication now occurring in the manipulation of multi component composites, it has been desirable to make an extension of the initial composite nomenclature, establishing rules of precedence for active phases and considering possible changes in connectivity produced by external variables. In the piezoelectric hydrophone materials work on the chemically co-precipitated powders has shown excellent properties even using just a simple lead titanate powder with $d_h g_h \sim 4{,}000.10^{-15}$ m^2/N. For the $PbTiO_3$:$BiFeO_3$ using conventional preparation techniques properties are markedly improved by doping to control conductivity. Work has continued on the fired composites which permit a larger filling factor for the piezoelectric phase and gives an extended range of properties between conventional 0:3 composites and monolithic PZT.

In a new topic area work has been started on exploring the possible application of piezo resistive composites for sensing both static and dynamical pressure changes. Such materials could have considerable interest for application as low K fillers in piezoresistive towed arrays.

Extending work from our dielectric center, where extensive modeling of flawed multilayer capacitors has been accomplished using finite element and finite difference methods, these techniques have now been adapted to model the effects of electric field on cracks in piezoelectric and electrostrictive ceramics.

2.2 Extension of Composite Nomenclature

A new nomenclature scheme based on the principles of connectivity, property type, tensor rank size scale and orientation is proposed and families of connectivity patterns for diphasic and triphasic composites are listed to reflect the new considerations. The concept of a quasi-composite is introduced in order to clarify relations between constituent phases in the more complex systems, also modifications to the connectivity due to the influence of external variables are considered.

2.3 0:3 Composites for Hydrophone Applications

2.3.1 Lead Bismuth Titanate Ferrate Compositions

Following up on the original studies by J. Giniewicz which established the advantages of the $PbTiO_3$:$BiFeO_3$ materials a more extensive study has now been completed using Mn as a modifier ion to improve the resistivity. It was evident from the dielectric loss data at low frequency, that for compositions containing 50 mole% or more of $BiFeO_3$ there is a considerable improvement in resistivity and consequently on improvement in polarizability of the 0:3 composite. Even for doped samples however, the best results were obtained at the 50% bismuth ferrate composition.

2.3.2 Chemically Co-Precipitated Lead Titanate

For pure lead titanate as a filler in the 0:3 composite original studies had used normal mixed oxide techniques to prepare the powders. In this study co-precipitated powders were generated from $Pb(NO_3)_2$ and $TiCl_4$. After calcining at 900°C the precipitates yielded highly crystalline powders with a very narrow size distribution. X-ray measurements on poled echo-gel polymer composites indicate very complete poling at 100 Kv/cm and $d_h g_h$ values over 4,000 x 10^{-15} m^2/V have been achieved.

2.3.3 Fired 0:3 Polymer Ceramic Composites

Current work has concentrated upon the transducing capability of the fired 0:3 as a broadband send/receive transducer, and as an impedance matching layer for PZT based transducers.

2.3.4 High $d_h g_h$ and ϵ Composites

Using a modification of the Safari structure PZT elements which have a very shallow intercavity have been explored. The effect upon a hydrostatic stress is such that the transverse component can become effectively tensile so that d_{33} and d_{31} contributions exhibit the same sign, leading to a device structure with high $d_h g_h$ and high ϵ

Typical values for experimental elements fabricated to this design are:

d_h = 150 pc/N
g_h = 19 x 10^{-3} Vm/n
$\epsilon 33$ = 810

The elements have a flat frequency response up to about 30 kHz.

2.3.5 Resonance Measuring Technique for the Complex Coefficients of Ceramic Composites

Two methods have been devised for measuring the complex coefficients of PZT:polymer composites. The first measures the real coefficient using a lumped circuit equivalent, the second models the complex coefficients based on an analytical solution for a single mode. Expansion for conductance and capacitance vs frequency and for Q_m are derived.

Experimentally coefficients have been derived for a wide range of 0:3 composites and for polyvilidene film transducers.

2.3.6 A Complex Impedance Cubes Model for Piezoelectric Composites

The simple cube model developed by Banno of NGK Japan has been extended to include complex dielectric, piezoelectric and elastic coefficients. The relations derived are useful for understanding the interrelation between d", ϵ " and s" in the polymer:ceramic composites, given

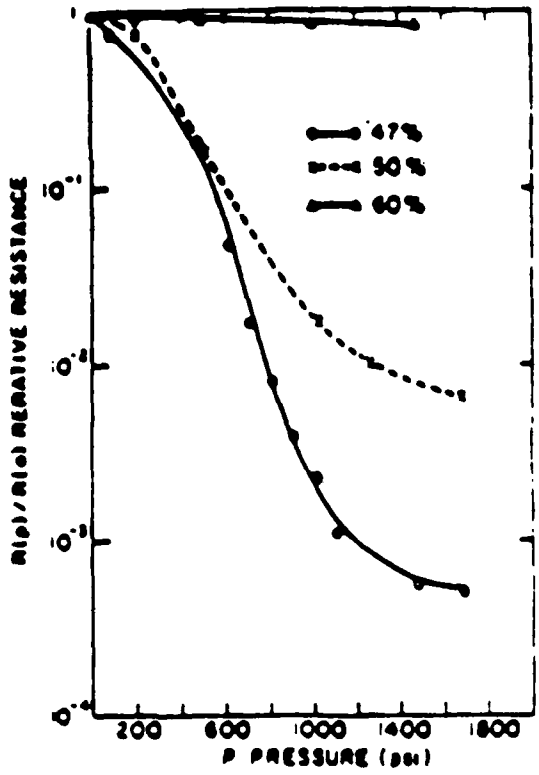

Fig. 2.3.7.1. Pressure dependence of the DC resistivity in an 0:3 Fe_3O_4:Epoxy composite as a function of semiconductor loading.

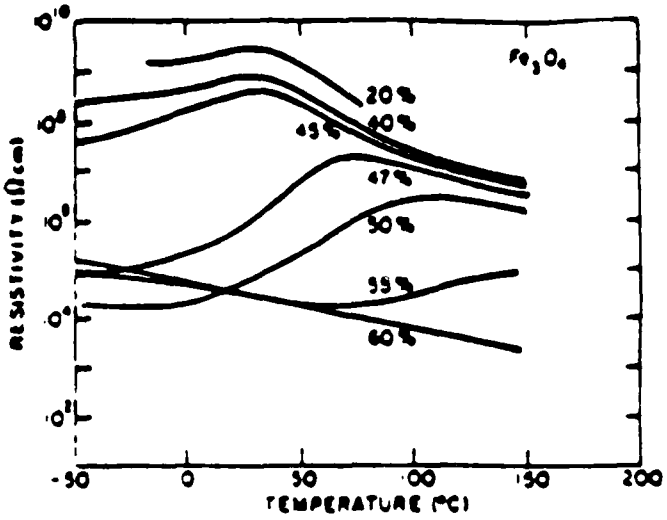

Fig. 2.3.7.2. Pressure dependence of the DC electrical resistivity in an 0:3 Fe_3O_4: Epoxy polymer composite as a function of the loading of the semiconductor phase.

the very disparate mechanical properties of the two components. The formulae show quite clearly that d" is more effected by ϵ" than s" in these systems.

2.3.7 Composite Sensor for Static and Dynamic Pressure

It was clear from earlier work on the composite thermistor that the major effect on the transport in semiconductor:polymer 0:3 composites at compositions near the critical percolation threshold arises from the thermal expansion of the polymer attenuating the connectivity of the conductive filler. Obviously if the same material is subjected to hydrostatic stress, partial phase connection could be restored and the material used as a stress sensor. Unlike the piezoceramic however, the transport will be modulated just as effectively by a DC stress field as by an alternating field.

In the concept being explored, the proposal is to balance the thermal PTC effect of the composite by using a semiconducting filler which will itself have a large NTC effect. Preliminary data, Fig. 2.3.7.1 and Fig. 2.3.7.2 suggest that the PTC effect can be minimized even at compositions which show a very strong pressure sensitivity in their resistivity.

3. ELECTROSTRICTION

3.1 Introduction

During the past year the major theoretical effort has focussed upon the effect of many body forces that arise from interionic charge transfer upon the magnitude and temperature dependence of the electrostriction and of the third order elastic constants. To provide experimental data for this work, T.O.E. constants and their temperature dependence were measured last year. This year the dielectric compressometer was adapted to permit the measurement of the temperature dependence of the electrostrictive Q constants.

In the practical electrostrictors, a very wide range of our work on relaxor ferroelectrics has been summarized. The balance of evidence for the model of micro polar regions in the relaxors was presented and many of the proposed nanostructural features were confirmed in TEM studies by Barber and co-workers at Essex and by Harmer at Lehigh.

For practical electrostrictor compositions work has continued on grain size effects in lead magnesium niobate:lead titanate, and on attempts to control the desirable perovskite phase in lead zinc niobate, and in lead zinc niobate-lead titanate solid solutions both by chemical doping and by processing methods.

In aging studies, work has been extended to the phenomena associated with aging under DC bias and have given the first direct quantitative evidence of the effective internal field associated with the defect ordering.

3.2 Theory of Electrostriction

The objective of this work is to investigate theoretically the magnitude and temperature variation of the electrostriction coefficients of ionic crystals in order to account for, and ultimately predict, tendencies in the effects of crystal structure and of the properties of the constituent ions.

During the previous year theoretical work focussed on the effect of many-body forces that arise from interionic charge transfer. Application to MgO and perovskite oxides and fluorides is in progress.

Supporting experimental studies of the single crystal third order elastic constants of $KMnF_3$ versus temperature were completed. These data are needed in order to determine the nonlinearity parameters required as input for the theoretical model for the electrostriction calculations. With only one exception the temperature dependence is linear, indicating that the effect of the improper ferroelastic transition at 186K (manifest in elastic anomalies) is no longer present above 300K, and permitting us to eliminate the effect of zero point and thermal motion by extrapolation to absolute zero. The static T.O.E. constants thus obtained differ significantly from the R.T. values. Both static and R.T. values exhibit large deviations from the Cauchy relations, demonstrating the inadequacy of pair potentials for describing the interionic short range overlap interactions on emphasizing the importance of many-body forces for a quantitative understanding of the electrostriction coefficients and other anharmonic properties.

At room temperature the second pressure derivatives of the elastic constants were also measured. Analysis of the data on the basis of a model with Coulomb and short range central force interactions indicates anomalously large fourth derivatives of the Mn-F and F-F pair potentials. A calculation of the temperature dependence of the elastic Gruneisen parameter is consistent with models for the acoustic anomaly according to which coupling between strain and order parameter fluctuations is limited to frequencies less than the relaxation rate of the soft R_{25} mode.

In order to study theoretically the effect of pretransformation modulated microstructures on the electrostriction behavior in the vicinity of the transformation temperature we have derived a Landau-Ginsburg continuum model for the improper ferroelastic O_h^1-D_{4h}^{18} phase transition in the perovskite structure compounds ABX_3. By employing group theoretical methods the gradient coefficients for the 3-component primary order parameter (the rotation angles of the BX_6 octahedra) can be expressed in terms of the soft phonon mode dispersion near the R-point. Analytic and numerical kink-type soliton solutions for both the antiphase and the twin boundaries in the tetragonal phase have been obtained.

The model has been applied to calculate the thickness and energy of both interphase boundaries versus temperature in $SrTiO_3$.

3.3 Low Level Electrostriction

Last year, the dielectric compressometer was adapted to measure small samples and the first single crystal measurements on $KMnF_3$ were accomplished. Over the current year an environment chamber has been added which permits measurements over the temperature range from 20 to 150°C. Data of the change in capacitance as a function of pressure is taken at each temperature and from the slope, the data summarized in Fig. 3.3.1 is produced.

From these measurements, it is simple to deduce both M and Q constants and the temperature dependence of Q is shown in Fig. 3.3.2. It is evident that like the T.O.E. constants the R point instability at low temperature does not reflect strongly in the Q constants which are only weakly temperature dependent.

A preliminary fitting to the anharmonic shell model however, using the method of Barsch and Achar, shows that for any of the models chosen (Table 3.3.1) it is not possible to fit both the third order elastic constants and the electrostriction constants with the same model parameters.

Table
Anharmonic shell model parameters, TOE constants ($10^{11}N/m^2$), and electrostriction constants (m^4/c^2).

Model	C1	C2	C3	C_{111}	C_{112}	Q_h	Q_s	Q_{1212}
1	-13.0	-2193	-392	-25.3	-3.835	.274	-0.629	.275
2	-122	992	-48.8	7.56	-2.284	.274	.5426	-.263
3	-13.4	189.1	-387	-2.98	-3.80	1.64	.539	.275
4	-74.1	-840	5218	-1.394	1.805	.354	.0372	.278
exp				-13.66	-0.253	.274	.5426	.275

3.4 Practical Electrostrictors

3.4.1 Relaxor Ferroelectrics

A wide spectrum of evidence from the macroscopic dielectric, elastic, electrostrictive and electro-optic behavior of relaxor ferroelectrics in the perovskite and tungsten bronze families has been reviewed. The balance of evidence is suggested to support a model in which local compositional heterogeneity gives rise to a broad distribution of local Curie points in very small $(100A)^3$ regions of the sample. Evidence from order:disorder studies in $Pb(Sc_{1/2}Ta_{1/2})O_3$ show

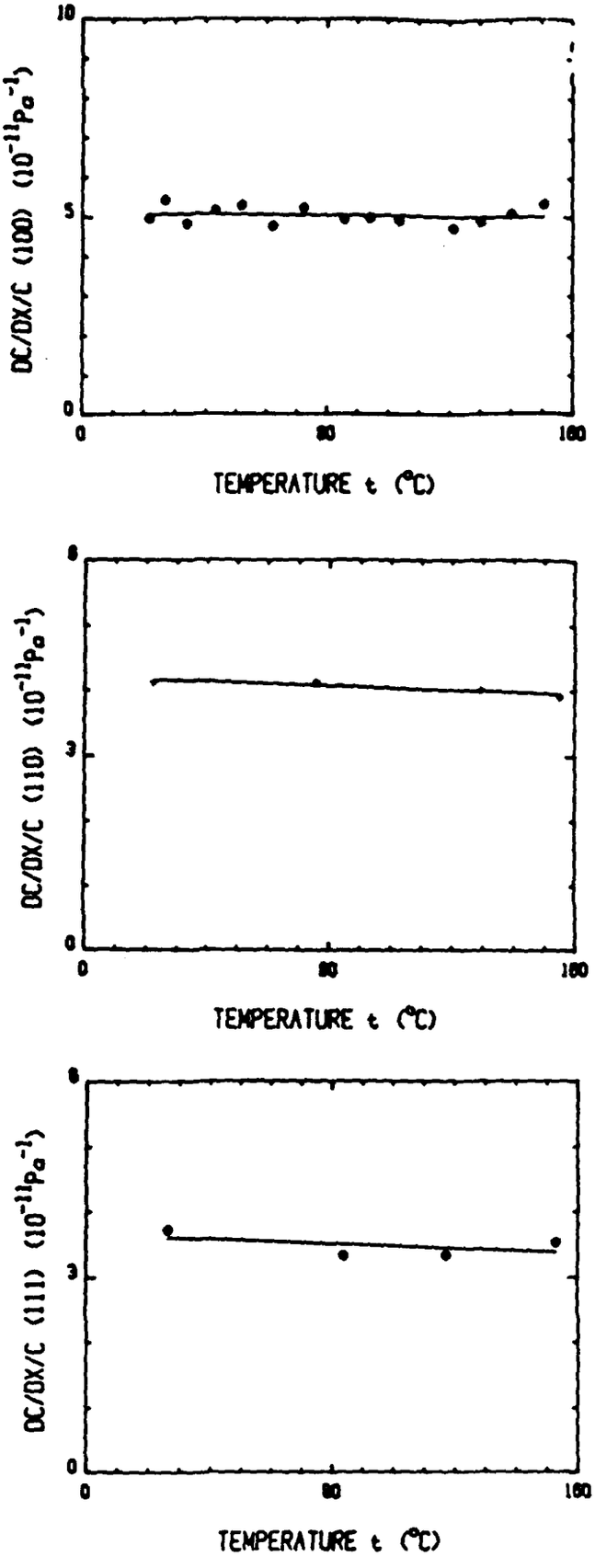

Fig. 3.3.1. Change of capacitance under uniaxial stress for 100, 110, and 111 oriented crystals of $KMnF_3$.

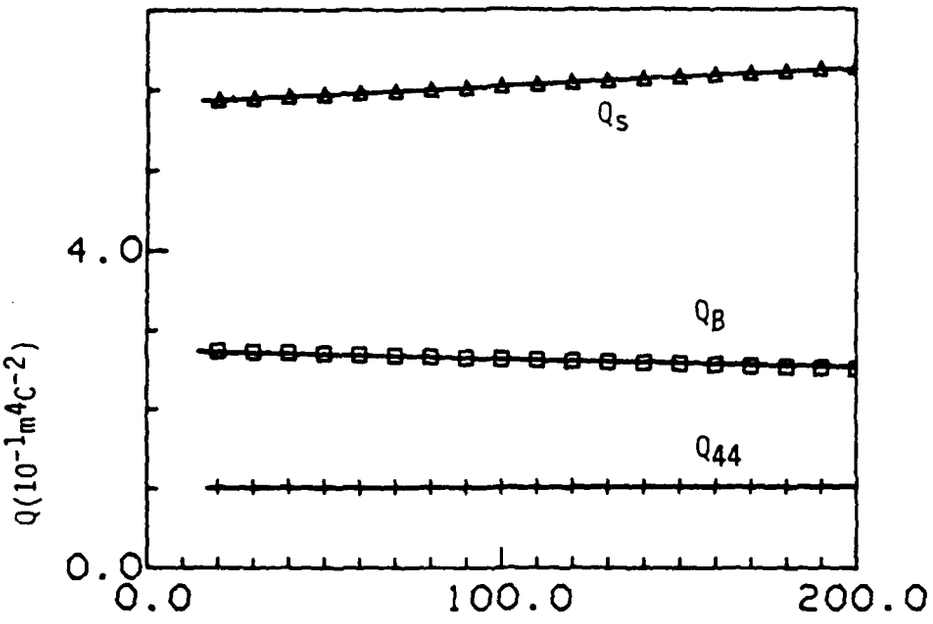

Fig. 3.3.2. Electrostriction constants deduced from the dielectric compressometer data $Q_S = Q_{11} - Q_{12}$
$Q_B = Q_{11} + Q_{12}$.

the critical role of local heterogeneity in the relaxation behavior and are now strongly supported by TEM analysis by Barber and his group in Essex and by Harmer and co-workers at Lehigh.

3.4.2 Aging Studies in $Pb(Mg_{1/3}Nb_{2/3})_3$:$PbTiO_3$

To further explore the role of aliovalent defects in PMN:PT which have been shown to be responsible for the preferential aging out of the frequency dependent part of the dielectric permittivity in PMN:PT doped with MnO_2, aging studies have been carried out under DC bias fields.

For a 10 mole% $PbTiO_3$ composition which has a depoling transition below room temperature an ordered micro domain state can be established at room temperature under high DC bias (10 Kv/cm). In an annealed sample cooled quickly to low temperature, no remanent polarization is established. For a sample aged under DC bias then short circuited and cooled however, a strong remanent polarization appears equivalent to that generated by cooling under a DC bias of ~ 2.5 Kv/cm.

We believe that aging the ordered micro domain status, establishes an ordered component in the defect dipole structure stabilizing the domain orientations, but because of its slow time constant for build up and decay this ordered component will persist even when the macro polarization has been relieved by short circuiting, and will thus again order the domains on cooling.

It would appear that this experiment offers the first clear evidence of the magnitude of the effective equivalent field generated in the defect ordering associated with the aging processes.

3.4.3 Grain Size Effects in Relaxor Ferroelectrics

Studies on this contract include measurements of grain size effects upon lead magnesium niobate (PMN) and lead lanthanum zirconate titanate (PLZT) relaxors. In PMN based systems both the dielectric permittivity K and the electrostrictive field coefficients M depend on grain size, but the polarization related Q constants do not. The dependence is not simple and other factors such as the diffuseness of the phase transition are also altered.

For PLZT, using grain grown samples it is possible to measure the grain size effect over a much wider range and to begin also to look at intrinsic thickness effects in single grain thick samples. Again the effects are complex, depending critically on the boundary conditions on the grain under study. A detailed account of this work will be given next year.

3.5 Preparative Studies of Relaxors

The composition $PbZn_{1/3}Nb_{2/3}O_3$ presents a continuing challenge to ceramic processing. It is known that single crystals of PZN, and of PZN:PT solid solutions have quite exceptional piezoelectric properties (d_{33} ~ 2,000 pc/N). So far however, it has proven impossible to densify polycrystal samples without inversion to a more stable pyrochlore structure which has totally uninteresting properties.

Stabilization of the ceramic form has been achieved by solid solution with $BaTiO_3$ with $SrTiO_3$ and $PbTiO_3$ and by low temperature sol-gel processing. In all cases, however, there is a degradation of the properties of the pure perovskite PZN either due to the chemical doping, or to the presence of some unwanted pyrochlore phase.

4. THERMODYNAMIC PHENOMENOLOGY AND PROPERTIES OF PRACTICAL ELECTROSTRICTORS

4.1 Introduction

Perhaps the major accomplishment on this year's contract has been the completion of a thermodynamic phenomenology for the whole $PbZrO_3$:$PbTiO_3$ solid solution family. We believe that this study by M. Haun and co-workers the continuation of a study which started some 10 years ago by A. Amin will provide a tool for calculating the intrinsic single domain parameters for any composition in the $PbZrO_3$:$PbTiO_3$ system from pure $PbZrO_3$ to pure $PbTiO_3$ at any temperature. The method of derivation makes use of, and cross correlates the most reliable current data on PZT, and no doubt the function will be updated and improved as new measured values are incorporated.

Application of the theory to pure lead titanate gives very good agreement with measured values and permits the prediction of single domain properties which have not yet been measured.

Derivation of the coefficients in the energy function has required new experimentation on a range of compositions which had to be prepared specially for these measurements. Dielectric and piezoelectric studies also had to be carried down to very low temperatures to freeze out defect and domain contributions and permit derivation of the orientation averages of the intrinsic constants.

In related studies a detailed analysis of the nature of the anisotropy in the modified lead titanate ceramics has been included for completeness.

4.2 Thermodynamic Phenomenology for PZT

Over the last 10 years, a full Landau:Ginsburgh:Devonshire (LGD) phenomenological theory has been developed for the $PbZrO_3$:$PbTiO_3$ solid solution system. In the Taylor series expansion for the elastic Gibbs free energy, the basic assumption is that all temperature dependence is carried in the lowest order terms. A second assumption is that the coefficients in the energy function only mutate slowly and continuously with chemical composition and that the phase changes which occur are associated with the crossover between alternative solutions in different polar or antipolar forms.

To permit the description of the antiferroelectric lead zirconate rich phases, a two sublattice model is required, but so that this model will have the same form as in all the major ferroelectric species, the expansion is made in terms of sum and difference of the sub lattice polarization, i.e.:

$$P_F = P_a + P_b$$
$$p_A = P_a - P_b$$

In the final refinement, additional parameters must be used to permit the description of the phases in which the oxygen octahedra take up rotated positions about the polar axis.

These rotation coordinates θ change the shape of the PZT crystal so that new coupling constants which we designate rotostriction constants are required. Since positive and negative rotations produce the same shape change, it is clear that the constants are rotostriction and not piezorotation descriptors. Similarly for the antiferroelectric phases which are characterized by non-zero values of the antipolarization p_i the antipolarizations will be shape changing through antiferroelectric striction constants Z_{ij} analogous to the Q_{ij} constants.

The full theory is described in a sequence of six papers, preprints of which are appended to this report.

4.3 Experimental Measurements on PZT Samples

Pure homogeneous ceramic samples of specific PZT compositions which were required to provide experimental data missing from the literature were prepared by sol-gel methods. X-ray powder diffraction was used to study calcining and to select optimum conditions. For measurement, the powders were sintered at temperatures in the range from 1000 to 1250°C to produce high density (96 to 97% theoretical) bodies with uniform microstructures.

Excess lead was included in the starting powders to improve densification by the fugitive liquid phase.

Powders from these samples were used for x-ray characterization of spontaneous strain. Bulk ceramic samples were measured at very low temperatures to determine averaged dielectric properties.

4.4 Derivations from the Phenomenology

4.4.1 Lead Titanate

The phenomenological theory has been used to model the dielectric and piezoelectric properties of single crystal lead titanate and to calculate the intrinsic behavior of poled polycrystal $PbTiO_3$.

The phenomenological calculations show good agreement with the low temperature dielectric behavior of lead titanate and permit the calculation of single crystal piezoelectric parameters which have not yet been measured experimentally.

In the ceramic calculations, upper and lower limits can be predicted for the averaged electrostrictive, dielectric permittivity spontaneous polarization and piezoelectric coefficients. Experimental data falls between these two bounds. The large piezoelectric anisotropy d_{33}/d_{31} is

traced to anisotropy in the single crystal electrostriction constants Q_{11}/Q_{12} and Q_{44}/Q_{12} with the possibility of a change in sign of d_{31} due to slight changes in the single crystal anisotropies.

4.4.2 Electrostriction in PZTs

Electrostriction constants Q_{12} measured on ceramic samples were used together with single crystal data to approximate the composition dependence of electrostriction across the phase diagram. Series and parallel models analogous to the Voight and Reuss models for elastic constants were used to relate the ceramic and single crystal constants and to derive bounds for the ceramic constants from the calculated single crystal parameters.

5. ASSOCIATED PROGRAMS

Each year, a major effort is required in the preparation and characterization of perovskite and related oxide materials to service the needs of the property measurement groups. This year we would list:

1) Preparation of fine powders of $PbTiO_3$:$BiFeO_3$ and of $PbTiO_3$ for composite studies.
2) Growth of single crystals of perovskite fluorides for electrostriction studies.
3) Extensive studies on pure and on chemically modified $Pb(Zn_{1/3}Nb_{2/3})O_3$ for piezoelectric and electrostrictive applications.
4) Preparation of highly homogeneous PZTs at many compositions across the phase diagram to aid in final development of the thermodynamic phenomenology.

These studies have been reported in the earlier sections.

In work closely related to the phenomenological studies of the PZTs, a detailed study has been going on in MRL of the nature and characteristics of the highly anisotropic modified lead titanate ceramics.

For both calcium and samarium modified compositions, it is possible to choose composition and poling condition such that d_{31} and consequently k_p the planar coupling goes to zero at a particular temperature.

The phenomenological studies suggest that part of the origin of this useful practical performance lies in the basic anisotropy of the single crystal electrostrictive Q constants which assure that d_{31} will be unusually low. In closely related studies however it has been shown that for a proper modelling of the resonance behavior a complex d^* is absolutely required and that whilst the real part of d_{31} goes to zero in an appropriate temperature depending upon preparation, chemistry and poling, the imaginary component does not.

The strong suggestion is that extrinsic factors turn the already low d_{31} and are in fact responsible for the observed temperature behavior. Reports of these studies are appended for completeness.

6. PUBLICATIONS, PRESENTATIONS, HONORS, AND AWARDS

1. Papers Published in Refereed Journals

1. M.J. Haun, E. Furman, S.J. Jang, H.A. McKinstry, L.E. Cross. "Thermodynamic Theory of $PbTiO_3$," J. Appl. Phys., 62(8), 3331 (1987).
2. D. Damjanovic, T.R. Gururaja, S.J. Jang, L.E. Cross. "Temperature Behavior of the Complex Piezoelectric d_{31} Coefficient in Modified Lead Titanate Ceramics," Materials Letters, 4(10), 414 (1986).
3. D. Damjanovic, T.R. Gururaja, S.J. Jang, L.E. Cross. "Possible Mechanisms for the Electromechanical Anisotropy in Modified Lead Titanate Ceramics," Ultrasonics Symposium, p. 633 (1986).
4. D. Damjanovic, T.R. Gururaja, L.E. Cross. "Anisotropy in the Piezoelectric Properties of Modified Lead Titanate Ceramics," Bull. Am. Ceram. Soc., 66(4), 699 (1987).
5. A. Halliyal, U. Kumar, R.E. Newnham, L.E. Cross. "Dielectric and Ferroelectric Properties of Ceramics in the $Pb(Zn_{1/3}Nb_{2/3})O_3$-$BaTiO_3$-$PbTiO_3$ System," J. Am. Ceram. Soc., 70(2), 119 (1987).
6. A. Halliyal, U. Kumar, R.E. Newnham, L.E. Cross. "Stabilization of the Perovskite Phase and Dielectric Properties of Ceramics in the $Pb(Zn_{1/3}Nb_{2/3})O_3$:$BaTiO_3$ System," Am. Ceram. Soc. Bull., 66, 671 (1987).
7. L.E. Cross. "Relaxor Ferroelectrics," Ferroelectrics, 76, No. 3 and 4, 241 (1987).
8. J.M. Hayes, T.R. Gururaja, G.L. Geoffrey, L.E. Cross. "Sol-Gel Processing of $0.91Pb(Zn_{1/3}Nb_{2/3})O_3$:$0.09PbTiO_3$ Stabilization of the Perovskite Phase," Materials Letters 5(10, 396 (1987).
9. L.E. Cross, R.E. Newnham. "History of Ferroelectrics," Ceramics and Civilization, Vol. 3, 289 (1987).
10. A.S. Bhalla, R. Guo, L.E. Cross, G. Burns. "Measurements of Strain and of Optical Indices in the Ferroelectric $Ba_{0.4}Sr_{0.6}Nb_2O_6$:Polarization Effects," Phys. Rev. B, Vol. 36(4), 2030 (1987).
11. S.L. Swartz, A.S. Bhalla, L.E. Cross, W.N. Lawless. "Low Temperature Dielectric Properties of $SrTiO_3$ Glass Ceramics," J. Appl. Phys., 60(6), 2069-2080 (1986).
12. J. Giniewicz, R.E. Newnham, A. Safari. "$(Pb,Bi)(Ti,Fe,Mn)O_3$-Polymer 0-3 Composites for Hydrophone Applications," Ferroelectrics, 73(3-4):405-418 (1987).
13. R.E. Newnham, S.A. Markgraf. "Classic Crystals: A Book of Models," Materials Education Council, 48 pp., Penn State University Press, University Park, PA (1987).
14. R.E. Newnham. "Composite Electroceramics (Part II)," Chem. Tech., 17(1):38-45 (1987).
15. B.V. Hiremath, R.E. Newnham, A. Amin. "Fabrication and Characterization of a Multilayer PTCR Thermistor," Ferroelectrics Letters, 8:1-9 (1987).

16. J.R. Belsick, A. Halliyal, U. Kumar, R.E. Newnham. "Phase Relations and Dielectric Properties of Ceramics in the $Pb(Zn_{1/3}Nb_{2/3})O_3$-$SrTiO_3$-$PbTiO_3$ System." Amer. Ceram. Soc. Bull., 66(4):664-667 (1987).

17. A. Safari, Y.H. Lee, A. Halliyal, R.E. Newnham. "0-3 Piezoelectric Composites Prepared by Coprecipitated $PbTiO_3$ Powder," Amer. Ceram. Soc. Bull., 66(4):668-670 (1987).

18. S. Trolier, Q.C. Xu, R.E. Newnham. "Preparation of Chemically Etched Piezoelectric Resonators for Density Meters and Viscommeters," Mat. Res. Bull. 22(9):1267-1274 (1987).

19. S.M. Pilgrim, R.E. Newnham, L.L. Rohlfing. "An Extension of the Composite Nomenclature Scheme," Mat. Res. Bull., 22:677-684 (1987).

20. Q.C. Xu, A.R. Ramachandran, R.E. Newnham. "Resonance Measuring Technique for Complex Coefficients of Piezoelectric Composites," J. Wave-Material Interaction, 2(2):105-122 (1987).

21. Thomas R. Shrout, Umesh Kumar, Mohammed Megherhi, Ning Yang, Sei-Joo Jang. "Grain Size Dependence of Dielectric and Electrostriction of $Pb(Mg_{1/3}Nb_{2/3})O_3$-Based Ceramics," Ferroelectrics, 76:479-487 (1987).

22. M.J. Haun, Y.H. Lee, H.A. McKinstry, L.E. Cross. "High Temperature X-ray Diffraction Study of Sol-Gel Derived PZT Powder," Advances in X-ray Analysis, 30:473 (1987).

23. T.R. Gururaja, Q.C. Xu, A.R. Ramachandran, A. Halliyal, R.E. Newnham, A. Safari. "Preparation and Piezoelectric Properties of Fired 0:3 Composites," IEEE Ultrasonics Meeting, Denver, CO, pp. 703 (1987).

24. Q.C. Xu, A.R. Ramachandran, R.E. Newnham. "Measurement of Complex Coefficients for Thick PVDF Polymer," IEEE Ultrasonics Meeting, Denver, CO (1987).

3. Presentations

a) Invited

L.E. Cross

1. "Present Trends and Future Prospects in Dielectric and Piezoelectric Ceramics," keynote address, Canadian Ceramic Soc. 85th Annual Meeting and Convention, Feb. 22-27, 1987, Ottowa, Canada.
2. "Ferroic Crystal Design for Tensor Property Optimization," 1987 Gordon Research Conference on Crystal Growth, Feb. 23-27, 1987, Santa Barbara, CA.
3. "Relaxor Ferroelectrics--Polarization and Strain Behavior," 20th Meeting, U.K. Dielectric Society, April 7-9, 1987, Cambridge, England.
4. "Electrostrictive Materials for Actuator Applications," 89th Annual Meeting of the American Ceramic Society, April 26-30, 1987, Pittsburgh, PA.
5. "Electro-optic Materials," IRIS Speciality Group on Infrared Materials, June 8-10, 1987, NBS, Washington, DC.
6. "Polarization and Deformation Mechanisms in Relaxor Ferroelectrics," Gordon Conference, "Solid State Studies in Ceramics," July 27-31, 1987, Plymouth, NH.
7. "Unusual Primary Ferroic Crystals and Devices," 2nd U.S./China Meeting of Ceramic Materials, keynote paper, U.S. Chairman on the meeting, Sept. 8-11, 1987.
8. "Electronic Ceramics for the 21st Century," 172nd Meeting of the Electrochemical Society, Oct. 18-23, 1987, Honolulu, Hawaii.
9. "At the Frontiers of Ceramic Science: Current Salients," The Institute of Ceramics: Basic Science Section, "Electroceramics," Dec. 16-18, 1987, King's College, London.

R.E. Newnham

10. "Dielectric Properties of Azo Dye-Poly (Methylmethacrylate) Mixtures," American Physical Society Meeting, L. Du, J. Runt, A. Safari, R.E. Newnham, March 16-20, 1987, New York, NY.
11. "The Golden Age of Electroceramics," American Ceramic Society Meeting, R.E. Newnham, April 27, 1987, Pittsburgh, PA.
12. "Structure-Property Relations in Electroceramics," Fifth International Symposium on Ferroelectric Semiconductors, R.E. Newnham, June 3, 1987, Rostov-on-Don, USSR.
13. "Composite Electroceramics," Gordon Research Conference, R.E. Newnham, July 27, 1987, Plymouth State College, NH.
14. "Crystal Structures and Crystal Optics," XIVth International Congress, International Union of Crystallography, R.E. Newnham, Aug. 12-20, 1987, Perth, Australia.
15. "Nanocomposites," U.S./China Seminar on Ceramics, R.E. Newnham, Sept. 10, 1987, Gaithersburg, MD.

16. "Structure-Property Relationships in Perovskite Materials," American Geophysical Union, Chapman Symposium on Perovskites, R.E. Newnham, Oct. 30, 1987, Bisbee, AZ.

b) Contributed

1. (6-EP-87) "Potential Distribution in $BaTiO_3$ During Electrical Degradation," D. Anderson, W. Huebner, L.E. Cross, Penn State University, University Park, PA 16802, Am. Ceram. Soc. Meeting, Pittsburgh, PA, May (1987).
2. (18-EP-87) "Piezoelectric Properties of Sol-Gel-Derived Sm- and Dy-Modified lead Titanate Ceramics," J.M. Hayes, T.R. Gururaja, L.E. Cross, G.L. Geoffrey, Penn State University, University Park, PA 16802, Am. Ceram. Soc. Meeting, Pittsburgh, PA, May (1987).
3. (22-EP-87) "Processing Studies on (1-x) PMN-x PT Ceramics," U. Kumar, A. Halliyal, L.E. Cross, Penn State University, University Park, PA 16802, Am. Ceram. Soc. Meeting, Pittsburgh, PA, May (1987).
4. (16-EP-87) "Preparation of PZN-PT Powder Near the Morphotropic Boundary," U. Kumar, A. Halliyal, L.E. Cross, Penn State University, University Park, PA 16802, Am. Ceram. Soc. Meeting, Pittsburgh, PA, May (1987).
5. (28-EP-87) "Fabrication and Characterization of Pure, Homogeneous PZT Ceramics from Sol-Gel-Derived Powders," Z. Zhuang, M.J. Haun, S.J. Jang, L.E. Cross, Penn State University, University Park, PA 16802, Am. Ceram. Soc. Meeting, Pittsburgh, PA, May (1987).
6. (113-E-87) "Dielectric Properties of Single Grain in Grain-Grown PLZT Ceramics," D.N. Huang, L.E. Cross, Penn State University, University Park, PA 16802, Am. Ceram. Soc. Meeting, Pittsburgh, PA, May (1987).
7. (114-E-87) "Application of $Pb_{1-x}Ba_xNb_2O_6$ Single Crystals as Sensors in Electro-optical Devices," S.G. Sankar, Carnegie Mellon University, Pittsburgh, PA; R. Guo, Z.P. Chang, A.S. Bhalla, L.E. Cross, Penn State University, University Park, PA 16802, Am. Ceram. Soc. Meeting, Pittsburgh, PA, May (1987).
8. (33-E-87) "New Composite Materials for Magnetic Field Sensor Applications," G. Harshe, S. Rajan, A.S. Bhalla, R.E. Newnham, L.E. Cross, Penn State University, University Park, PA 16802, Am. Ceram. Soc. Meeting, Pittsburgh, PA, May (1987).
9. (35-E-87) "Investigations of Electrostriction Effects in Glass," Y. Sun, L.E. Cross, Penn State University, University Park, PA 16802, Am. Ceram. Soc. Meeting, Pittsburgh, PA, May (1987).
10. (36-E-87) "Elastic Strain Developed by Phase Switching in Ferroelectric Crystals and Ceramics," W.Y. Pan, Q.M. Zhang, A.S. Bhalla, L.E. Cross, Penn State University, University Park, PA 16802, Am. Ceram. Soc. Meeting, Pittsburgh, PA, May (1987).

11. (39-E-87) "Quasistatic Measurements of PLZT 9.5/65/35 Ceramics," W. Gu, E. Furman, L.E. Cross, Penn State University, University Park, PA 16802, Am. Ceram. Soc. Meeting, Pittsburgh, PA, May (1987).
12. (40-E-87) "Investigation of the Electrical Conductivity in PLZT Ceramics," E. Furman, W. Gu, L.E. Cross, Penn State University, University Park, PA 16802, Am. Ceram. Soc. Meeting, Pittsburgh, PA, May (1987).
13. (66-E-87) "The Growth and Pyroelectric Properties of Alanine- and Phosphorus-Substituted Triglycine Selenate (TSGe) Single Crystals," X.S. Lin, A.S. Bhalla, L.E. Cross, Penn State University, University Park, PA 16802, Am. Ceram. Soc. Meeting, Pittsburgh, PA, May (1987).
14. (62-E-87) "Pyroelectric Properties of Lead Zirconate-Lead Zinc Niobate Ceramics," T. Takenaka, A.S. Bhalla, L.E. Cross, Penn State University, University Park, PA 16802, Am. Ceram. Soc. Meeting, Pittsburgh, PA, May (1987).
15. S.W. Choi, T.R. Shrout, S.J. Jang, A.S. Bhalla. "Dielectric and Pyroelectric Properties of $Pb(Mg_{1/3}Nb_{2/3})_3$-$PbTiO_3$ Solid Solution Ceramics," Am. Ceram. Soc. Meeting, Pittsburgh, PA, May (1987).
16. T.R. Shrout, M. Megherhi, U. Kumar, N. Yang, S.J. Jang. "Grain Size Dependence of Dielectric and Physical Properties of PMN Based Ceramics," Am. Ceram. Soc. Meeting, Pittsburgh, PA, May (1987).
17. S.M. Pilgrim, A. Halliyal, R.E. Newnham. "Piezoelectric Composites as Vibration Absorbers."
18. M.H. Lee, A. Halliyal, R.E. Newnham. "Piezoelectric Properties of Coprecipitated $PbTiO_3$ Powder/Polymer Composites with 0-3 Connectivity."
19. Q.C. Xu, A. Halliyal, A.R. Ramachandran, D. Damjanovic, T.R. Gururaja, R.E. Newnham. "Piezoelectric Properties of 0-3 Composites as a Function of Temperature."
20. K.A. Klein, A. Halliyal, R.E. Newnham, J. Runt, A. Safari. "Thin Film Polymer-Electroceramic Composites."
21. A.R. Ramachandran, A. Halliyal, T.R. Gururaja, Q.C. Xu, R.E. Newnham. "Piezoelectric Coefficients of 'Fired' Composites with 0-3 Connectivity."
22. J.H. Adair, D.V. Miller, R.E. Newnham. "The Surface Chemistry of Barium Titanate in Aqueous Suspension."
23. W.B. Carlson, R.E. Newnham. "Simulations of Electromechanical Properties of Composite Multilayers via Finite Difference Numerical Techniques."
24. M.H. Lee, A. Halliyal, R.E. Newnham. "Crystallization and Morphology of Lead Titanate Prepared by a Coprecipitation Method."

25. J.R. Belsick, A. Halliyal, U. Kumar, R.E. Newnham. "Phase Relations and Dielectric Properties in the $Pb(Zn_{1/3}Nb_{2/3})SrTiO_3$-$PbTiO_3$ System."
26. S. Trolier, Q.C. Xu, A. Halliyal, R.E. Newnham. "Chemically Etched Piezoelectric Devices from PZT Disks."
27. S. Baumler, J. Belsick, A. Halliyal, R.E. Newnham. "Piezoelectric Properties of Modified $Pb(Zn_{1/3}Nb_{2/3})O_3$-$PbTiO_3$ Ceramics."
28. D.J. Taylor, R.E. Newnham. "Effects of Electric Field on Mechanical Fracture in Ceramic Capacitors and Transducers."
29. Thomas R. Shrout, Beth Jones, J.V. Biggers, James H. Adair. "Enhanced Processing of Perovskite $Pb(Mg_{1/3}Nb_{2/3})O_3$ Relaxors Through Understanding the Surface Chemistry of the Component Powders," Fall Meeting of Amer. Ceram. Soc., Orlando, FL (1987).
30. D.A. Anderson, J.H. Adair, D. Miller, J.V. Biggers, T.R. Shrout. "Surface Chemistry Effects on Ceramic Processing of $BaTiO_3$ Powder, Fall Meeting of Amer. Ceram. Soc., Orlando, FL (1987).
31. T.R. Gururaja, Q.C. Xu, R.E. Newnham. "Fired 0-3 Piezoelectric Composite Materials for Biomedical Ultrasonic Imaging Applications," IEEE Ultrasonics Symposium, Denver, CO, Oct. 14-16 (1987).
32. Q.C. Xu, A.R. Ramachandran, R.E. Newnham. "Measurement of Complex Coefficients of Thick Film PVDF Polymer."

Lectures to Industry, Government, and Universities

1. R.E. Newnham. "Structure-Property Relations in Electroceramics," Israel Institute of Technology (Technion), Haifa, Jan. 1, 1987
2. R.E. Newnham. "Transducers, Sensors and Actuators," Ben Gurion University of the Negev, Beersheva, Israel, Jan. 5, 1987.
3. R.E. Newnham. "Recent Advances in Electroceramics," National Materials Board, Washington, DC, Feb. 10, 1987.
4. R.E. Newnham. "Electroceramic Components and Systems," State College, PA, Chapter IEEE, Feb. 19, 1987.
5. R.E. Newnham. "Electronic Packaging," Alcoa Research Lab. Seminar, Pittsburgh, PA, Feb. 24, 1987.
6. R.E. Newnham. "Transducers, Sensors and Actuators," W.R. Grace Co., Columbia, MD, March 31, 1987.
7. R.E. Newnham, L.E. Cross. "Composite Superconductors," DARPA Seminar, Washington, DC, April 15, 1987.
8. R.E. Newnham. "Integrated Electroceramics," Ceramic Process Systems, Boston, MA, April 1 16, 1987.

9. R.E. Newnham. "Electroceramic Materials and Devices," E.C. Britton Symposium, Dow Corning Corp., Midland, MI, April 23, 1987.
10. R.E. Newnham. "Piezoelectric Materials for Control of Fluid--Solid Interface," ONR Flow Noise Symposium, Washington, DC, May 6, 1987.
11. R.E. Newnham. "Crystal Chemistry of Electro-Optic Materials," Electronic and Electro-optic Materials Symposium, Redstone Arsenal, Huntsville, AL, May 14, 1987.
12. R.E. Newnham. "Ceramic Superconductors," AMP Inc. Seminar, Harrisburg, PA, May 20, 1987.
13. R.E. Newnham. "Ceramic Superconductors," Alcoa Seminar, Pittsburgh, PA, May 21, 1987.
14. R.E. Newnham. "Composite Electroceramics," Institute of Crystallography, Moscow, USSR, June 8, 1987.
15. R.E. Newnham. "Electroceramics: Structure-Property Relationships," Center for Fundamental Materials Research, Michigan State University, East Lansing, MI, June 11, 1987.
16. R.E. Newnham. "Electroceramics: The Coming Age of Miniaturization and Integration," Center for Fundamental Materials Research, Michigan State University, East Lansing, MI, June 12, 1987.
17. R.E. Newnham. "Recent Advances in Electroceramics," Dow Chemical Seminar, Waltham, MA, July 1, 1987.
18. R.E. Newnham. "Structure-Property Relationships," Armstrong World Industries, Lancaster, PA, July 10, 1987.
19. R.E. Newnham. "Short Course on Electroceramics," Dow Corning Seminars, Midland, MI, July 16-17, 1987.
20. R.E. Newnham. "Composite Piezoelectrics," McQuarrie University, Sydney, Australia, Aug. 10, 1987.
21. R.E. Newnham. "Recent Advances in Electroceramics," Hewlett-Packard Corp., Andover, MA, Oct. 23, 1987.
22. R.E. Newnham. "Composite Electroceramics," Carnegie-Mellon University, Pittsburgh, PA, Sept. 15, 1987.
23. R.E. Newnham. "The Golden Age of Electroceramics," U.S. Army Materials Technology Lab., Watertown, MA, Oct. 6, 1987.
24. R.E. Newnham. "Composite Electroceramics," U.S. Army Materials Technology Lab., Watertown, MA, Oct. 7, 1987.
25. R.E. Newnham. "The Golden Age of Electroceramics," Sprague Electric Co., Multilythics Div., Hudson, NH, Oct. 13, 1987.

26. R.E. Newnham. "The Golden Age of Electroceramics," Brandeis University, Waltham, MA, Oct. 22, 1987.
27. R.E. Newnham. "Composite Superconductors," Celanese Research Co., Summit, NJ, Nov. 9, 1987.
28. R.E. Newnham. "Composite Electroceramics," Rutgers University, New Brunswick, NJ, Nov. 10, 1987.
29. R.E. Newnham. "Electroceramics," Monsanto Chemical Co., St. Louis, MO, Dec. 14, 1987.

Manuscripts in Preparation

1. Z.Q. Zhuang, M.J. Haun, S.J. Jang, L.E. Cross. "Fabrication and Characterization of Pure Homogeneous PZT' Ceramics from Sol-Gel Derived Powders," J. Am. Ceram. Soc., accepted.
2. M.J. Haun, E. Furman, S.J. Jang, L.E. Cross. "Modeling of Electrostrictive, Dielectric and Piezoelectric Properties of Ceramic $PbTiO_3$," IEEE Trans. on Ultrasonics, Ferroelectrics and Frequency Control, accepted.
3. M.J. Haun, Z.Q. Zhuang, E. Furman, S.J. Jang, L.E. Cross, "Electrostrictive Properties of the Lead Zirconate Titanate Solid Solution System," J. Am. Ceram. Soc., submitted.
4. J.N. Kim, M.J. Haun, S.J. Jang, L.E. Cross, X.R. Xue. "Temperature Behavior of Dielectric and Piezoelectric Properties of Samarium Doped Lead Titanate Ceramics," IEEE Trans. on Ultrasonics, Ferroelectrics and Frequency Control, submitted.
5. M.J. Haun, T.J. Harvin, M.T. Lanagan, Z.Q. Zhuang, S.J. Jang, L.E. Cross. "Thermodynamic Theory of Lead Zirconate," in preparation.
6. M.J. Haun, E. Furman, S.J. Jang, L.E. Cross. "Thermodynamic Theory for the Lead Zirconate-Titanate Solid Solution System, Part I, Phenomenology," in preparation.
7. M.J. Haun, E. Furman, H.A. McKinstry, L.E. Cross. "Thermodynamic Theory for the Lead Zirconate-Titanate Solid Solution System, Part II, Tricritical Behavior," in preparation.
8. M.J. Haun, Z.Q. Zhuang, E. Furman, S.J. Jang, L.E. Cross. "Thermodynamic Theory of the Lead Zirconate-Titanate Solid Solution System, Part III, Curie Constant and Sixth Order Polarization Interaction Dielectric Stiffness Coefficients," in preparation.
9. M.J. Haun, E. Furman, T.R. Halemane, L.E. Cross. "Thermodynamic Theory of the Lead Zirconate-Titanate Solid Solution System, Part IV, Tilts of the Oxygen Octahedra," in preparation.
10. M.J. Haun, E. Furman, S. J. Jang, L.E. Cross. "Thermodynamic Theory of the Lead Zirconate-Titanate Solid Solution System, Part V, Theoretical Calculations," in preparation.

11. Xing-Jiao Li, Wuyi Pan, L.E. Cross. "Experimental Analysis of Ferroelectric Domain Layer Wave," IEEE Trans. on Ultrasonics, Ferroelectrics and Frequency Control, submitted.

12. M.Q. Zhang, W.Y. Pan, L.E. Cross. "Laser Interferometer for the Study of Piezoelectric and Electrostrictive Strains," J. Appl. Phys., accepted.

13. W.Y. Pan, Q.Y. Jiang, L.E. Cross. "Isothermal Aging of the Complex Dielectric Permittivity in MnO Doped Lead Magnesium Niobate:Lead Titanate Relaxor Ferroelectric Ceramics," Ferroelectrics, accepted.

14. C.M. Lawson, A. Halliyal, A.S. Bhalla, S.J. Jang, L.E. Cross. "Piezoelectric Fiber Optic Electric Field Sensor," Ferroelec. Lett. (March 1988).

15. M.T. Lanagan, J.H, Kim, S.J. Jang, R.E. Newnham. "Microwave Dielectric Properties of Antiferroelectric Lead Zirconate," J. Am. Ceram. Soc., in press.

4. Books

1. T.R. Gururaja, A. Safari, R.E. Newnham, L.E. Cross. Electronic Ceramics: Properties, Devices and Applications, Chapter on Recent Advances in Piezoelectric Ceramics with R.C. Pohanka and P.L. Smith, Lionel M. Levinson, Marcel Dekker.

2. Glass and Glass Ceramics, Chapter on Polar Glass Ceramics: New Materials for Piezoelectric and Pyroelectric Devices, P.W. McMillan, Academic Press.

Name of Person Receiving Award	Recipient's Institution	Name of Award	Sponsor of Award
R.E. Newnham	Materials Research Lab	Elected Fellow of the American Ceramic Society, May 1987	
L.E. Cross	Materials Research Lab	Elected to ADCOM of IEEE for the Ultrasonics, Ferroelectrics and Frequency Control Section, Sept. 1987	
Susan E. Trolier	Materials Research Lab	1987 Xerox Award Winner for the best M.S. thesis in Materials at Penn State	
Glenn R. Fox	Materials Research Lab	1987 Xerox Award Winner for the best B.S. thesis in Materials at Penn State	

Degrees Earned

Ph.D.:

1. William Butler Carlson. "Numerical Analysis of Electrostrictive Ceramic Devices," Ph.D. Engineering Science and Mechanics.

2. Steven Alan Markgraf. "Structure-Property Relations and Phase Transitions in Fresnoite-Type Crystals," Ph.D. Solid State Science.

3. Steven Michael Pilgrim. "Application of Piezoelectric Polymer Composites to Passive and Active Vibration Absorption," Ph.D. Solid State Science.

4. Michael T. Lanagan. "Microwave Dielectric Properties of Antiferroelectric Lead," Ph.D. Ceramic Science.

5. Eugene Furman. "Dielectric Breakdown and Related Properties in PLZT," Ph.D. Solid State Science.

6. Michael J. Haun. "Phenomenology of Ferroelectricity in the $PbZrO_3$:$PbTiO_3$ Solid Solution System," Ph.D. Solid State Science.

7. Dragan M. Damjanovic. "Highly Anisotropic Piezoelectric Properties in Modified Lead Titanate Ceramics," Ph.D. Solid State Science.

M.S.:

1. Susan E. Trolier. "Use of Photolithography and Chemical Etching in the Preparation of Miniature Piezoelectric Devices from PZT Ceramics," M.S. Ceramic Science.

2. Joseph Sopko. "A Quantitative Method for Determining the Dynamic Response Characteristics of Pyroelectric Materials," M.S. Electrical Engineering.

3. Deborah Taylor. "Finite Element Analysis of Failure in Electrostrictive Ceramic Actuators," M.S. Solid State Science.

B.S.:

1. Russell L. Bryant. "Integrated Ceramics: Magnetoelectric Effect in the $BaTiO_3$-$CoFe_2O_4$ System," B.S. Ceramic Science.

2. Glen R. Fox. "Coprecipitation of $PbTiO_3$ Nanocomposite Fillers for Electro-optic Composites," B.S. Ceramic Science.

3. Christopher L. Geist. "Tape-Casting of PZT and Fabrication of Thin Layer Structures Using PZT Tape," B.S. Ceramic Science.

4. Alan Ingram. "Piezoelectric Paint," B.S. Ceramic Science.

5. Lorianne Jones. "Miniature Transducers for Ultrasound Diagnostic Equipment," B.S. Ceramic Science.

6. David Leandri. "$(V_{1-x}Cr_x)_2O_3$ Composite Thermistors," B.S. Ceramic Science.

7. Laura Stearns. "A Study of the Behavior of PZT at High Temperatures," B.S. Ceramic Science.

8. Charles Wilt. "Amorphous Z_2O_3 and Carbon Black Composites," B.S. Ceramic Science.

7. **Applied Science Apprenticeships**

It is the purpose of this program to provide opportunity for high school students to become acquainted, during their summer break, with the workings of a major research laboratory and the fascination of research and discover. The objective is to have a maximum of four students in this category who could work closely with the post-doctoral fellows and graduate assistants in the Materials Research Laboratory on problems associated with our ONR program in the Center and Dielectric Studies and on the program of research on Piezoelectric and Electrostrictive Materials for Transducer Applications. These programs which encompasses the preparation, characterization, and measurement of properties of a wide range of new electroceramic and ceramic-plastic composites offer many opportunities in which the "extra pair of hands" and quick perceptions of a well-motivated high school student provides invaluable assistance.

We believe that the relaxed atmosphere and constant interchange between faculty, post-doctoral fellows, graduate assistants, and technical aides, and the continuous presence of many eminent foreign visiting scientists provides a very stimulating environment for the young student who may be at a critical juncture in making decisions as to longer range career plans.

A secondary but not insignificant advantage of the program is in the additional component which it provides in the education of our graduate students. Most of these young men and women will go out into responsible positions in Government and Industry where they will be called upon to organize and supervise the work of many junior engineers and technicians. This program, which attaches the technical aid to a graduate assistant, gives him the chance to organize the work of a second person to speed his own program, but also the responsibility of the associated human problems of scheduling and humane management. We believe it has been a most valuable experience for the graduate assistants who have participated and has given them very useful insights into both the problems and the rewards of "people management."

For the last three years, we have developed a much closer relationship with the University's Upward Bound Program, who are able to draw well-motivated black students from the Philadelphia School System. Over the years it has become our custom to issue each student participant a certificate on completion of the term at a small internal ceremony in MRL. Copies of certificates given to our last three successful apprentices are appended.

PUBLISHED PAPERS

Piezoelectric and Related Composites

Mat. Res. Bull., Vol. 22, pp. 677-684, 1987. Printed in the USA.
0025-5408/87 $3.00 + .00

AN EXTENSION OF THE COMPOSITE NOMENCLATURE SCHEME

S. M. Pilgrim, R. E. Newnham, and L. L. Rohling
Materials Research Laboratory
The Pennsylvania State University, University Park, PA 16802

(Received February 4, 1987; Refereed)

ABSTRACT

An expanded version of composite nomenclature is presented. This nomenclature is based on the principles of connectivity, property type, tensor rank, size scale, and orientation. Families of connectivity patterns for diphasic and triphasic composites are listed. These families adequately reflect the possibilities of composite connectivities. The concept of quasi-composites is introduced in order to clarify the relations among constituent phases in a composite. An extension of the nomenclature to encompass dependence of the connectivity on external variables is also included. The nomenclature scheme conforms to intuitive ideas of importance; however, it is based on rigorous application of rules of precedence.

MATERIALS INDEX: Composites, Nomenclature, Piezoelectric

Introduction

The use of composite materials for piezoelectric, pyroelectric, dielectric, and mechanical applications is well documented. The advantages of composites for improving performance as compared to single phase materials have been demonstrated on several size scales. These size scales extend from the nanometer scale to the centimeter scale. The nanometer scale of composite materials can be found in some polymer blends and copolymers, particularly those used for mechanical applications. The ABS (acrylonitrile-butadiene-styrene) blended copolymers typify this scale and use. The ABS composite consists of discrete, interlocking phase separated regions with a distinct boundary phase. All phase domains are present on the nanometer scale. The micron size scale is typified by some piezoelectric composites. In this case, the composite may consist of piezoelectric ceramic particles embedded in a polymer matrix [1]. The particle size is on the micron scale. Piezoelectric composites may also be made on the millimeter scale [2]. This is the case when macroscopic machining is done to a monolithic piece of piezoelectric ceramic. The final size scale for composites is the centimeter scale. Reinforced concrete can be viewed as a centimeter scale composite. Both the reinforcing rod diameters and the inter-rod separation are on the centimeter scale.

Although composite materials can be formed on dimensional scales covering at least seven orders of magnitude, the underlying principles are the same. The connectivities of the constituent phases within the composite, and the relative sizes of the phases with respect to each other and to the interrogating field, are critical. In order to fully exploit the possibilities of composite materials, a scheme of nomenclature is necessary. Fabricating a composite requires both the proper constituent phases and also the optimum spatial connectivity. Connectivity has been defined as the number of dimensions in which a phase is self-connected [3]. The connectivity of the constituent phases can alter the physical properties of the

composite by many orders of magnitude.

The importance of connectivity is illustrated in Figure 1. Figure 1 presents a simple insulator composed of a minor, conductive phase and a major nonconductive phase. In the insulator shown in Figure 1a, the conductive phase is present as discrete particles; however, in Figure 1b the conductive phase is present as a three dimensionally connected network. Clearly the insulator with discrete conductive regions will have a massively different response than that of the insulator with connected conductive regions. Proper phase choice and connectivity are not the only important factors in fabricating a composite. The symmetry of the composite is also important, since physical properties are related to symmetry through tensor relations.

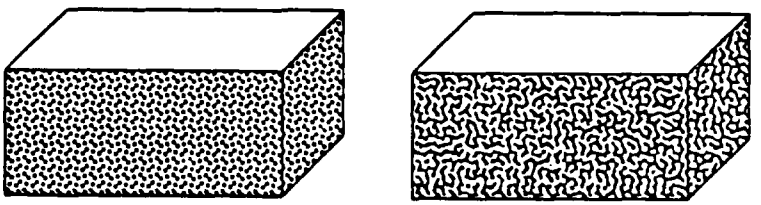

FIG. 1a and FIG. 1b
{0-3} and {3-3} Connected Composites

The type of excitation or interrogation which evokes the desired response is also important. Its nature will determine on what size scale the connectivity and symmetry should be specified. The size scale of the composite in relation to the size scale of the interrogating field is important in interactions with acoustic and optical fields. If the phase connectivity is on a smaller scale than the wavelength of the interrogating field, the composite will respond as an apparently single phase material. An additional consideration is the nature of the physical property under investigation. Physical properties may be linear results of the effects shown by the constituent properties, or more complicated results of the effects.

Van Suchtelen has defined two types of effects in diphasic composites--sum and product properties [4]. Sum properties are the result of an 'averaging' of a physical property common to both constituent phases. Young's modulus and the dielectric constant are both sum properties. The manner of the 'averaging' is dependent on the connectivity, symmetry, and orientation of the phases. A large number of averaging schemes for various properties are available in the literature [5]. Product properties are more complex. In a product property, the excitation of phase (A) stimulates a response which in turn acts as an excitation of phase (B) to generate the final response. Product properties can therefore result in a physical property effect which is present in neither constituent phase.

An example of a product property is the superconductivity stabilizer by W. N. Lawless [6]. In this product property, a superconducting cable of Nb_3Sn is sheathed with a paramagnetic ceramic of $CdCr_2O_4$. Temperature variations cause portions of the superconducting cable to revert to normal metallic conduction. This results in a decrease in the electric current and a decrease in the accompanying magnetic field which is supported in the ceramic. The decrease in the magnetic field demagnetizes the paramagnetic $CdCr_2O_4$ and thus reduces its temperature. This in turn cools the Nb_3Sn cable causing it to return to the superconducting state. Regardless of the composite system, the possible types of physical properties and their magnitudes are intimately related to the connectivity.

Connectivity

Connectivity is a vital feature in characterizing and predicting the response of a composite. In order to describe the connectivity of a composite the connectivities of the constituent phases are written in order [3]. The concept of ordered mixing also plays a part when considering connectivity [7].

For diphasic composites ten connectivities are possible: 0-0, 1-0, 2-0, 3-0, 1-1, 2-1, 3-1, 2-2, 3-2, 3-3. However, in considering only ten diphasic connectivities the fact that two composites of the same phases and connectivity could differ radically was ignored. Specifically, no convention for the ordering of the phase connectivities was established. For example, a composite formed from $Pb(Zr,Ti)O_3$ rods embedded in a polymer matrix has markedly different piezoelectric properties than a monolithic

$Pb(Zr,Ti)O_3$ with polymer filled channels within it [8,2]. Considering just the ten diphasic connectivities both composites would possess 3-1 connectivity. Recent usage has considered the former as a 1-3 connected composite and the latter as a 3-1 connected composite. In this convention the active phase connectivity is written first. By accepting the active-first convention six additional diphasic connectivities are generated:0-1, 0-2, 0-3, 1-2, 1-3, 2-3. These sixteen diphasic connectivities form ten families, where a family is denoted by braces i.e. {3-1}. The {3-1} consists of the connectivities 1-3 and 3-1 when the connectivity of the active phase is written first. In some cases one of a family of connectivities has been referred to as an inverted connectivity. An example of this is the 3-0 connectivity member of the {0-3} [9]

Applying the active-first convention to triphasic composites generates more than the twenty connectivity patterns previously enumerated [3].

TABLE

Diphasic Composites	
Family	members
{0-0-0}	1
{0-0-1}	3
{0-0-2}	3
{0-0-3}	3
{0-1-1}	3
{0-1-2}	6
{0-1-3}	6
{0-2-2}	3
{0-2-3}	6
{0-3-3}	3
{1-1-1}	1
{1-1-2}	3
{1-1-3}	3
{1-2-2}	3
{1-2-3}	6
{1-3-3}	3
{2-2-2}	1
{2-2-3}	3
{2-3-3}	3
{3-3-3}	1

In fact the twenty patterns are actually twenty families of connectivities. These twenty families and the number of their members are listed in Figure 2. Each family contains one, three, or six members. As an extension of the active-first convention, the phase connectivities should be written in order of activity. An active phase is considered to be one which possesses a desirable physical property not shared by another constituent phase. Next in precedence are those phases which phase. possess a particularly desirable property coefficient. Lastly the connectivity of the phase possessing no especially desirable physical property or property coefficients is written. Briefly this order of precedence can be given as active-inactive-inert. For larger numbers of phases the following rules of precedence apply:

1 Unique desired property (property possessed by only one phase)
2 Desired property coefficient in a shared property
3 Tensor order of coefficient or property
4 Volume fraction
5 Weight fraction
6 Formula weight or repeat unit weight

Quasi-composites

In order to properly define a composite connectivity the principle of quasi-composites is used. A quasi-composite is formed when one phase is entirely within another or when there is a large difference in size scales within the composite. In Figure 2a, phases A and B form a quasi-composite with {3-1} connectivity which is embedded in a matrix C. Quasi-composite (A-B) is one dimensionally connected in the total composite. The resultant total composite connectivity is {3-1(3-1)}. This is clearly different than the {1-1-3} composite of A, B, and C shown in Figure 2b.

Size scale differences may also generate quasi-composites. If a group of phases exists on a size scale more than two orders of magnitude larger or smaller than the other size scales present, the group forms a quasi-composite. Assume a polymer matrix (A) loaded with a particulate piezoelectric (B) and a particulate conductor (C), whose particle size is two orders of magnitude smaller than that of phase (B). In this case phases (A) and (C) form a quasi-composite and generate a total composite connectivity which is pseudo-diphasic. The phases in the pseudo-diphasic are the particulate piezoelectric (B) and the 0-3 diphasic quasi-composite of (C) and (A). The total composite connectivity is designated as 0-3(0-3). This connectivity is derived from B-3(C-A). It should be noted that the rules of precedence still apply--the connectivity of (B) is still written first since it is an active phase. The connectivity of the quasi-composite is written next since it contains only a desirable shared property. The total connectivity of the quasi-composite is given in parantheses following its overall connectivity.

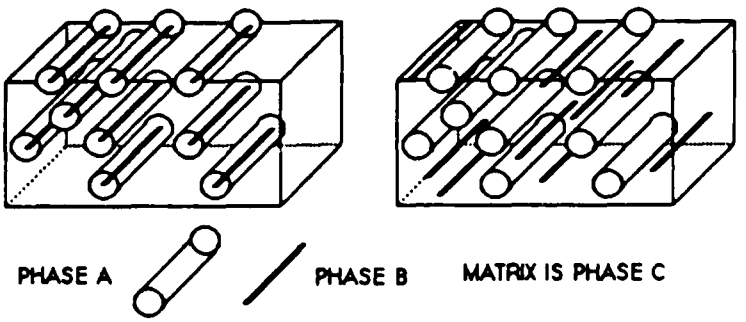

FIG. 2a and 2b
(3-1(3-1)) and (1-1-3) Connected Composites

The scheme of forming quasi-composites when phase sizes differ by more than two orders of magnitude is both instructive and extensible. It clarifies the connectivity, but does not obscure the basic underlying connectivity. Connectivities with quasi-composites are to connectivites what space groups are to point groups; they provide additional information without obscuring the essentials. The technique is extensible since no restrictions on the number of phases present have been assumed. In the case of 'n' phases, the individual quasi-composites are grouped beginning with the smallest size scale present. Then, while considering 'p' of the 'n' phases to form 'q' quasi-composites for a resultant number of constituents 'n-p+q', the rules of precedence are applied. For example, the total connectivity of a six phase mixture composed of:

(A) 0.1 μm particulate conductor
(B) 10 μm particulate piezoelectric
(C) 10 μm particulate
(D) 1.0 mm conductive mesh
(E) 1.0 cm nonconductive rods
(F) matrix

would be found by following the rules of precedence and the flowchart given in Figure 3.

The series of progressive expansions of this composite are shown in Figure 4. Phases (A) and (F) form a quasi-composite with connectivity 0-3. Phases (B) and (C) and quasi-composite (A-F) form a quasi-composite with connectivity 0-3(0-3)-0. Phase (D) and quasi-composite (B-3(A-F)-C) form a quasi-composite with connectivity 3(0-3(0-3)-0)-2. The quasi-composite has precedence over phase (D) as a result of its piezoelectric activity. The quasi-composite (3(B-3(A-F)-C)-D) and phase (E) form the complete composite 3(3(B-3(A-F)-C)-D)-E with connectivity 3(3(0-3(0-3)-0)-2)-1. On considering this composite from the final total connectivity, this material is composed of a three dimensionally connected quasi-composite matrix with precedence over a rod-like phase. On a smaller scale the matrix is composed of a three dimensionally connected quasi-composite matrix with precedence over a mesh-like material. On a yet smaller scale the matrix is composed of two particulate phases, of which one has precedence over a three dimensionally connected quasi-composite matrix. At the smallest size scale, at least six orders of magnitude smaller than the largest scale present, the quasi-composite matrix is composed of a particulate phase with precedence over the actual matrix phase.

Orientation

No reference to the orientation of the one or two dimensionally connected phases has been made previously. Consequently the composites in Figure 5 are indistinguishable by connectivity alone. Some of this ambiguity can be removed for composites which possess an accepted unique axis of orientation. Polar , mechanically stretched, electrically excited, and extruded materials all contain a conventional axis of interest. This conventional axis of interest can be considered as an axis of orientation. If the connectivity within a one dimensionally connected phase is perpendicular to the orientation axis, the connectivity

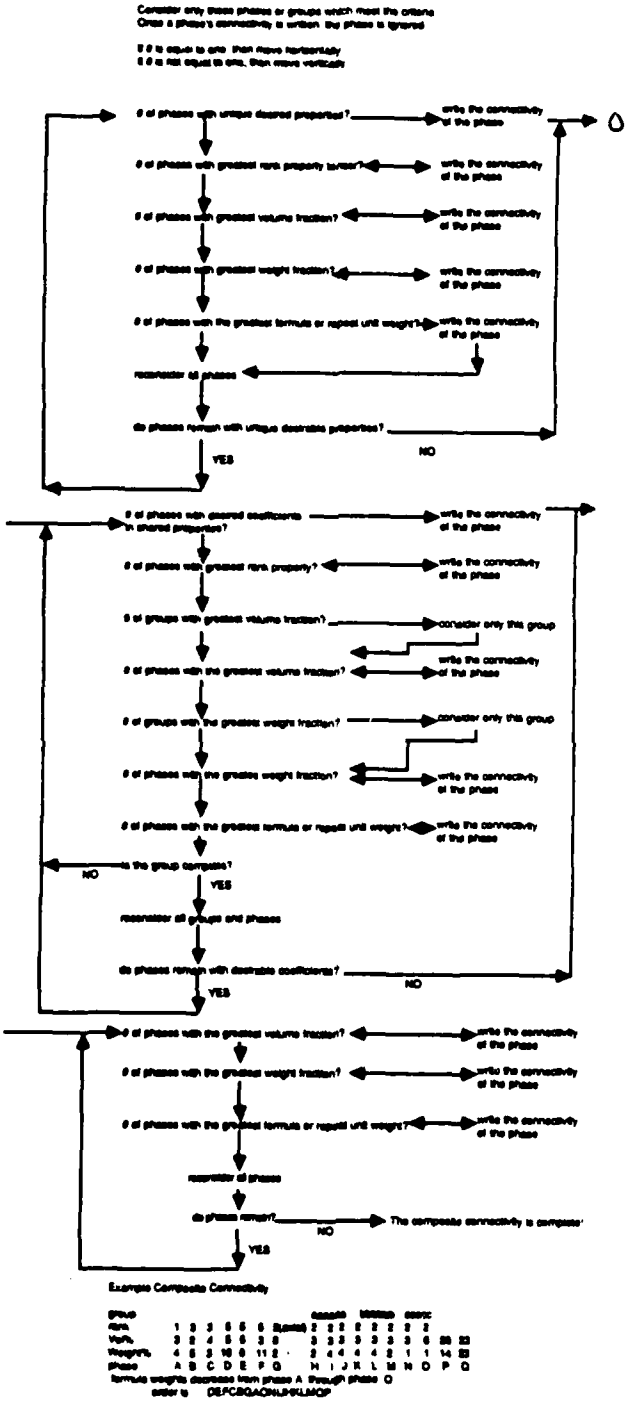

FIG. 3
Flowchart for Determining Composite Connectivity with Example

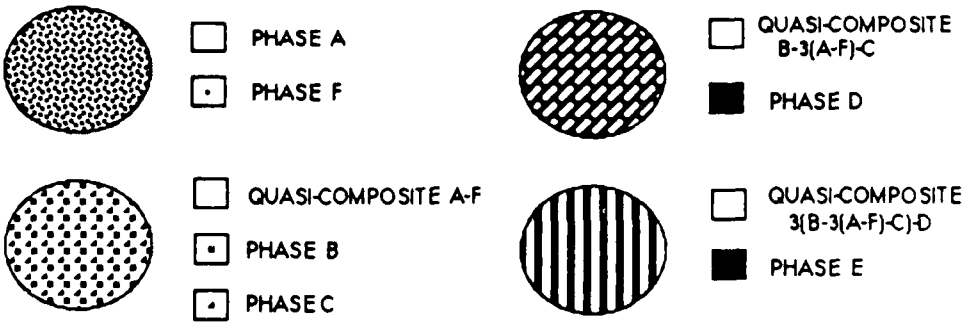

FIG. 4
Progressive Expansions of Six Phase Composite

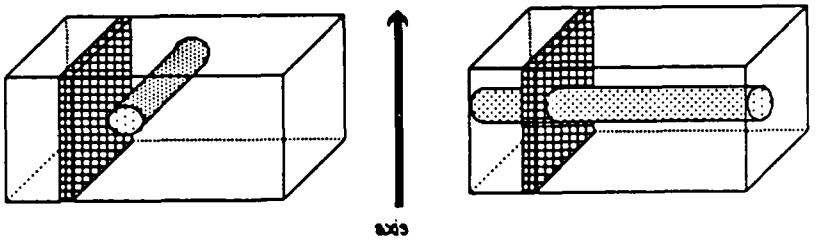

FIG. 5a and 5b
{1-2-3} and {1+2-3} Connected Composites

should be preceded by a '+' instead of a '-'. Additionally, if the normal to a two dimensionally connected phase is perpendicular to the orientation axis the phase connectivity should also be preceded by a '+'. By this convention the composites of Figure 5 can be distinguished. Figure 5a possesses {1-2-3} connectivity; Figure 5b possesses {1+2-3} connectivity.
The six phase composite discussed previously would be have 3(3(0-3(0-3)-0)-2)-1 connectivity if the rods (E) are parallel to the orientation axis and if the normal to mesh (D) is parallel to the axis of orientation. If both the rod axis and the mesh normal are perpendicular to the orientation axis the connectivity would be denoted as 3(3(0-0-3(0-3))+2)+1. This convention does not distinguish between Figures 6a and 6b. Both are {+1+2-3} connected composites.

Transitions

The nomenclature appropriate to a composite may change as a function of externally applied fields or effects. Such variables include temperature (T), voltage (V), and stress(σ). Applied variables which result in second order effects i.e. electrostriction (EE), and cross properties such as magnetoelectricity (BE) are also included as external variables. Two types of transitions may result from a change in external variables. In the case of a phase property transition, the transition occurs within a phase. A connectivity transition does not involve any change in phase properties, but may alter the composite properties or connectivity. In order to denote a transition, a prototypic connectivity is required. The prototype is taken to be the connectivity present at 0 K with no externally applied fields or forces. Transitions are denoted by

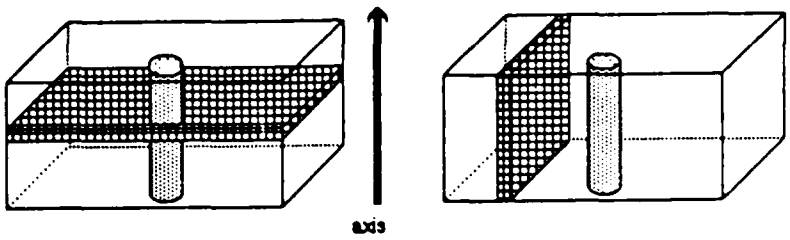

FIG. 6a and 6b
{+1+2-3} and {+1+2-3} Connected Composites

writing the prototypic symmetry, the external variable(s), type of transition ('p' for phase property transitions or 'c' for connectivity transitions), and the new connectivity.

Taking a 30 Vol% V_2O_3-polyethylene composite thermistor as an example, the nomenclature would yield a 3-3 prototypic connectivity. The polyethylene connectivity is listed first since both phases are inert and it is the majority phase. The V_2O_3 phase has a temperature induced phase property transition (NTC) at -135 °C which is denoted Tp. This transition results in a 3-3 connectivity. It must be noted that the order of phases is now reversed. The conductive V_2O_3 now takes precedence over the inert polyethylene. This transition is denoted: 3-3Tp3-3.

Another example involves a composite varistor sandwiched between insulators. The composite is composed of a quasi-composite of conducting ZnO and insulating Bi_2O_3 with 2-3 connectivity, an insulating Al_2O_3 phase, and a minor electrode phase. The prototype has 2-2(2-3)-2 connectivity. The electrode connectivity is first (conductivity has precedence), and the quasi-composite connectivity is second since it is present in a larger volume fraction than the Al_2O_3. Applied voltage causes a phase property transition in the quasi-composite which makes it conductive. The resulting connectivity is 2(2-3)-2-2, with the quasi-composite now taking precedence as the largest volume fraction conductor. The entire transition is denoted: 2-2(2-3)-2Vp2(2-3)-2-2.

If multiple transitions occur they are listed as progressive deviations from the prototypic state. The thermistor composite mentioned above has a second transition at 130 °C. This transition is a temperature induced connectivity transition (Tc). This transition results in the breakup of the three dimensionally connected V_2O_3 phase into a discrete phase. This transition, 3-3Tc0-3, does not alter the order of the phases--the V_2O_3 phase is still first. The complete connectivity description for the composite thermistor is: 3-3Tp3-3Tc0-3. If multiple transitions are nonsequential or independent they are written in increasing tensor rank of the external variable. The nomenclature for a composite formed from a thermistor and a varistor would list the temperature transition before the voltage transition.

Summary

The idea of connectivity patterns has been expanded to form connectivity families for diphasic and triphasic composites. These families more adequately reflect the possibilities of composite connectivity than those given elsewhere. As a further improvement, an expanded version of composite nomenclature has been presented. This nomenclature is based on the principles of connectivity, quasi-composites, orientation, and transition.

The order of precedence for the connectivities within a composite has been defined. The order of precedence conforms to intuitive ideas of importance; however, it is based on rigorous application of the rules of precedence:

1 Unique desired property (property possessed by only one phase)
2 Desired property coefficient in a shared property
3 Tensor order of coefficient or property

4 Volume fraction
5 Weight fraction
6 Formula weight or repeat unit weight

These rules are applicable in a purely mechanical sense.

Quasi-composites were introduced to clarify the spatial and size relations among phases. Physically segregated phases form quasi-composites. Phases present on different size scales also form quasi-composites. In writing the total connectivity, quasi-composite connectivities are grouped by parantheses and conform to the rules of precedence for connectivities.

Orientation of one and two dimensionally connected phases has been denoted within the nomenclature scheme. If a one dimensionally connected phase, or the normal to two dimensionally connected phase, is perpendicular to the composite axis its connectivity is preceded by a '+'. In the case of a parallel or oblique relation to the composite axis the connectivity is preceded by a '-'.

Transitions as a result of external variables are described for composites. A concise method for writing the transition based on prototypic connectivity, external variable, and transition type is given.

These four major themes form the basis of the expanded composite nomenclature. The scheme is extensible to multiphase composite systems. It accurately reflects the physical relations of phases within composites.

Acknowledgements

This work supported by Corning Glass Works Foundation. We also thank our colleagues at the Marerials Research Laboratory whose creativity forced an extension of the composite nomenclature scheme.

References

1. R. E. Newnham, A. Safari, G. Sa-gong, J. Giniewicz, Proc. 1984 IEEE Ultrasonics Symposium, 501 (1985).

2. A. Safari, R. E. Newnham, L. E. Cross, and W. A. Schulze, Ferroelectrics, 41,197 (1982).

3. R. E. Newnham, D. P. Skinner, and L. E. Cross, Mater. Res. Bull., 13, 525 (1978).

4. J. van Suchtelen, Philips Res. Rpts., 27, 28 (1972).

5. L. K. H. van Beek, Prog. Dielectr., 7, 69 (1965).

6. W. N. Lawless, private communication

7. J. A. Hersey, Powder Tech., 11 41 (1975).

8. K. A. Klicker, J. V. Biggers, and R. E. Newnham, J. Amer. Ceram. Soc., 64, 5 (1981).

9. S. M. Pilgrim and R. E. Newnham, Mater. Res. Bull., 21,1447 (1986).

Composite electroceramics

Part 2

Robert E. Newnham

Part 1 of this article (CHEMTECH, December 1986, pp. 732–739) outlined some of the basic principles of composite electroceramics: sum and product properties, polychromatic percolation, and the effect of porosity, among others. In Part 2 we'll examine composite-material symmetry, we'll discuss Curie groups, magnetic Curie groups, and color groups, and we'll review their effects on physical properties.

Many varieties of symmetry are found in composite materials. In describing their symmetry, the basic idea is Pierre Curie's principle of symmetry superposition: Composite materials exhibit only those elements of symmetry that are common to their constituent phases and to the geometric arrangement of those phases.

The practical importance of Curie's principle rests with its influence on physical properties. Neumann's law from crystal physics sums this up: The symmetry elements of any physical property of a composite must include those of its crystallographic point group. Nye discusses applications of this law to single-crystal materials (*1*). A discussion of the more wide-ranging effects of symmetry has been given by Shubnikov and Koptsik (*2*).

Laminated composites are good illustrations of composite symmetry. The glass fibers of unidirectional laminates are aligned parallel to one another, and these laminates are said to have orthorhombic symmetry (crystallographic point group mmm [Figure 1]).

Mirror planes are oriented perpendicular to the laminate normal and perpendicular to an axis formed by the intersection of the other two mirrors. Therefore, the physical properties of a unidirectional laminate must reflect the symmetry elements of point group mmm. If the laminate is heated, thermal expansion will cause it to change shape. Less expansion will take place parallel to the fiber axis because glass is less prone to thermal expansion and has greater stiffness than polymers do. The laminate will expand anisotropically, but its symmetry will not change. The heated laminate continues to conform to point group mmm.

A cross-ply laminate is made up of a pair of unidirectional laminates bonded together with their fiber axes at 90° (Figure 2). Such a laminate belongs to tetragonal point group $\bar{4}2m$. The fourfold axis is perpendicular to the laminated sheets and to both sets of glass fibers. Its twofold symmetry axes are oriented perpendicular to the $\bar{4}$ axis and at 45° to the fiber axes. The tetragonal symmetry is maintained when the laminate is heated; double-curvature distortion occurs, but the symmetry elements of point group $\bar{4}2m$ are not violated.

Laminated composites with $\pm\theta$ angle-ply alignment exhibit orthorhombic symmetry consistent with point group 222 (they have three perpendicular twofold axes). In a $\pm\theta$ angle-ply laminate, the fibers in the first layer are oriented at an angle of $+\theta$ with respect to the edge of the laminate (Figure 3). Fibers in the second layer form an angle of $-\theta$ with the edge, and they form an angle of 2θ with respect to the fibers in the first layer. A pair of twofold symmetry axes bisects the fiber directions, and a third is perpendicular to the laminated layers. When heated, the fibers twist but the symmetry is unchanged.

The varieties of thermal strain exhibited by the three laminated composites are excellent examples of Neumann's law. In each case, the symmetry of the physical properties includes that of the point group of the composite. Other properties of the composite obey Neumann's law as well. The elastic properties of an angle-ply metal matrix are shown in Figure 4.

Maximum anisotropy in Young's modulus is observed when the fibers in the adjacent layers of the matrix are parallel to one another ($\theta = 0°$ or 90°). In this case, the symmetry of the composite is orthorhombic, but as θ approaches 45°, the anisotropy disappears until the symmetry becomes tetragonal at $\theta = 45°$. This corresponds to the symmetry of the cross-ply laminate.

The point groups for unidirectional laminates (mmm), cross-ply laminates ($\bar{4}2m$), and angle-ply laminates (222) are examples of crystallographic symmetry in composite materials. Three-dimensional composites use more complicated patterns. Woven carbon–carbon composites are made from carbon fibers infiltrated with pyrolytic carbon (*3*). Aerospace engineers have found that weaves with cubic geometries show excellent resistance to wear.

Cubic symmetry is obtained by weaving fibers in directions that correspond to important symmetry directions in a cube. In one such pattern, the fiber axes are aligned perpendicularly to one another along three

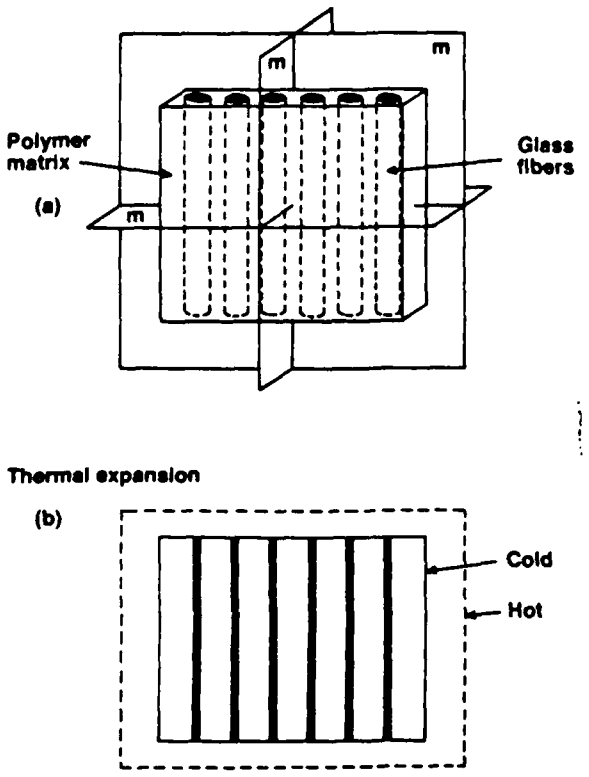

Figure 1. (a) Unidirectional laminate consisting of parallel glass fibers in an epoxy matrix has orthorhombic symmetry. (b) Symmetry of the composite is maintained when it is heated.

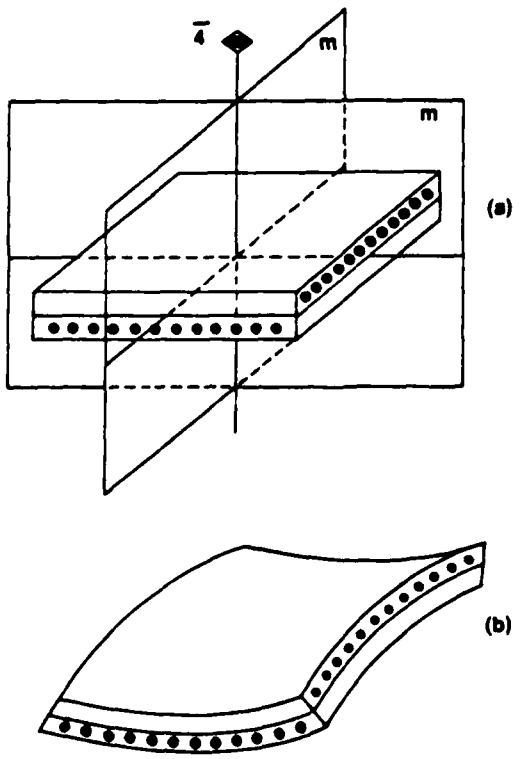

Figure 2. (a) Cross-ply laminate containing orthogonal fibers in adjacent layers has a fourfold inversion axis and two mirror planes, 4̄2m. (b) Double curvature occurs on heating, consistent with 4̄2m symmetry. Plywood is a cross-ply laminate.

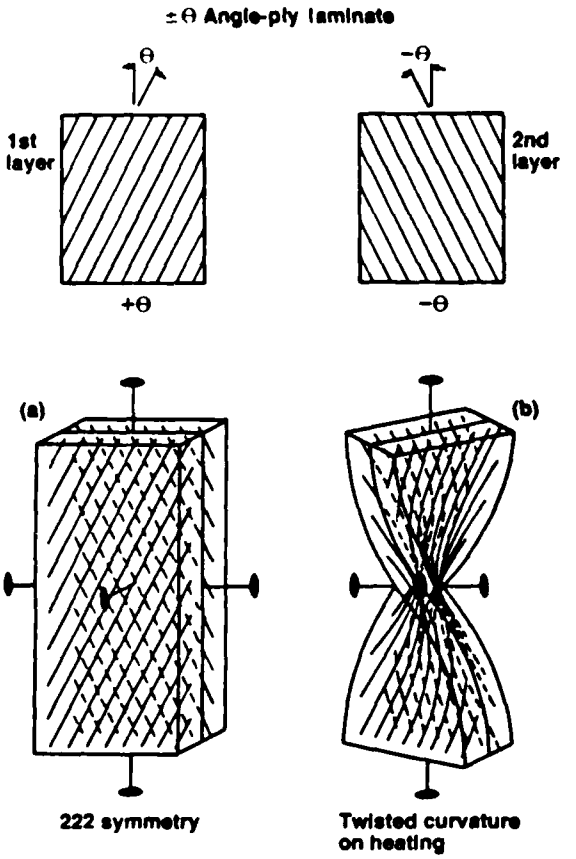

Figure 3. (a) $\pm\theta$ angle-ply laminate with 222 symmetry. (b) When heated, this laminate twists but keeps its original symmetry.

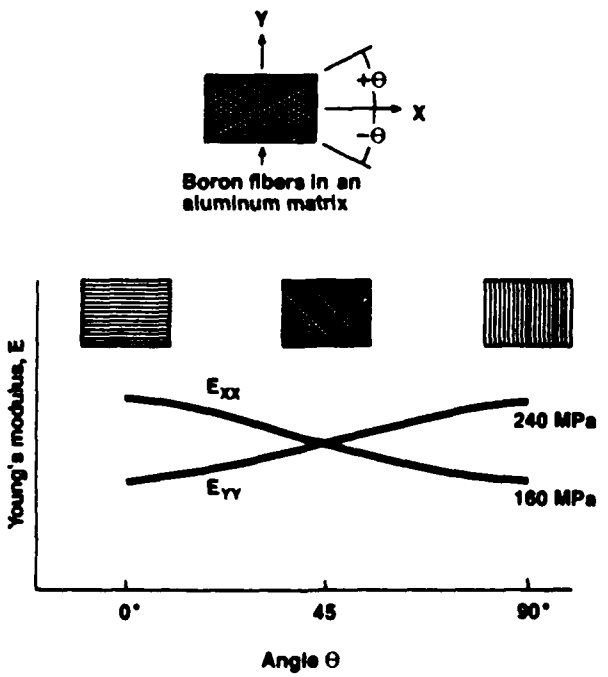

Figure 4. $\pm\theta$ angle-ply composite of boron fibers in an aluminum matrix. When $\theta = 0°$ or 90°, the fibers in the two layers are parallel. When $\theta = 45°$, the fibers are 90° from one another. Young's modulus as measured in the x and y direction is E_{xx} and E_{yy}. Symmetry changes from orthorhombic ($E_{xx} \neq E_{yy}$) to tetragonal ($E_{xx} = E_{yy}$).

Symmetry

Although the term symmetry is used to describe areas and objects as diverse as mathematics, electrical charge, magnetism, and crystals, in all it implies harmony—a sameness, or something that remains unchanged throughout an operation. In solid state chemistry, or crystallography, symmetry operations on materials are discussed in terms of symmetry elements, including

- *Rotation axis, n*
- *Mirror plane, m*
- *Inversion axis, n̄*
- *Center of symmetry, 1̄*

The elements noted are examples of those belonging to point symmetry, because at least one point in the material remains unchanged during the symmetry operation. Crystals have been found to belong to one of 32 possible combinations of point elements; each combination is called a point group.

nonintersecting <100> directions. Another has four nonintersecting <111> directions as fiber directions. An even more complex weave is obtained by combining the <100> and <111> patterns in a seven-directional weave with faceted strands. In the carbon–carbon composites, 60–75% of the volume is occupied by carbon fibers.

Extruded geometries

Other symmetry elements can be introduced during processing. The extruded honeycomb ceramic used as a catalytic substrate is one interesting example (4). By suitably altering the die used to extrude the ceramic slip, a large number of different symmetries can be incorporated into a composite body when the extruded form is filled with a second phase. Figure 5 illustrates three extruded geometries with hexagonal, tetragonal, and orthorhombic symmetries. The orthorhombic pattern (Figure 5a) resembles the cellular structure of wood in which cell walls terminate on adjacent transverse walls. Such a structure offers excellent resistance to mechanical and thermal shock.

Lead zirconate titanate (PZT) honeycomb ceramics have been transformed into piezoelectric transducers by poling them and adding electrodes. Honeycomb transducer symmetry depends on the symmetry of the extruded honeycomb and on the poling direction. For a square pattern, the symmetry of the unpoled ceramic is tetragonal (4/mmm) with a fourfold axis parallel to the extrusion direction. When the honeycomb is poled parallel in the same direction as the extrusion, the symmetry changes to 4mm.

Longitudinally poled PZT composites have been investigated by Shrout and co-workers (5). Transversely poled, epoxy-filled composites are especially sensitive to hydrostatic pressure waves (6); their symmetry belongs to the orthorhombic point group mm2 (Figure 6).

Not all composites have crystallographic symmetry. Some belong to the seven limiting groups that have infinite-fold symmetry axes (Figure 7). The best known of the Curie groups are those with spherical (∞ ∞ m), cylindrical (∞/m m), and conical (∞ m) symmetry (2). The other four groups exhibit right- and left-handed characteristics, which can best be illustrated by various liquids.

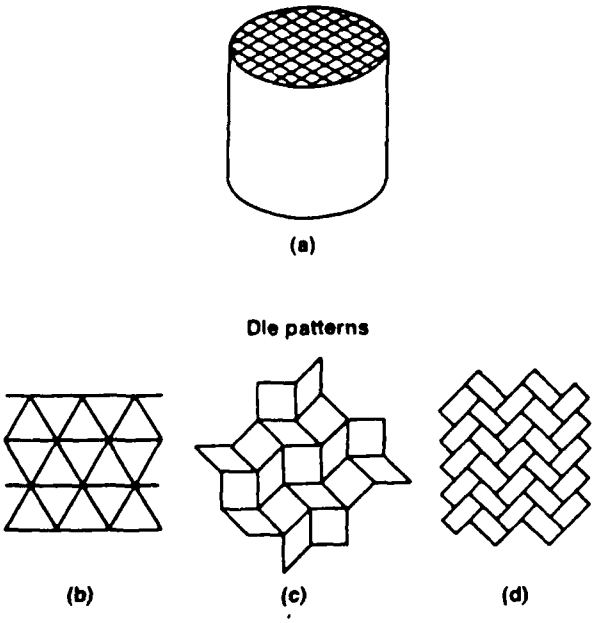

***Figure 5.* (a) Electroceramic bodies with many different symmetries can be extruded by using dies. (b) An end-on view of a hexagonal monolithic honeycomb pattern. (c) A tetragonal pattern with square and diamond faces. (d) An orthorhombic pattern**

An ordinary liquid, such as water or benzene, has spherical symmetry. The molecules have no alignment or handedness, and hence there are infinite numbers of infinite-fold axes and mirror planes, corresponding to Curie group ∞ ∞ m. All other limiting groups are subgroups of ∞ ∞ m, as indicated in Figure 7.

The mirror planes are lost when the liquid possesses handedness. A simple way to impart handedness is to dissolve sugar in water. Although randomly oriented in water, the sucrose molecules are all of the same handedness, thereby making the solution optically active. When dissolved in water, dextrose and levose—the right- and left-handed forms of sugar—give rise to the enantiomorphic forms of point group ∞ ∞. This symmetry can be imposed on a composite material by incorporating randomly oriented, left- or right-handed molecules within the body.

Point groups ∞ ∞ m and ∞ ∞ are consistent with random orientation of crystallites as well. A polycrystalline body of alumina (single-crystal symmetry 3m) belongs to ∞ ∞ m. The symmetry group of polycrystalline quartz (enantiomorphic single-crystal group 32) depends on the relative population of right- and left-handed grains. If the two are equal in population, as is normally the case, the symmetry of the randomly oriented polycrystalline body is ∞ ∞ m. If left-handed grains were systematically excluded, for example by grinding up a right-handed crystal, the symmetry group would be ∞ ∞.

Composite bodies that have texture or direction may belong to one of the five remaining Curie groups: ∞/mm, ∞ m, ∞/m, ∞ 2, or ∞. Texture is added to a composite when it is mechanically processed. All five groups have special symmetry axes. Liquid crystals have an orientational order that conforms to Curie group symmetry. In nematic liquid crystals, the molecules are parallel to one another, giving cylindrical symmetry

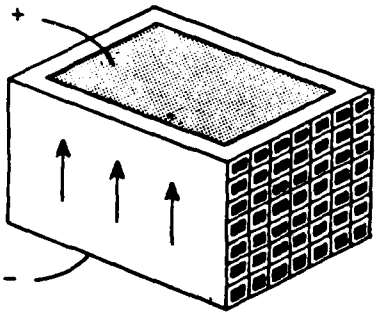

Figure 6. **Honeycomb pressure sensor extruded with tetragonal 4/mmm symmetry, transversely poled to give orthorhombic mm2 symmetry.**

∞/mm. Conical symmetry (∞ m) is achieved when the molecules are parallel *and* polar. And if the liquid crystal molecules have handedness or are stacked helically, as in cholesteric liquids, the symmetry group is ∞ 2. Group ∞/m occurs in the unlikely circumstance that right- and left-handed molecules align with opposite polarity. Certain ferroelectric crystals, such as $Pb_5Ge_3O_{11}$, exhibit ambidextrous behavior. Right- and left-handed ferroelectric crystals, however, are in the polar point group ∞, the lowest-symmetry Curie group.

Mixed liquids can lead to some interesting symmetry changes. Mixing an enantiomorphic liquid (∞ ∞) with a nematic liquid crystal (∞/mm) creates a "mixed drink" with symmetry ∞ 2, in accordance with the principle of symmetry superposition.

Physical forces or fields can be assigned to certain symmetry groups. Consider a temperature gradient dT/dx. This is a vector that can be imposed on a composite material during processing, and if the material has a "memory," the vector nature of the temperature gradient will be retained after the gradient is removed.

Polar glass–ceramic materials illustrate this principle (7). A glass is crystallized under a strong temperature gradient, and polar crystals grow like icicles inward from the surface. Certain glass–ceramic systems, such as $Ba_2TiSi_2O_8$ and $Li_2Si_2O_5$, show sizable pyroelectric and piezoelectric effects when prepared in this manner. They belong to Curie point group ∞ m, the group of a polar vector. As the glass crystallizes in a temperature gradient, its symmetry changes from spherical (∞ ∞ m) to conical (∞ m), the same as that of a poled ferroelectric ceramic.

Magnetic Curie groups

Other physical forces can be classified into Curie group symmetries. To describe magnetic fields and their properties it is necessary to introduce the so-called black-and-white Curie groups illustrated in Figure 8. Magnetic fields are represented by axial vectors with symmetry ∞/mm′. The symbol m′ indicates that the mirror planes that are parallel to the magnetic field are accompanied by time reversal (essentially a reversal of the magnetic field to maintain symmetry). The symbol 1′ is added to the Curie group symbols to indicate that in normal Curie groups all symmetry elements occur twice—once with and once without time reversal.

Polar vectors, such as temperature gradient or electric field, belong to Curie group ∞ m1′. Tensile stress, which

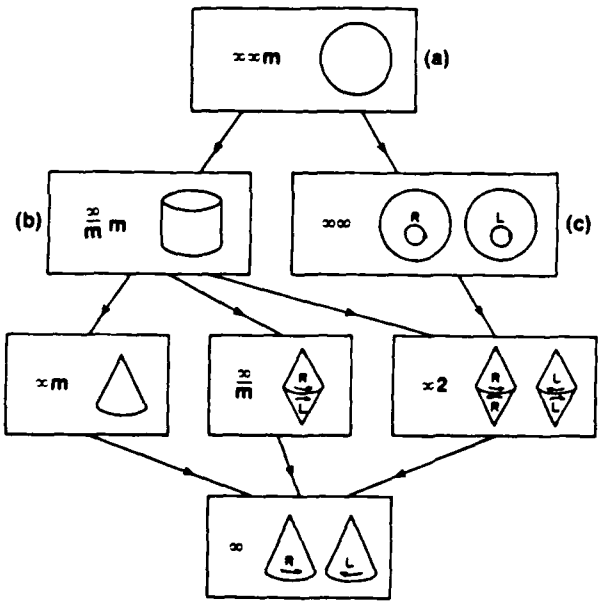

Figure 7. **The seven limiting symmetry groups with infinite-fold axes, called Curie groups. These apply to aggregates rather than to single crystals. (a) Water and benzene have spherical symmetry, ∞ ∞ m. Spheres contain an infinite number of infinite-fold axes and mirror planes. (b) Cylindrical symmetry, ∞/m m, provides one axis with infinite-fold symmetry and a mirror plane parallel to the axis. Polymers often have cylindrical symmetry created by extruding them through dies or by pulling them lengthwise. (c) The mirror planes of spheres are lost when the liquid is right- or left-handed, as when sucrose is dissolved in water. The point group is ∞ ∞. The remaining groups (unlabeled) have directionality, as do collections of dipoles.**

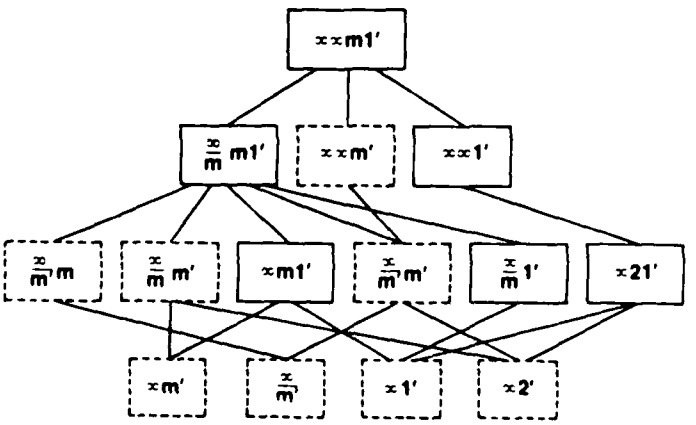

Figure 8. **Magnetism can be classified into Curie groups but because every magnetic field has a direction, one symmetry operation that appears is time reversal (essentially an imaginary flopping of the magnetic field), indicated by m′. Normal Curie groups (solid boxes) contain symmetry elements both with and without time reversal. Magnetic derivatives are dotted boxes; m′ indicates that the mirror operation is accompanied by time reversal.**

More than two phases

Connectivity patterns for more than two phases are similar to the diphasic patterns but are more numerous. There are 20 three-phase patterns and 35 four-phase patterns, but only 10 two-phase patterns (Figure 10). For n phases the number of connectivity patterns is $(n + 3)!/3!n!$. Triphasic connectivity patterns are important when electrode patterns are incorporated into disphasic ceramic structures.

depends on two forces operating in equal and opposite directions, is represented by a second-rank tensor that belongs to cylindrical group ∞/mm1′.

The symmetry superposition principle applies to the point groups in Figure 8. In the magnetoelectric composites made from ferroelectric and ferromagnetic phases, the symmetry of the poling fields is retained. If the electric and magnetic poling fields are applied in the same direction, the symmetry of the composite is ∞ m′. When the poling fields are perpendicular to one another, the symmetry is 2′mm′.

To summarize, some composites belong to crystallographic point groups (cross-ply laminates to $\bar{4}$2m), some belong to limiting groups (polar glass–ceramics to ∞ m), and some belong to black-and-white limiting groups (magnetoelectric composites to ∞ m′). Composites that contain more than two phases can be described by color group symmetry.

The magnetoelectric composite is an excellent illustration of the importance of symmetry in composite materials. Figure 9 shows the change in symmetry going from single domain—single crystals of $CoFe_2O_4$ and $BaTiO_3$ through multidomain and polycrystalline states—to a polycrystalline composite that has been poled and magnetized in parallel electric or magnetic fields. In combining a magnetized ceramic such as $CoFe_2O_4$ (symmetry group ∞/mm′) with a poled ferroelectric ceramic such as $BaTiO_3$ (symmetry group ∞ m1′), the symmetry of the composite is obtained by retaining the symmetry elements common to both groups: ∞ m′.

An interesting feature of symmetry is its effect on physical properties. According to Neumann's law, the symmetry of a physical property of a material must include the symmetry elements of the point group. The separate symmetries of a magnetized ceramic and a poled ferroelectric forbid the occurrence of magnetoelectricity, but their combined symmetry (∞ m′) allows it. By incorporating materials of suitable symmetry in a composite, new and interesting product properties can be expected to occur.

Connectivity

Connectivity is an important feature in property development in multiphase solids because physical properties can change by many orders of magnitude depending on the manner in which connections are made (8). For instance, if an electric wire's metallic conductor and rubber insulation were connected in series rather than in parallel, its resistance would be far higher.

Each phase in a composite can be connected to material in the same phase in zero, one, two, or three dimensions. It is natural to confine attention to three perpendicular axes because all property tensors are referred to such systems. If we limit discussion to diphasic composites, there are 10 connectivities (8), as shown in Figure 10: 0–0, 1–0, 2–0, 3–0, 1–1, 2–1, 3–1, 2–2, 2–3, and 3–3. A 2–1 connectivity pattern, for example, has one phase that is two-dimensionally self-connected, whereas the second phase is in the form of chains or fibers. Connectivity patterns generally are not unique. In the case of a 2–1 pattern, the fibers of the second phase might be perpendicular to the layers of the first, or they might be parallel.

The past few years have seen development of processing techniques for making ceramic composites with different connectivities (9). Extrusion, tape-casting, and replamine (lost-wax process) methods have been especially successful. The 3–1 connectivity pattern in Figure 10 is ideally suited to extrusion processing. A ceramic slip extruded through a die gives a three-dimensional, connected pattern with one-dimensional holes, which can later be filled with a second phase (Figure 6).

Another variety of connectivity suited to processing is the 2–2 pattern of alternating layers of the two phases. Tape casting multilayer capacitors that have alternating or interleaved layers of metal and ceramic is one way to produce 2–2 connectivity. In this arrangement, both

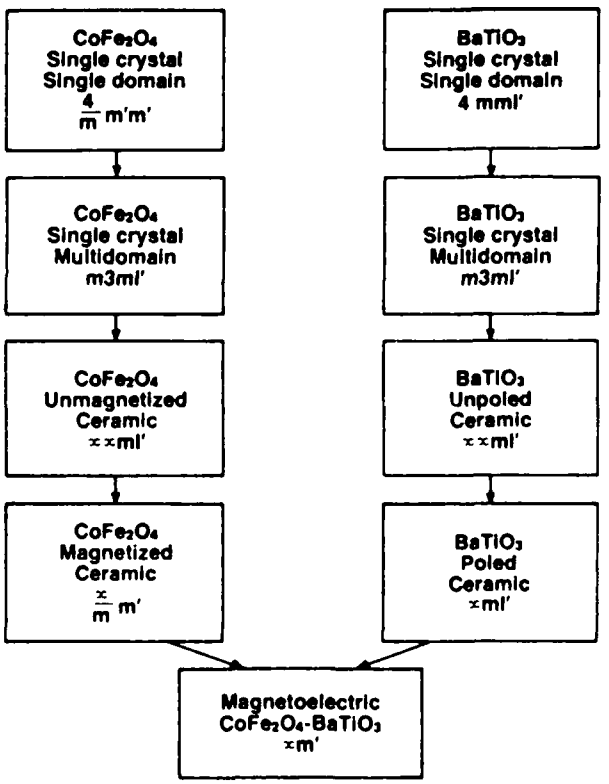

Figure 9. **Symmetry derivation for a polycrystalline $BaTiO_3$–$CoFe_2O_4$ magnetoelectric composite, poled and magnetized in parallel electric and magnetic fields**

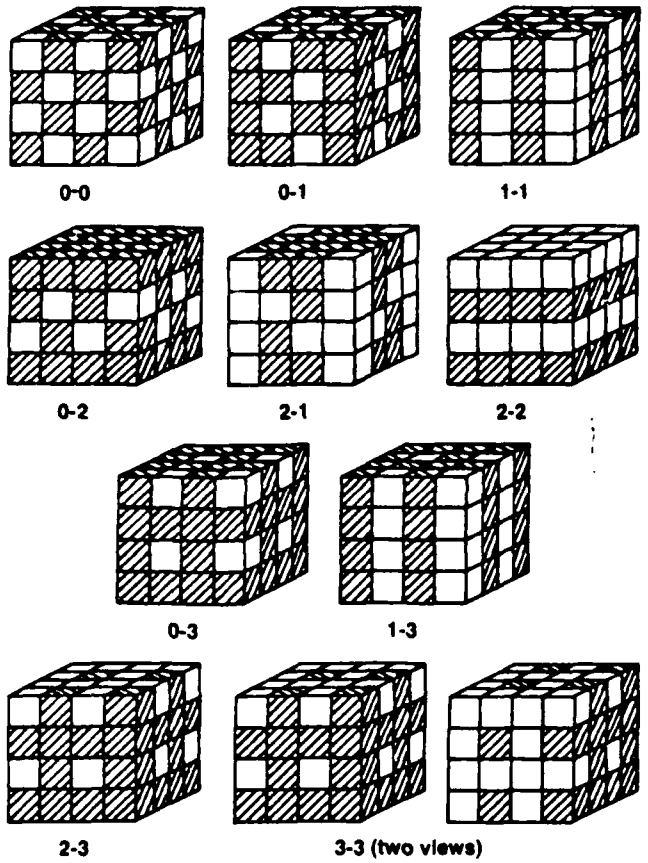

Figure 10. **Ten connectivity patterns used to describe the tensor properties of diphasic composites**

phases are self-connected in the lateral x and y directions, but they are not connected to the layer along z.

In 3–2 connectivity, one phase is connected in three dimensions, the other is connected in two. This pattern can be considered a modified multilayer pattern with 2–2 connectivity. If holes are left in the layers of one phase, the layers of the second phase can connect through these holes to give three-dimensional connectivity.

The most complicated and perhaps the most interesting pattern is 3–3 connectivity in which the two phases form interpenetrating, three-dimensional networks. These patterns often occur in living systems, such as coral, in which organic tissue and an inorganic skeleton penetrate one another. These structures, as well as the connectivity patterns found in foam, wood, and other porous materials, can be replicated in other materials using the replamine process (*10*).

Stress concentration

The importance of stress concentration in composite materials is well known from structural studies, but its relevance to electroceramics is not so obvious. Stress concentration is important to many piezoelectric composites made from polymers and ferroelectric ceramics (*9*). By focusing the stress on the piezoelectric phase, some of the piezoelectric coefficients can be enhanced while others are reduced (*8*).

As an example, consider a piezoelectric composite in which both the tensile stress and the resulting electric field are parallel to the poling direction. If the two phases of the composite are arranged in parallel, the stress acting on the more compliant phase will be transferred to the stiffer one. A composite of interest here is made from a ferroelectric ceramic (phase 1) in parallel with a compliant polymer (phase 2).

If 90% of the composite volume is polymer, then the volume fraction of the ferroceramic is 0.1, and the piezoelectric voltage coefficient is 10 times larger than the voltage coefficient of the ceramic alone. Excellent designs for hydrophones—instruments that direct and register the distance and direction of sound in water—are obtained in this way (*9*).

The advantages of internal stress transfer also can be used in pyroelectric coefficients. If the two phases have different thermal expansion coefficients, there is a stress transfer between the phases, which generates the electric polarization through the piezoelectric effect. In this way it is possible to make a composite pyroelectric in which neither phase is pyroelectric (*8*).

Electric field concentration

The multilayer design used for ceramic capacitors is effective for concentrating electric fields. By interleaving metal electrodes and ceramic dielectrics, relatively modest voltages can produce highly electric fields.

Multilayer piezoelectric transducers are made in the same way that multilayer capacitors are (*11*). Oxide powder is mixed with an organic binder and tape cast by spreading it with a blade on a surface. After the material dries, the tape is stripped from the substrate and electrodes are applied with a screen printer and electrode ink. The pieces of tape are then stacked, pressed, and fired to produce a ceramic that has internal electrodes. After leads are attached, the multilayer transducer is packaged and poled.

When compared with a simple piezoelectric transducer, the multilayer transducer offers a number of advantages:

- The internal electrodes make it possible to generate larger fields for smaller voltages, eliminating the need for transformers for high-power transmitters. A 10-V difference across a tape-cast layer 100 μm thick produces an electric field of 10^5 V/m, not far from the depoling field of PZT.
- The inherent higher capacitance of multilayer design also may help in impedance matching.
- Many electrode designs can be used to shape poling patterns, which in turn control the mode of vibration and ultrasonic beam patterns.
- Additional design flexibility is possible by interleaving layers of different composition. Ferroelectric and antiferroelectric layers can be alternated, thereby increasing the depoling field.
- Grain-oriented piezoelectric ceramics also can be tape cast into multilayer transducers. This enhances piezoelectric properties by aligning the crystallites parallel to internal electrodes (*12*).

- Arrangement of thin dielectric layers in a multilayer transducer provides improved strength against electric breakdown. Gerson and Marshal measured the breakdown strength of PZT as a function of specimen thickness (*13*). The d.c. breakdown field for 1-cm-thick ceramics was less then half that of 1-mm-thick samples. It is likely that this extends to even thinner specimens and leads to improved poling and more flexible transducers.

Perhaps an even more important factor is the enhancement of electrostrictive efforts. Electrostriction is a second-order electromechanical coupling of strain and electronic field. For small fields, electrostrictive strains are small compared with piezoelectric strain, but this is not true for the high fields generated in multilayer transducers.

Multilayer electrostrictive transducers made from ferroelectrics, such as lead magnesium niobate (PMN) (*14*), can generate strains larger than those of PZT (Figure 11). Moreover, poling is not required, and there are no aging effects. The concentration of electric fields makes nonlinear effects increasingly important.

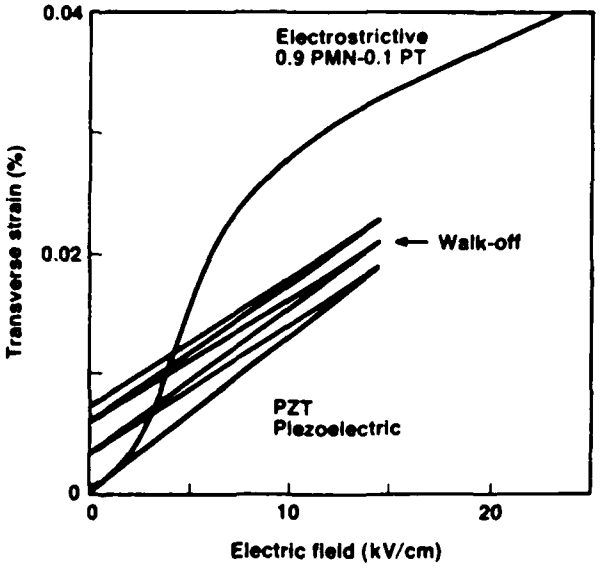

Figure 11. **Comparison of electrostrictive and piezoelectric micropositioners. PMN is lead magnesium niobate, PT is lead titanate, and PZT is lead zirconium titanate. Although it does not show a linear response to an electric field, a PMN-PT mixture generates more strain than does PZT. PZT also shows a shift in its strain response when the electric field strength returns to zero.**

Multilayer thermistors

For many applications it is desirable to lower room temperature resistance because thermistor elements often are connected in series with the circuit elements they are designed to protect. It is possible to lower the resistivity of the composite by altering the components, but the resistivity cannot be lowered indefinitely without degrading the effect of a thermistor when its resistance is increased suddenly at high temperatures; that is, when it has a positive temperature coefficient (PTC).

Placing internal electrodes in a thermistor reduces the resistance per unit volume without affecting temperature characteristics. Thermistor devices are being fabricated as ceramic disks or as composite wafers. We recently developed a way to make multilayer $BaTiO_3$ PTC thermistors with greatly lowered room temperature resistance (*15*). $BaTiO_3$ powder doped with rare-earth ions is mixed with an organic binder and tape cast on glass slides. Electrodes are then screen-printed on the tapes, which are stacked, pressed, and fired. The internal electrode configuration is similar to that of a multilayer capacitor.

The basic idea involves comparison of a single-layer disk thermistor with a multilayer thermistor of the same external dimensions. The multilayer device is assumed to have n ceramic layers and $n + 1$ electrodes. A represents the area of the single-layer thermistor, t is its thickness, and ρ is the resistivity. The resistance of the disk thermistor is

$$R_s = \rho t/A$$

For the multilayer thermistor, the area of the electrodes is nA (without margins) and the thickness is t/n (neglecting the electrode thickness). The resistance of the multilayer device is

$$R_M = \rho(t/n)/nA = R_s/n^2$$

The resistivity of the thermistor is lowered by a factor of $1/n^2$ with $n - 1$ internal electrodes.

We have demonstrated the feasibility of this idea with a multilayer device that contains four tape-cast layers. As predicted, the resistance of the multilayer specimen is about $n^2 (= 16)$ times smaller, with very little change in the temperature characteristic.

Summary

We've reviewed some of the basic ideas underlying composite electroceramics.

Sum properties involve the averaging of similar properties in the component phases, with the composite values that lie between those for series and parallel models. A simple sum property is the dielectric constant: The constant of the composite lies between those of the individual phases. This is not true for combination properties based on two or more properties. Acoustic velocity depends on stiffness and density, and because the mixing rules for these two properties are often different, the acoustic velocity of a composite can be smaller than those of its constituent phases.

Product properties are even more complex than sum properties are because three properties are involved: Different properties in the constituent combine to yield a third property in the composite. In a magnetoelectric composite, the piezoelectric effect in $BaTiO_3$ acts on the magnetostrictive effect of cobalt ferrite to produce a composite magnetoelectric effect.

Connectivity patterns are an important feature of

composite electroceramics. The self-connectivity of the phases determines whether series or parallel models apply and thereby minimizes or maximizes the properties of the composite. The three-dimensional nature of the connectivity patterns makes it possible to minimize some tensor components while maximizing others.

Concentrated field and force patterns are possible with carefully selected connectivities. Using internal electrodes, electrostrictive ceramics can produce strains comparable with those of the best piezoelectric materials. Stress concentration is achieved by combining stiff and compliant phases in parallel. Several hydrophone designs are based on this principle.

Periodicity and scale are important factors when composites are to be used at the high frequencies that produce resonance and interference. When wavelengths are on the same scale as the component dimension, the composite no longer behaves as a uniform solid. The colorful interference phenomena observed in opal and feldspar minerals are interesting examples of natural composites. Acoustic analogues occur in the PZT–polymer composites that are used as biomedical transducers.

Symmetry governs the physical properties of composites just as it does in single crystals. The Curie principle of symmetry superposition and Neumann's law can be generalized to cover fine scale composites, thereby elucidating the nature of their tensor properties. As in the case of magnetoelectric composites, sometimes a composite belongs to a symmetry group that is lower than any of its constituent phases. Unexpected product properties occur in this case.

Interfacial effects can lead to interesting barrier phenomena in composites. $ZnO–Bi_2O_3$ varistors and carbon–polymer PTC thermistors are important examples of barrier effects. Barrier layer capacitors made from conducting grains separated by thin insulating grain boundaries are another example.

Polychromatic percolation is an interesting concept that has yet to be fully explored. Composites fabricated from two or more conducting phases can have several kinds of transport paths, both single-phase and mixed, depending on percolation limits and volume fractions. Carbon–PZT–polymer composites can be poled because polychromatic percolation established flux continuity through ferroelectric grains. The SiC–BeO composites under development as substrate ceramics are another example. These diphasic ceramics are simultaneously excellent thermal conductors and poor electrical conductors. A thin layer of BeO-rich carbide separates the SiC grains, insulating them from one another electrically but providing a good acoustic impedance match, which ensures phonon conduction.

Coupled-phase transformations in polyphasic solids introduce additional possibilities. Recently discovered NTC–PTC composites made from V_2O_3 powder and embedded in polyethylene combine matrix and filler materials with complementary properties. At low temperatures the V_2O_3 particles are in a semiconducting state and in intimate contact with one another. On passing through a semiconductor–metal transition, the electrical conductivity increases by five orders of magnitude. Further heating rapidly expands the polymer, which pulls the V_2O_3 particles apart. As a consequence, the electrical conductivity decreases by eight orders of magnitude. In addition to this "window material" with a controlled conductivity range, several other composites are subject to coupled-phase transformation.

Porosity and inner surfaces play special roles in many electroceramic composites used as sensors. Humidity sensors made from Al_2O_3 and LiF have high inner surface area because of thermally induced fractures. The high surface area and hygroscopic nature of the salt result in the excellent moisture sensitivity of the electrical resistance. Chemical sensors based on similar principles can be constructed in the same way.

References

(1) Nye, J. F. *Physical Properties of Crystals;* Oxford University: Oxford, England, 1957.
(2) Shubnikov, A. V.; Koptsik, V. A. *Symmetry in Science and Art;* Plenum: New York, 1974.
(3) Gebhardt, J. J. ACS Symposium Series 21; American Chemical Society: Washington, D.C., 1976, w976, p. 212.
(4) Lachman, I. M.; Bagley, R. D.; Lewis, R. M. *Bull. Am. Ceram. Soc.* **1981**, *60*, 202.
(5) Shrout, T. R., et al. *Mater. Res. Bull.* **1980**, *15*, 1371.
(6) Safari, A.; Halliyal, A.; Newnham, R. E.; Lachman, I. M. *Mater. Res. Bull.* **1982**, *17*, 302.
(7) Halliyal, A., et al. *Mater. Res. Bull.* **1983**, *18*, 1007.
(8) Newnham, R. E.; Skinner, D. P.; Cross, L. E. *Mater. Res. Bull.* **1978**, *13*, 535.
(9) Newnham, R. E., et al. *Mater. Eng.* **1980**, *II*, 93.
(10) White, R. A.; Weber, J. N.; White, E. W. *Science* **1972**, *176*, 922.
(11) Dayton, G. O.; Schulze, W. A.; Shrout, R. T.; Swartz, S.; Biggers, J. V. *Adv. Ceram.* **1984**, *9*, 115.
(12) Granahan, M.; Holmes, M.; Schulze, W. A.; Newnham, R. E. *J. Am. Ceram. Soc.* **1981**, *64*, C68.
(13) Gerson, R.; Marshal, T. C. *J. Appl. Phys.* **1959**, *30*, 1650.
(14) Uchino, K.; Nomura, S.; Cross, L. E.; Newnham, R. E.; Jang, S. J. *J. Mater. Sci.* **1981**, *16*, 569.
(15) Hiremath, B. V., Hu, K. A.; Newnham, R. E., in preparation.

Robert E. Newnham works and teaches at the Materials Research Laboratory at Pennsylvania State University (University Park, Pa. 16802; 814-865-1451). He uses his background in mathematics, physics, and mineralogy (Ph.D., Pennsylvania State University) and crystallography (Ph.D., Cambridge University) to design composite transducers, sensors, and actuators. A recipient of the Wilson Prize for Outstanding Teaching, he is an active member of the American Ceramics Society, the American Physical Society, and the Mineralogical Society of America.

Ferroelectrics, 1987, Vol. 73, pp. 405–417
Photocopying permitted by license only

(Pb, Bi)(Ti, Fe, Mn)O_3/POLYMER 0–3 COMPOSITES FOR HYDROPHONE APPLICATIONS

J. R. GINIEWICZ, R. E. NEWNHAM, A. SAFARI and DAWNE MOFFATT

Materials Research Laboratory, The Pennsylvania State University, University Park, PA 16802

(Received 3 July 1986)

The hydrostatic piezoelectric response of composite materials incorporating $(Pb_{1-x}Bi_x)(Ti_{1-x}Fe_x)O_3$ ceramic fillers from the highly anisotropic tetragonal region of the solid solution system in the vicinity of the morphotropic phase boundary were measured and compared. The considerable difficulty in poling and, hence, the diminished piezoelectric response encountered as the composition of the filler is shifted closer to the phase boundary was determined to be largely due to the high conductivity of the $BiFeO_3$-rich compositions. The ceramic was modified with Mn in an attempt to lower its conductivity. Composites incorporating the Mn-doped filler poled more rapidly and easily than the undoped material and ultimately achieved a hydrostatic figure of merit, $d_h g_h$, 40% better than that observed for the undoped samples. Among the samples investigated, the highest hydrostatic figures of merit were exhibited by samples containing the doped and undoped $x = 0.5$ fillers. The hydrostatic response remains stable over a broad pressure range.

INTRODUCTION

The development of new polymeric materials, that has occurred in the past few decades, has spurred a growing interest in composite material design for the optimization of a variety of physical properties. Among the composite materials most actively investigated at present are those classified as electronic composites. Multilayer dielectric materials and piezoelectric ceramic/polymer composites are of particular importance as technological and industrial advances demand more versatile and responsive sensors and actuators.

This investigation deals primarily with 0–3 piezoceramic/polymer designs or materials which consist of a three-dimensionally connected polymer matrix within which the ceramic phase is dispersed as discrete particles. Piezoceramic/polymer composite materials have been found to exhibit piezoelectric properties superior to those exhibited by homogeneous piezoelectric materials.[1-3] The piezoceramic and polymer components of the composite materials may be arranged in a variety of configurations thereby optimizing overall piezoelectric performance.[4] In addition, certain features such as elastic compliance and low density make these materials attractive candidates for versatile pressure sensitive devices. 0–3 materials are among the simplest of all the composite designs where the ceramic component is embedded in a polymer matrix as a particulate suspension. Although less responsive overall than its more elaborately configured relatives, this material has certain distinctly advantageous features.

Perhaps one of the most attractive features of the 0–3 design is its versatility in assuming a variety of forms including thin sheets, extruded bars and fibers, and

certain molded shapes. This investigation explores the preparation and hydrostatic piezoelectric performance of the material in the form of sheets prepared by a conventional polymer compounding and forming technique incorporating undoped and Mn-doped fillers from the highly anisotropic phase boundary compositions of the $PbTiO_3$–$BiFeO_3$ solid solution system. The flexible nature of the sheet design makes it a viable candidate for a variety of applications. Piezoelectric sheets are suitable materials for pressure sensitive devices which require a material that is able to conform to the contours of various surfaces. Such devices as pressure sensitive keyboards, transducing gloves and blood pressure gauges are a few products currently produced from piezoelectric sheet composites.[5,6]

HYDROPHONE MATERIALS: AN OVERVIEW

A number of poled ceramic materials, such as $Pb(Zr, Ti)O_3$, (PZT),[7] and certain piezoelectric polymers, such as polyvinylidenefluoride, (PVDF),[8] exhibit a piezoelectric response when subjected to a hydrostatic pressure. Such materials are well-suited for transducer applications, in particular for those devices employed as underwater pressure sensors, hydrophones. Three of the most important properties required of a good transducer are: (1) voltage sensitivity or the material's ability to convert the applied pressure to an electrical signal, (2) low density to enable adequate impedance coupling between the device and the transmitting medium and (3) compliance for enhanced durability and conformability, and reduced "ringing" or echo effects within the device. The conventional figure of merit focuses on the sensitivity of the material and is expressed in terms of the hydrostatic piezoelectric strain coefficient, d_h, the hydrostatic piezoelectric voltage coefficient, g_h, and the dielectric constant, K_{33}, as

$$d_h g_h = (d_{33} + 2d_{31})^2/\varepsilon_0 K_{33}$$

where ε_0 is the permittivity of free space. The leading piezoelectric ceramic material, PZT, exhibits only a modest hydrostatic response due to a relatively large negative d_{31} coefficient (-175 pC/N) with respect to its d_{33} coefficient (400 pC/N). The hydrostatic performance of the leading piezoelectric polymer, PVDF, is also limited by a similar inhibition of d_h and a relatively low melting temperature.

Piezoceramic/polymer composites are a class of materials that effectively overcome these limitations and hence are found to be more responsive and versatile transducer devices.[1-3] The composite constituents provide complementary properties which, when combined, produce a superior hydrostatic piezoelectric material. The polymer phase lowers the density of the material providing better acoustic coupling to water than that obtained for a high density homogeneous ceramic. The low dielectric constant of the polymer phase effectively increases the g_h coefficient and the figure of merit. Finally, the piezoelectric properties of the ceramic are easily adjusted within the composite whose constituent phases may be suitably arranged to effectively distribute the applied stress in a manner that encourages the maximum piezoelectric response.[4]

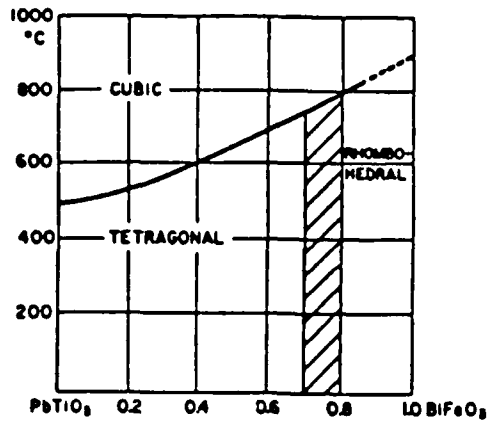

FIGURE 1 $PbTiO_3$–$BiFeO_3$ structural phase diagram.[10]

THE $PbTiO_3$–$BiFeO_3$ SYSTEM

The $(Pb_{1-x}Bi_x)(Ti_{1-x}Fe_x)O_3$ solid solution system is of particular interest for its promising piezoelectric properties. The system possesses a morphotropic phase boundary ($0.7 < x < 0.8$) between a tetragonal ($0.0 \leq x \leq 0.7$) and rhombohedral ($0.8 \leq x \leq 1.0$) modification of the perovskite structure (Figure 1) very much analogous to that observed for $PbTiO_3$–$PbZrO_3$.[9-10] The $PbTiO_3$–$BiFeO_3$ system is distinctive, however, for the extremely large structural anisotropy attained for compositions in the tetragonal region.[10] This considerable distortion gives rise to a potential for highly anisotropic piezoelectrics from the composition range near or on the morphotropic phase boundary. Unfortunately, as is the case for $PbTiO_3$, it is this very feature which, on the one hand, makes possible an outstanding piezoelectric response, also deters the production of strong, dense ceramics. Samples prepared in the tetragonal range generally fracture upon cooling through the transition temperature, T_c, with the degree of specimen disruption increasing as the composition approaches the phase boundary.

The variation of the lattice parameters with compopsition is shown in Figure 2a. The tetragonal lattice parameters c and a are found to vary quite considerably as the composition approaches the phase boundary. The magnitude of c increases dramatically from 4.40 A for $x = 0.5$ to 4.53 A at $x = 0.7$ while a decreases in a more gradual manner from 3.85 A for $x = 0.5$ to 3.81 A at the phase boundary. The c/a ratio is exceptionally high for all the compositions recorded attaining a maximum value of 1.19 at the morphotropic phase boundary (Figure 2b). This represents a strain of nearly 20% in materials prepared from this portion of the solid solution system where ceramic samples are rarely strong and generally fracture upon cooling through the transition temperature.

All modifications of the solid solution are ferroelectric. No reports appear in the literature, however, regarding the observation of a hysteresis loop for any composition, presumably because of a high coercive field and the low resistivity of the material. The variation of ferroelectric Curie point with composition as

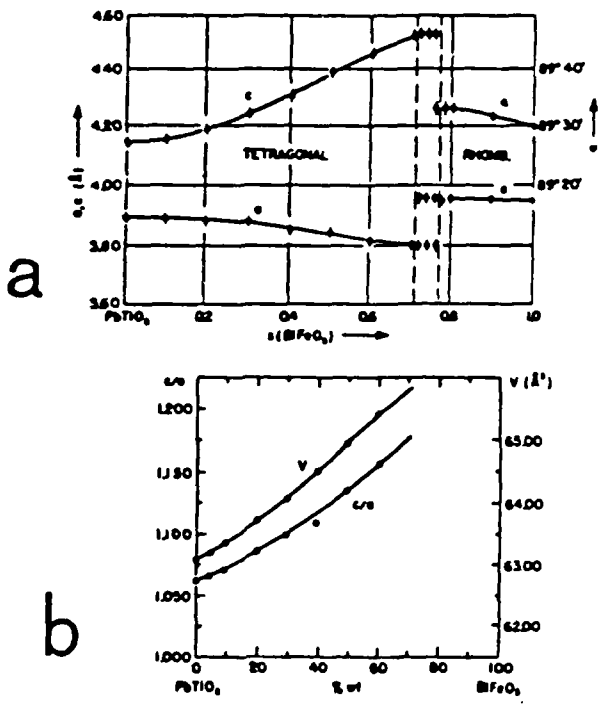

FIGURE 2 (a) Variation of the lattice parameters with composition, (b) variation of tetragonal c/a and volume with composition.[10]

depicted in Figure 1 is seen to increase in a nearly linear fashion from 490°C for $PbTiO_3$ to 850°C for $BiFeO_3$.

The Curie point dielectric constant is depicted in Figure 3a as a function of composition measured at 25°C and a frequency of 530 MHz. Its value is observed to decrease with increasing $BiFeO_3$ content.[11] The dissipation factor is plotted as a function of temperature for selected compositions in Figure 3b. The losses generally increase with increasing $BiFeO_3$ content and are likely due to to a substantial *n*-type conductivity associated with the ferrite.[11] A complex variation of conductivity with composition has been reported and has been attributed to the relative contributions of several possible conductivity mechanisms operating across the composition range.[10] The greatest contributors to the conductivity for compositions with a high $BiFeO_3$-content are likely to be the Fe^{2+} ions present with the Fe^{3+} ions on the B-sites of the perovskite lattice which are oxidized via the reaction $Fe^{2+} \rightarrow Fe^{3+} + e^-$ thereby liberating electrons to the system.[12-14] Where $PbTiO_3$ and $BiFeO_3$ are both semiconductors it can be assumed that the high losses at elevated temperatures are primarily conductive.[11]

OBJECTIVES OF THE INVESTIGATION

The prime objective of this investigation was to produce easily fabricated, thin, responsive piezoelectric sheets for hydrophone applications. The

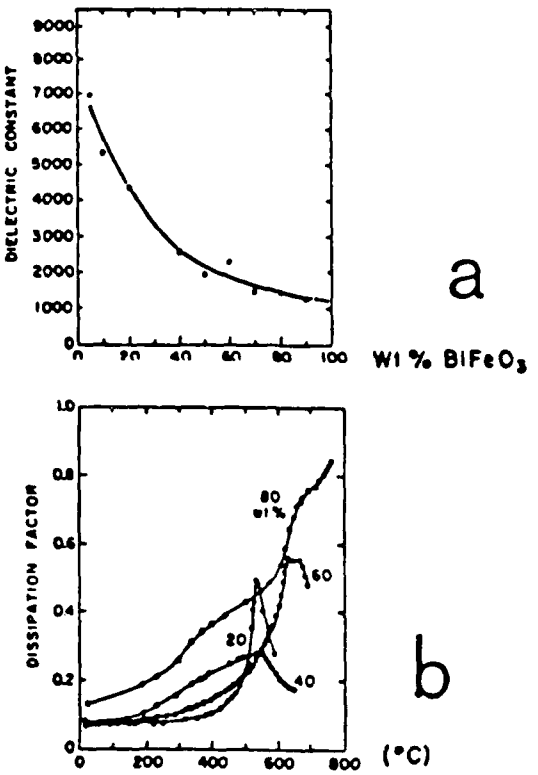

FIGURE 3 (a) Curie point dielectric constant as a function of composition (25°C, 530 MHz), (b) dissipation factor as a function of temperature (530 MHz).[11]

(Pb, Bi)(Fe, Ti)O_3/polymer 0–3 composites satisfy all the desired requirements of a good hydrophone material. The high anisotropy of $(Pb_{1-x}Bi_x)(Ti_{1-x}(Fe, Mn)_x)O_3$ compositions in the range $x = 0.5$–0.7 permits considerable hydrostatic sensitivity. 0–3 composites incorporating this filler are, therefore, more responsive than 0–3 designs currently produced containing $PbTiO_3$ or PZT. In addition, very thin sheets of the material may be produced due to the fine particle sizes obtained by quenching the filler powders. The high strain present in ceramics prepared in the $x = 0.5$–0.7 composition range allows for the production of fine particles on quenching with minimal damage to individual crystallites. Sheets made with single crystallites created in this way are found to more easily poled and to have an enhanced piezoelectric response over composites made with fine particles produced by grinding.

Little has been reported in the literature regarding the piezoelectric properties of materials produced from the $PbTiO_3$–$BiFeO_3$ system. Most studies on the system have been conducted mainly to better determine the nature of $BiFeO_3$ which is difficult to characterize alone. Further, any investigation of the piezoelectric character is restricted by the brittle nature and high conductivity of

the material, especially in the prime area of interest near the morphotropic phase boundary. The aim of this investigation was to examine the hydrostatic piezoelectric nature of the binary system as the filler component of a 0–3 composite. The one problem of brittle fracture is resolved and, in fact, exploited in this way. The difficulties related to the high conductivity are alleviated by modifying the filler compositions with small concentrations of a Mn-dopant. It has already been pointed out that the greatest contributors to the conductivity for composition with x greater than 0.5 are most likely to be the Fe^{2+} ions present with the Fe^{3+} ions on the B-sites of the perovskite lattice which are oxidized via the reaction $Fe^{2+} \rightarrow Fe^{3+} + e^-$ thereby liberating electrons to the system. The Mn dopant is added in an attempt to counter this electron liberating oxidation by oxidizing the ferrous ions via the reaction: $Mn^{3+} + Fe^{2+} \rightarrow Fe^{3+} + Mn^{2+}$ thereby lowering the conductivity of the ceramic. The hydrostatic piezoelectric performance of composite samples incorporating both the undoped and Mn-doped filler are examined and compared.

PREPARATION OF THE CERAMIC

The $(Pb_{1-x}Bi_x)(Ti_{1-x}(Fe_{1-y}Mn_y)_x)O_3$ powders were prepared by a conventional double-firing process. Green mixtures were batched with compositions in the range $x = 0.5$–0.7 and $y = 0.0$ and 0.02 from the oxides PbO, TiO_2, Bi_2O_3, Fe_2O_3, and MnO_2. The green powders were contained in covered alumina crucibles and subjected to a primary low-temperature firing in air at 800°C for 1.5 hours. The calcined powders were loosely compacted, placed in covered alumina crucibles and subjected to a second firing at 1000°C for 1.5 hours. The pellets were quenched to room temperature directly following the soak period. The quenched samples generally fractured completely upon quenching and required only the slightest grinding with mortar and pestle to break up agglomerates.

The intergranular nature of the fracture and particle morphology are apparent in scanning electron micrographs of powders representing any of the tetragonal compositions investigated. Disruption of the microstructure is observed to occur entirely at the grain boundaries. No fractured particles are observed. Particles produced for all tetragonal compositions are generally discrete, approximately spherical crystallites.

The particle size distribution curves for samples prepared from each composition were determined by means of a Sedigraph 5000D Particle Size Analyser (Figure 4). Samples prepared closer to the phase boundary produced the narrowest distributions with the smallest mean particle size reflecting a more thorough disruption of the microstructure as the strain in the system increases. The mean particle size range is 5–10 μm for compositions $x = 0.5$–0.7 where the finest particles are produced for powders with composition $x = 0.7$.

PREPARATION OF THE COMPOSITE

Composite samples were prepared containing 50–60 volume percent (Pb, Bi)(Ti, Fe)O_3 filler and 40–50 volume percent polymer from the epoxy-based

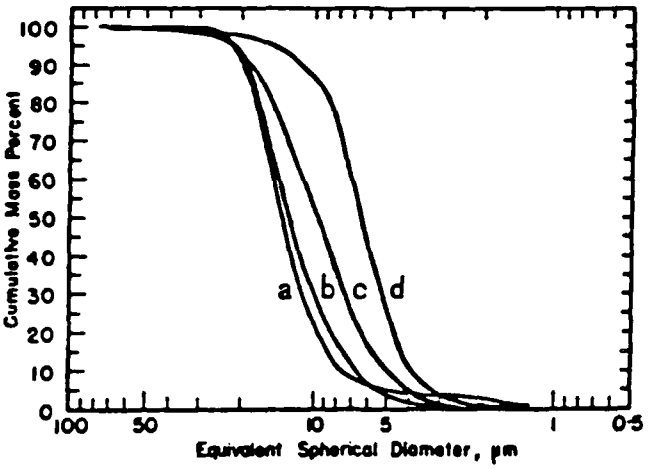

FIGURE 4 Sedigraph particlfie size distribution curves for selected tetragonal compositions. (All samples fired and quenched at 1000°C with a soak period of 1.5 hours—(a) $x = 0.5$, (b) $x = 0.6$, (c) $x = 0.65$, (d) $x = 0.7$).

Eccogel series (Eccogel-Series 1365 # 25—Emerson and Cuming, Dewey and Almy, Chemical Division, Canton, Ma.). The filler was initially blended with the liquid components of the Eccogel system and compounded by a high-shear hand-mixing technique. The mixture was then formed into a sheet by hot-rolling at a temperature in the range 40–60°C. The formed sheets were initially cured under a low pressure applied by means of a hydraulic press at 90°C for 2.0 hrs and then post-cured for an additional 3.0–4.0 hours at 70°C.

The cured composite sheets were polished with a fine silicon carbide emery paper to smooth out rough or pitted areas on the surfaces. The sheet was then cut into rectangular sections measuring approximately 0.5–1.0 cm^2. The sheet was sectioned in this manner to better evaluate homogeneity. In addition, poling of the material was more easily accomplished on small, thin sections than on larger sheets. The rectangular sections were subsequently polished to a uniform thickness of approximately 0.2–0.5 mm and dried in a 70°C furnace for 2.0–3.0 hours. The polished sections were electroded with an air-dry silver paint for poling and for dielectric and piezoelectric testing.

PIEZOELECTRIC AND DIELECTRIC MEASUREMENT

Two series of samples were prepared for dielectric and piezoelectric testing. The samples constituting these series are listed in Table I. The series were selected to investigate both the effects of filler composition and Mn doping of the filler on the degree of poling achieved and, hence, on the hydrostatic piezoelectric response. The first series was examined in order to monitor the change in piezoelectric response with increasing $BiFeO_3$-content for tetragonal compositions in the vicinity of the morphotropic phase boundary. The samples constituting the second series were prepared incorporating both undoped and Mn-doped $(Pb_{0.5}Bi_{0.5})(Ti_{0.5}Fe_{0.5})O_3$ fillers. Mn ions substituted for 2% of the Fe^{3+} ions in

TABLE I

Poling fields, poling periods, and d_{33} coefficients for Series I and II samples

	x	y	Practical E (KV/cm)	Period (min.)	d_{33} (pc/N)
Series I					
501	0.50	0.00	110	30	45
651	0.65	0.00	100	15	23
701	0.70	0.00	100	10	16
Series II					
501	0.50	0.00	110	30	45
501M	0.50	0.02	100	15	55

the doped samples. The purpose of this second series was to investigate the effects of Mn-doping on the polarization and ultimate piezoelectric performance of composites incorporating this filler. Investigation of the dielectric and piezoelectric properties included: (a) determination of the optimum poling conditions for each sample, (b) determination of the nature and degree of poling achieved as evidenced by the magnitude of the longitudinal strain coefficient, d_{33}, and the inversion of the $00l/h00$ x-ray diffraction peaks of the filler, (c) measurement of low frequency (KHz) dielectric constant and dissipation factor, both before and after poling, and, finally, (d) measurement of the hydrostatic piezoelectric coefficients, d_h and g_h.

Poling the Composites

The optimum poling temperature, poling field, and time are determined primarily by the relative dielectric constants and conductivities of the composite components, the polymer melting temperature, and the composite integrity. The relative dielectric constants and conductivities of the two components, in particular, affect, to a considerable extent, the degree of poling achieved.[3]

The electric field acting on the piezoelectric element within an insulating 0–3 composite will be similar to the applied field only if the dielectric constants of the components are nearly equivalent. This is generally not the case, however, for ceramic/polymer systems where the difference in dielectric constant may be one or two orders of magnitude. The local field acting on the ceramic particles, therefore, will only be about 5% of the applied field strength.

The relationship between the electric fields acting upon each component and their respective conductivities, where the *dc* poling field is applied for a period longer than the relaxation time, is defined by the Maxwell–Wagner model[15] as

$$E_{(1)}/E_{(2)} = \sigma_{(2)}/\sigma_{(1)} = \rho_{(1)}/\rho_{(2)}$$

where the subscripts 1 and 2 refer to the ceramic and polymer phases respectively. The magnitude of the electric field acting on the ceramic, $E_{(1)}$, is

optimized, therefore, by allowing for the highest possible conductivity ratio. In most cases, where the conductivity of the ceramic is particularly high, only a very small fraction of the poling field will act on the piezoelectric filler.

The considerable differences in dielectric constant and conductivity between the two components of the composite system establishes the need for a poling field of at least 75 KV/cm to produce any significant polarization of the material. The relatively low melting temperature of the Eccogel matrix sets the upper limit for the poling temperature. The optimum poling temperature of 75°C was established on the basis of a general survey made for representative samples selected from the two series and applied for the poling of all the samples investigated.

Optimum poling fields and times were similarly determined by systematically varying the parameters and monitoring the degree of poling achieved and the incidence of breakdown. The results of this study are presented in Table I. The practical poling field established represents that field strength at which the highest degree of poling is achieved with minimum breakdown. The poling time corresponds to that period required to achieve maximum poling under the influence of the practical field. The magnitudes of the longitudinal strain coefficient, d_{33}, exhibited by samples poled under these conditions are listed for each specimen as an indicator of the degree of poling attained. The d_{33} value recorded is an average of those sections from the original composite sheet that achieved a maximum degree of poling with a deviation ±5 pC/N. d_{33} measurements were made on a Berlincourt d_{33} meter (Model CPDT 3300—Chanel Products, Inc., Ohio).

Series I samples were found to be increasingly resistant to poling as the filler composition approached the morphotropic phase boundary. The maximum degree of poling as indicated by the longitudinal strain coefficient, d_{33}, was consequently observed to decrease significantly as the composition became increasingly rich in $BiFeO_3$. Mn-doping of the filler was found to significantly enhance the poling of the 50I composite material as indicated by the d_{33} coefficients recorded for Series II samples in Table I. Samples doped with 2 mol% Mn were observed to achieve maximum poling in half the time required to pole an undoped sample at similar field strengths.

The intensity ratios of the $00l/h00$ x-ray diffraction peaks from samples constituting Series II were monitored both before and after poling in order to detect the possible contribution of 90° domain reorientation or the rotation of single domain crystallites to the ultimate degree of poling attained for the composite. The $00l/h00$ peaks for both poled and unpoled samples from this series are depicted in Figures 5a and 5b. Both the 50I and 50IM samples exhibited similar inversions after poling with about a 10% increase in the intensity of the $00l$ peaks. Unlike the rigid environment of a solid ceramic or a stiffer polymer matrix, the compliant Eccogel Polymer used for this composite system is apparently better able to accommodate the distortion of the ceramic particles that accompanies 90° domain wall motion or the rotation of single domain crystallites. The 10% inversion indicates that complete poling has not been fully realized and, hence, that optimum poling of the (Pb, Bi)(Ti, Fe)O_3/polymer system is likely to be significantly greater than what has been observed in this investigation.

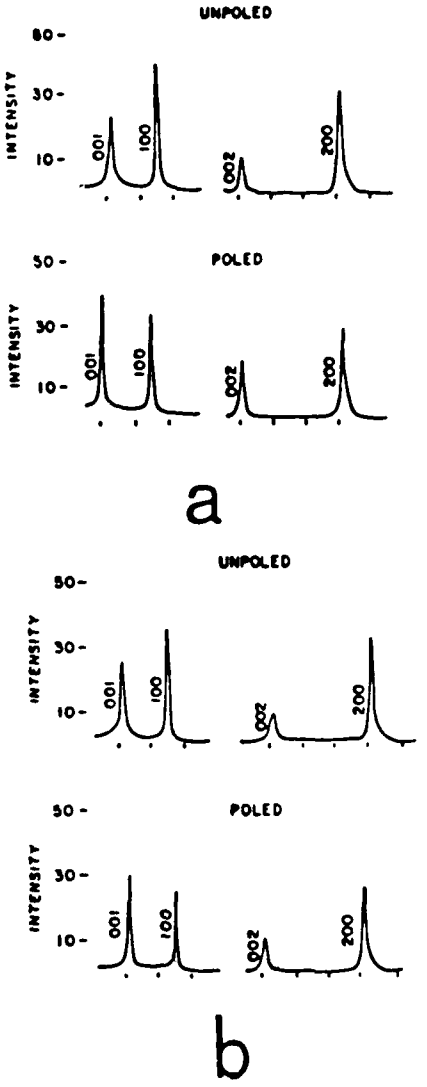

FIGURE 5 001/h00 x-ray diffraction peaks (a) Sample 50I (b) Sample 50IM.

Dielectric Data

Dielectric constant and dissipation factor were recorded for each sample both before and after poling. The dielectric constant was calculated in terms of the sample dimensions and capacitance. Capacitance and dissipation measurements were made at 1 KHz on a Hewlett–Packard 4270A automatic capacitance bridge. The data appear in Table II. The values represent an average of measurements made for several specimens taken from a particular composite sheet with a

TABLE II

Dielectric and piezoelectric data for Series I and Series II composite samples

	K		D		d_h	g_h	$d_h g_h$
	Before	After	Before	After	(pC/W)	(mVm/N)	(fm^2/N)
Series I							
501	45	40	0.13	0.09	25	65	1625
651	55	50	0.17	0.10	15	30	450
701	45	45	0.12	0.08	5	15	75
Series II							
501	45	40	0.13	0.09	25	65	1625
501M	45	40	0.12	0.05	30	90	2700

deviation of ±5 and ±0.01 for dielectric constant and dissipation factor respectively.

The dielectric constant and dissipation factor for each sample both before and after poling were found to be similar in magnitude. The dielectric constant was observed to decrease somewhat for those samples that were sufficiently poled. This reflects the reorientation of the K_{33} within the piezoelectric filler where the alignment in the poling direction will be manifested by a decrease in the dielectric constant of the composite. Dissipation factors were typically about 10% for all samples with a slight decrease after poling.

Hydrostatic Piezoelectric Data

Hydrostatic piezoelectric measurement was made by a dynamic technique[16] by which means the voltage coefficient, g_h, was evaluated and the strain coefficient, d_h subsequently derived. Hydrostatic data are recorded in Table II. The values of the coefficients recorded are averages of those measured on the portions of the composite sheets that achieved a maximum degree of poling. The deviation of d_h and g_h are ±5 (pC/N) and ±10 (mV-m/N) respectively for the 50I and 50IM samples and, of those specimens representing the 65I and 70I samples, the deviations are less than ±5 (pC/N) and ±5 (mV-m/N) respectively. Hydrostatic measurements were taken as a function of pressure on a sample representative of the undoped filler composition $x = 0.5$. The results of that investigation are shown in Figure 6.

The increased inhibition to poling of the Series I samples as the composition approches the morphotropic phase boundary is reflected in the steady decrease of the hydrostatic response from a figure of merit of nearly 2000 (fm^2/N) for the 50I sample to barely 100 (fm^2/N) for sample 70I. The hydrostatic response of the Mn-doped sample, 50IM, as represented by the hydrostatic figure of merit, $d_h g_h$, is found to increase approximately 40% over that exhibited by the undoped sample, 50I, again reflecting the enhanced poling of samples prepared with the Mn-dopant. In addition, the response is observed to be highly stable over a broad pressure range. The hydrostatic performance exhibited by the Series II samples, in particular, the exceptionally high voltage sensitivity and pressure stability, establishes, therefore, this material's merit as an effective and reliable hydrostatic pressure sensor.

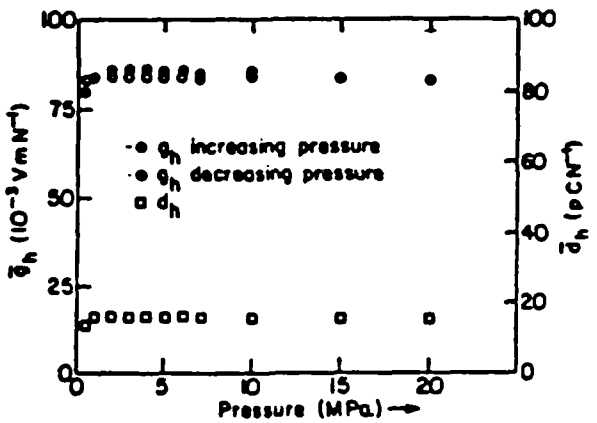

FIGURE 6 Hydrostatic piezoelectric coefficients as a function of pressure (Measurements made at the facilities of the Underwater Sound and Reference Division of the Navy, Orlando, FL).

SUMMARY

A prototype 0–3 sheet design was developed composed of a (Pb, Bi)(Ti, (Fe, Mn))O_3 filler and an epoxy (Eccogel) matrix. The hydrostatic piezoelectric responses of composite materials representing $(Pb_{1-x}Bi_x)(Ti_{1-x}Fe_x)O_3$ compositions from the highly anisotropic tetragonal region in the vicinity of the morphotropic phase boundary were measured and compared.

Samples incorporating filler compositions in the range $x = 0.5$–0.7 (Series I) poled with an applied field of about 100 KV/cm in oil at 75°C exhibited an increased resistance to poling as the filler composition approached the phase boundary. This is reflected in the steady decrease of the hydrostatic response from a figure of merit of nearly 2000 (fm^2/N) for the sample representing $x = 0.5$ to barely 100 (fm^2/N) for that incorporating the phase boundary composition $x = 0.7$.

The high conductivity of samples prepared in the composition range investigated is most likely associated with the presence of Fe^{2+} ions on the B-site of the perovskite lattice which initiate the liberation of electrons via the reaction $Fe^{2+} \rightarrow Fe^{3+} + e^-$. The filler was modified by doping with Mn in an attempt to effectively counter this detrimental reaction by oxidizing the Fe^{2+} via the reaction $Fe^{2+} + Mn^{3+} \rightarrow Fe^{3+} + Mn^{2+}$ thereby reducing the conductivity of the filler.

The merit of the (Pb, Bi)(Ti, Fe, Mn)O_3/Eccogel 0–3 composite as a sensitive and stable hydrostatic piezoelectric transducer has been demonstrated by the hydrostatic performance of those samples containing the doped and undoped fillers (50I and 50IM). Composites incorporating the Mn-doped filler poled more rapidly and easily than the undoped material and ultimately achieved a hydrostatic piezoelectric figure of merit, $d_h g_h$, of 2700 (fm^2/N), a value approximately 40% better than that exhibited by the undoped sample of 1625 (fm^2/N). The (Pb, Bi)(Ti, (Fe, Mn))O_3/Eccogel composites containing the

$x = 0.5$ fillers were found to be superior to PZT, PVDF, and most of the $PbTiO_3$ and PZT composite sheet materials currently reported in the literature.[5-6] Further work is underway to optimize the filler composition, the composite preparation and the poling procedure. The results obtained in this study indicate that the composite system, prepared under these optimized conditions, should prove to be an exceptionally sensitive and stable hydrophone material.

ACKNOWLEDGEMENT

The authors are grateful for the financial support received from the Office of Naval Research and the Celanese Research Company.

REFERENCES

1. R. E. Newnham, L. J. Bowen, K. A. Klicker, and L. E. Cross, *Materials in Engineering*, **112**, 93 (1980).
2. R. E. Newnham, A. Safari, J. Giniewicz, and B. H. Fox, *Ferroelectrics*, **60**, 15 (1984).
3. R. E. Newnham, A. Safari, G. Sa-Gong, and J. Giniewicz, *Proceedings of IEEE Ultrasonic Symposium*, 501 (1984).
4. R. E. Newnham, D. P. Skinner, and L. E. Cross, *Materials Research Bulletin*, **13**, 525 (1978).
5. Hisao Banno and Shigeo Saito, *Japanese Journal of Applied Physics*, **22**, Supp. 22-2, 67 (1983).
6. Hisao Banno, *Ferroelectrics*, **5**, 3 (1983).
7. Bernard Jaffe, William R. Cook, Jr., and Hans Jaffe, Piezoelectric Ceramics, (Academic Press, London and New York, 1971).
8. H. Kawai, *Japanese Journal of Applied Physics*, **8**, 975 (1969).
9. S. A. Fedulov, P. B. Ladyshinski, I. L. Pyatigorskaya, and Yu. N. Venevtsev, *Soviet Physics-Solid State*, **6**, 375 (1964).
10. S. A. Fedulov, Yu. N. Venevtsev, G. S. Zhandov, E. G. Smazhevskaya, and I. S. Rez, *Soviet Physics—Crystallography*, **7**, 62 (1962).
11. R. T. Smith, G. D. Achenbach, R. Gerson, and W. J. James, *Journal of Applied Physics*, **39**, 70 (1968).
12. J. Smit and H. P. J. Wijn, Ferrites, (John Wiley and Sons, New York, 1959).
13. E. P. Wohlfarth, ed., Ferromagnetic Materials, vol. 2, (North Holland Publishing Co., New York, 1980).
14. R. F. Soohoo, Theory and Application of Ferrites, (Prentice-Hall, Inc., New Jersey, 1960).
15. A. R. Von Hippel, Dielectrics and Waves, (John Wiley and Sons, 1954).
16. J. R. Giniewicz, (Pb, Bi)(Ti, Fe)O_3/Polymer 0-3 Composite Materials for Hydrophone Applications, M.S. Thesis, The Pennsylvania State UNiversity (1985).

In Memorium: Issai Lefkowitz

Life goes by too quickly. It was 25 years ago, but it seems like only yesterday that Lef and I met at the International Union of Crystallography meeting in Cambridge, England. Lef was enjoying a sabbatical at the Cavendish Laboratory working with Helen Megaw on the $NaNbO_3$ structures. I remember his happy smile and his enthusiastic approach to research; sometimes the words came so fast he seemed to bubble over with fun.

That enthusiasm never left him. At the Penn State IMF meeting in 1981, Lef was very sick, but he wasn't about to give up. He was full of optimism and talked about his latest copper chloride results with great feeling. That was Lef—an inspiration to us all—he showed us how to make the most out of life. He taught us how to live, and how to die.

Bob Newnham

Am Ceram Soc Bull., 66 [4] 668-70 (1987)

0-3 Piezoelectric Composites Prepared by Coprecipitated $PbTiO_3$ Powder

AHMAD SAFARI*
Rutgers University, Piscataway, NJ 08854

YOUNG H. LEE, ARVIND HALLIYAL,* and ROBERT E. NEWNHAM*
Pennsylvania State University, University Park, PA 16802

Pure lead titanate powder was prepared by a coprecipitation technique using $Pb(NO_3)_2$, $TiCl_4$, and NH_4OH as starting raw materials. The coprecipitated powder was calcined at 900°C to yield highly crystalline particles with a narrow particle size distribution. The 0-3 composites were prepared with this powder using a polymer. X-ray diffraction patterns taken on the surface of the composites before and after poling indicated that almost saturation poling was achieved at 100 kV/cm. The hydrostatic charge and voltage coefficients, d_h and g_h, were ≈ 45 (pCN^{-1}) and 95 ($10^{-3}VmN^{-1}$), respectively. The composites showed no aging effect.

Piezoelectric phenomenon exhibited by certain piezoelectric crystals, polarized polymers, and composites is used in a number of electromechanical transducers such as hydrophones, vibration sensors, and pressure and stress sensors. In hydrophone, the active sensing element is a solid piezoelectric ceramic material such as PZT. Piezoelectrically active ceramic components convert underwater sound pressure waves to electrical signals, which are then amplified and displayed. The sensitivity of a sound receiver material is characterized by a hydrophone figure-of-merit (FOM), commonly taken as the product of the hydrostatic piezoelectric charge (d_h) and voltage (g_h) coefficients.

During the past few years, piezoelectric ceramic-polymer composites with many different connectivity patterns have been designed and fabricated for improved hydrostatic pressure sensitivity.[1-3] Among the composites studied so far, the simplest types are those with 0-3 connectivity,[4] which consist of a three-dimensionally connected polymer matrix loaded with piezoelectrically active ceramic particles. One of the most attractive features of the 0-3 design is its versatility in assuming a variety of forms including thin sheets, extruded bars and fibers, and certain molded shapes. This type of composite is also easy to fabricate and amenable to mass production. By using the right kind of polymer, the composite can be made flexible to conform to curved surfaces.

Early attempts to fabricate flexible composites with piezoelectric ceramic particles were made by Kitayama and Sugawaru,[5] Pauer,[6] and Harrison.[7] These composites were prepared by embedding PZT particles, 5 to 10 μm in size, in a polymer matrix. An improved version of the 0-3 composite was fabricated by Banno and Saito.[8] Rather than using PZT as the ceramic filler, pure or modified $PbTiO_3$ was employed because of its greater piezoelectric anisotropy. The $PbTiO_3$ filler was prepared by water-quenching the ceramic, thereby exploiting the high strain present in the material to produce fine powders. The average particle size was ≈ 5 μm. The $PbTiO_3$ powder was mixed with chloroprene rubber, hot-rolled at 40°C into sheets 0.5-mm thick, and then pressed at 190°C for 20 min under 13 kg/cm^2 pressure. The composites were poled at 60°C in silicone oil with a field of 100 kV/cm for 1 h. The hydrostatic voltage coefficient, g_h, of these pure $PbTiO_3$ composites was found to be comparable to that of PVDF polymer ($100 \cdot 10^{-3}VmN^{-1}$), and the d_h value was ≈ 35 pCN^{-1}.

Recently the sol-gel process has been used to prepare $PbTiO_3$ powder for use in 0-3 composites.[9,10] The merits of sol-gel processing such as high purity, molecular homogeneity, and lower processing temperatures are obvious advantages over the conventional mixed-oxide processing method.[9] In this study $PbTiO_3$ powder was prepared by the coprecipitation method, and flexible 0-3 composites were prepared by incorporating the powder in a dielectric gel polymer.[9] Dielectric and piezoelectric properties of these composites are reported in this paper.

Powder Preparation

The $PbTiO_3$ powder was prepared by precipitation from an aqueous solution, in which the reactants were mixed in one molar stoichiometric quantities. The starting raw materials were $Pb(NO_3)_2$, $TiCl_4$ and NH_4OH. The aqueous solutions were mixed in the following order: first deionized water was taken in a large container and heated to 45°C and the $TiCl_4$ solution was added. After the solution was mixed, $Pb(NO_3)_2$ solution was added to the container followed by the addition of H_2O_2 solution. The pH of the resulting solution was adjusted to ≈ 8.95 to 9.25 by adding NH_4OH. The precipitated aqueous solution was washed with deionized water and dried at 100°C. The dried material was ground using a mortar and pestle and calcined at 900°C for 1 h to yield highly crystalline $PbTiO_3$ particles with a very narrow particle size distribution. Figure 1 shows the complete flow chart of the procedure used to prepare $PbTiO_3$ powder. The SEM micrograph of the $PbTiO_3$ powder prepared by coprecip-

*Member, the American Ceramic Society
[9]Eccogel 1365-0, W. R. Grace & Co., Lexington, MA.
[10]4270A, Hewlett-Packard Co., Palo Alto, CA
[11]Using a piezo d_{33} meter, Berlincourt
[12]3538A, Hewlett-Packard Co., Palo Alto, CA

Received January 13, 1987, approved February 5, 1987

Peer Reviewed Contribution

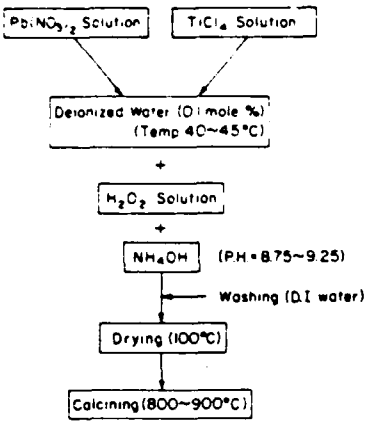

Fig. 1. Procedure used for preparing $PbTiO_3$ powder by the coprecipitation method.

Fig. 2. SEM micrograph of the $PbTiO_3$ powder prepared by the coprecipitation method. (bar = 10 μm)

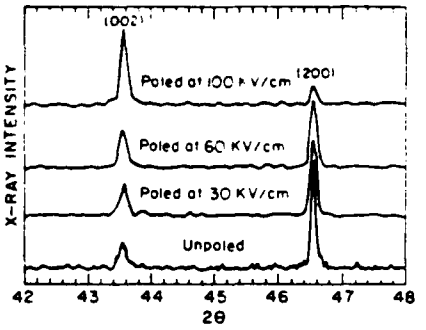

Fig. 3. Intensities of 002 and 200 XRD peaks as a function of applied voltage.

itation method is shown in Fig. 2. It can be seen that the particles are almost spherical with average particle size of ≈ 3 μm.

Composite Preparation

To prepare the composite, $PbTiO_3$ powder was dispersed in a dielectric gel polymer and then mixed by hand with a spatula for ≈ 10 min. The volume fraction of $PbTiO_3$ filler particle in the composite was 67%. The mixture was then placed in a mold and the composite formed under a pressure of 15 000 psi (100 MPa). After the composites were cured at 80°C for ≈ 10 h, they were polished lightly to ensure that the faces were parallel. Electrodes of air-dried silver paste were applied to the surfaces of the composite. The samples were poled at 75°C with a field of 100 kV/cm for 30 min. All the samples were aged for at least 24 h prior to measurements.

Measurements

The capacitance and dissipation factors were measured at 1 KHz using a multi-frequency LCR meter.[†] The d_{33} coefficient was measured dynamically[‡] at a frequency of 100 Hz.

The d_h coefficient was determined by the dynamic ac technique. An electromagnetic driver was used as an ac stress generator to apply pressure waves to the sample and a PZT standard, which was also under a static pressure from the hydraulic press. The charges produced from the sample and the standard were buffered with an impedance converter and the voltages produced were measured by a spectrum analyzer.[§] The ratio of the voltages produced was proportional to the d_h coefficients. By accounting for the sample geometries, the d_h coefficient of the sample was calculated. The hydrostatic piezoelectric coefficient g_h was then calculated from the relation, $g_h = d_h/\varepsilon_0 k$.

Results and Discussion

The intensity ratio of the 002/200 X-ray diffraction (XRD) peaks from the surface of the composites was monitored both before and after poling to detect the possible contribution of domain reorientation or the rotation of the single-domain crystallites during poling. There is a possibility that fine crystallites produced by the coprecipitation method are single domain but randomly oriented within the polymer matrix before poling. In this case, polarization will occur with a movement of the single-domain particles themselves so as to align the polar axis of each particle in the direction of the poling field. The intensities of 002 and 200 peaks for the samples at increasing electric field up to 100 kV/cm are compared with those for the unpoled samples in Fig. 3. A complete reversal of the intensities of the two peaks at 100 kV/cm indicates that almost saturation poling has been achieved. This behavior also indicates the reorientation of 90° domain walls or the rotation of single-domain crystallites.

The dielectric and piezoelectric properties of composites are summarized in Table I and compared with those of composites prepared by using $PbTiO_3$ powder prepared by different processing methods.[11] The dielectric constant of the composite prepared by the coprecipitation method is comparable to that of composites prepared by the sol-gel and mixed-oxide methods. The piezoelectric d_{33}, d_h and g_h coefficients of the composites prepared by the coprecipitation method are about two times larger than those of composites prepared by other processing methods. This difference is probably due to the greater purity and approximate spherical geometry of powder prepared by the coprecipitation method. The values of g_h and d_h of the 0-3 composites prepared by the coprecipitation method showed no pressure dependence up to 1000 psi, as shown in Fig. 4. These composites also showed no significant aging, as is clear from Fig. 5, where no change in the XRD peak intensities is seen with time.

Table I. Dielectric and Piezoelectric Properties of $PbTiO_3$-Polymer Composites Prepared by Using Different $PbTiO_3$ Powder

$PbTiO_3$ filler prepared by	Vol% $PbTiO_3$	K_{33}	d_{33} (pCN^{-1})	d_h (pCN^{-1})	g_h (10^{-3} VmN^{-1})	$d_h g_h$ (10^{-15} m^{2}N^{-1})	Ref.
Coprecipitation	67	50	60	43	97	4170	Present work
Sol-gel	70	50	35	26	59	1530	11
Mixed oxide	70	45	25	13	33	430	11

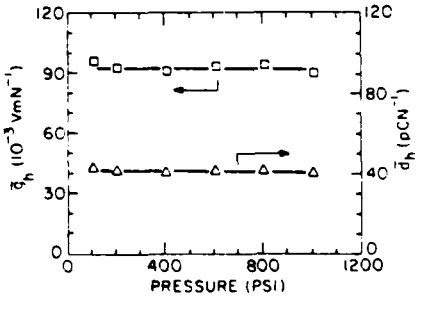

Fig. 4. Variation of d_h and g_h with pressure (measured at 75 HZ) for 0-3 composite prepared by using coprecipitated $PbTiO_3$ powder.

Ahmad Safari

Ahmad Safari is assistant professor in the Ceramic Dept. at Rutgers University, and he is also a member of the Center for Ceramics Research. He earned his B.S. in 1972 and M.S. in 1974, both in physics from Tabriz University, and his Ph.D. in solid-state science in 1983 from Pennsylvania State University. Prior to joining Rutgers University, he worked at the Materials Research Lab at Penn State.

Young H. Lee is associate professor in the Dept. of Electronic Materials, Kwangwoon University, Korea. He received his B.S. in 1973, M.S. in 1975, and Ph.D. in 1981, all in electrical engineering from Yonsei University. His research interests include PTC thermistors, electrooptic materials, and composites. He worked as a visiting scientist in the Materials Research Lab at Pennsylvania State University during 1985–86.

Arvind Halliyal is a research associate with the Materials Research Lab, Pennsylvania State University, University Park, PA. His photograph and biographical sketch appear on page 676.

Robert E. Newnham is professor of solid-state science at Pennsylvania State University, University Park, PA. His photograph and biographical sketch appear on page 676.

Summary

Lead titanate powder prepared by a coprecipitation method yielded highly crystalline particles with a very narrow particle-size distribution. Composites were prepared using a dielectric gel polymer with 67 vol% loading of $PbTiO_3$ powder. The XRD of composites before and after poling indicated that almost saturation poling was achieved in these composites. The composites prepared using coprecipitated $PbTiO_3$ powder as filler particles yielded the highest $d_h g_h$ figure of merit for 0-3 type composites.

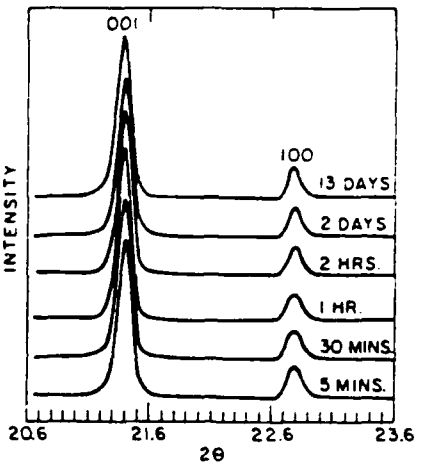

Fig. 5. Effect of aging on the intensities of 001 and 100 XRD peaks for a 0-3 composite prepared by using coprecipitated $PbTiO_3$ powder.

References

[1]R. E. Newnham, L. J. Bowen, K. A. Klicker, and L. E. Cross, "Composite Piezoelectric Transducers," *Mater. Eng.*, **112**, 93–106 (1980).

[2]R. E. Newnham, A. Safari, G. Sa-Gong, and J. Giniewicz, "Flexible Composite Piezoelectric Sensors"; pp. 501–506 in Proceeding of The IEEE Ultrasonic Symposium. Institute of Electrical and Electronics Engineering, New York, 1984.

[3]A. Safari, "Perforated PZT-Polymer Composites with 3-1 and 3-2 Connectivity for Hydrophone Applications"; Ph. D. Thesis, Pennsylvania State University, 1983.

[4]R. E. Newnham, D. P. Skinner, and L. E. Cross, "Connectivity and Piezoelectric-Pyroelectric Composites," *Mater. Res. Bull.*, **13**, 525–36 (1978).

[5]T. Kitayama and S. Sugawara, "Flexible Piezoelectric Materials," *Rep. Proc. Gr. Inst. Elec. Comm. Eng. Jpn.*, CPM27-17 (1972).

[6]L. A. Pauer, "Flexible Piezoelectric Materials," *IEEE Intl. Conf. Res.* 1-5 (1973).

[7]W. B. Harrison, "Flexible Piezoelectric Organic Composites," Proceedings of the Workshop on Sonar Transducer Materials," Naval Research Lab. (1976).

[8]H. Banno and S. Saito, "Piezoelectric and Dielectric Properties of Composites of Synthetic Rubber and $PbTiO_3$ and PZT," *Jpn. J. Appl. Phys.*, **22** [Supp 22-2] 67–69 (1983).

[9]S. R. Gurkovich and J. B. Blum, "Crystallization of Amorphous Lead-Titanate Prepared by a Sol-Gel Process," *Ferroelectrics*, **62**, 189–95, (1985).

[10]D. L. Monroe, J. B. Blum, and A. Safari, "Sol-Gel Derived $PbTiO_3$-Polymer Piezoelectric Composites," *Ferroelectrics Lett.*, **5**, 39–46 (1986).

[11]Y. H. Lee, M. J. Haun, A. Safari, and R. E. Newnham, "Filler Preparations for $PbTiO_3$-Polymer Piezoelectric Composites"; in Proc. IEEE International Symposium on Applications of Ferroelectrics, Lehigh University, 1986. ■

Ferroelectrics Letters, 1987, Vol. 8, pp. 1-9
Photocopying permitted by license only

FABRICATION AND CHARACTERIZATION OF A MULTILAYER PTCR THERMISTOR†

B.V. HIREMATH*, R.E. NEWNHAM, AND AHMED AMIN‡
Materials Research Laboratory, The Pennsylvania State University, University Park, PA 16802, U.S.A.

(Received for Publication September 27, 1987)

Abstract A method has been developed to decrease the room temperature resistance of a PTCR barium titanate ceramic by introducing internal electrodes in a configuration analogous to multilayer capacitors. A multilayer thermistor containing four (n=4) tape cast layers of PTCR barium titanate was fabricated with internal electrodes. A reference sample of the same PTCR barium titanate without internal electrodes was fabricated with the same external dimensions as those of the multilayer thermistor. As predicted by theory, it was found that the resistance of the multilayer thermistor is approximately 16 (n^2=16) times smaller than the test specimen with little change in the PTCR effect of the multilayer thermistor.

INTRODUCTION

PTCR Thermistors exhibit a positive temperature coefficient of resistance with a steep rise in resistance as the temperature increases. This anomalous change of the resistance with temperature has been used in a wide range of electronic applications. Important markets for PTCR devices include television degaussers, automotive electric chokes, motor starters, crankcase heaters for refrigeration and air conditioning compressors, air heaters for hair dryers, hair culers, food warmers, and a wide range of current limiters. Annual worldwide production has increased to more than 10^8 units.[1]

The PTCR effect is observed in semiconducting barium titanate[2] with the resistivity increasing dramatically near the Curie tem-

---

*Engineering Research Center, AT&T, Princeton, NJ 08540.
‡Texas Instruments, Inc., Attleboro, MA 02703.

†Communicated by Dr. G. W. Taylor

perature. For many applications, it is desirable to lower the room temperature resistance because the thermistor elements are often connected in series with the circuit elements which are to be protected. The resistivity of a PTCR device can be lowered by altering the chemical composition,[3] but only at the expense of degrading the PTCR thermistor effect.

Thermistor devices are normally fabricated as ceramic disks or as composite wafers. In this paper we discuss a method of introducing internal electrodes into a PTCR ceramic in order to reduce the resistance per unit volume without affecting the temperature characteristics. The internal electrode configuration is very similar to that in multilayer capacitors.

To illustrate the basic idea, we compare a single layer disk thermistor with a multilayer thermistor of the same external dimensions. The resistance of the disk thermistor (R_D) is given by equation (1)

$$R_D = \frac{\rho t}{A} \tag{1}$$

where ρ is the resistivity, t the thickness, and A the cross-sectional area of the disk thermistor. For a comparable multilayer thermistor made up of n active layers, the total electroded area is nA (neglecting margins). The thickness of each layer is t/n, neglecting the electrode thickness. The resistance of the multilayer device (R_m) is therefore

$$\begin{aligned} R_m &= \rho(t/n)nA \\ &= \frac{R_D}{n^2} \end{aligned} \tag{2}$$

The resistance of the multilayer is lowered by a factor of $1/n^2$ with respect to a disk thermistor of the same external dimensions.

EXPERIMENTAL PROCEDURE

Verification of the reduction in resistance was obtained from barium titanate PTCR thermistors. Raw materials*, $BaCO_3$, La_2O_3 and TiO_2 were batched according to the chemical formula $Ba_{99.97}La_{0.03}TiO_3$. Figure 1 shows a flow chart of the powder preparation. The ingredients were rolled in a polyethylene jar for about ten hours using zirconia grinding media. The slurry was dried at 110°C for about four hours. The dried powder was calcined at 1200°C for 2 hours using high density alumina crucibles. The calcined powder is again ball milled for 8 hours and the slurry was dried at 110°C for four hours.

Multilayer thermistors were fabricated in accordance with the flow chart shown in Figure 2. The same ceramic composition described earlier was milled with a commercial binder** for 6 hours in a polyethylene jar. The slurry was filtered through a 100 size mesh and deaired. Tapes were cast on a moving glass plate using the doctor blade technique. Platinum electrodes were screen printed on one square-inch tapes. Lamination of these tapes was carried out in a method similar to that used in the multilayer ceramic capacitor industry. The binder burnout was carried out by heating the samples at the rate of 4°C/hr to a peak temperature of 550°C and holding at the peak temperature for 2 hours. Total binder burnout required about 120 hours. These samples were then placed on a zirconia setter and sintered at 1350°C for one hour in air. The heating rate was 200°C/hr. The samples were cooled in the furnace after sintering by switching off the power to the furnace.

The edges of the sintered multilayer thermistors were lightly polished to expose the internal electrodes. Termination was carried out by coating the ends with a conducting silver epoxy and attaching silver wire leads. The multilayer thermistor prepared in this fashion contained four active ceramic layers.

*Fisher Scientific Co., Fairlawn, NJ.
**CB73115 binder, Cladan, Inc., San Marcus, CA.

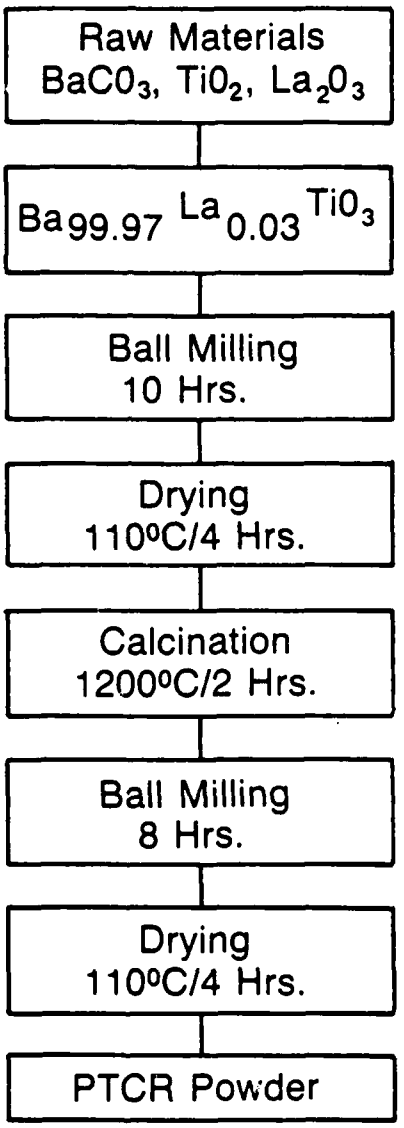

FIGURE 1. Flow chart for the preparation of PTCR powder

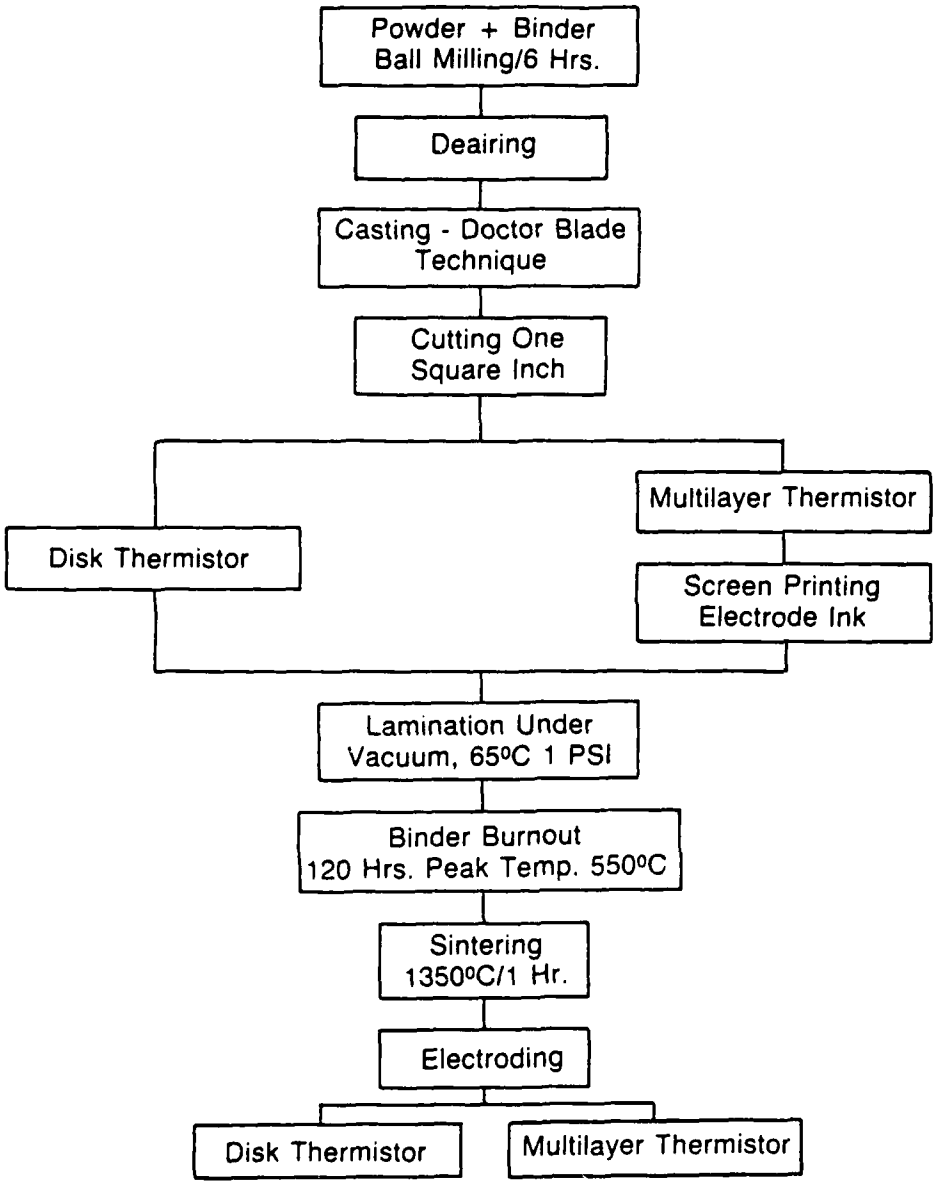

FIGURE 2. Flow chart for the preparation of disk and multilayer PTCR thermistors

A reference specimen without internal electrodes fabricated from four square tapes each one square inch in area. The four tapes were stacked between two electrodes and laminated. Sintering was carried out in a similar method to that used for the multilayer thermistor. The reference test specimen was essentially a disk thermistor.

Resistivity measurements were carried out as a function of temperature on both the disk and multilayer thermistors. The dc resistance was measured using a Kiethley* electrometer. The temperature was controlled by a hot oil bath and monitored with a thermocouple. I-V characteristics were measured using a picoammeter** at room temperature.

RESULTS AND DISCUSSION

The room temperature resistance of the devices was calculated by measuring the slopes of I-V curve at low field levels. The average resistance of the multilayer thermistors was 6.25×10^5 ohms whereas the resistance of the disk thermistor was 1.02×10^7 ohms. The resistance of the multilayer thermistor is found to be 1/16.32 times that of the test specimen in agreement with equation (2).

Figure 3 shows the variation of the resistance with temperature of the disk thermistor and the multilayer thermistor. The multilayer thermistor displays a similar temperature characteristic but it has only resistance 16 times lower than that of the disk thermistor over the range of temperature measured. This work shows that by introducing the internal electrodes into the bulk PTCR ceramic, the room temperature resistance can be lowered without deteriorating the PTCR effect of the bulk ceramic.

As shown in Figure 3, the change of resistance between room temperature and 190°C is only about three orders of magnitude,

*Kiethley Electrometer Model 610A Keithley Instruments, Cleveland, OH.

**Picoammeter 4140B PA meter, Hewlett Packard, Palo Alto, CA.

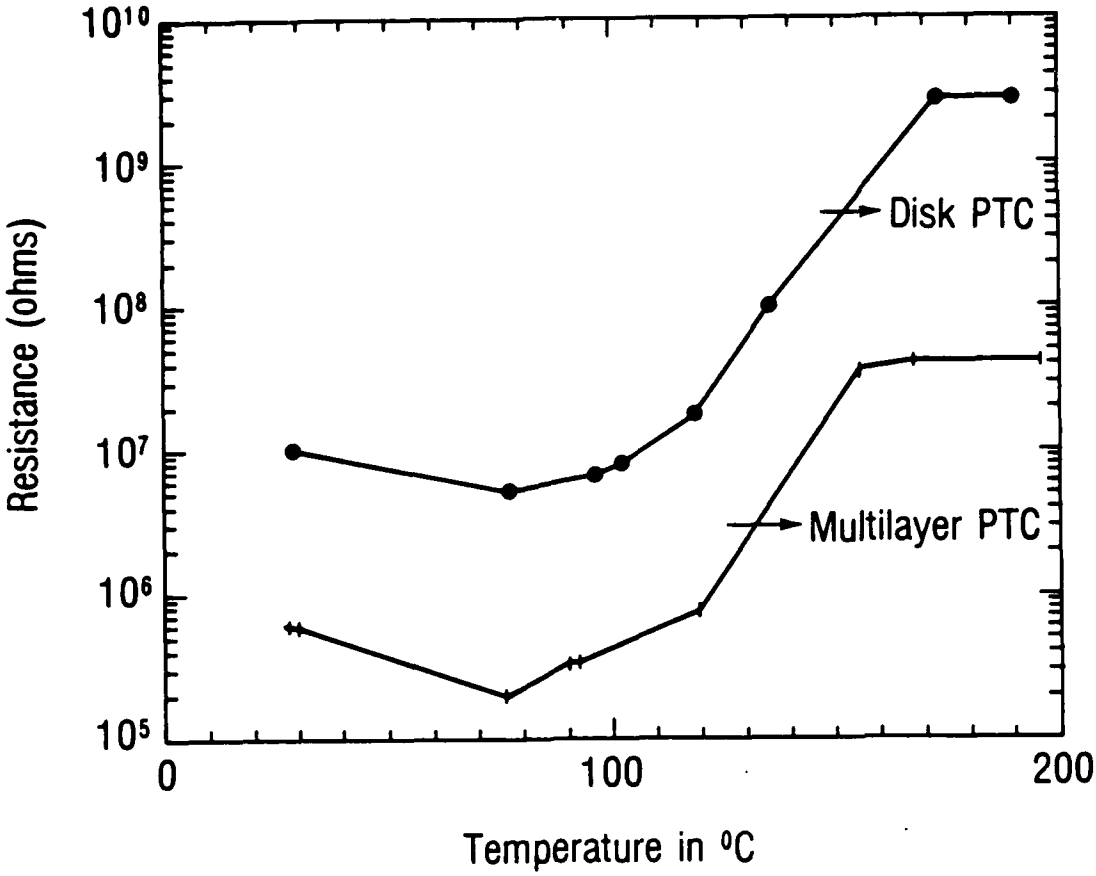

FIGURE 3. Temperature variation of resistance of disk and multilayer thermistors with some external dimensions.

somewhat smaller than the increase observed in commercial thermistors. This is because the powder processing and sintering condition of the samples were not optimized to obtain six or seven orders of magnitude of resistance change as reported in the literature.[2] The main emphasis of the work is to show a method of reducing the room temperature resitance by introducing internal electrodes in a PTCR ceramic.

Comparing the current-voltage characteristics of the test disk and the multilayer thermistor, the I-V relation for the disk thermistor is more ohmic than that of the multilayer thermistor. The disk thermistor did not contain internal electrodes whereas the multilayer thermistor had four internal electrodes. The non-ohmic behavior of the I-V characteristic for the multilayer thermistor can be attributed to the effect of the internal electrodes. In order to improve electrical contact between electrodes and the ceramic layers, a fugitive electrode technique has been investigated.[4] In the process, porous layers are created in the sintered ceramic and then the porous layers are backfilled with electrode materials, thereby avoiding the cofiring of the ceramic and electrode materials. With the fugitive electrode technique, it is possible to use base metals or conducting oxides as external electrodes, thereby enhancing ohmic contact.

CONCLUSION

This work showed that internal electrodes in PTCR ceramics lower the room temperature resistance without deteriorating the PTCR effect. This technique can be used where the resistivity of the bulk PTCR ceramic cannot be reduced further by changing the ceramic composition.

Usually PTCR disks are manufactured with aluminum, aluminum copper alloy or nickel as electrodes which form ohmic contact with the ceramic. Palladium-based thick film pastes have also been developed for this purpose.[5] In our work we have used platinum as

internal electrodes because the electrode and ceramic layers were cofired in air. In order to use Al or Ni as internal electrodes, the fugitive electrode technique[4] can be employed.

REFERENCES

1. B. M. Kulwicki, Am. Ceram. Soc., 1, 138 (1980).
2. O. Saburi, J. Phys. Soc. Jpn., 14(9), 1159 (1959).
3. T. Matsuoka, Y. Matsuo, H. Sasaki, and S. Hayakawa, J. Amer. Ceram. Soc., 55(2), 108 (1972).
4. B. V. Hiremath, Ph.D. Thesis, The Pennsylvania State University (1986).
5. R. J. Lisauskas and V. Shukla, Ceram. Bull., 60(3), 402 (1981).

PREPARATION OF CHEMICALLY ETCHED PIEZOELECTRIC RESONATORS FOR DENSITY METERS AND VISCOMETERS

Susan Trolier, Q. C. Xu, R. E. Newnham
Materials Research Laboratory
The Pennsylvania State University
University Park, PA 16802

Pergamon Journals

New York • Oxford • Beijing • Frankfurt • São Paulo • Sydney • Tokyo • Toronto

Mat. Res. Bull., Vol. 22, pp. 1267-1274, 1987. Printed in the USA.
0025-5408/87 $3.00 + .00

PREPARATION OF CHEMICALLY ETCHED PIEZOELECTRIC RESONATORS FOR DENSITY METERS AND VISCOMETERS

Susan Trolier, Q. C. Xu, R. E. Newnham
Materials Research Laboratory
The Pennsylvania State University
University Park, PA 16802

ABSTRACT Photolithography and chemical etching were investigated as a potential means of fabricating miniature piezoelectric devices. Among the acids studied, concentrated HCl demonstrated the fastest etching of PZT disks over a wide temperature range. HCl also proved to be compatible with some commercially available photoresists and so could be incorporated into a simple processing procedure for delineating and etching patterns in the ceramic.

Using this technique, flexural mode resonators similar to tuning forks were generated with fundamental resonances between 10 and 115 kHz. These devices were then used to provide simultaneous measurements of the density and viscosity of liquids by monitoring the position of the resonance frequency and the width of the resonant peak, respectively.

MATERIALS INDEX: lead zirconate titanate (PZT)

Introduction

The advent of the microcomputer was presaged by the development of a fabrication procedure which permitted the semiconductor industry to mass produce miniature electronic devices. This technology, and hence the whole realm of integrated circuit manufacture, hinges on the ability to create very fine patterns on the surface of a silicon wafer by selectively removing minute quantities of material. In order to accomplish this, a multi-step process is employed wherein a pattern masking portions of the wafer surface is first delineated so that unprotected areas can later be etched away (1). The process, pictured in Fig. 1, is thus largely analogous to the production of pictures by the printing plate method. This technique was adapted to piezoelectric ceramic transducers because miniature devices of these materials could be useful as sensors or actuators.

The design chosen to test this processing procedure was a flexural mode resonator. In this study, four cantilevers, arranged around a center bar so that the whole looked like a capital "H", were etched out of a sheet of PZT poled in the thickness direction. With one face electroded as demonstrated in Fig. 2 and the other completely metallized and allowed to act as a floating electrode, anti-parallel electric fields were established in the two halves of each cantilever. Due to the

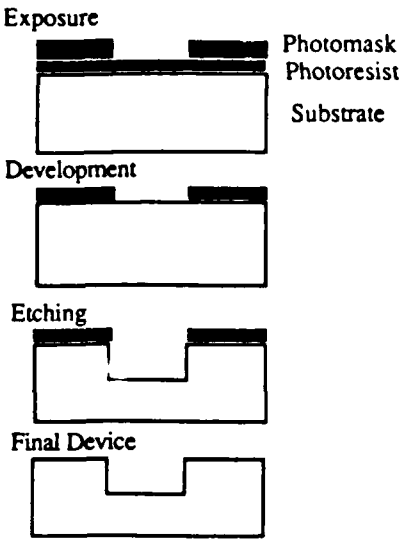

FIG. 1:
Fabrication process

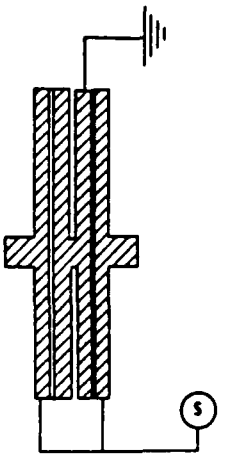

FIG. 2:
Electrode pattern for flexural resonator

converse piezoelectric effect $\varepsilon_i = d_{ij} E_j$ (2), a strain field arises in which one half of the leg expands while the other contracts. This fulfills the condition for flexure, and the cantilevers wag in the horizontal plane. By utilizing four cantilevers arranged so that they are symmetric about the center bar, the root of each cantilever is effectively clamped by the motion of the others. This then permits each of the cantilevers to act as though fixed on one end.

Density Meter

Whenever a transducer is excited in a fluid medium, an effective mass is forced into oscillatory motion. This quantity includes contributions from the transducer itself, i.e. the piezoelectric and the electrode, and an additional term known as the radiation mass due to the displaced fluid surrounding the ceramic. For vibrations in air, this radiation mass is very small, and so in many circumstances is considered negligible. In the case of a transducer vibrating in a liquid, however, the weight of the disturbed fluid cannot be neglected and so the effective mass is far higher.

As an approximate treatment of the effect of the mass-spring damping on the system, consider the resonance of the transducer in air to be undamped (a valid assumption for a high Q_m transducer) so that it follows the equation

$$m\frac{d^2x}{dt^2} + sx = 0$$

(3) where m is mass, x is position, t is time, and s the spring stiffness constant. Solution of this equation gives the resonant frequency in terms of s and m:

$$f_r = \frac{1}{2\pi}\sqrt{\frac{s}{m}}$$

(3). For vibrations in air, m includes only the mass of the transducer and the resonance can be expressed as

$$f_r = \frac{1}{2\pi}\sqrt{\frac{s}{B\rho_{ceramic}}}$$

for B = constant and $\rho_{ceramic}$ = density of the ceramic. When the oscillator is immersed in a liquid, however, the mass of the transducer is augmented by that of the displaced fluid, m_l, so that

$$f_r = \frac{1}{2\pi}\sqrt{\frac{s}{m + m_l}}$$

Since $m_l = A \times \rho_{liq}$ and $m = B \times \rho_{ceramic}$ for A and B constant, the equation can be expressed as

$$f_r = \frac{1}{2\pi}\sqrt{\frac{s}{A\rho_{liq} + B\rho_{ceramic}}}$$

$$\frac{1}{f_r^2} = A'\rho_{liq} + B'\rho_{ceramic}$$

when λ, the wavelength of the vibration in the fluid, is much greater than the size of the transducer (A' and B' are constants). If this last condition is not fulfilled, the transducer can no longer be considered a point source of radiation, and m_l becomes frequency dependent. For cases in which the equation does hold, however, it is clear that a plot of f_r^{-2} versus ρ_{liq} should yield a straight line.

From this treatment it is expected that a flexural mode resonator would undergo shifts in the resonant frequency when oscillated in liquids of different densities. By calibrating this change, the device can be used as a density meter.

Viscometer

In addition to the effect of fluid on the value of the resonant frequency, the nature of the surroundings also influences the shape of the resonance peak, and hence Q_m. Previous work utilizing this effect has hinged on monitoring the amplitude of vibrations for torsional or flexural mode quartz resonators immersed in various fluids (4-6). In this study, an alternate functional dependence of the viscosity on the width of the resonance peak is derived which is applicable to the geometry utilized for density determinations.

To derive the effect of the viscosity of the liquid on Q_m, consider the wave equation (3,7) written as

$$\rho\frac{\delta^2 u}{\delta t^2} = q\frac{\delta^2 u}{\delta x^2} + \eta\frac{\delta^2}{\delta x^2}\left(\frac{\delta u}{\delta t}\right)$$

where ρ = density, u = displacement, t = time, q = real elastic constant, and η = coefficient of viscosity defined as $\eta = v' + {}^4/_3 v''$ where v' = volume coefficient of viscosity and v'' = shear viscosity. For harmonic oscillations

$$u = u_0 e^{j\omega t}$$

which, when substituted into the wave equation, gives

$$\rho\frac{\delta^2 u}{\delta t^2} = \frac{\delta^2 u}{\delta x^2} q\left[1 + \frac{j\eta\omega}{q}\right]$$

With the elastic constant rewritten as a complex quantity,

$$q^* = q(1 + j\tan\delta) = q(1 + j\frac{1}{Q_m})$$

(8) it is clear that

$$\frac{\eta\omega}{q} = \frac{1}{Q_m}$$

This final equation suggests that a piezoelectric resonator should make an accurate viscometer. Thus, with correct calibration, analysis of the resonance behavior (peak position and peak width) of an oscillator vibrating in a fluid should simultaneously provide measurements of the density and viscosity of the liquid.

Experimental Procedure

Poled PZT blanks were polished to the desired thickness using a series of Al_2O_3 powders. Because the clarity of the photolithographic pattern was enhanced by smooth wafer surfaces, final polishing was done with 3 μm grit. Prior to applying the photoresist, the samples were spun on an Integrated Technologies spin coater for 25 seconds at 2000 rpm to remove dust. Then, working under yellow lights to prevent premature resist exposure, enough resist was placed on the surface to cover 2/3 of the disk and the spin cycle was repeated. The second face was coated in a similar fashion. All samples were then placed in a light tight container and baked for 20 minutes at 80°C. The dried photoresist was exposed under an array of white light bulbs for approximately 25 minutes using a 35 mm film negative as a photomask. Shipley Microposit S1400-27 positive photoresist was chosen for use because it was capable of withstanding the attack of the most promising etchant, HCl, for over an hour.

After exposure, the wafers were developed in a dilute Shipley Microposit Developer for 1.5 minutes to remove exposed areas. They were then post-baked, usually for 50 minutes at 80°C to further harden the remaining resist.

Following patterning, the disks were placed in a bath of warm concentrated HCl for etching. In order to remove reaction products from the surface and so present fresh acid to the cavities (1), it was necessary to agitate the liquid. Once the pattern was completely etched, the piece was rinsed in distilled water and the resist was removed with a spray of acetone.

Electrodes were hand-painted on to device surfaces using an air-dry silver paint; any necessary electrical connections were then made by gluing silver wires to the silvered surface with a conducting epoxy.

Resonance frequency data, including capacitance, conductance and impedance values, were collected using a Hewlett Packard 4192A LF Impedance Analyzer interfaced to a personal computer. Flexure mode "H" cantilever devices were suspended from the sample holder by wires affixed to the center bar so that they hung freely in a liquid bath. These same wires also served as electrical connections. In order to minimize hysteritic effects caused by subjecting a ferroelectric to large alternating fields, oscillation voltages of 0.1 volts were utilized throughout these experiments. Resonant frequencies were determined by taking the maximum value in plots of conductance versus frequency. To monitor the peak width as a function of viscosity, plots of capacitance versus frequency were examined and frequencies f_1 and f_2, the maximum and minimum capaci-

tance values respectively, were determined to the nearest 0.01 kHz. The difference $f_2 - f_1$ was then used as the peak width at half height. Reference viscosities, used as "true" viscosity values for each liquid were determined using a Brookfield model LVF Viscometer.

Relation Between Peak Shift and Density

As predicted by theory, vibrating an "H" transducer in liquids of disparate densities caused marked changes in the resonant frequency. This trend is illuminated in Fig. 3, where f_r^{-2} is plotted as a function of the density. Error bars given for the y axis data points arise from the fact that peak broadening obscured the exact resonance frequency. Within these limits, however, the data points were reproducible.

The graphs in Fig. 3 illustrate a good fit to the predicted linear correlation between f_r^{-2} and the density. It should be noted, however, that the least squares fits to the lines (given immediately above the graphs) do not extrapolate to the resonant frequency of the device in air, implying that the meter would be applicable only above some lower density limit. It was also found that measurements taken with ~18.8 and ~37 kHz transducers were more accurate than those derived from transducers oscillating at 10 kHz.

Despite the adherence of most of the points to the prediction, it is also clear that some of the data deviate significantly from the line. Potential causes for this behavior are numerous. For example, moderate electrical conductivity caused peaks to shift too far below the readings in air, while high conductivity caused peaks to shift rapidly and erratically with time. This problem could easily be eliminated by coating the transducer with a thin layer of compliant plastic to electrically insulate it. Attempts of this kind were made, but it was difficult to attain a truly impermeable layer of Eccogel-0. Waterproofing of parts is, however, common industrially and would probably not constitute a major obstacle. A second problem which could prove more insidious results from the fact that the theory assumes that the transducer is a point source radiating into an infinite medium. This imposes several restraints on the sizes of both transducer and container and is considered more thoroughly in the following section.

Potential Geometric Limitations

The theory which predicts a linear change in f_r^{-2} as a function of density is derived for a point acoustic source radiating into an infinite medium. Practically, this implies 1) the resonator size should be much smaller than the wavelength of sound in the medium: size $<< {}^1/_6 \lambda$.
2) the resonator should be surrounded with 2-3 wavelengths of liquid on all sides.

Unfortunately, it proved difficult to simultaneously satisfy both conditions in the case of flexure mode resonators. Although the 10 kHz transducer with cantilever dimensions of 7.5mm x 1.5mm did just fulfill the size requirement, the quantities of liquid used in measurement were far too small, particularly in those cases where v approached 2000 $^m/_s$. This could account for the fact that better data were obtained for transducers with higher frequencies.

There are two potential means of sidestepping this problem. The first is to manufacture a transducer which approximately fulfills the requirements for a wide range of acoustic velocities (900-2000 $^m/_s$). This would probably require a transducer with an intermediate frequency (i.e. 40-50 kHz) which had a maximum dimension near 4.5mm. Preliminary attempts were made to fabricate a resonator with these specifications, but the bars were too thin to permit painting the split electrodes by hand. A second method by which these conflicting restraints could be circumvented is to utilize a series of transducers, each of which fulfils both requirements for a limited range of acoustic velocities.

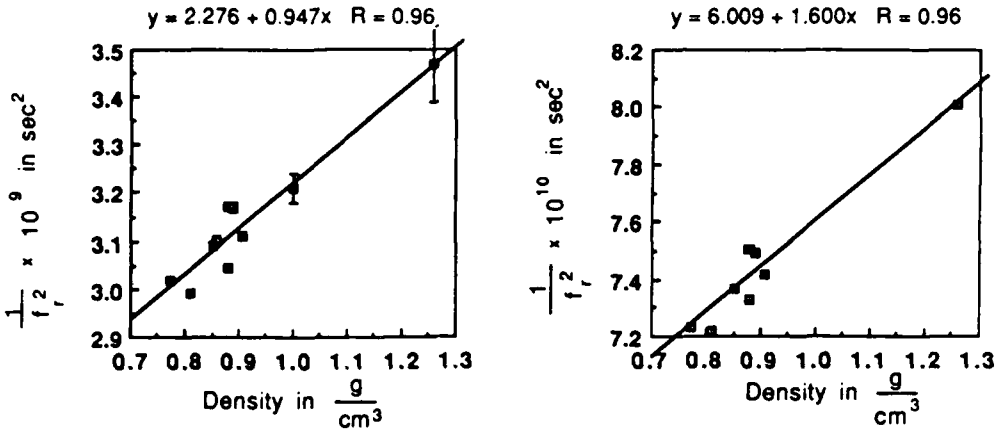

(a) (b)

FIG. 3:
Relation between resonant frequency and density for (a) 18 kHz hard PZT transducer with dimensions of 1cm x 2mm x 0.2mm and (b) 37 kHz soft PZT transducer with dimensions of 6mm x 2mm x 0.2mm

Relation Between Viscosity and Peak Width

As predicted by the theory, Fig. 4 shows the width of the resonant peak to be directly proportional to the viscosity. It is interesting to note that for Fig. 4(b), the least squares fit to the line does not extrapolate correctly to the value obtained for Δf in air ($\Delta f = 0.036$ kHz in air). Consequently, since a knee in the curve must appear at some viscosity, it is not surprising that values for $\eta \sim 1$-2 cp (black diamonds) do not fit the curve. Above this cut-off, however, the device seems to be at least as reproducible as the Brookfield viscometer. Again, data taken at ~18.8 and ~37 kHz were more accurate than those derived from a 10 kHz transducer.

Conclusions

PZT disks fabricated by conventional techniques were prepared for patterning by polishing with 3μm grit and spin-coating the photoresist onto the wafer. After soft-baking to remove the solvent, the resist was exposed through a high contrast 35mm film negative patterned with the negative image of the final device. Wafers were then developed, post-baked, and etched to transfer the design to the PZT.

Using this technique, several small piezoelectric devices were prepared from thin (~0.2mm thick) ceramic disks. The flexural mode transducers consisted of four cantilevers arranged around a center bar so that the device looked like a capital "H". By varying the geometry, fundamental resonances between 10 and 115 kHz could be generated.

"H" transducers were then used as density meters by tracking the change in the resonant frequency during vibrations in different liquids. Plots of f_r^{-2} versus ρ were linear for the density

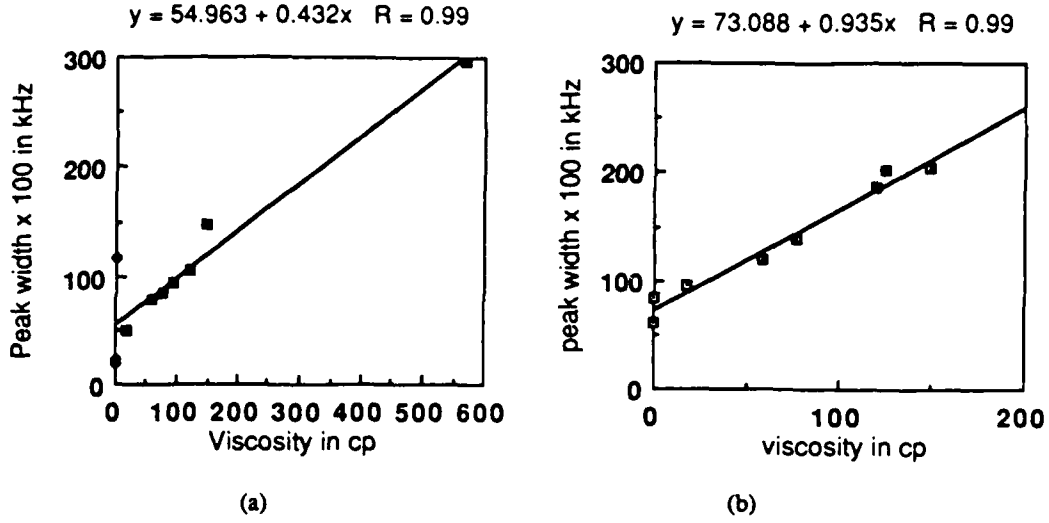

FIG. 4:
Relation between peak width and viscosity for (a) 18.8 kHz hard PZT transducer with dimensions of 1cm x 2mm x 0.2 mm and (b) 37 kHz soft PZT transducer with dimensions of 6mm x 2mm x 0.2mm

range of ~0.78 - 1.3 $^{g}/_{cm^3}$. Nevertheless, there are some outstanding questions concerning the sizes of the resonator and the fluid bath required for the most accurate operation of the meter.

Measurement of the viscosity of the fluid medium could also be made with an "H" transducer. It was found that due to the attenuation of sound radiated into the liquid, the peak width decreased in direct proportion to the viscosity. The device appeared to be similar in accuracy to the Brookfield viscometer used for calibration.

The advantages this type of configuration offers over previous work include the fact that a single run of data can be used to simultaneously determine the density and viscosity of a liquid. Furthermore, utilization of the microfabrication technique has significantly reduced the size of the transducer, permitting operation of the device in small quantities of fluid.

References

(1) Ivor Brodie and Julius J. Muray. The Physics of Microfabrication. New York: Plenum Press, 1982.

(2) J. F. Nye. Physical Properties of Crystals. New York: Oxford University Press, 1985.

(3) Lawrence E. Kinsler and Austin R. Frey. Fundamentals of Acoustics. New York: John Wiley and Sons, Inc., 1962.

(4) M. R. Fisch, R. P. Moeller, and E. F. Carome, "Improved Acoustic Viscometer Technique," J. Acoust. Soc. Am.60(3), 623-625 (1976).

(5) Benjamin Welber, "Damping of a Torsionally Oscillating Cylinder in Liquid Helium at Various Temperatures and Densities," Phys. Rev. 119(6), 1816-1822 (1960).

(6) Dwain E. Miller, "Measurements of the Viscosity of Parahydrogen," J. Chem. Phys. 42(6), pp. 2089-2100 (1965).

(7) C. H. Hun and Y. F. Chao. (Q. C. Xu, trans.) The Fundamentals of Acoustic Theory. Beijing, China: Defense Industrial Publishing Company, 1981.

(8) A. E. Semple and W. Thompson Jr. Improvements to the Transfer Method for Determining the Complex Dynamic Modulus of Polymer Composites. Technical Memorandum File No. TM No. 85-138. Applied Research Laboratory, Pennsylvania State University Aug. 5, 1985.

Acknowledgements

This material is based upon work supported under a National Science Foundation Graduate Fellowship.

RESONANCE MEASURING TECHNIQUE FOR COMPLEX COEFFICIENTS OF PIEZOELECTRIC COMPOSITES

Q. C. XU, A. R. RAMACHANDRAN and R. E. NEWNHAM
Materials Research Laboratory
The Pennsylvania State University
University Park, PA 16802

ABSTRACT

Composite electroceramics have found a number of applications, e.g., in medical imaging and for target location. Tradaitional measurement procedures are not easily adaptable for characterising these materials. Two techniques based on the resonance method have been devised for the present purpose. One is for measuring the real coefficients based on the lumped circuit equivalent. The other is for complex coefficients and is based on an analytical solution for a single mode. Expressions for conductance vs. frequency, capacitance vs. frequency and Q_m are derived. Experimentally obtained values for the complex dielectric, elastic, and piezoelectric coefficients of 0-3 composites (NTK-306, Japan), 0-3 fired composites (Penn State), PTBF 0-3 composites (Celanese), and polyvinylidene film (Raytheon) are presented.

1. INTRODUCTION

Composite electroceramics have found a number of important applications [1]. Many of the piezoelectric composites exhibit lower Q_m and Q_e than ceramics and exhibit electromechanical properties which vary rapidly with frequency. Thus the traditional measurement methods such as the IEEE standard [2] and other techniques used for ceramics [3,4] are difficult to apply in the case of composites. Quasistatic methods are limited to very low frequencies ($\leq$ 100 Hz) [5]. A resonance method has been used in measuring the real part of the piezoelectric coefficients of polyvinylidene fluoride (PVDF), but electrical loss was neglected [6]. Consideration of this loss is important in composite materials [7].

Knowledge of the complex coefficients is of importance in several areas including medical imaging [8], accurate target location [9], and transfer function determination between electrical and mechanical signals. For these problems, it is necessary to know phase information in addition to amplitude data. From the viewpoint of materials science, the imaginary part of the property coefficients relative to the microstructure of the material, provides a fundamental understanding of loss mechanisms. Techniques for determining the complex coefficients of piezoelectric ceramics based on admittance measurement at three frequencies have been used for more than a decade [10-12], but there are difficulties in applying these techniques for low Q composites. Koga and Obigashi [13] measured the electromechanical properties of PVDF by the admittance fitting method assuming that h_{33} is real as done by Ikeda [14], but this assumption needs to be verified by experiment.

In this paper, two techniques based on the resonance method are described; one is for measuring the real coefficients based on a lumped equivalent circuit representation, the other is for measuring complex coefficients and is based on an analytical solution for a single mode. Expressions for conductance vs. frequency, capacitance vs. frequency and Q_m are derived. Experimentally obtained values for the complex dielectric, elastic, and piezoelectric coefficients of 0-3 composites (NTK-306, Japan), 0-3 fired composites (Penn State), PTBF 0-3 composites (Celanese), and polyvinylidene film (Raytheon) are presented.

2. REAL PARAMETER MEASURING TECHNIQUE

(a) Analysis of Admittance

When piezoelectric characteristics are determined using an equivalent circuit with lumped parameters (Fig.1), the results are valid only near the resonant frequency of a single mode. For very high electromechanical coupling coefficients, harmonic circuit elements should be included in the dynamic branch.

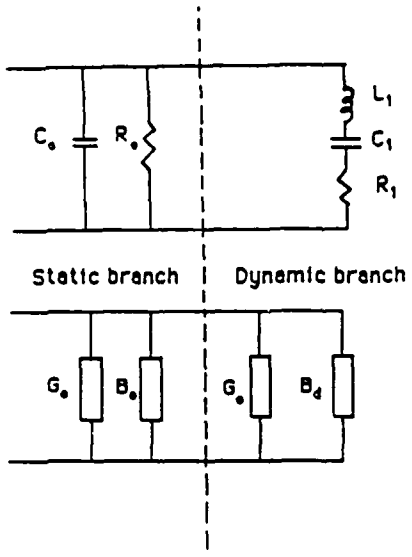

Figure 1 Equivalent circuit of a single mode piezoelectric resonator.

The admittance is given by

$$Y = \left[\omega C_o \tan \delta_e + \frac{R_1}{R_1^2 + (\omega L_1 - 1/\omega C_1)^2} \right] + j \left[\omega C_o - \frac{(\omega L_1 - 1/\omega C_1)}{R_1^2 + (\omega L_1 - 1/\omega C_1)^2} \right] \tag{1}$$

$$= G + jB = (G_o + G_d) + j(B_o + B_d)$$

where G is the conductance and B, the susceptance. Subscripts o and d refer to the static and dynamic contributions respectively; thus,

$$G_o = \omega C_o \tan \delta_e \tag{2}$$

$$G_d = \frac{R_1}{R_1^2 + (\omega L_1 - 1/\omega C_1)^2} = \frac{G_{rd}}{1 + Q_m^2 (\omega_s^2/\omega^2)(\omega^2/\omega_s^2 - 1)^2} \tag{3}$$

where $G_{rd} = 1/R_1$ is the dynamic conductance when $f = f_s$ and $f_s = 1/2\pi\sqrt{(L_1 C_1)}$, i.e., the series resonance frequency;

$$Q_m = 1 / \omega_s R_1 C_1 . \tag{4}$$

In the case of the susceptance, the static and dynamic parts are respectively,

$$B_o = \omega C_o$$

and

$$B_d = -\frac{(\omega L_1 - 1/\omega C_1)}{R_1^2 + (\omega L_1 - 1/\omega C_1)^2} = \omega C_1 \frac{(1 - \omega^2/\omega_s^2)}{(\omega^2/\omega_s^2)(1/Q_m^2) + (1 - \omega^2/\omega_s^2)^2} .$$

From Eq. (1), it can be seen that if the loss component R_1 or R_e^{-1} is high, Y is dominated by the static part, $(G_o + jB_o)$. We have to subtract the static contribution from Y to obtain the dynamic part, $(G_d + jB_d)$. The

capacitance vs. frequency curve is represented by (see Fig. 2)

$$C(f) = \frac{B_o + jB_d}{\omega} = C_o + \frac{(1 - \omega^2/\omega_s^2)\, C_1}{(\omega^2/\omega_s^2)\,(1/Q_m^2) + (1 - \omega^2/\omega_s^2)^2} \quad . \tag{5}$$

From Eqs. (1) - (3), we obtain the G(f) curve near f_s (see Fig. 3). The dotted line represents G_o.

When $f = f_s$, we obtain

$$G_d = G_{rd} = 1/R_1 = \omega_s C_1 / \tan \delta_m \quad , \tag{6}$$

$$G_o = G_{ro} = \omega_s C_o \tan \delta_e \quad . \tag{7}$$

(b) Determination of Low Q_m Values

Q_m can be evaluated from the C(f) or G(f) curves. From Eq. (5), $C = C_o$ at $\omega = \omega_s$. By equating $\partial C/\partial \omega$ to zero, we can get the extremum frequency values f_1' and f_2' (see Fig. 2), corresponding to the maximum and minimum capacitances respectively, and thus obtain

$$f_1' = (1 - 1/Q_m)^{1/2}\, f_s$$

$$f_2' = (1 + 1/Q_m)^{1/2}\, f_s$$

where

$$Q_m = 2f_s^2 \Big/ \left\{ (f_2' + f_1')(f_2' - f_1') \right\} \quad . \tag{8}$$

However in the case of low values of $Q_m k^2$, f_1' and f_2' cannot be obtained exactly from Fig. 2 because of the broadened nature of the curve near f_1' and f_2'. Under these circumstances, Q_m can be estimated from Fig. 3 even though the G(f) curve does not have a sharp narrow peak. From Eqs. (3) and (4), we can see that there exist two frequencies f_1, f_2 which satisfy the following relations:

$$(\omega_1 L_1 - 1/\omega_1 C_1) = -R_1/N \; ; \quad (\omega_2 L_1 - 1/\omega_2 C_1) = R_1/N \quad . \tag{9}$$

In these expressions, N can be any positive real number. This leads to the result,

$$G_d(f_1) = G_d(f_2) = R_1 \Big/ \left\{ R_1^2 (1 + 1/N^2) \right\} = N^2 G_{rd} / (N^2 + 1) \quad . \tag{10}$$

From Eq. (9),

$$\omega_1 = (\omega_s / 2Q_m) \left(\sqrt{(1/N^2) - 4Q_m^2} - 1/N \right)$$

$$\omega_2 = (\omega_s / 2Q_m) \left(\sqrt{(1/N^2) + 4Q_m^2} + 1/N \right)$$

$$Q_m = f_s / (f_2 - f_1)\, N \tag{11}$$

According to Eqs. (10) and (11), if Q_m is small, i.e., the peak in the G(f) curve is broad, N will take on high values such as N = 3, in obtaining Q_m.

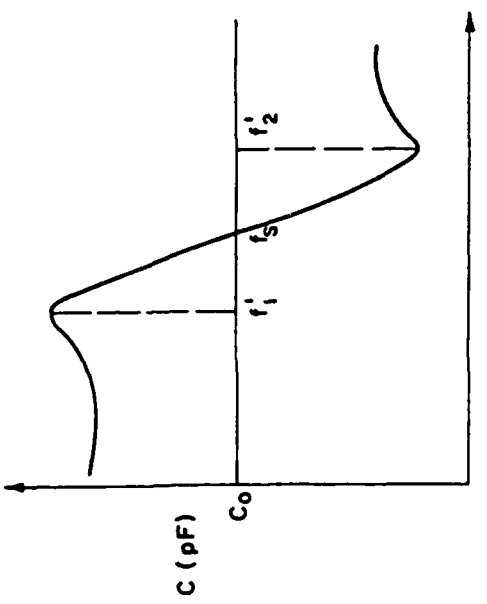

Figure 2 Frequency spectrum of capacitance.

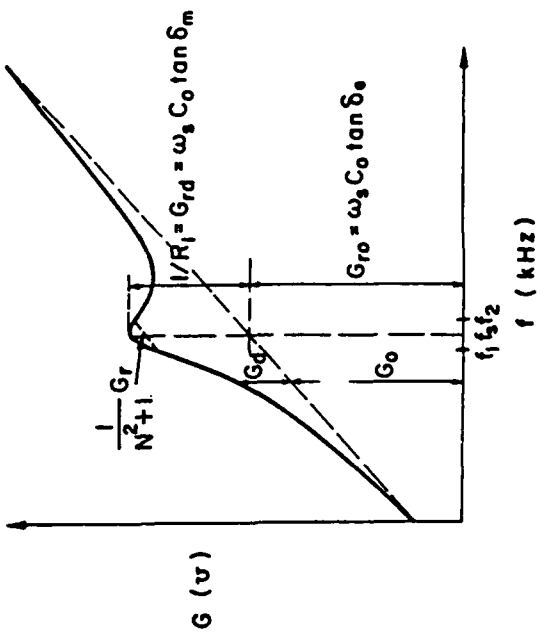

Figure 3 Frequency spectrum of conductance.

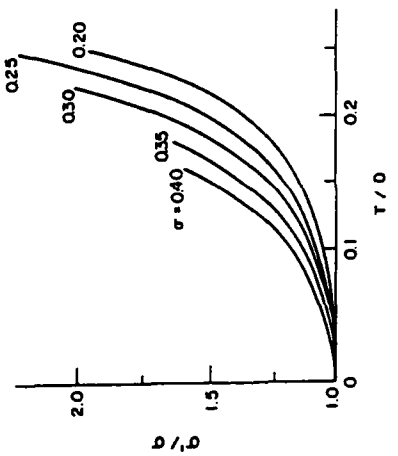

Figure 4 σ'/σ vs. T/D

(c) Parameters for a Disk-Shaped Sample

(1) Relationships for the TE mode

$$f_S = f_{STE} \; ; \; C_1 = 1/(\omega_S R_1 Q_m) \; ; \; k_t^2 = \frac{\pi^2}{8}(C_1/C_o) \; ; \; V = 2T f_S / (1-k_t^2)^{1/2} \; ;$$

$$C_{33}^D = \rho V^2 \; ; \; \varepsilon_{33}^S = C_o T / \frac{\pi}{4} D^2 \varepsilon_o \; ; \; \tan\delta_e^S = G_{ro}/\omega_S C_o$$

$$\tan\delta_m = 1/Q_m$$

$$e_{33} = k_t \sqrt{C_{33}^D \varepsilon_{33}^s \varepsilon_o}$$

$$h_{33} = e_{33}/(\varepsilon_{33}^s \varepsilon_o)$$

The parallel resonance frequency, f_{PTE} is given by,

$$f_{PTE} = f_{STE} / (1 - 8k_t^2/\pi^2)^{1/2} .$$

(2) Relationships for the radial (PE) mode [2]

$$f_S = f_{Sp} \; ; \; C_{1p} = 1/\omega_S R_{1p} Q_{mp} \; ; \; V_p = \pi D f_{Sp}/R_1$$

$$\varepsilon_{33p}^S = C_{op} T / (\frac{\pi}{4} D^2 \varepsilon_o) \; ; \; \tan\delta_e^S = G_{rop} / (2\pi f_{pS} C_{op})$$

$$S_{11}^E = 1/\rho(1-\sigma^2) V_p^2 \; ; \; S_{12}^E = -S_{11}^E \sigma$$

Defining

$$P = 2(1+\sigma)/\left(R_1^2 - (1-\sigma^2)\right) \text{ and } P_1 = C_{1p}/C_{op} P \; ;$$

we get,

$$k_p = \left\{ P_1 / (1+P_1) \right\}^{1/2}$$

From measurements performed on the disk shaped sample which is convenient to fabricate, the following coefficients can be calculated.

$$k_{31} = k_p \left((1-\sigma)/2 \right)^{1/2}$$

$$\varepsilon_{33p}^T = \varepsilon_{33p}^s / (1-k_p^2)^{1/2} \; ; \; g_{31} = d_{31}/(\varepsilon_{33}^T \varepsilon_o)$$

$$d_{31} = k_{31} / (\varepsilon_{33}^T S_{11}^E \varepsilon_o)^{1/2}$$

$$k_{33} = (k_t^2 + k_p^2 - 2k_t^2 k_p^2)^{1/2}$$

$$d_{33} = k_{33} (\varepsilon_{33}^T S_{11}^E \varepsilon_o)^{1/2}$$

$$g_{33} = d_{33} / (\varepsilon_{33}^T \varepsilon_o)$$

Hydrostatic coefficients:

$$d_h = d_{33} + 2d_{31}$$

$$S_h^E = (2S_{11}^E + S_{33}^E) + (2S_{12}^E + 4S_{13}^E)$$

$$k_h = d_h / (S_h^E \varepsilon_{33}^T \varepsilon_o)^{1/2}$$

It is necessary to measure the second harmonic frequency f_{2sp} in addition to f_{sp} in order to obtain the Poisson ratio, σ. [2,14,15] (see Table 1 and Fig. 4).

TABLE 1. σ VS. R_1 AND f_{2sp} / f_{1sp} FOR THIN DISK

σ	R_1	R_2/R_1
0.25	2.0172	2.6669
0.26	2.0236	2.6595
0.27	2.0300	2.6520
0.28	2.0363	2.6447
0.29	2.0426	2.6375
0.30	2.0489	2.6304
0.31	2.0551	2.6234
0.32	2.0612	2.6165
0.33	2.0674	2.6096
0.34	2.0735	2.6029
0.35	2.0795	2.5963
0.36	2.0855	2.5897
0.37	2.0915	2.5833
0.38	2.0974	2.5769
0.39	2.1033	2.5706
0.40	2.1072	2.5643
0.45	2.1380	2.5342
0.50	2.1659	2.5059
0.55	2.1929	2.4793
0.60	2.2192	2.4541
0.65	2.2443	2.4304

R_1 is the root of the equation: $xJ_o(x)/J_1(x) = 1 - \sigma$

$R_2/R_1 = f_{2sp}/f_{1sp}$

It should be noted that in some composites such as the NTK-306, the apparent velocity varies rapidly with frequency, and in this case the Poisson ratio can be obtained from a bar sample and a disk sample driven near the fundamental resonance frequencies. The fundamental frequencies of the two samples must be reasonably close to each other.

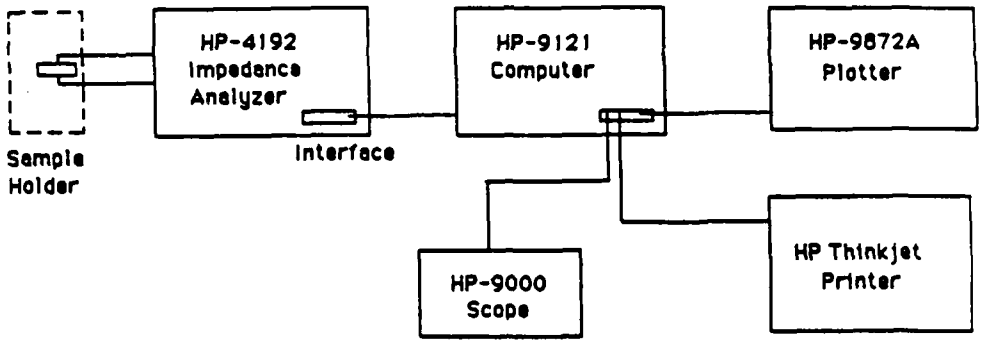

Figure 5 Schematic diagram of the measurement technique.

(d) Other Modes

In principle, other vibrational modes, such as the LE (3-1) mode, the LE (3-3) mode and shear modes can be excited and studied by methods similar to those described above but require suitable sample geometries. For very low Q_m (< 5) composite samples like the NTK-306 0-3 composite, the shear mode is very difficult to excite because of the very high damping coefficient.

(e) Experimental Results and Calculations

Four different piezoelectric samples were studied and their coefficients were evaluated using the technique described above viz., 0-3 composite (NTK), fired 0-3 composite (PSU), 0-3 PTBF composite and PVDF films.

Figure 5 shows a block diagram of the measuring apparatus.

The samples were suitably electroded to minimise problems of surface resistance. Figure 6 shows the G(f), C(f), and ϕ(f) curves near the radial and thickness resonance frequencies. The ϕ (f), [$\phi = \tan^{-1}$ (B/G)] curve is helpful in determining f_s. A computer program was written to calculate the different coefficients. The coefficients for the fired 0-3 composite disk (PSU) and PTBF 0-3 composite (Celanese) were evaluated similarly. Figures 7 and 8 show their G(f), C(f) and ϕ(f) curve for these samples.

Thick PVDF film samples (T = 540 μm) were also studied (see Fig. 9). Thin PVDF film samples (T = 50 μm) were excited only in the LE (3-1 and 3-2) mode. Another computer program was written to calculate the coefficients in this case. It was necessary to mount the thin film sample carefully so that it was straight and unconstrained. Experimental results for thin PVDF sample are shown in Fig. 10.

3. COMPLEX COEFFICIENT MEASUREMENT TECHNIQUE

(a) Relations for the Thickness Mode of a Plate (TE)

We assume that all of the dielectric, elastic and piezoelectric coefficients are complex, so that

$$C_o^* = C_o(1 - jD) \quad ; \quad D = \tan \delta_e \tag{12}$$

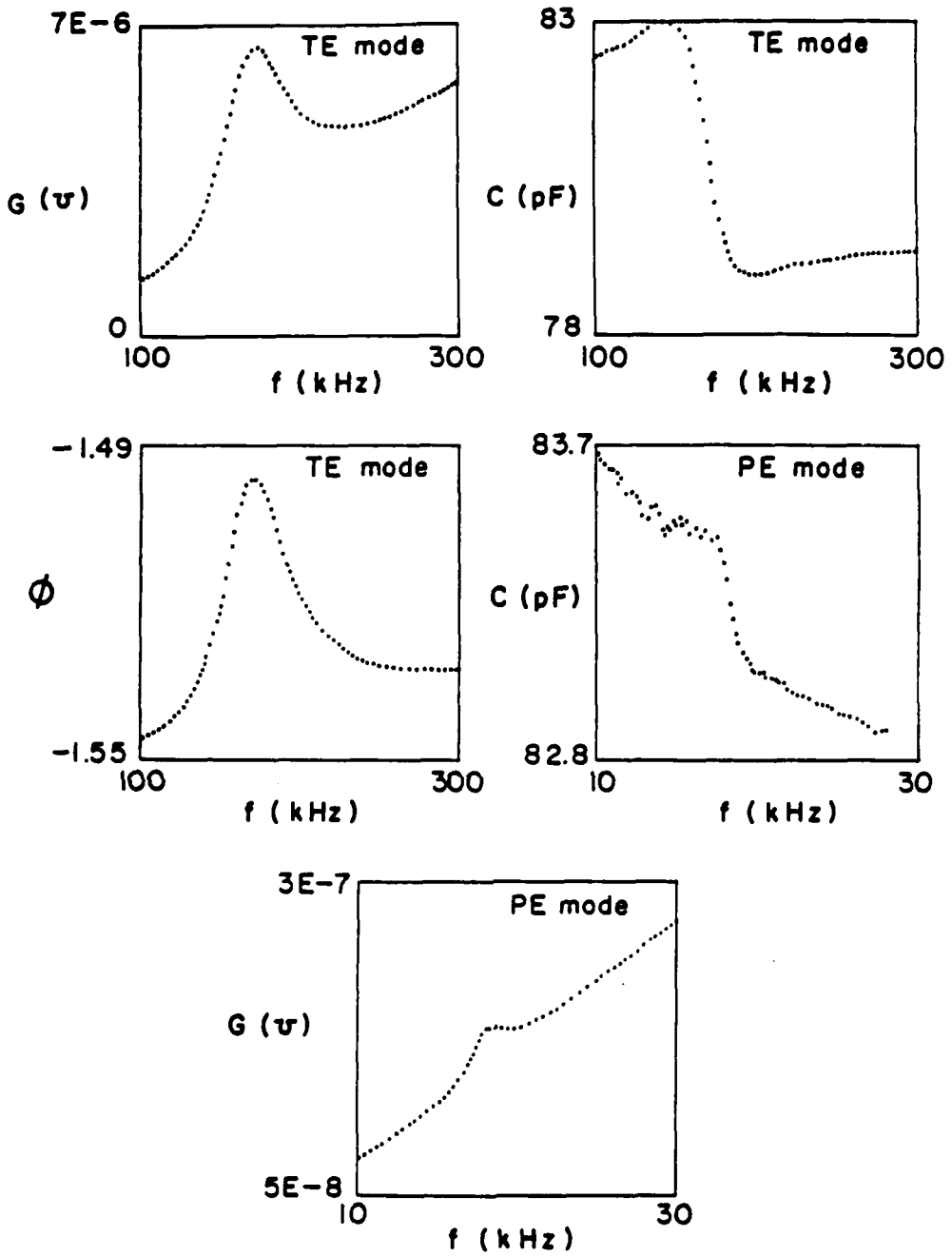

Figure 6 Experimental curve for NTK 0-3 composite.

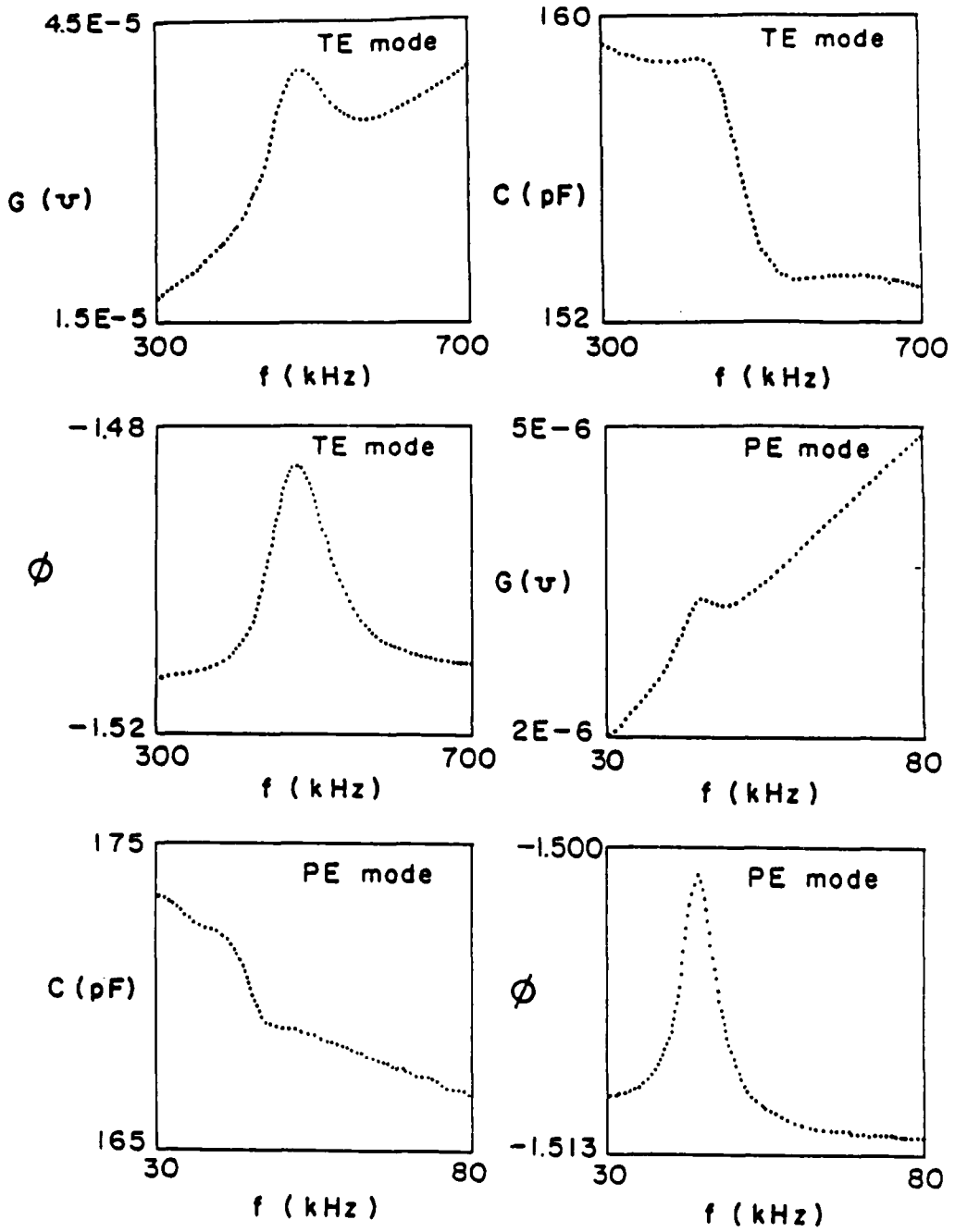

Figure 7 Experimental curves for fired 0-3 composite.

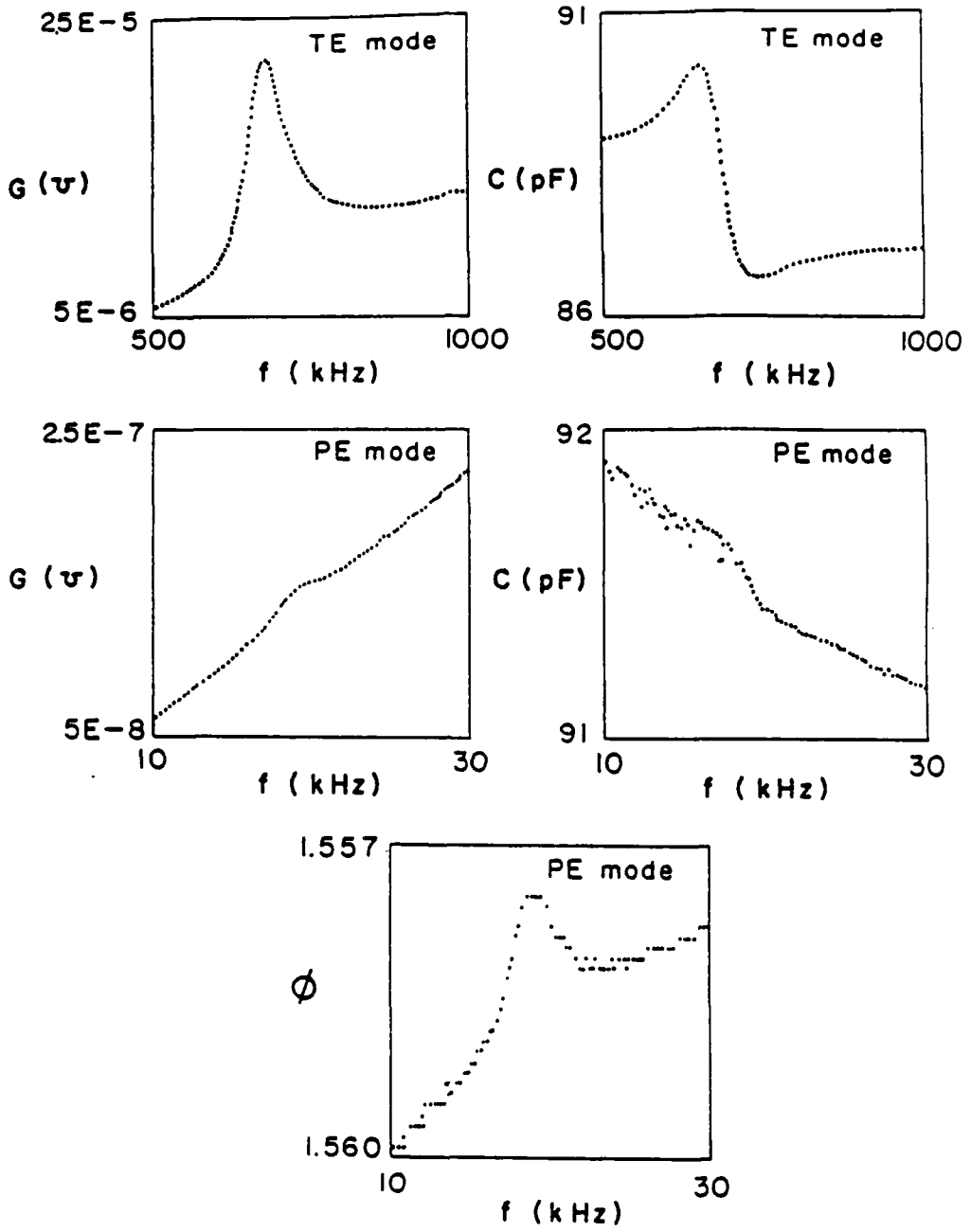

Figure 8 Experimental curves for PTBF 0-3 composite.

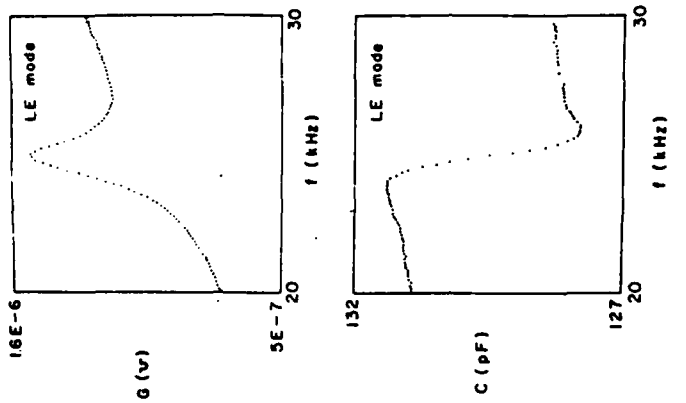

Figure 10 Experimental curves for biaxially oriented thin PVDF film.

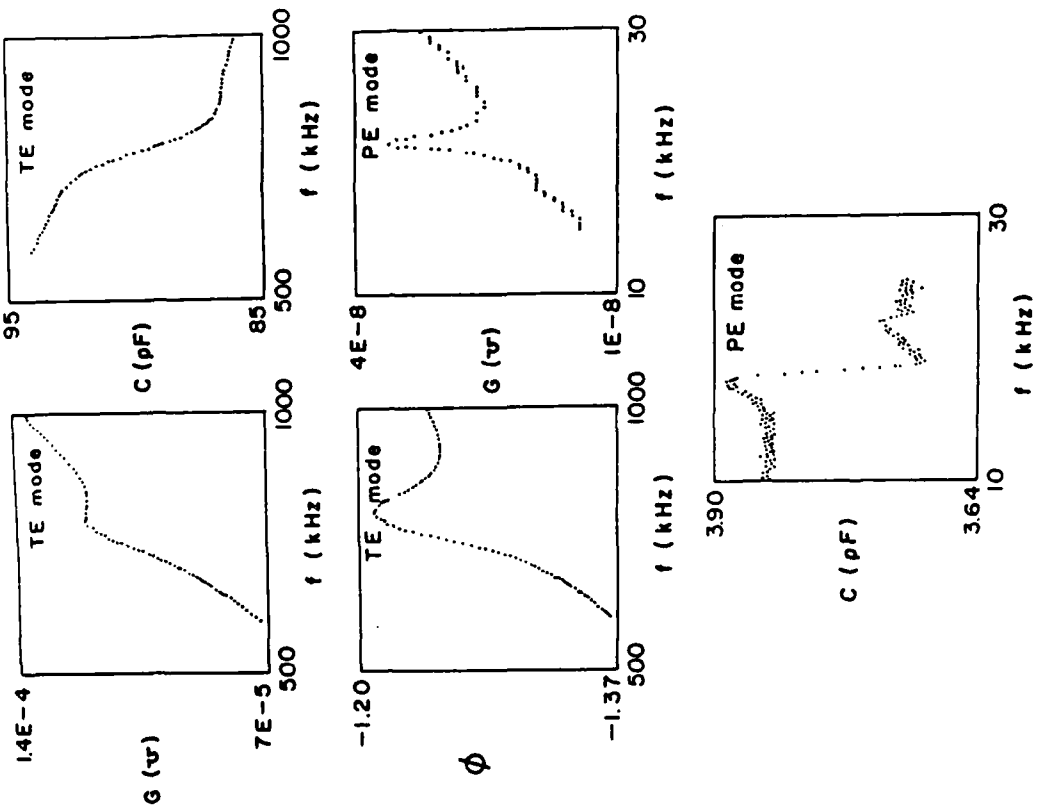

Figure 9 Experimental curves for thick PVDF film.

$$C_{33}^{D*} = C_{33}^{D}(1 + jJ) \quad ; \quad J = \tan \delta_m \tag{13}$$

and

$$k_t^* = k_t(1 + jP) . \tag{14}$$

The impedance of the thickness mode is

$$Z = \left(1/j\omega C_o^* \right) \left(1 - (k_t^{*2} \tan b^* / b^*) \right) \tag{15}$$

where,

$$b^* = (\omega T / 2V^*) .$$

Since D^2, J^2 and P^2 are much lesser than 1, the following equations hold with sufficient accuracy. (As long as D, J and P < 0.5, the error is less than 0.14%).

$$V^* = \left(C_{33}^{D^*} / \rho \right)^{1/2} = \left(C_{33}^{D} / \rho \right) \left(1 + j (J / 2) \right) = V \left(1 + j (J / 2) \right) \tag{16}$$

$$b^* = (\omega T / 2V^*) = (\omega T / 2V) \left(1 - j (J / 2) \right) = b \left(1 - j (J / 2) \right) \tag{17}$$

$$k_t^{*2} = k_t^2 (1 + 2jP) . \tag{18}$$

Substituting Eqs. (12), (16), (17) and (18) into Eq. (15), we have,

$$Z = R + jX$$

where,

$$R = \frac{1}{\omega C_o} \left\{ D + (k_t^2/b) \frac{[(1 + \tan^2 b) \tanh(bJ / 2) - (D + (J / 2) + 2P)(1 - \tanh^2(bJ / 2)) \tan b]}{[1 + \tan^2 b \tanh^2 (bJ / 2)]} \right\} \tag{19a}$$

$$X = \frac{1}{\omega C_o} \left\{ -1 + (k_t^2 / b) \frac{[1 - \tanh^2 (bJ / 2) \tan b + (D + (J / 2) + 2P) \tanh (bJ / 2) \sec^2 b]}{[1 + \tan^2 b \tanh^2 (bJ / 2)]} \right\} \tag{19b}$$

Eq. (19a) can be rewritten as,

$$\omega_i C_o R_i - D = \alpha_i = K (\eta_i - \beta \gamma_i) / \chi_i \tag{20}$$

where,

$$\chi_i = b_i (1 + \tan^2 b_i \tanh^2 (b_i J / 2)) \tag{21}$$

$$\gamma_i = \tan b_i (1 - \tanh^2 (b_i J / 2)) \tag{22}$$

$$\eta_i = (1 + \tan^2 b_i) \tanh (b_i J / 2) \tag{23}$$

$$\beta = D + J/2 + 2P \tag{24}$$

$$K = k_t^2 \tag{25}$$

$$b_i = (\omega_i T / 2V) \tag{26}$$

$$C_s = C_o \left(1 + [1 - (8/\pi^2)] - 0.145\,[K/(1-K)]\right) .$$

For three selected frequencies, f_1, f_2, f_3, and the corresponding resistances. R_1, R_2, R_3, respectively, application of Eq. (20) leads to the expressions,

$$\beta = (\chi_1 \alpha_1 \eta_2 - \chi_2 \alpha_2 \eta_1) / (\chi_1 \alpha_1 \gamma_2 - \chi_2 \alpha_2 \gamma_1) \tag{27}$$

$$K = \chi_1 \alpha_1 / (\eta_1 - \beta \gamma_1) \tag{28}$$

$$\phi = -S_1 \pm (\sqrt{S_2}/2E_1) \;,\; J = (1/b_3) ln\left((1+\phi)/(1-\phi)\right) \tag{29}$$

where,

$$S_1 = E_2/(2E_1)$$

$$E_1 = (1/K)\,\alpha_3 b_3 \tan^2 b_3 - \beta \tan b_3$$

$$E_2 = -(1 + \tan^2 b_3)$$

$$E_3 = \left(\alpha_3 b_3 / K\right) + \beta \tan b_3$$

$$S_2 = E_2^2 - 4E_1E_3$$

An iterative method is used for obtaining the values of k_t, P, J and V. ${\varepsilon_{33}}^S$ and D can be determined directly from C_s and G_{ro}. The iteration is carried out in the following steps:

(1) Beginning with initial input value of J_o and taking $V_o = 2f_s T$ and using Eqs. (27) and (28), K_1, and P can be estimated from f_1, f_2, R_1 and R_2 to give $V_1 = V_o / 1 - K_1)^{1/2}$ (The subscripts on V and K refer to the iteration step).

(2) Using V_1 as the new value for V, step (1) is repeated to give K_2 and P_2. This iteration procedure continues until the K and P values converge. In practice, four iterations are sufficient.

(3) Taking the values of K_4, β_4, V_4, f_3 and R_3 and using Eq. (29), we obtain a new value, $J = J_1$.

(4) Taking J_1 and V_4, steps (1), (2) and (3) are repeated to obtain $J = J_2$.

(5) This iteration procedure is continued until the condition, $(1 - J_i / J_{i-1}) < 10^{-5}$ is satisfied. This yields the complex coefficients, ${\varepsilon_{33}}^S(1 - jD)$, $V(1 + j(J/2))$, $k_t(1 + jP)$, ${C_{33}}^D(1 + jJ)$.

Some other complex coefficients are calculated as follows

$$h_{33}^* = k_t \left(C_{33}^D / \varepsilon_{33}^S\right)^{1/2} \left(1 + j\,(P + J/2 + D/2)\right) \tag{30}$$

$$e_{33}^* = k_t (C_{33}^D \varepsilon_{33}^S)^{1/2} \left(1 + j\,(P + J/2 - D/2)\right) \tag{31}$$

(b) Relationships for the Length (3-3) Mode of a Bar (LL)

$$Z = 1/(j\omega C_o^*)\left(1 - (k_{33}^{*2}\tan b^*/b^*)\right) \tag{32}$$

where

$$b^* = \omega L / 2V^*$$

$$V^* = (\rho S_{33}^{D*})^{-1/2} = V\left(1 + j(J/2)\right)$$

$$V = (\rho S_{33}^{D})^{-1/2} = 2f_s L/(1 - k_{33}^2)$$

$$S_{33}^{D*} = S_{33}^{D}(1 - jJ)$$

$$k_{33}^* = k_{33}(1 + jP)$$

The method used to evaluate the coefficients of the LL mode is very similar to that used for the TE mode described above. The following coefficients are obtained from the analysis of the LL mode:

$$k_{33}^*,\ S_{33}^{D*},\ d_{33}^*,\ g_{33}^*,\ \varepsilon_{33}^{T*},\ \text{etc.}$$

(c) Relationships for the Thickness-Shear (TS) Mode of a Plate

$$Z = (1/j\omega C_o^*)\left(1 - (k_{15}^{*2}\tan b^*/b^*)\right). \tag{33}$$

Again, the method is the same as for the TE mode, carried out in Section 3(a). The coefficients k_{15}^*, C_{55}^{D*}, h_{15}^*, ε_{33}^{S*}, etc., are evaluated by analysis of this mode.

(d) Relationships for the Length (3-1) Mode of a Bar (LE)

The admittance is given by,

$$Y = j\omega C_o^*\left(1 + \frac{k_{31}^{*2}}{(1 - k_{31}^{*2})}\ \frac{\tan(\omega L/2V^*)}{\omega L/2V^*}\right) \tag{34}$$

As previously done, we assume,

$$C_o^* = C_o(1 - jD)\ ;\ K = k_{31}^2$$

$$S_{11}^{E*} = S_{11}^{E}(1 - jJ)\quad ;\quad b = \omega L/2V \tag{35}$$

$$k_{31}^* = k_{31}(1 + jP)\ ;\ V = 2f_s L$$

$$V^* = (\rho S_{11}^{E*})^{-1/2} = V\left(1 + j(J/2)\right)$$

$$D = G_{ro}/2\pi f_s C_o .$$

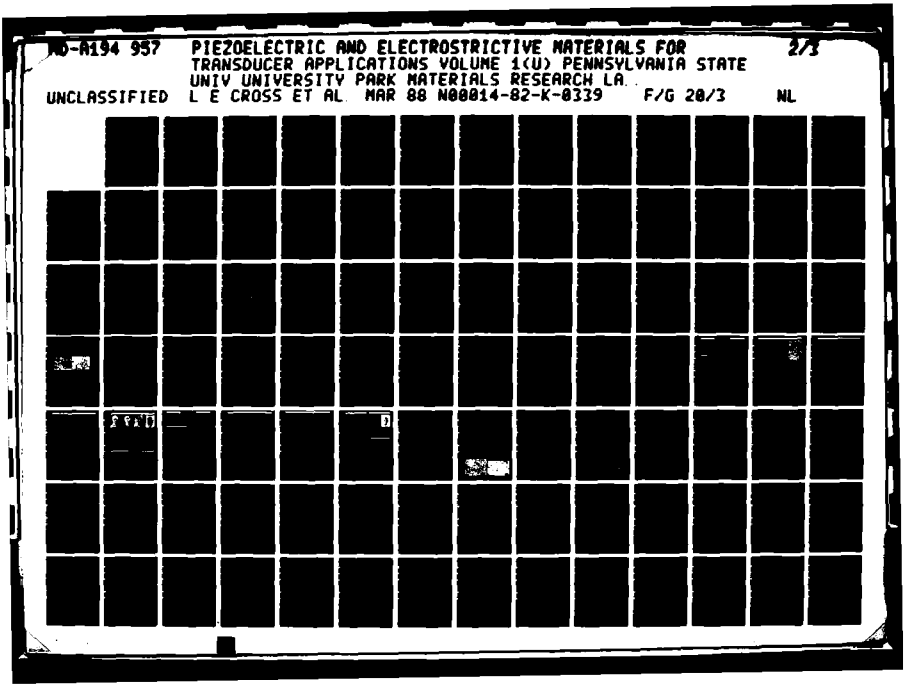
AD-A194 957 PIEZOELECTRIC AND ELECTROSTRICTIVE MATERIALS FOR 2/3
TRANSDUCER APPLICATIONS VOLUME 1(U) PENNSYLVANIA STATE
UNIV UNIVERSITY PARK MATERIALS RESEARCH LA
UNCLASSIFIED L E CROSS ET AL MAR 88 N00014-82-K-0339 F/G 20/3 NL

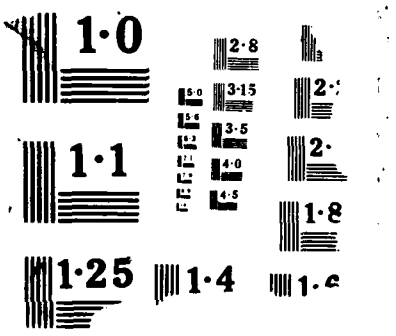
1·0
1·1
1·25
1·4
2·8
3·15
3·5
4·0
4·5
2·
1·8

Substituting these above relations into Eq. (34), we arrive at,

$$Y = G + jB$$

where,

$$G = \omega C_o \left\{ D + \frac{K\,[\,D - J/2 - 2P\,(1+K)]\;[1 - \tanh^2(bJ/2)]\tan b + K\tanh(bJ/2)\sec^2 b}{b\,[1 + \tan^2 b \tanh^2(bJ/2)]} \right\} \tag{35a}$$

$$B = \omega C_o \left\{ 1 + \frac{K[J/2 + 2P(1+K) - D]\,(1+\tan^2 b)\tanh(bJ/2) + K[1 - \tanh^2(bJ/2)]\tan b}{b[1 + \tan^2 b \tanh^2(bJ/2)]} \right\} \tag{35b}$$

Eq. (35a) can be rewritten as,

$$\left(G_i / \omega_i C_o\right) - D = \alpha_i = K\,(-\beta\gamma_i + \eta_i)/\chi_i\,. \tag{36}$$

Here,

$$\beta = (D - J/2 - 2P(1+K)$$

The definitions of χ_i, γ_i and η_i are given in Eqs. (21-23). Substituting three frequencies and the corresponding three conductance values in Eq. (36), we get,

$$K = \chi_1\alpha_1 / (\eta_1 - \beta\gamma_1) = K_{31}^2 / (1 - K_{31}^2) \tag{37}$$

$$\beta = (\chi_1\alpha_1\eta_2 - \chi_2\alpha_2\eta_1) / (\chi_1\alpha_1\gamma_2 - \chi_2\alpha_2\gamma_1) = (J/2) + 2P(1+K) - D \tag{38}$$

$$d_{31} = k_{31}\,(\varepsilon_{33}^T S_{11}^E \varepsilon_o)^{1/2} \tag{39}$$

$$d_{31}^* = d_{31}\left\{1 + j\left(-D/2 - J/2 + \frac{P}{1+k_{31}^2}\right)\right\} \tag{40}$$

$$g_{31}^* = g_{31}\left(\,1 + j\,(\,D/2 - J/2 + P)\,\right) \tag{41}$$

The iteration procedure is very similar to the one described in Section 3(a). Here, we make use of the conductances measured at three distinct frequencies. The following complex coefficients are obtained:

$$\varepsilon_{33}^{T*} = \varepsilon_{33}^T\,(1 - jD^T) \tag{42}$$

$$S_{11}^{E*} = S_{11}^E\,(1 - jJ) = \rho(2f_s L)^2\,(1 - jJ) \tag{43}$$

TABLE 2. PROPERTY COEFFICIENTS MEASURED USING THE TECHNIQUE AT 25° C

Parameter	NTK	Fired	PTBF	PVDF[1]	PVDF[2]
Complex dielectric coefficients	33.4(1-0.021j) (f=18.6kHz)	45(1-0.020j) (f=101kHz)	41.2(1-0.012j) (f=19kHz)	7.5(1-0.022j) (f=1kHz)	11(1-0.016j) (f=1kHz)
ε_{33}^*	32(1-0.037j) (f=172kHz)	44(1-0.040j) (f=1.32kHz)	39.4(1-0.023j) (f=676kHz)	6.0(1-0.24j) (f=792kHz)	10.8(1-0.054j) (f=27.7kHz)
Complex elastic coefficients $C_{33}^{D*}(N/m^2)$	$8.1\times10^9(1+0.26j)$ (f=172kHz)	$13.9\times10^9(1+0.088j)$ (f=1.32MHz)	$7.7\times10^9(1+0.094j)$ (f=676kHz)	$1.09\times10^9(1+0.25j)$ (f=792kHz)	
Complex Piezoelectric Coefficient					
$e_{33}^*(C/m^2)$	0.19(1-0.003j)		0.11(1-0.017j)	0.036(1-0.2j)	
$h_{33}^*(V/m)$	$6.7\times10^8(1+0.034j)$		$3.2\times10^8(1+0.015j)$	$6.8\times10^8(1+0.035j)$	
Electromechanical Coupling Coefficient K					
k_t^*	0.13(1-0.12j)	0.27	0.07(1-0.06j)	0.15(1-0.21j)	
k_{31}	$\simeq$ 0.01	0.040	= 0.014	k_{31}^*=0.094 (1-0.008j)	k_{31}^*=0.069 (1-0.011j)
k_p	$\simeq$ 0.02	0.066	$\simeq$ 0.026	$k_{32}\leq0.01$	
k_{33}	0.12	0.28	0.092		
k_h	0.17	0.16	$\simeq$ 0.12		
Piezoelectric Coefficient (pC/N)					
d_{33}	39	48	52	-27	-16
d_{31}	-3.8	- 7.0	-7.7	d_{31}^*=15(1-0.093j)	d_{31}^*=13(1-0.088j)
d_h	31	34	37		
Density (Kg/m^3)	4.23×10^3	4.4×10^3	5.5×10^3	1.46×10^3	1.78×10^3
Compliance (m^2/N)					
S_{11}^E	3.64×10^{-10}	0.76×10^{-10}	9.22×10^{-10}	3.75×10^{-10}	2.9×10^{-10} (1-0.1j)
S_{12}^E	1.64×10^{-10}	0.19×10^{-10}	2.67×10^{-10}		

1 Voided uni-stretched thick film
2 Non-voided bi-stretched thin film

$$V^* = 2f_s L\left(1 + j\,(J/2)\right) \tag{44}$$

$$d_{31}^* = k_{31}(\varepsilon_{33}^T S_{11}^E \varepsilon_o)^{1/2}\left(1 + j(-D/2 - J/2 + P)\right) \tag{45}$$

$$g_{31}^* = d_{31}(\varepsilon_{33}^T \varepsilon_o)^{-1}\left(1 + j(D/2 - J/2 + P)\right) \tag{46}$$

(e) Selection of the Three Frequencies

The selection of the three frequencies is important for the iteration procedure to lead to converging values. We therefore, recommend the following choices.

$$f_1 \cong (1 - 0.2/Q_m) f_s \quad ; \quad f_2 \cong (1 + 0.2/Q_m) f_s \quad ; \quad f_3 \cong (1 + 0.1/Q_m) f_s \tag{47}$$

If the frequencies selected are too far from f_s, the material parameters may be different from those at f_s since they change with frequency. On the other hand, if these three frequencies are too close to f_s, error is introduced due to error in measurement.

As long as the vibration is a single mode, the iteration converges rapidly within 3 minutes on a HP-9121 computer.

(f) Computer Programs and Experimental Results

In order to carry out the analysis described above, two computer programs, named ITRESTE and ITCONLE for TE and LE modes respectively, were written.

These programs automatically print out the measured values of the complex coefficients along with the total iteration time required for convergence.

The complex coefficients of the NTK-306 0-3 composite, fired 0-3 composite, PTBF 0-3 composites and polyvinylidene fluoride are listed in Table 2.

4. SUMMARY

1) A measurement technique for evaluating the complex coefficients of piezoelectric materials of low Q_m has been described. As long as the figure of merit, $M = k^2 Q_m$ is greater than 0.001, the technique for estimating the real parts of the coefficients can be utilized even for piezoelectric materials with $Q_m < 4$.

2) The experimental results indicate that the piezoelectric coefficient h_{33} is complex, contrary to the usual assumption that it is real.

3) Using just one disk shaped sample of the material, it is possible to estimate all of the real coefficients for the LE, LL, TE, PE and hydrostatic modes.

4) The error in the evaluation of the coefficients can be reduced to less than 5% when the vibration mode is pure.

5) In the case of the iterative method for the evaluation of the complex coefficients, the choice of the three measurement frequencies which lead to rapid convergence is outlined.

6) The technique for measuring real coefficients can be applied to single mode vibrations of low Q_m transducers vibrating in a liquid or attached to a solid. The effective electromechanical coupling coefficient, the conversion efficiency and the bandwidth can be estimated in this manner.

7) These techniques can be used to evaluate property parameters as a function of frequency if the sample size is changed.

8) These techniques are not suitable for high Q_m piezoelectric ceramics, but are useful for measuring property coefficients of materials like piezoelectric composites and PVDF.

ACKNOWLEDGEMENTS

We would like to express our sincere thanks to Dr. L. E. Cross for his suggestion that h_{33} may also be complex, Drs. Ilmar Kalnin, Roger H. Tancrell and H. Banno, for supplying the samples, and Mr. P. Moses for his assistance with computer calculations.

We would also like to acknowledge the financial support given by the Research Center for the Engineering of Electronic and Acoustic Materials, The Pennsylvania State University, which made this work possible.

REFERENCES

1. R.E. Newnham, "Composite Electroceramics," *Ann. Rev. Mat. Sci.* **16**, 47-68 (1986).

2. IEEE Standard on Piezoelectricity, *IEEE SU-31* **2**, 8-55 (1982).

3. G. E. Martin, "Determination of Equivalent Circuit Constants of Piezoelectric Resonator of Moderately Low Q by Absolute Admittance Measures," *JASA* **26**, 413-420 (1954).

4. K. Shihayama, "Measurement of Small Values of Electromechanical Coupling Coefficient in Piezoelectric Transducers," *JASA* **34**, No. 12, 1883-1886 (1962).

5. T. Furukawa et al., "Computer-Controlled Apparatus for Measuring Complex Elastic, Dielectric and Piezoelectric Constants of Polymer Films," *Rev. Sci. Instrum.* **57**, 2 (1986).

6. H. Obigashi, "Electromechanical Properties of Polarized Polyvinylidene Fluoride Films as Studied by Piezoelectric Resonance Method," *J. Appl. Phys.* **47**, No. 3, 949 (1976).

7. M.B. Moffett, "On the Impedance of a Lossy Transducer," Technical Memorandum No. 85-1045, Naval Underwater Research Center, New London Lab. (1985).

8. J.P. Jones, "Ultrasonic Tissue Characterization: A Review," *JASA Suppl. 1* **79**, Spring S44 (1986).

9. W.J. Bangs and P.M. Schulthesiss, "Space-Time Processing for Optimum Parameter Estimation," *Proc. NATO Advanced Study Institute on Signal Processing*, August 1972.

10. R. Holland, "Measurement of Piezoelectric Phase Angles in a Ferroelectric Ceramic," *IEEE SU-17*, 123-124 (1970).

11. J.G. Smits, "Iterative Method for Accurate Determination of the Real and Imaginary Parts of the Materials Coefficients of Piezoelectric Ceramics," *IEEE SU-23*, 393-402 (1976).

12. S. L. Chen, "Method and Program for Determination of Complex Dielectric, Piezoelectric and Elastic Coefficients of Piezoelectric Ceramics," *J. Chinese Silicate Soc.* **9**, No. 3 265-275 (1981) (in Chinese).

13. K. Koga a.' '. Obigashi, "Piezoelectricity and Related Properties of Vinylidene Fluoride and Trifluoroethylene Copolymers," *J. Appl. Phys.* **59**, No. 6, 21-42 (1986).

14. T. Ikeda, "Fundamentals of Piezoelectric Materials Research," *Ohom Sha*, 83-87 (1984) (in Japanese).

15. T. Tanaka, K. Okazaki and N. Ichiro, "*Piezoelectric Ceramic Materials*," Nihon Gakkai Sha (1973) (in Japanese).

16. P. Moses, "Circle," Materials Research Laboratory, The Pennsylvania State University.

ADDENDUM

RESONANCE MEASURING TECHNIQUE FOR COMPLEX COEFFICIENTS OF PIEZOELECTRIC COMPOSITES

Q. C. XU, A. R. RAMACHANDRAN and R. E. NEWNHAM
Materials Research Laboratory
The Pennsylvania State University
University Park, PA 16802

[Note: The following list of symbols was added immediately prior to the printing of this issue.]

List of symbols

C = capacitance

C_0 = static capacitance

R_e = electric loss

$R_e = (\omega C_0 \tan\delta_e)^{-1}$

$\tan\delta_e$ = electric loss tangent

f = frequency

L_1 = dynamic inductance

C_1 = dynamic capacitance

R_1 = mechanical loss

$R_1 = (\tan\delta_m / \omega_s C_1)$

ω_1 = angular frequency

$\omega = 2\pi f$

Q_m = mechanical quality factor = $1/\tan\delta_m$

$\tan\delta_m$ = mechanical loss tangent

Y = admittance

G = conductance

G_o = static conductance

G_d = dynamic conductance

G_{rd} = dynamic conductance at f_s

B = suspectance

B_o = static suspectance

B_d = dynamic suspectance

ω_s = series resonance frequency

K = piezoelectric coupling coefficient

f_1, f_2 = frequencies used to determine Q_m from G(f) curve

T = thickness of sample

ρ = density

V = Acoustic velocity

D = Diameter of sample or electric loss

C_o^* = static complex capacitance

C_{33}^{D*H} = complex stiffness coefficient

$J = \tan\delta_m$

k_t^* = complex thickness coupling coefficient

P = phase angle of k_t^*, k_{33}^*

Z = impedance

b^* = dimensionless parameter (= $\omega T / 2V^*$)

V^* = complex acoustic velocity

L = length of bar sample

k_{31}^* = complex coupling coefficient of LE mode

k_h = coupling coefficient of hydrostatic mode

MEASUREMENT OF COMPLEX COEFFICIENTS FOR THICK PVDF POLYMER*

Q.C. Xu, A.R. Ramachandran and R. E. Newnham
R.H. Tancrell+

M. R. L. , Pennsylvania State University; University Park, PA 16802
+ Raytheon Research Division, Lexington, MA 02173

ABSTRACT

A new measuring technique of complex coefficients for low k^2Q_m piezoelectric materials has been described. The complex elastic, dielectric and piezoelectric coefficients for the longitudinal length mode and for the thickness mode of thick polymer produced at Raytheon, and their temperature and frequency dependence are measured by this technique. Following the method of time-temperature superposition, $\log\omega a_T$ is plotted as abscissa. The real parts of d_{33}, d_h, poisson ratio and their temperature dependence are also obtained.

1. Introduction

In general, piezoelectric composites and polymer materials exhibit large piezoelectric imaginary components, marked temperature/frequency dependence and lower k^2Q_m than ceramics, so measurement of their complex coefficients is useful for many applications [1], such as piezoelectric acoustic absorbers, active noise control and acoustic target location.

The other methods for determination of complex coefficients of piezoelectric materials are: (1) Gain-band-width method by Holland and Ernisse [2]. (2) Interactive method by Smith [3]. (3) Quasistatic (<100Hz) method by Hayakawa and Furukawa [4]. (4) Admittance fitting method by Ohigaski [5]. In the case of materials with $k^2Q_m<0.01$, it is difficult to obtain convergence by the first two methods. Further, method (4) listed above assumes that h_{33} is real.

In section II of this paper, the complex coefficient measurement technique is presented. The temperature/frequency dependence of the various coefficient are presented in section III, in addition, the real coefficients d_h, d_{33}, σ are also presented. In section IV, the results are summarized and discussed.

* This work was supported by the Research Center for the Engineering of Electronic and Acoustic Materials, The Pennsylvania State University

II Measurement Technique

The analytical solution for single vibration mode, assuming that all the piezoelectric, elastic and dielectric coefficients are complex, is as follows:

(1) Impendance of thickness mode (TE mode)

$$Z=1/(j\omega C_0)[1-k_t^2\tan b/b]=R+jX$$
$$R=D/(\omega C_0')+k_t'^2[\tanh(Jb'/2)\sec^2b'-(D+J/2+pH)\operatorname{sech}^2(Jb'/2)\tan b']/\{[1+\tan^2b'\tanh^2(Jb'/2)](\omega C_0'b')\}=R_0+R_d \quad (1)$$

(2) Admittance of length mode (LE mode)

$$Y=j\omega C_0\{1+k_{31}^2\tan b/[b(1-k_{31}^2)]\}=G+jB$$
$$G=\omega C_0'D+\{K\omega C_0'[D-J/2-pH(1+K)]\tan b'\operatorname{sech}^2(b'J/2)+\tanh(Jb'/2)\sec^2b'\}/\{b'[1+\tan^2b'\tanh^2(b'J/2)]\}=G_0+G_d \quad (2)$$
$$C=C_0'\{1+K/b'[\tan b'\operatorname{sech}^2(Jb'/2)+(D-J/2-pH(1+K))\tanh(b'J/2)\sec^2b']\}/[1+\tan^2b'\tanh^2(b'J/2)]=C_0'+C_d$$

Here, the subscript"0" stands for the static part,and "d" for the dynamic part. For the TE mode, all the complex coefficients are assumed as shown below:

$k_t=k_t'+jk_t''=k_t'(1+jPH)$,
$v=(c_{33}D/\rho)^{0.5}=[c_{33}D^*(1+jJ)/\rho]^{0.5}=v'(1+jJ)^{0.5}$
$b'=\omega T/(2v')$, $J=(\tan\delta_m)_D$, T is thickness.

For LE mode, $k_{31}=k_{31}'+jk_{31}''=k_{31}'(1+jPH)$, $K=k_{31}'^2/(1-k_{31}'^2)$, $v=[(1/\rho s^E(1-jJ)]=v'/(1-jJ)$, $b'=\omega L/(2v')$ L is length. Using the Mittag-Leffler theorem,

$$C_s=C_0'\{1+[(1-8/\pi^2)-0.145K]K/(1-K)\} \quad (3)$$

where, C_s is the capacitance when $f=f_s$. C_s can be obtained from the C vs. f curve. f_s is obtained from the G vs. f curve.See Figs 1-2. From C_s and G_0(or R_0), ε_{33}^s and $\tan\delta$ are obtained. From equation (1) or (2), selecting three frequencies f_1,f_2,f_3 on the R vs. f or G vs.f curve,the corresponding values of R_1,R_2,R_3 for TE mode(or G_1,G_2,G_3 for LE mode) can be obtained.Taking these values and using an iterative method, k_t' (or k_{31}'),PH and $\tan\delta_m$ can be obtained [6]. Since only three parameters are being determined, the convergence is very fast and easy. Further, velocity and elastic coefficients can also be obtained. All the complex coefficients are determined near by f_s in this technique.

Because of the low value k^2Q_m and the weak resonance peak, local amplification of the dynamic conductance G_d (or R_d) is necessary, see Fig. 1. In order to improve the accuracy, it is better to use the G (or R) vs. f curve than the C vs. f curve. It is necessary to separate the pure electrical conductance G_0 (or R_0) from the total conductance G (or R). The frequency selected for the iterative method are important. We suggest $f_1=f_s(1-0.2/Q_m)$, $f_2=f_s(1+0.2/Q_m)$, $f_3=f_s(1+0.1/Q_m)$. The schematic diagram of measurement equipment is shown in Fig. 3 .

Published at: IEEE Ultrasonic Symposium 1987, Denver, CO.

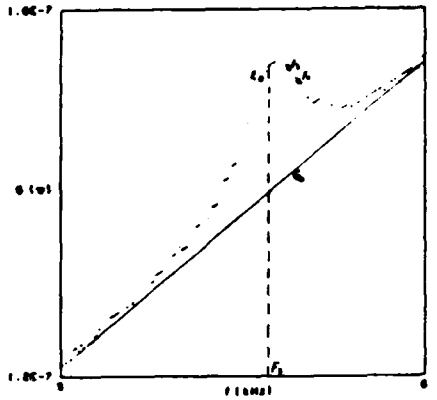

Fig.1, Conductance G vs. frequency f.

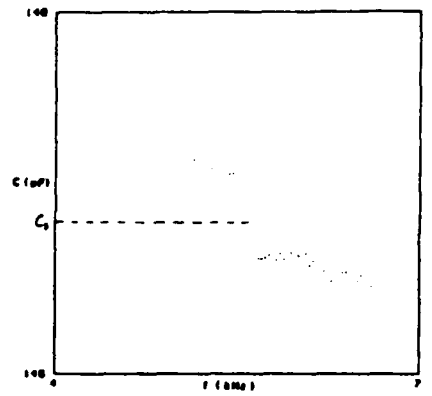

Fig.2, Capacitance C vs. frequency f.

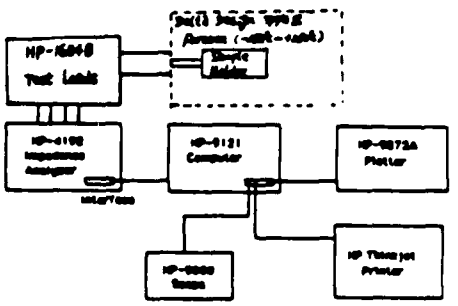

Fig.3, Schematic diagram of the measurement equipment.

The real coefficients d_h', d_{33}' are interesting for hydrophone application [7]. They can be obtained approximately as follow:

$$d_{33}'=e_{33}'/C_{33}'+(d_{31}'+d_{32}')\sigma/(1-\sigma),$$
$$d_h'=d_{33}'+d_{31}'+d_{32}' \qquad (4)$$

Using a square plate sample of PVDF, the poisson ratio σ can be obtained appoximately [8].

$$\sigma=(1-f_1^2/f_2^2)/[1+8f_1^2/(\pi^2 f_2^2)] \qquad (5)$$

here, f_1, f_2 are the first two resonance frequencies of the square sample.

III The Temperature/Frequency Dependence of the Property Coefficients of the Thick PVDF

Following the WLF equation for polymer, $\log\omega a_T=\log 2\pi f\cdot C_1(T-T_R)/[C_2+(T-T_R)]$. For the thick PVDF, let T_R=20°C, the coefficients C_1 and C_2, determined by dielectric measurement, are 6.2 and 118.6 respectively, therefore

$$\log a_T=-6.2(T-20)/(98.6+T)$$

a_T, being the shift factor, plotting $\log\omega a_T$ as the abscissa. we can represent the frequency dependence in a very wide range. Fig.4 shows the dielectric properties of TE mode (f:500 KHz-1000 KHz) and LE mode (f: 4 KHz-7 KHz). We see that two peaks have same $\log\omega a_T$ value, however, the vertical correction factor has not been considered here, therefore, the $\tan\delta_e$ for TE is higher than for LE [9].

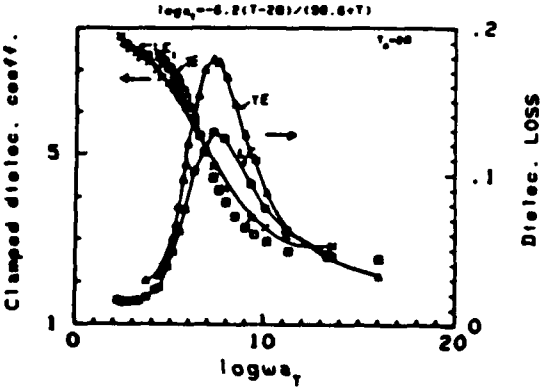

Fig.4, T and f dependence of dielectric coefficient.

The elastic properties behave in a similar fashion to the dielectric properties and are shown in Fig. 5 and have $s_{22}^E=1.5s_{11}^E$. The real part of e_{33}, e'_{33} is almost independent of frequency and temperature, its imaginary part shows a peak ($e''_{33}/e'_{33}=0.5$) at $\log\omega a_T=6$. The results show that h_{33} is complex; the peak value $h''_{33}/h'_{33}=0.6$. The coefficient d_{31} is shown in Fig.6, and $d'_{32}=d'_{31}/6$.

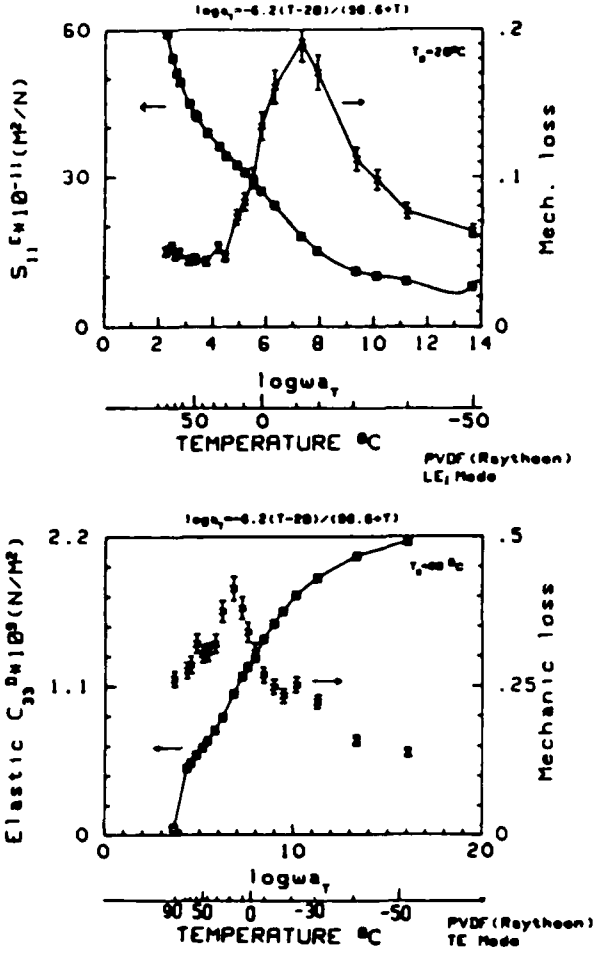

Fig.5. T and f dependence of elastic properties.

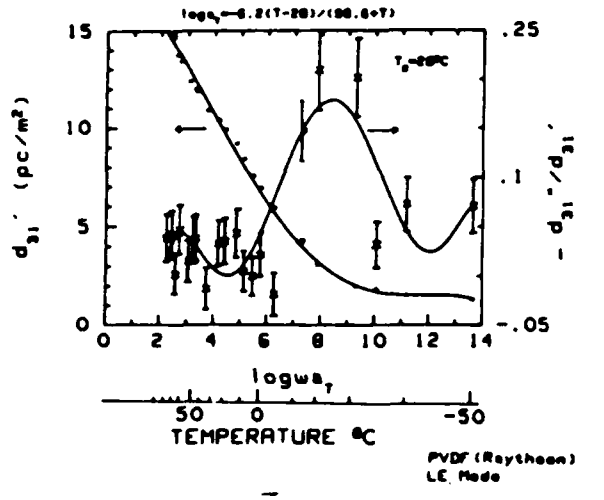

Fig.6. d vs. $\log\omega a_T$ and T.

Fig.7 shows the complex coupling coefficients. The loss tangent (k"/k') does not refer to the piezoelectric energy loss. It is as follows:

$$k''/k' = \tan\delta_A + \tan\delta_m - 2d''/d' \qquad (7)$$

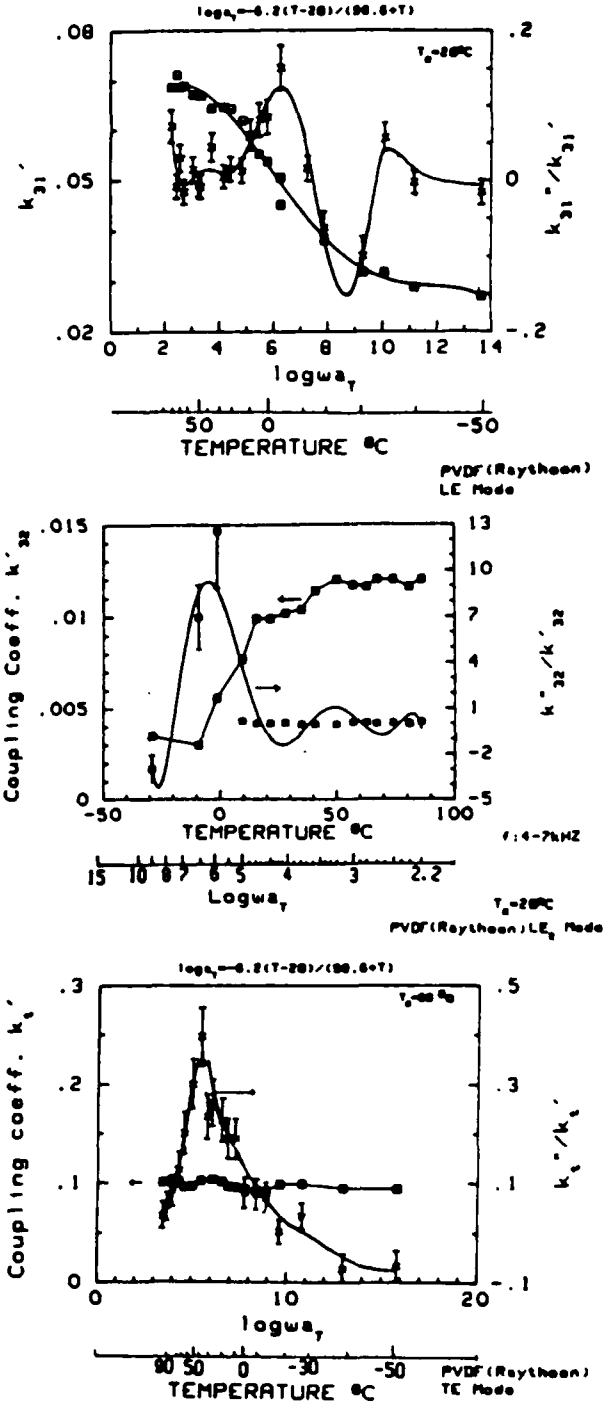

Fig.7, Coupling coefficients k vs. $\log\omega a_T$ and T.

The temperature dependences of d'_h, d'_{33} and poisson ratio σ are shown in Fig.8-9. This technique has also been used successfully for evaluating 0-3 composites, such as the NTK-306, the Celanese PTBF and fired composite (MRL).

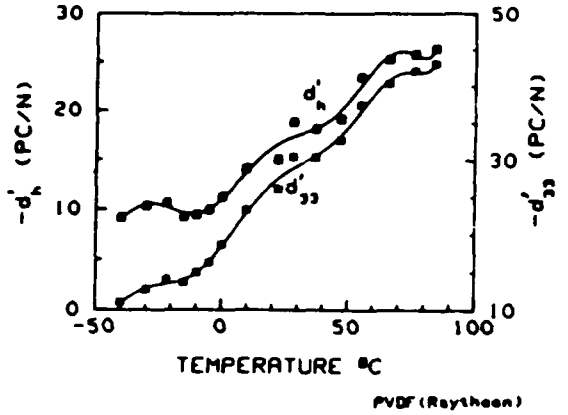

Fig.8, d_h' and d_{33}' vs. temperature.

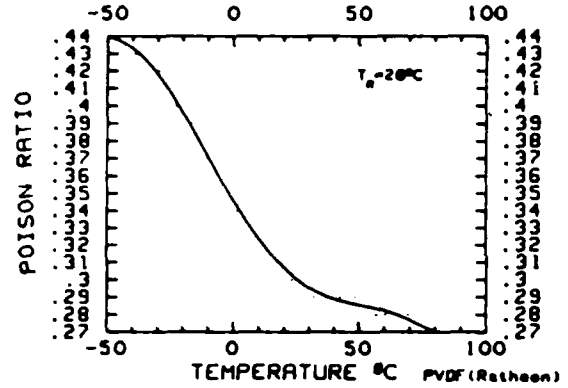

Fig.9, Poisson ratio σ vs. temperature.

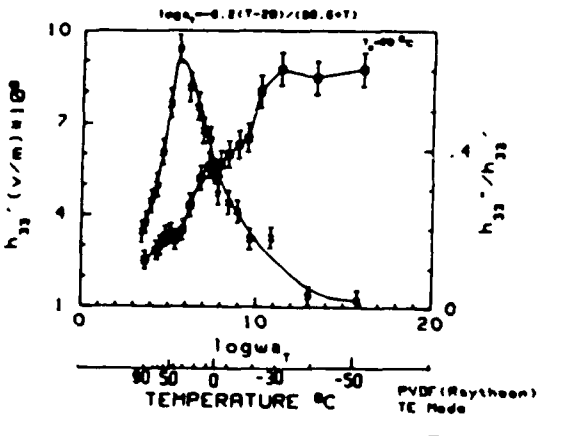

Fig.10 h_{33} vs. $\log\omega a_T$ and T.

IV. Summary

(1) This measurement technique is appropriate for PVDF and 0-3 composites (flexible ceramics) with $k^2Q_m>0.004$ and $Q_e>10$. The relative error in measurement can be <10% when the vibration mode is pure. This iterative process converges more easily than smits's method for low k^2Q_m sample. The choice of three frequencies is critical for convergence.
(2) This PVDF is a three phase structure with crystalline and amorphous regions and voids. The temperature dependence of poisson ratio (Fig.9) is probably due to the existence of void. In addition, e_{33} does not show marked temperature dependence as opposed to thin PVDF.
(3) The composite abscissa, $\log\omega a_T$, is convenient for considering the frequency and temperature dependence. The vertical correction factor needs to be obtained in future. The thick PVDF material exhibits high dielectric, elastic and piezoelectric loss near $\log\omega a_T$=6-8, this data is useful for designing piezoelectrical acoustic absorbers or vibration dampers.
(4) The results show that, h_{33} also is complex for thick PVDF, as shown in Fig.10

REFERENCES

1. R.E. Newnham, "Composite Electroceramics," Ann. Rev. Mat. Sci.16, 47-68 (1986)
2. R. Holland, "Measurement of Piezoelectric Phase in a Ferroelectric Ceramic," IEEE SU-17, 123-124 (1970)
3. J.G. Smits, "Iterative Method for Accurate Determination of the Real and Imaginary Parts of the Materials Coefficients of Piezoelectric Ceramics," IEEE SU-23, 393-402 (1976)
4. T. Furukawa et al., "Computer Controlled Apparatus for Measuring Complex Elastic, Dielectric and Piezoelectric Constants of Polymer Films," Rev. Sci. Instrum. 57, 2 (1986).
5. H. Ohigashi, "Elektromechanical Properties of Polarized Polyvinylidene Flouride Films as Studied by Piezoelectric Resonance Method," J. Appl. Phys. 47, No.3, 949 (1976).
6. Q.C. Xu, A.R. Ramachandran and R.E. Newnham, "Resonance Measuring Technique for Complex Coefficients of Piezoelectric Composites," (will be published on Jou.of Int. of Wave and Mat.)
7. R.H. Tancrell et al., "Properties of PVDF for Sonar," Proceedings of IEEE Ultrasonics Symposium pp. 624-629 (1985)
8. H. Ekstein, "Free Vibrations of Anisotropic Bodies" Physical Review V66 No.6 p108 (1944)
9. A. Klonis etc. "Introduction to Polymer Viscoelasticity", Wiley Interscience (1972)

Electrostriction Studies

Ferroelectrics, 1987, Vol. 76, pp. 241-267
Photocopying permitted by license only

RELAXOR FERROELECTRICS

L. ERIC CROSS
Evan Pugh Professor of Electrical Engineering and Director of the Materials Research Laboratory
The Pennsylvania State University, University Park, PA 16802

Abstract--This article attempts to review a number of macroscopic measurements which have been used to explore the electrical, mechanical, thermal, and optical characteristics of relaxor ferroelectrics and to authenticate the compositional heterogeneity model which was first proposed by G.A. Smolenskii to describe these materials. In this connection the work of N. Setter on order disorder in lead scandium tantate is discussed to clearly establish the role of compositional heterogeneity. To demonstrate the very wide temperature range above the dielectric permittivity maximum T_m over which large values of RMS polarization persists, electrostrictive spontaneous strain and quadratic electro-optic measurements on lead magnesium niobate and on the tungsten bronze structure ferroelectric barium strontium niobate are introduced. In order to validate the hypothesis that the polar micro regions which exist above T_m are in dynamical disorder, measurements of the field induced electrostriction are reviewed. From the aging behavior of suitably doped relaxor compositions it is suggested that because of internal heterogeneity local and global symmetries differ in the relaxor and the consequences of these differences are discussed with respect to the poling: depoling behavior and to the low temperature dispersion in lead barium niobate bronze structures.

INTRODUCTION

The relaxor ferroelectric may be distinguished from normal ferroelectric crystals by three distinct families of properties highlighted in (Fig. 1), which reviews the behavior of lead magnesium niobate $PbMg_{1/3}Nb_{2/3}O_3$ (PMN) a typical relaxor composition. In the dielectric response (Fig. 1a) the weak field dielectric permittivity reaches a high peak value ~ 20,000 typical for a ferroelectric perovskite near T_c, but the dielectric maximum clearly does not mark a phase change into a ferroelectric form as the temperature of the maximum increases with frequency in a manner typical of a relaxation dielectric. The associated maximum in ϵ'' ($\tan\delta$) is also typical of relaxor response.

From behavior in high alternating fields however, it is clear that the PMN is ferroelectric at low temperature with bona-fide dielectric hysteresis, a necessary and sufficient condition. However, we note again from Fig. 1b that the hysteretic response slowly degenerates into just nonlinearity as the temperature increases, i.e., that the spontaneous polarization is not suddenly lost at the T_c of a first or second order transition but decays more gradually to zero.

Perhaps the most startling behavior is that to longer coherence length probing radiations where samples cooled to very low temperature show no evidence of optical anisotropy, or of the x-ray line splitting which would be characteristic of a macro-volume changing to a polar phase (Fig. 1c).

An explanation which has been offered for these relaxor ferroelectric behaviors by G.A. Smolenskii (1) is that in for example $PbMg_{1/3}Nb_{2/3}O_3$ the Mg and Nb ions do not order, so that

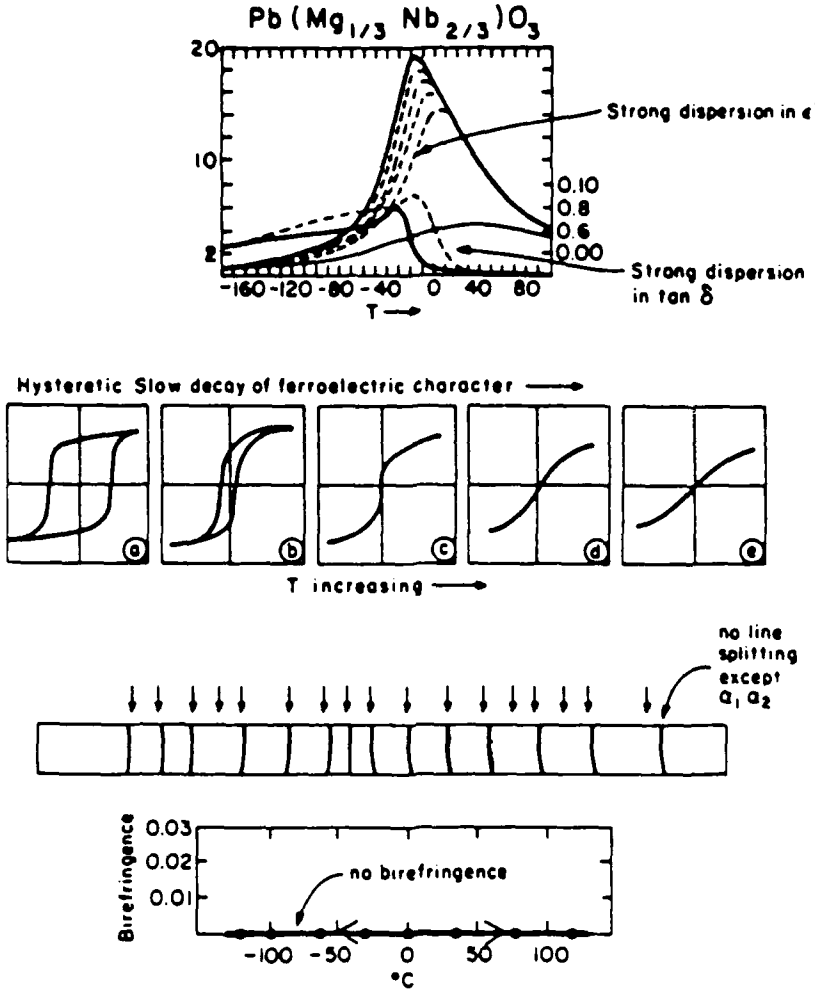

Figure 1. Characteristic features of a ferroelectric relaxor.

Figure 1a. Dielectric dispersion in Lead Magnesium Niobate (PMN) as a function of temperature and frequency.

Figure 1b. Dielectric hysteresis in PMN as a function of temperature.

Figure 1c. Optical and x-ray evidence for the absence of a macroscopic phase change below the Curie maximum (T_c).

across any trace in the crystal there are fluctuations in Mg: Nb concentration. It is suggested that these statistical composition fluctuations lead to large fluctuations in the Curie temperature Fig. 2a, and that thus over a wide temperature range there is an intimate mixture of ferroelectric (Polar) and para-electric (Non Polar) regions, with the balance becoming steadily more polar as the temperature is reduced. Clearly, if the scale of the heterogeneity is of order 100-200 A^{o} as proposed and the polar directions set in at random over the available domain states (8 states for the polar phase in rhombohedral PMN) then for interrogation by a probing radiation such as x-ray or optical frequency, the random array will still reflect the prototypic cubic symmetry.

A second potential facet of behavior which was not in the original Smolenskii model appears if one considers the likely stability of very small polar micro regions. Using Devonshire or a similar formalism the free energy as a function of polarization for one of the polar regions must appear as in Figure 2b. For a domain of macroscopic volume, the energy full separating alternative domain states is many many times kT and the domain is quite stable. Since however, ferroelectricity is a cooperative phenomenon, all energies scale with the volume so that on continued scale reduction (near a dimension of $(100\ A^{o})^{3}$ for a typical perovskite) the barrier in ΔG becomes comparable to kT and the polar region unstable against thermal aggitation.

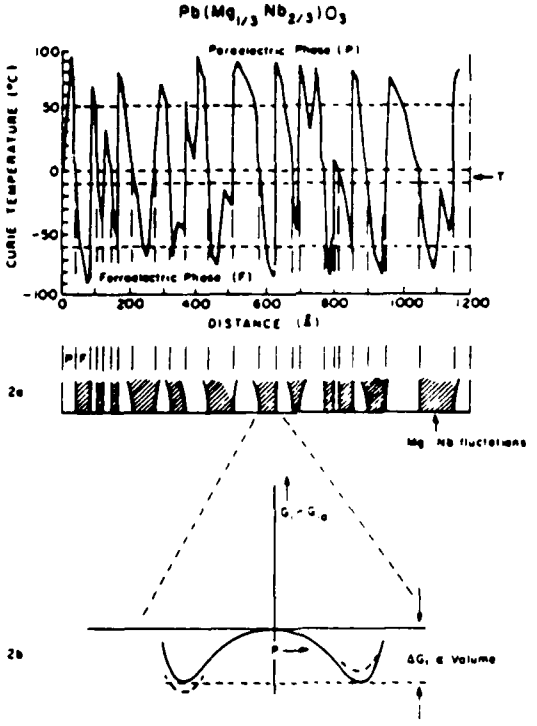

Figure 2a. One-dimensional illustration of the Smolenskii model of compositional heterogeneity giving rise to wide fluctuations in Curie temperature over a short scale.

Figure 2b. Schematic illustration of the Elastic Gibbs Free Energy in one of the polar micro regions.

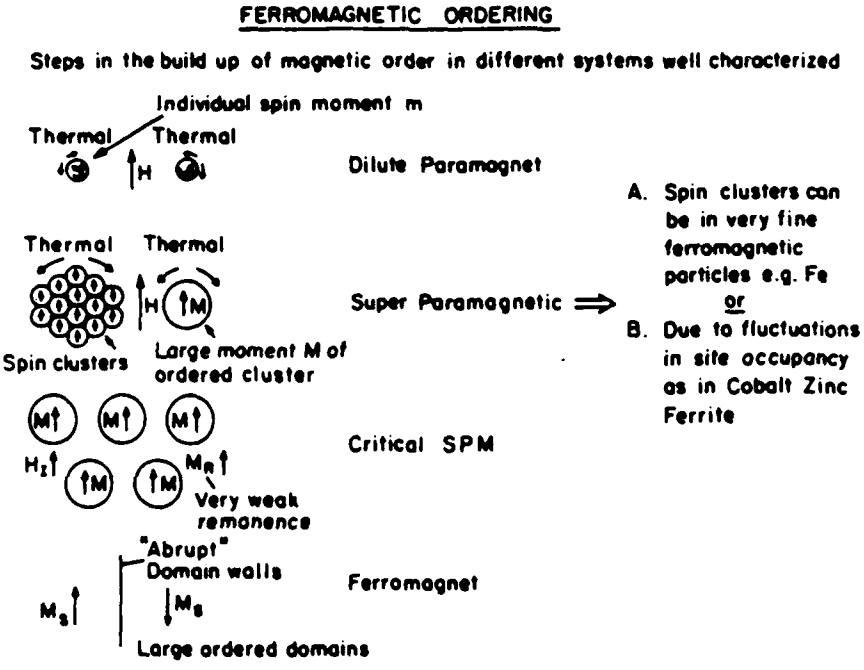

Figure 3. Schematic illustration of the build-up of magnetic ordering with scale in a simple Ferromagnetic system.

In magnetism, the build-up of ordered states from isolated spins is well understood (Fig. 3) and the superparamagnetic state in which small ordered spin clusters establish an inadequate magnetocrystalline anisotropy energy to remain stable against thermal motion is well documented. For the build-up of ferroelectric order no such detailed scheme has yet been delineated, however, it is tempting to suggest that the small polar micro-volumes postulated to exist in the relaxor ferroelectric could over some range of sizes, be unstable in a similar manner, giving rise to analogous superparaelectric properties.

To prove out the Smolenskii model for the perovskite relaxor, and to explore the added caveat of potential superparaelectric behavior, three questions need to be answered.

1. Are fluctuation in the concentration of B_1, B_2 cations responsible for the diffuse nature of the phase change in a $Pb(B_1, B_2)O_3$ perovskite relaxor ferroelectric?

2. Is there direct evidence for a substantial value of $\sqrt{P^2}$, the RMS polarization at temperatures well above the dielectric maximum (T_c)?

3 Are the polar regions in this high temperature range 'flipping' in orientation as in the superparamagnet or are they fixed in orientation?

It would appear that each of these questions can now be answered in the affirmative. However, aging studies in pure and doped materials confirm that the simple model of a perfect microcrystal in a co-joining high permittivity matrix phase is inadequate and that as might be expected the symmetry of the local region is lower than that of the bulk. This difference between local and

global symmetries has important consequences not only in the aging behavior, but also in the manner in which global polarization builds up under electric field, the grain size and thickness dependence of the permittivity and on the behavior of $(Pb_{1-x}Ba_x)Nb_2O_6$ crystals at compositions close to the tetragonal: orthorhombic morphotropic phase boundary.

THE ROLE OF MICROHETEROGENEITY

A critical test for the Smolenskii model would be to find a system exhibiting ferroelectric properties which could, without changing composition, be taken from a completely homogeneous (regular) distribution of cations upon the B site of a $Pb(B_1B_2)O_3$ perovskite to a completely random distribution which must then show local heterogeneity. The idea is depicted schematically in two dimensions in Fig. 4. The schematic in Fig. 4a was developed by tossing a coin and recording the head (black) and the tail (white) dots on a regular lattice--clearly there are large black/white heterogeneities. If however, that structure is ordered Fig. 4b, full translational symmetry is recovered, and the composition is completely uniform down to the unit cell scale. If the Smolenskii hypothesis is correct we expect to see diffuse, dispersive relaxor behavior in the disordered state, and sharp normal ferroelectric transitions in the fully ordered state.

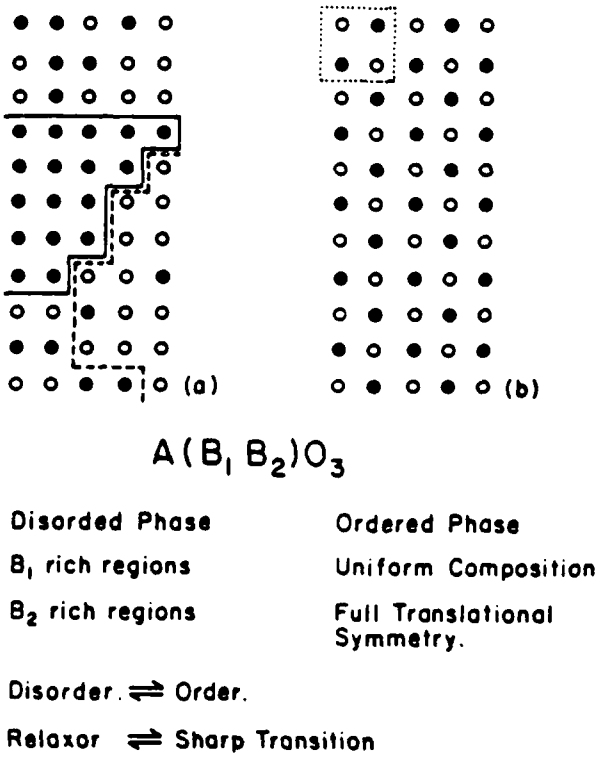

Figure 4. Two-dimensional illustration of order-disorder in a hypothetical B_1:B_2 system, and expected consequences for $Pb(B_1:B_2)O_3$ perovskite.

Studies by N. Setter (2) and A.J. Burggraaff (3) lead to the discovery and evaluation of order disorder in $Pb(Sc_{1/2}Ta_{1/2})O_3$ (PST). Because of the large difference in x-ray scattering the degree of order in the crystal or ceramic can be evaluated from the superlattice reflection which appears as a consequence of the doubling of all dimensions of the unit cell (Fig. 5). Also, by comparing the width of base lattice and superlattice reflections the size of the ordered domains may be estimated.

The major conclusions of the PST study are summarized in Fig. 6 which exhibits the structures for ordered and disordered forms and the manner in which with on ordering the dispersion is lost, the depolarization becomes much more abrupt and the optical properties revert to those of a normal macrodomain ferroelectric exhibiting clear optical anisotropy below the Curie temperature.

Recently more direct confirmation of the order disorder behavior in PST has been obtained by C. Randal et al., as discussed in another article in this journal, where the ordered lead ion displacements in the crystal which carry the ferroelectric response of the ordered state have also been identified.

The conclusion then regarding the first question is tabulated in Table 1 and confirms the original Smolenskii model.

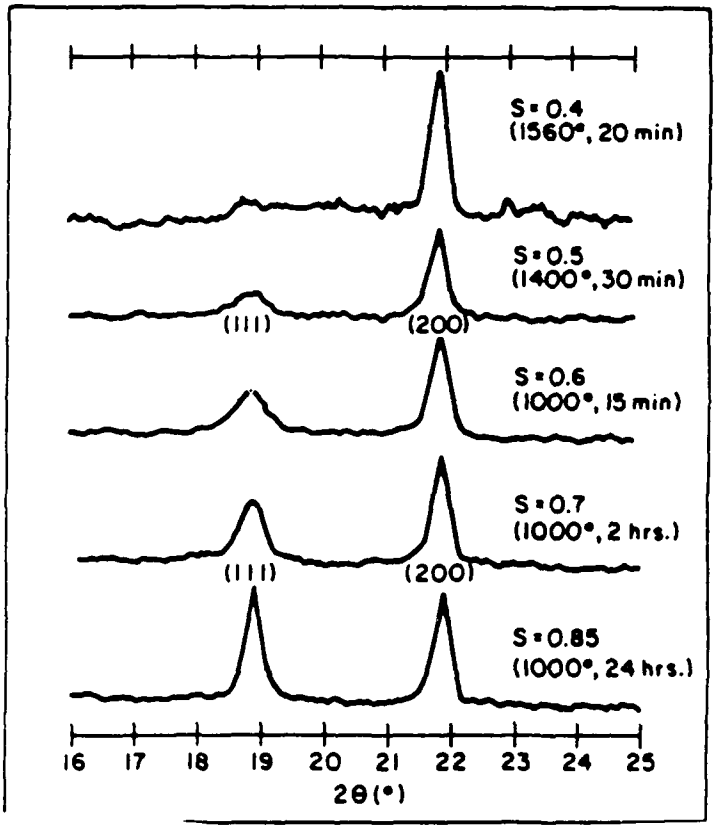

Figure 5. Superlattice line intensity as a function of annealing time in $Pb(Sc_{1/2}Ta_{1/2})O_3$ showing change from disorder to order with thermal annealing.

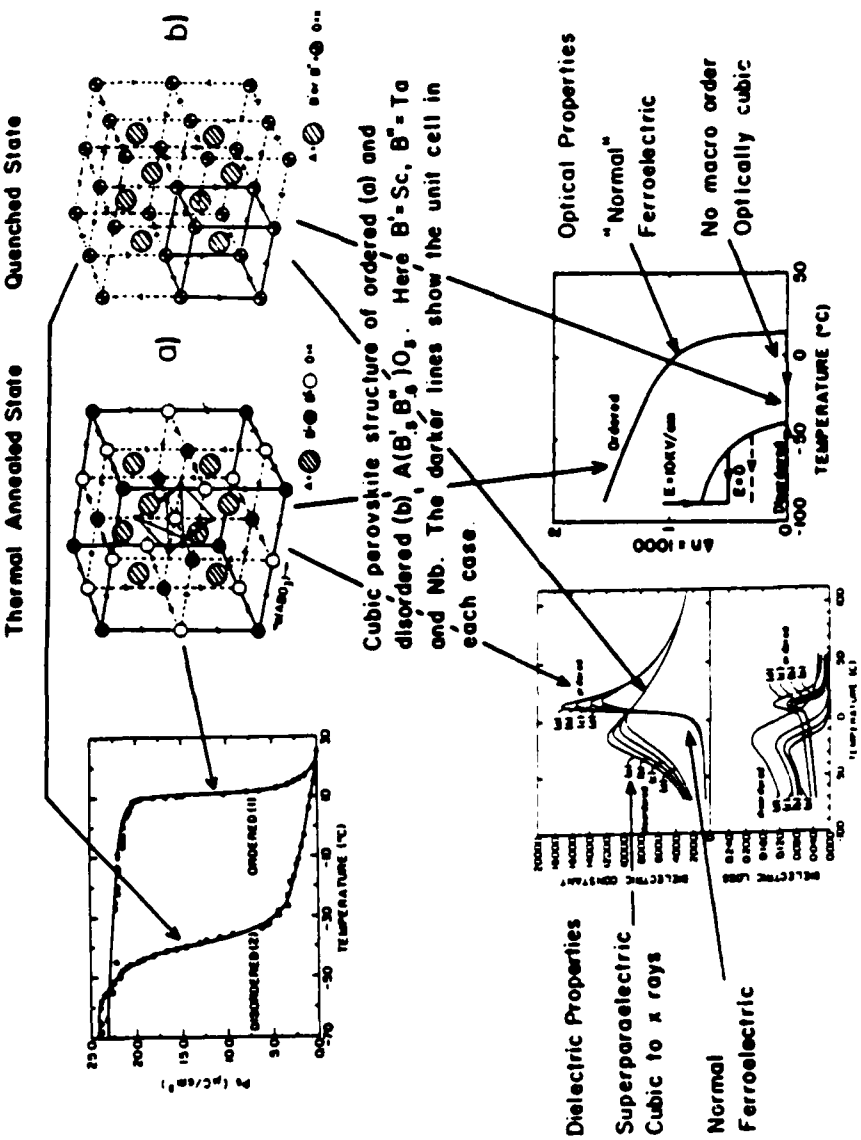

Figure 6. Illustration of the major differences in properties between highly ordered and disordered $Pb(Sc_{1/2}Ta_{1/2})O_3$.

TABLE 1

Conclusion from the experiments upon cation ordering in $PbSc_{1/2}Ta_{1/2}O_3$.

In $PbSc_{1/2}Ta_{1/2}O_3$

For the Annealed Cation Ordered State - no cation composition fluctuations.

Normal Ferroelectric Properties

1) Sharp 1st order change at T_c
2) Stable remanent polarization
3) No frequency dependence at radio frequencies in ferroelectric state
4) Stable birefringence
5) Rhombohedral

For the Quenched Cation Disordered State - must have statistical fluctuations in Sc:Ta distribution on B

Superparaelectric Properties

1) Diffuse phase change
2) No stable remanence
3) Strong frequency dependence
4) No stable birefringence
5) Cubic macro symmetry to both x-rays and optical frequencies

THE PERSISTENCE OF MICRO POLAR REGIONS ABOVE T_c

To address the second question it is useful to focus attention upon properties of the crystal which are controlled by the square of the electric polarization P^2. Clearly if random + - fluctuations occur in P above T_c, $P = 0$ but $P^2 \neq 0$, i.e., a property which depends on P^2 should begin to be affected at temperatures well above T_c.

In PMN, electrostrictive strain is given by

$$x_{11} = Q_{11}P^2_1 + Q_{12}P^2_2 + Q_{12}P^2_3 \quad a$$
$$x_{22} = Q_{12}P^2_1 + Q_{11}P^2_2 + Q_{12}P^2_3 \quad b$$
$$x33 = Q_{12}P^2_1 + Q_{12}P^2_2 + Q_{11}P^2_3 \quad c \qquad 3.1$$
$$x44 = Q_{44}P_2P_3 \quad d$$
$$x55 = Q_{44}P_2P_3 \quad e$$
$$x66 = Q_{44}P_1P_2 \quad f$$

Looking now at the thermal expansion in PMN, above a temperature $T_o \sim 350^o$ C, the thermal expansion follows a normal linear law of the form (Fig. 7).

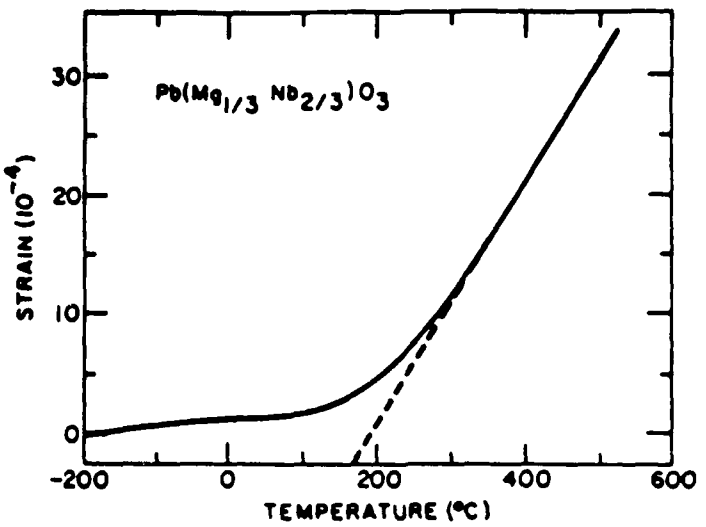

Figure 7. Thermal strain S_{11} vs. temperature for ceramic $Pb(Mg_{1/3}Nb_{2/3})O_3$.

$$\ell_T = \ell_0(1 + \alpha(T - T_0)) \qquad 3.2$$

where ℓ_T = length at T
ℓ_0 = length at T_0

α = thermal expansion coefficient

Clearly the thermal strain

$$x_{11} = x_{22} = x_{33} = \frac{\ell_T - \ell_0}{\ell_0} = \alpha(T - T_0) \qquad 3.3$$

Below 350° C, the rate of thermal contraction reduces continuously. If we attribute this reduction to the electrostrictive consequence of an escalating RMS P_s below 350° C. The strain produced is given by

$$x_{11} = x_{22} = x_{33} = (Q_{11} + 2Q_{12})P^2 \qquad 3.4$$

and since in PMN ($Q_{11} > -2Q_{12}$) the set electrostrictive strain is dilatational. Thus the total strain (thermal and electrostrictive) will be

$$x_{11T} = x_{22T} = x_{33T} = -\alpha(T_0 - T) + (Q_{11} + 2Q_{12})P^2_s \qquad 3.5$$

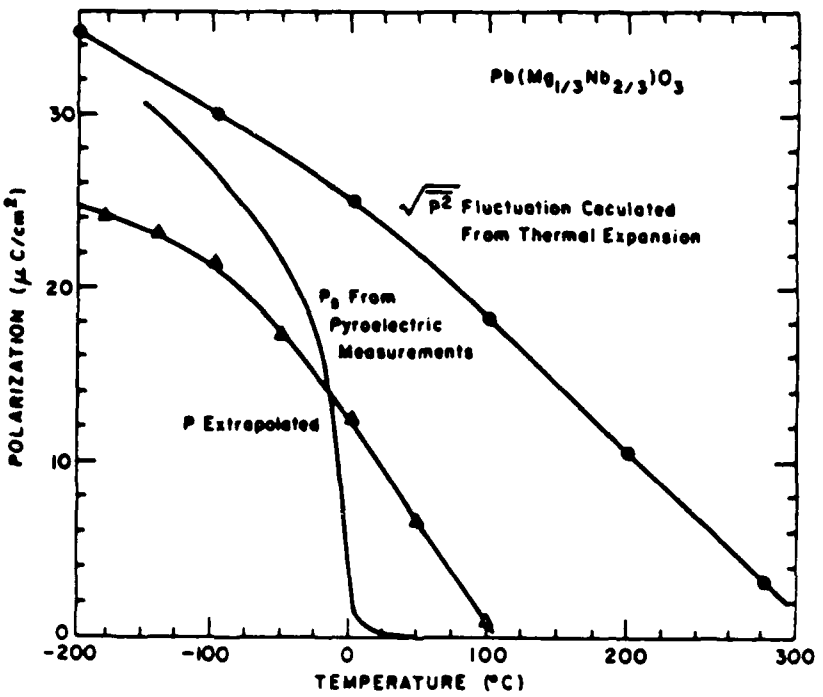

Figure 8. Calculated values of RMS polarization $\sqrt{P^2}$ derived from thermal strain data compared to hysteresis and pyroelectric measurements of P_s in ceramic PMN.

If the total thermal effect x_{11T} is measured then equation 3.5 may be rearranged to give

$$P^2_s = \frac{x_{11T} + \alpha(T_o - T)}{(Q_{11} + 2Q_{12})} \qquad 3.6$$

From known values of Q_{11} and Q_{12} and the higher temperature α the temperature dependence of P^2_s may be deduced. Figure 8 compares the calculated $\sqrt{P^2}_s$ against P_s measured from pyroelectric depolarization, and against an extrapolated P determined earlier from dielectric hysteresis by G.A. Smolenskii et al. (4). Evidentally $\sqrt{P^2}_s$ has substantial values well above the T_c given by the dielectric maximum in weak field permittivity.

The tungsten bronze structure crystal $(Ba_{0.40}Sr_{0.60})Nb_2O_6$ is also a relaxor ferroelectric due to fluctuations in the distribution of Ba and Sr over the five-fold and four-fold tunnels in the structure Fig. 9. Excellent single crystals of the 60:40 composition are available from a careful continuing growth program at Rockwell (R.R. Neurgaonkar 5,6,7).

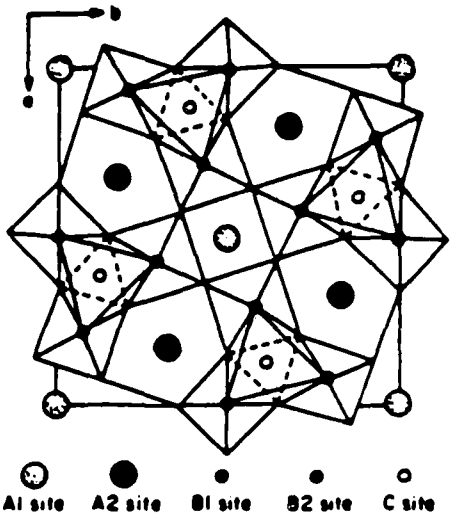

Site occupancy of some ferroelectric tungsten-bronze-type structures

Formula	A1	A2	C	B1	B2
$Ba_xSr_{5-x}Nb_{10}O_{30}$ ($x \approx 1.38$)	≈1.64 Sr	≈1.38 Ba ≈2.01 Sr	0	2 Nb	8 Nb
$Ba_{4+x}Na_{2-2x}Nb_{10}O_{30}$ ($x = 0.13$)	1.74 Na 0.13 Ba	4 Ba	0	2 Nb	8 Nb
$K_{6-x-y}Li_{4+x}Nb_{10+y}O_{30}$ ($x = 0.07$, $y = 0.23$)	1.75 K 0.25 Li	3.95 K 0.05 Li	3.77 Li 0.23 Nb	2 Nb	8 Nb

After Abrahams et al. 1971

Figure 9. Projection normal to the tetragonal c axis of the structure of $Ba_xSr_{1-x}Nb_2O_6$, illustrating the cation mixing on the A_1 and A_2 sites in the Tungsten Bronze structure ferroelectrics.

For the tetragonal tungsten bronze, the prototype symmetry is 4/mmm and the electrostrictive coupling takes the form

$$x_{11} = Q_{11}P^2_1 + Q_{12}P^2_2 + Q_{31}P^2_3 \quad a$$
$$x_{22} = Q_{12}P^2_1 + Q_{11}P^2_2 + Q_{31}P^2_3 \quad b$$
$$x_{33} = Q_{13}P^2_1 + Q_{13}P^2_2 + Q_{33}P^2_3 \quad c \qquad 3.7$$
$$x_{44} = Q_{44}P_1P_3 \quad d$$
$$x_{55} = Q_{44}P_1P_3 \quad e$$
$$x_{66} = Q_{66}P_1P_2 \quad f$$

In this crystal the ferroelectric symmetry is 4 mm so that polar fluctuations are largely $\pm P_3$ giving

$$x_3 = Q_{33}P^2_3 \qquad 3.8$$

Similarly for the transverse strain

$$x_{11} = x_{22} = Q_{31}P^2_3 \qquad 3.9$$

Typical thermal expansion data for c axis (3) orientation is given in Fig. 10a and again the temperature dependence of P^2_3 may be deduced from the departure from linearity below 350° C.

In 60:40 SBN, the high quality of the crystals now permit the use of the quadratic electro-optic effect to deduce P^2_3 from the temperature dependence of the optical birefringence, i.e.,

$$\Delta n = -1/2\, n_o^3(g_{33} - g_{31})P^2_3 \qquad 3.10$$

Again above 350° C Δn is a linear function of T of the form.

$$\Delta n = \Delta n_o + \beta(T - T_o) \qquad 3.11$$

Following the electrostriction relation then

$$P^2_3 = -\frac{\Delta nT - \Delta no + \beta(T - T_o)}{1/2 n_o^3(g_{33} - g_{31})} \qquad 3.12$$

The behavior of the optical birefringence for single crystal SNB 60:40 is given in Fig. 10b. Since both electrostriction and quadratic electro-optic constants are known for 60:40 SBN two independent checks for $\sqrt{P^2_3}$ can be made. Figure 11 compares deductions from opucal and electrostrictive measurements to the temperature dependence of P_3 deduced from pyroelectric studies (8). It is quite evident again that very substantial values of $\sqrt{P^2_3}$ exist for a wide range of temperature above T_c.

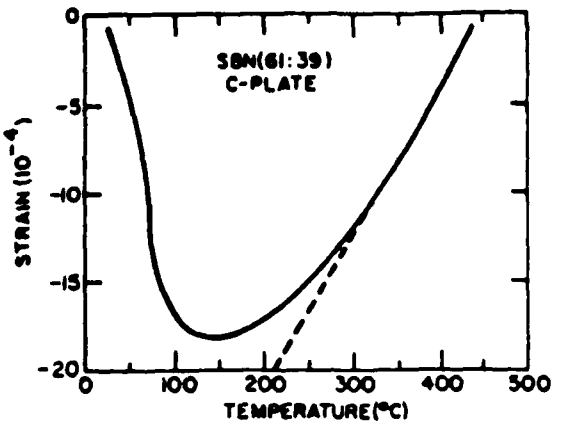

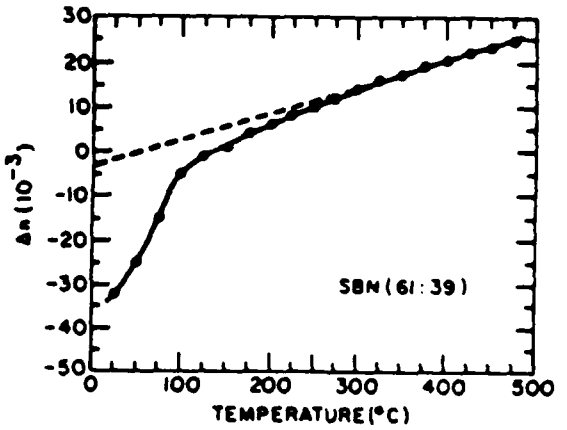

Figure 10a. Thermal strain measurements along the tetragonal c axis in single crystal SBN of composition $Ba_{0.39}Sr_{0.61}Nb_2O_6$.

Figure 10b. Optical birefringence Δn of an 'a' plate of SBN 61:39 as a function of temperature.

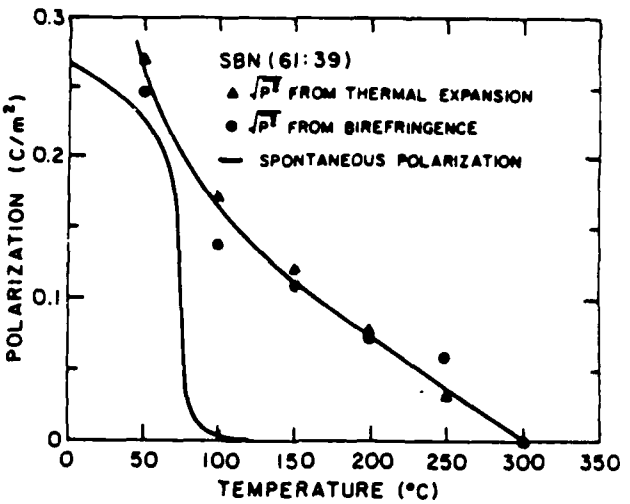

Figure 11. RMS polarization $\sqrt{P^2}$ deduced from thermal strain and optical birefringence data in single crystal SBN 61:39 compared to pyroelectric measurements of $\bar{P}_3$.

DYNAMICAL DISORDER IN RELAXORS

The third and probably most difficult question concerns the nature of the polar micro regions which clearly must exist for a wide (200° C) temperature range above T_c. Is the polarity static, leading to a glass-like structure, or is the disorder dynamical with polar micro regions undergoing switching between different orientation states as in the superparamagnet.

Some indirect evidence for dynamical disorder may be adduced from the mode of break-up of long-range polar order induced by electric field at low temperature. The fact that order 'unpicks' slowly on heating, and is not re-established on cooling suggests that polar micro regions can switch out of long range order at temperatures well below T_c. Above T_c additional evidence for dynamical disorder can be obtained by measurement of the induced electrostrictive strain. We have demonstrated that polar micro regions do exist for a range of temperature above T_c in the uniaxial $(Ba_{0.4}Sr_{0.6})Nb_2O_6$ bronze. Thus in this temperature range under external E field applied in the '3' (3) direction, there will be two very different mechanisms contributing to the electric polarization; (1) modulation of the switching of already polar micro regions by the external field (2) change of the intrinsic polarization in the micro region, in nonpolar regions and change of the volume of micro regions. Since as is evident from Figure 10a, the crystal has already adjusted its shape to the occurrence of P_s in the micro region and as $+P_s$ and $-P_s$ states have the same strain, mechanism (1) is not shape changing and would thus give zero contribution to electrostriction mechanisms (2) on the other hand, involves the induction of new polarization and are thus shape changing and contributing to electrostriction. If mechanism (1) becomes important in the temperature range above T_c, a measurement of the induced strain in this temperature region should show anomalously low values for electrostriction constant Q_{33}.

Polar micro regions must have P_s vectors which are dominantly along the four-fold axis so that switching of polar micro regions should not be induced by a field E_1 and Q_{11} should be normal.

Figure 12a,b shows measurements of Q_{33}, Q_{31} as a function of temperature and it is evident that the values are anomalously small approaching zero close to T_c. Measurements of Q_{11} on the other hand, show values which are quite normal, Fig. 11c.

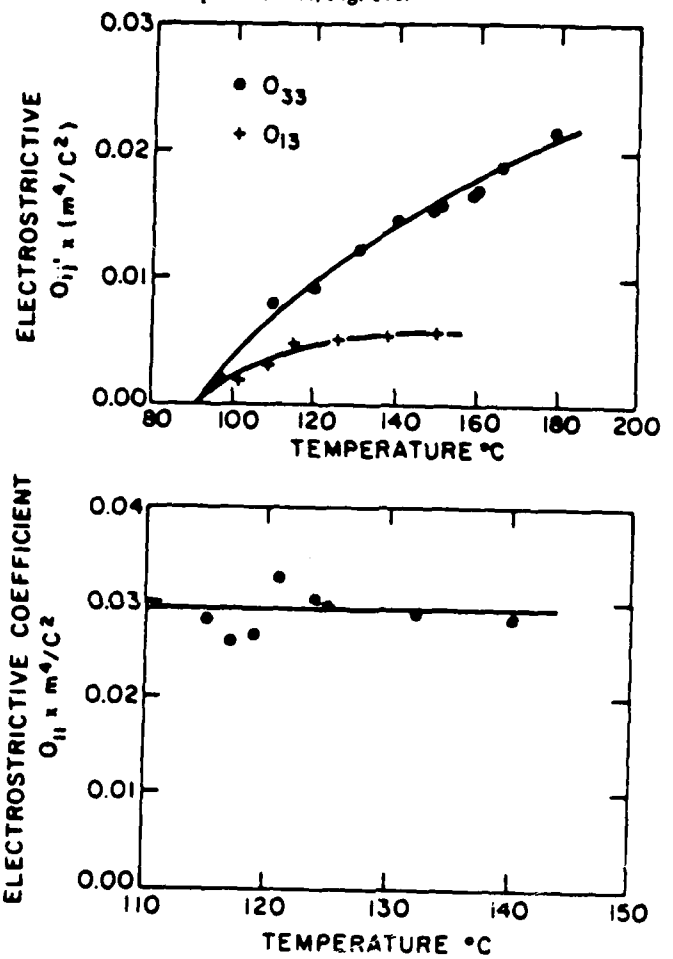

Figure 12. Measurements of induced electrostrictive strain in single crystals of SBN 61:39.

Figure 12a,b. Q_{33} and Q_{31} as a function of temperature.

Figure 12c. Q_{11} as a function of temperature.

PRELIMINARY CONCLUSION

From the evidence discussed it is suggested:

Fluctuations in the concentration of B_1B_2 cations on the B site of suitable $Pb(B_1B_2)O_3$ perovskites are responsible for the relaxor behavior.

The RMS polarization P^2 has substantial values at temperatures more than 200° C above the mean Curie point T_c.

The micro polar regions in the higher temperature region are being dynamically disordered by thermal motion.

Relaxor ferroelectrics are in some ways electrical analogues of the well-known superparamagnets.

CONSEQUENCES OF DIFFERING LOCAL AND GLOBAL SYMMETRY

Introduction

The original naive model for the expectation that polar micro regions should be undergoing dynamically disordering in the thermal field was based on consideration of a simple Landau:Ginsburgh:Devonshire (LGD) model for the multiaxial PMN ferroelectric in which the appearance of a polar vector along any one of the <111> directions would lead to a minimum in the energy of a certain value of P (P_s).

Clearly in the infinite perfect crystal all (111) directions are identically equivalent by symmetry and all energy minima are of equivalent depth, Fig. 13. Questioning now what dictates the magnitude

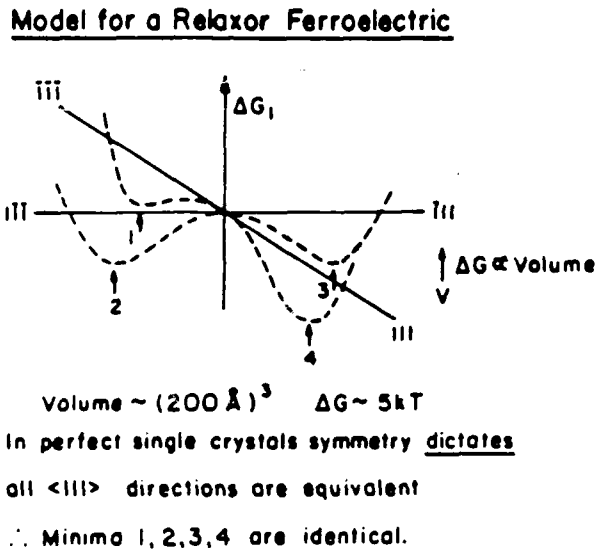

Figure 13. Sketch of Elastic Gibbs Free Energy ΔG_1 vs. polarization P for four of the eight equivalent <111> orientations in a perovskite ferroelectric in the rhombohedral phase.

of the energy hills between domain states it is evident that neglecting surface terms, the energy ΔG is proportional to the volume and that for a simple perovskite ferroelectric with Curie point close to 250^{o} C $\Delta G \sim 5$ kT when the volume approached $(200\ A)^3$.

In the relaxor ferroelectric, it is expected that the small micro polar regions are delineated by composition fluctuations which dictate strong local fluctuations in T_c. On this model however, (Fig. 1) it is very unlikely that the surrounding of each micro polar domain retains cubic or spherical symmetry. For example, in two dimensions (Fig. 14) it may be expected that composition gradients on each side of the micro region will not be identical and thus that the energy minimum for the 111 direction may be dissimilar to that for the $\bar{1}\bar{1}\bar{1}$ direction.

Generally then it must be expected that due to heterogeneity, the local symmetry will be lower than the global symmetry and for each polar micro region, the orientation states which must be identical in both energy and orientation in the perfect crystal are now inequivalent in the local domain.

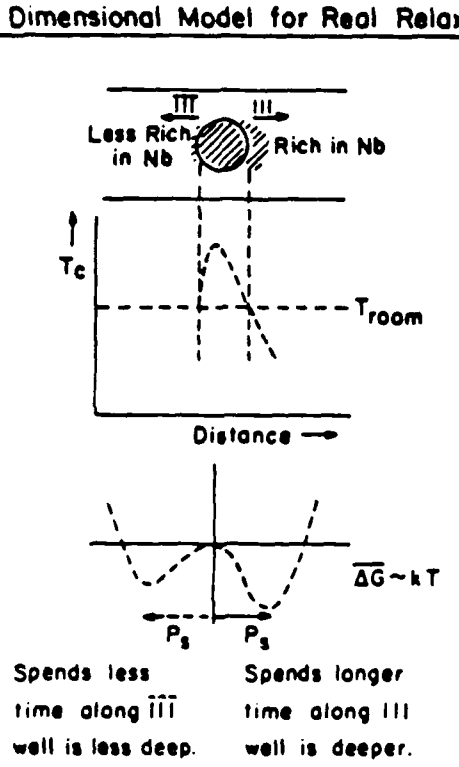

Figure 14. One-dimensional illustration of the expected departure from global crystal symmetry for a polar micro region delineated by a highly asymmetric composition profile.

Several important consequences ensue from this symmetry lowering.

1. If local minima are of differing depth and the polar region is of a size to permit dynamical disordering, the polar vector will spend longer time in the deepest minimum so that the micro region will have a net (weak) polar moment.
2. Crystal surfaces and grain boundaries in ceramics, will modify the symmetry for micro regions close to the bounding surface, unbalancing the potential distribution of vector states and thus probably reducing the fluctuation component of the polarizability.
3. Polar vector directions may be perturbed from the family of orientations dictated by the global symmetry and particularly in uniaxial systems, if the axial constant weakens off axis minima may become stable leading to unexpected dispersions in the dielectric response.

Aging Behavior

PMN and its solid solutions with lead titanate (PT) have been used for some time in surface deformable mirror technology because of the stability of dimensions, low effective thermal expansion (Fig. 7) and high electrostriction. The absence of a stable orientation for the micro polar regions at temperatures near T_c avoids problems with aging and self-stabilization in normal ferroelectrics and the fact that PMN is a stoichiometric compound means that with care it can be prepared without aliovalent defects. The fact however, that differences between local and global symmetry will give weakly preferred directions for P_s in the polar micro regions means that polar defects should be able to readjust to further stabilize P_s in the larger micro regions and thus to reduce the relaxation component of permittivity and of strain.

Pure PMN: 10% PT the electrostrictor composition of most interest can be prepared so as to exhibit no aging even after 1,000 hours at 25° C (Fig. 15a). Doping with 0.1 wt% MnO introduces a strong aging of the relaxation component of K^I and K^{II} (Fig. 15b) with the dispersive component being preferentially removed (Fig. 15c) but being recovered on cooling to temperatures below the aging temperature. Aging is obviously not a log: linear relation as in normal ferroelectrics, Fig. 16a and the magnitude depends strongly on the doping level, Fig. 16b.

From a plot of K^I vs. K^{II} over the full aging period, Fig. 17 following the method of Arlt it is evident that a broad range of relaxation times is involved and if as in normal ferroelectrics the intrinsic polarizability is almost loss free, it is evident that as expected the relaxation carries a major fraction of the total permittivity.

The aging behavior becomes explicable if we postulate that as in normal ferroelectrics polar defects will slowly readjust their orientation so as to lower the energy and stabilize existing domain states. In the Mn doped PMN: PT, Mn^{3+} with associated oxygen vacancies will form a defect dipole pair which can reorient by motion of the oxygen vacancy. Due to the lower local symmetry, polar micro regions will have a weakly preferred orientation which will act to reorient defects, further stabilizing the polar vector. Clearly larger regions which 'flip' less frequently will stabilize first so that longer relaxation times will be preferentially lost.

If as in normal ferroelectrics, aging is by volume stabilization of polar regions. Heating the sample does not introduce new polar regions and the dispersion stays low. Cooling the crystal below the aging temperature however, will introduce new unstabilized micro regions and dispersion is recovered. As in a normal ferroelectric, orientation of the defect structure is energetically equivalent to applying an internal electrical bias favoring the existing domain state.

For the relaxor ferroelectric, aging under DC bias provides an interesting way to quantify this pseudo bias. Aging under DC bias, short circuiting, then cooling without bias in a suitably doped relaxor (Fig. 18) leads to a poled condition where the poling has been induced by the oriented effective internal field E_D. Comparing poling levels with simple DC poling of freshly deaged samples shows that $E_D \sim 2.5$ Kv/cm which is consistent with the expectation.

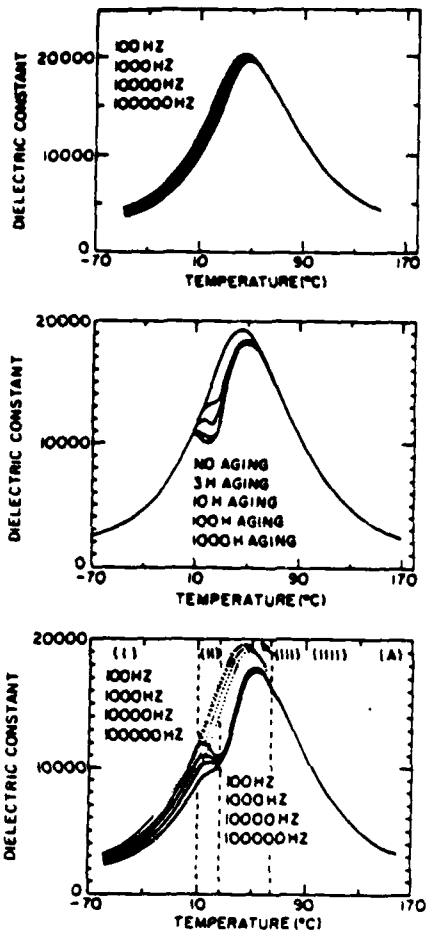

Figure 15. Aging behavior in pure and in 'doped' lead magnesium niobate: lead titanate (PMN:PT) solid solutions.

Figure 15a. Pure stoichiometric PMN:10% PT material showing no aging up to 1,000 hours at room temperature.

Figure 15b. Aging behavior of PMN:10% PT doped with 0.1 wt% MnO. Dielectric response K' vs. T after aging for different times at 20° C.

Figure 15c. Aging behavior of PMN:10% PT doped with 0.1 wt% MnO showing preferential aging of the dispersive component of K' which is however recovered for temperatures below the aging temperature.

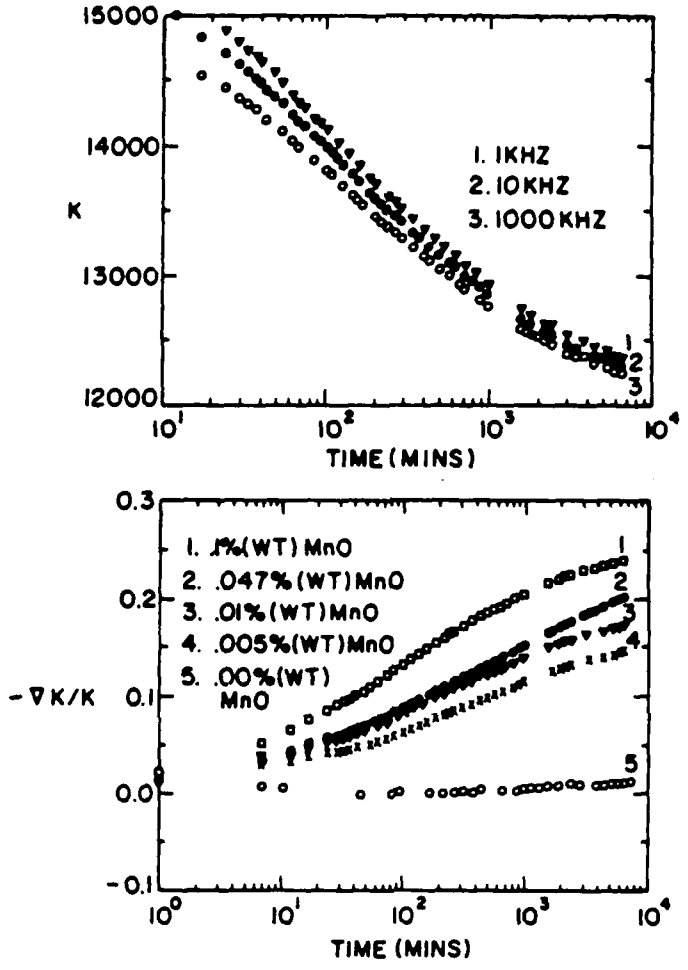

Figure 16. Isothermal aging of PMN:10% PT with MnO doping.

Figure 16a. Illustrating departure from the logarithmic aging law at longer times.

Figure 16b. Aging curves as a function of MnO concentration.

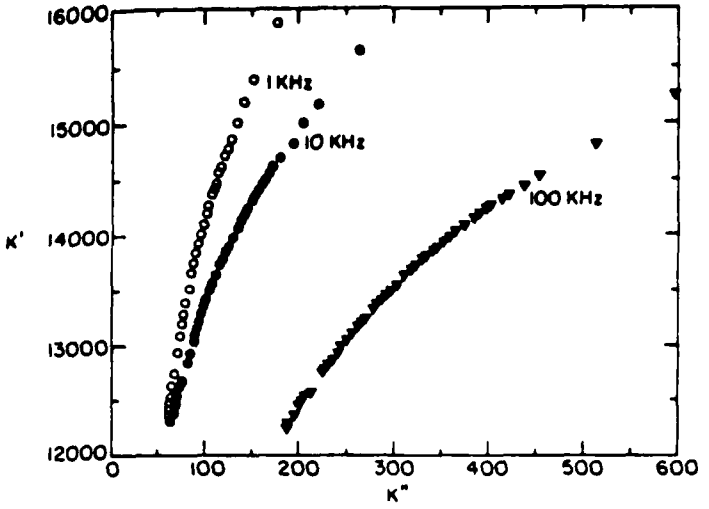

Figure 17. Plots of K' vs. K" over the full 1,000 hour aging period for PMN:10% PT with 0.1 wt% MnO doping.

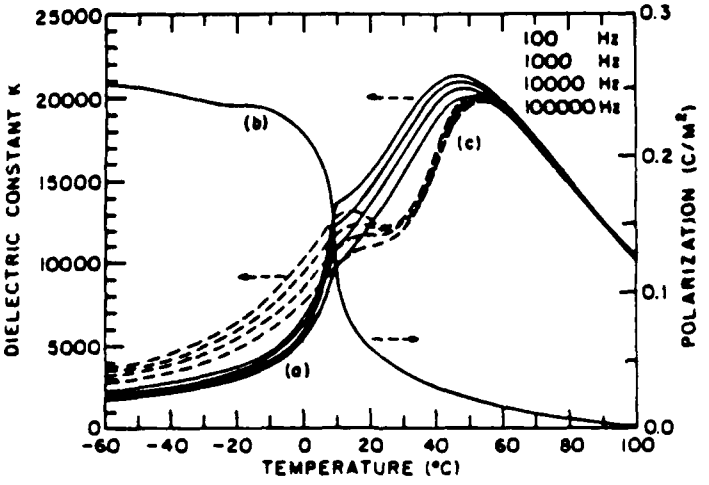

Figure 18. Dielectric constant (a) and thermal depolarization curve (b) for a ceramic PMN:10% PT doped with 0.1 wt% MnO and aged for 300 hours at 22 Kv/cm DC bias applied at room temperature (25° C).

Curve c is the conventional curve for a sample aged under similar conditions but without DC bias.

Poling, Depoling, Grain Size, and Surface Effects

Earlier studies by Yao Xi (8) using the ferroelectric relaxor PLZT at the composition 8.65:3 have shown that the poling and depoling of the hot-pressed transparent ceramic is consistent with th build-up and decay of macro domains from constituent micro domains. Ceramics can be quenche into a stable micro domain structure at low temperature, then under DC bias a stable macrodomai state can be induced with both field and temperature affecting the kinetics of the build-up. Mor recently similar studies have been carried forward on fully dense compositions with a wide range o grain sizes. These data (9) suggest that near the grain boundary there is a region of reduced weak field permittivity and enhanced asymmetry. Finer grain ceramics depolarize at lower temperature an take higher fields to repolarize. However, the saturation polarization is not affected by the grain siz eventhough the coercivity is markedly enhanced in the finer grained samples.

Using extremely grain grown PLZTs it has been possible very recently to explore the thicknes dependence of the properties of single grain thick samples. In these crystals it is evident that near th free surface there is again a region of low weak field permittivity. That these crystals exhibit highe coercivity than thick, but that the maximum polarization is not dependent upon thickness.

It is interesting to note that TEM studies by Clive Randal et al., reported in another paper in thi issue confirm the presence of micro domains in quenched samples of an 8.2:70:30 PLZT and show explicitly the build-up of a macro domain structure under electric bias.

Orientational Effects of Local Symmetry

A most interesting solid solution in the family of tungsten bronze ferroelectrics is that between $PbNb_2O_6$ and a hypothetical $BaNb_2O_6$ end member. In the range of the bronze compositions there is a fascinating morphotropic phase boundary (Fig. 19) separating orthorhombic (mm^2) and

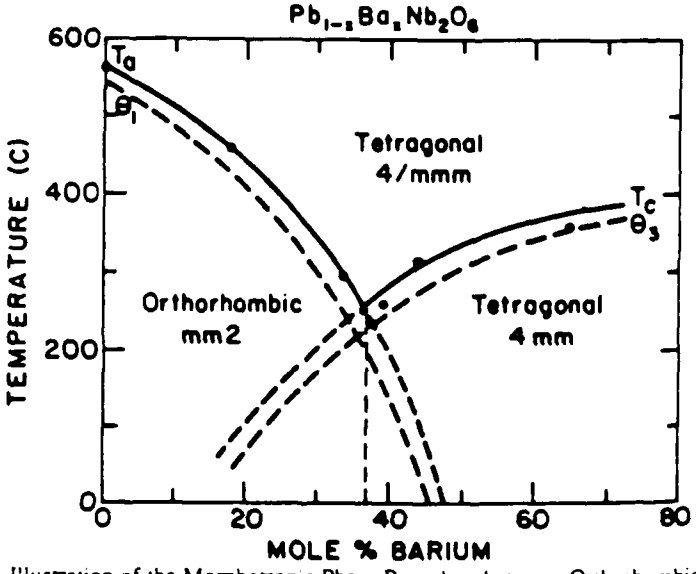

Figure 19 Illustration of the Morphotropic Phase Boundary between Orthorhombic (mm^2) an Tetragonal (4mm) phases in the $PbNb_2O_6$:$BaNb_2O_6$ tungsten bronze ferroelectri phase diagram.

tetragonal 4 mm ferroelectric phases. Since in the prototype 4/mmm symmetry, there is no coupling between four-fold and two-fold axes these two modes of polarization are unrelated and have separate Curie Weiss temperatures (θ_1 and θ_3). Evidently θ_1 decreases with Ba addition to $PbNb_2O_9$ and θ_3 increases so that near crossover the system switches from orthorhombic ferroelectric (P_s along 110) to tetragonal ferroelectric (P_s along 001).

From a simple L:G:D phenomenology (10) (11) it is possible to deduce the expected behavior of the anisotropic weak field permittivity in the orthorhombic, Fig. 20 and tetragonal, Fig. 21 regions. Since the electro-optic constants r_{33} and r_{51} depend on K_3 and K_1 respectively, the high values of permittivity which occur in the polar phases are of high practical as well as theoretical importance.

Experimental measurements in both phases confirm the broad features of the phenomenological expectation (Fig. 22, 23, and 24) however, at lower temperature it is evident that both K_1 and K_3 have relaxation character freezing out to much lower values. We believe that these are the first instances of strong relaxation in the permittivity perpendicular to the polar axis in a ferroelectric phase where clearly they can not be associated with a conventional domain wall relaxation.

On the basis of a relaxor model it is suggested that this unusual relaxor behavior may be associated with small departures of the polar axes from the simple <100> <110> family of directions in tetragonal and orthorhombic macro symmetries.

For the situation depicted schematically in Fig. 25 it could be that there are two types of barriers, for 100 and 110 type switching so that the deeper wells cause a freezing out of the switchability in the ferroelectric direction, at much higher temperatures than the weaker well freezes out the polarizability in the perpendicular direction.

Thus, even in the polar state, the orthogonal component of polarizability retains relaxation character to freeze out at much lower temperature. That the lower temperature maxima are not simple ferroelectric phase changes has been confirmed by pyroelectric tests which exhibit no current maxima in the vicinity of the freeze out.

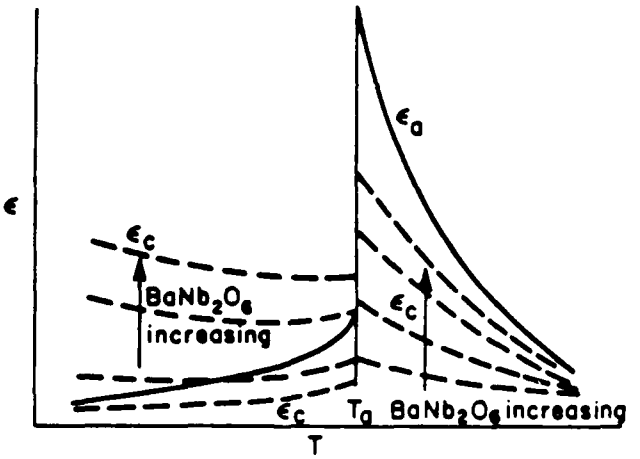

*With respect to the tetragonal axial system

Figure 20. Schematic diagram of the expected weak field dielectric behavior in the orthorhombic ferroelectric phase of $Pb_{1-x}Ba_xNb_2O_6$ as the composition approaches the morphotropic boundary from the lead rich side.

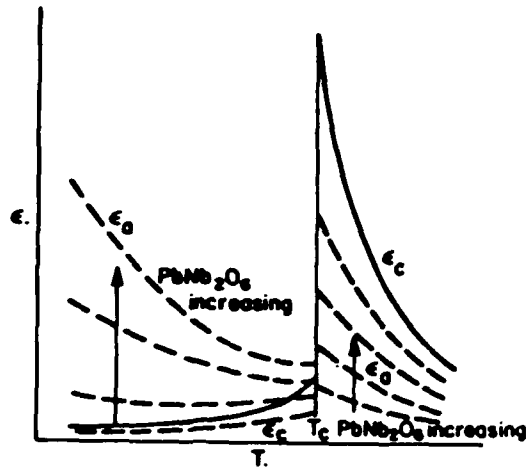

Figure 21. Schematic diagram of the weak field dielectric behavior in the tetragonal ferroelectric phase of $Pb_{1-x}Ba_xNb_2O_6$ from the barium rich compositions.

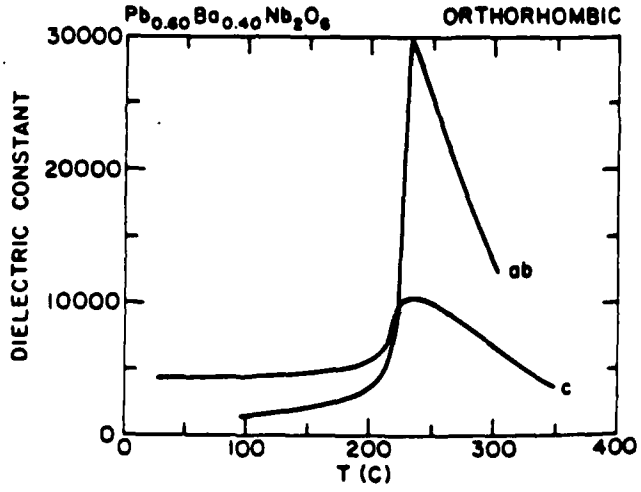

Figure 22. Weak field dielectric permittivity vs. temperature in $Pb_{0.6}Ba_{0.4}Nb_2O_6$ at a frequency of 100 kHz.

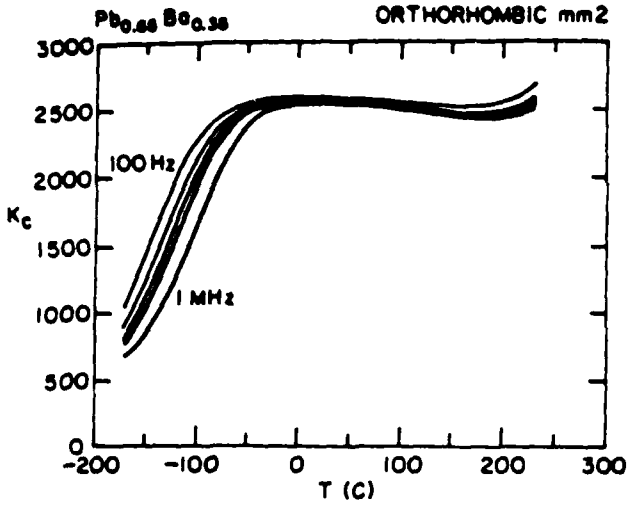

Figure 23. Low temperature dielectric dispersion in ϵ_c over the frequency range 100 Hz to 1 MHz in $Pb_{0.6}Ba_{0.4}Nb_2O_6$ a composition in the orthorhombic phase field close to the MPB.

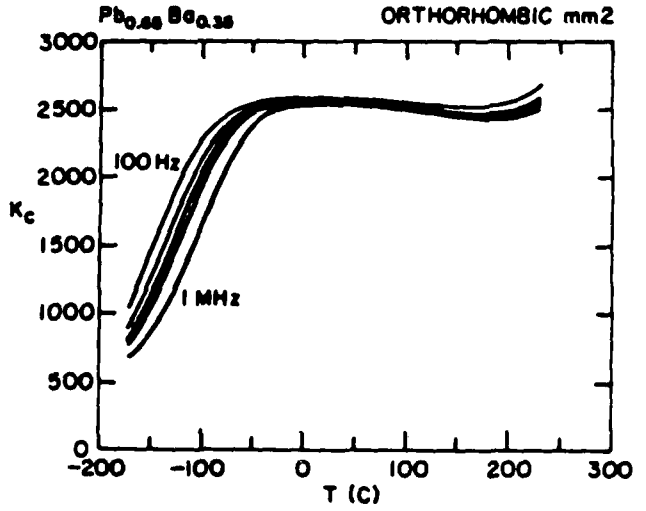

Figure 24. Low temperature dielectric dispersion in ϵ_a over the frequency range 100 Hz to 1 MHz in $Pb_{0.56}Ba_{0.44}Nb_2O_6$ a composition in the tetragonal phase field close to the MPB.

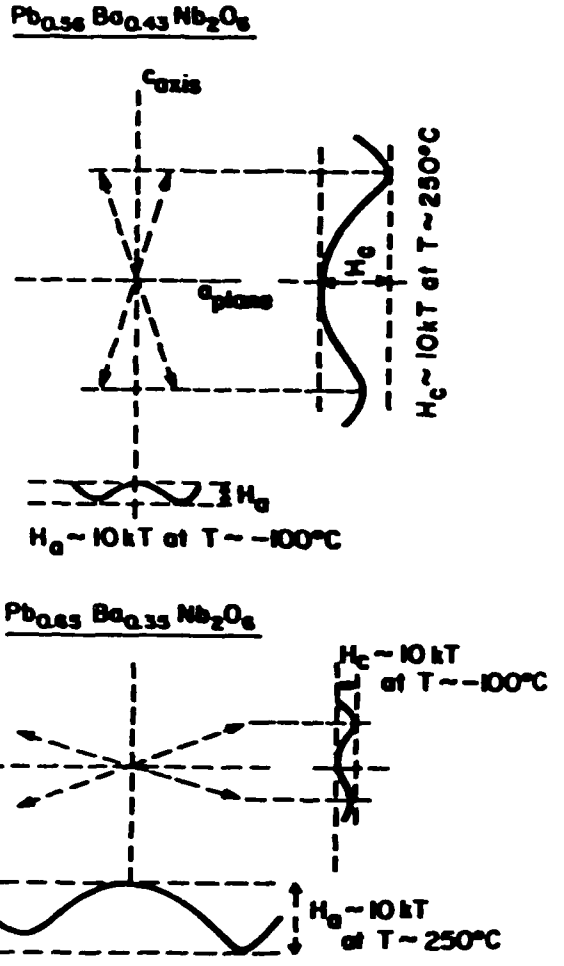

Figure 25. Schematic diagram of the proposed free energy in the tetragonal compositions close to the MPB (a) and in the orthorhombic compositions close in to the MPB (b).

Again it is postulated that due to compositional heterogeneity local symmetry is lower than the global symmetry of the crystal.

SUMMARY AND CONCLUSIONS

A broad family of experimental evidence has been presented which suggests that the relaxor ferroelectric crystals and ceramics may be the electrical analogues of superparamagnets. Ordering studies have shown that compositional heterogeneity leading to a breakdown of translational symmetry is responsible for relaxor character. Electrostrictive and electro-optic measurements demonstrate that the RMS polarization $\sqrt{P^2}_s$ has large values at temperatures well above T_c the mean Curie point, and induced electrostrictive distortion has been measured to establish that the fluctuations in P are dynamical above T_c.

Aging, poling, and depoling grain size and thickness dependence of the dielectric properties have been demonstrated to be consistent with a model in which the local symmetry of the fluctuating micro polar region is lower than the global symmetry, giving rise to an inequivalence between alternative orientation states. In the tungsten bronze structure ferroelectrics in the $Pb_{1-x}Ba_xNb_2O_6$ solid solution family at compositions close to the ferroelectric: ferroelectric morphotropic boundary, it is suggested that the lower symmetry of the local orientation states may be responsible for the most unusual dielectric dispersion evident in the polar phases.

REFERENCES

1. G.A. Smolenskii, A.I. Agranovskaya, Soviet Physics Solid State 1, 1429 (1959).
2. N. Setter, L.E. Cross, J. Appl. Phys. 51, 4356 (1980).
3. C.G.F. Stenger, F.L. Scholten, A.J. Burggraat, Solid State Comm. 32, 989 (1979).
4. G.A. Smolenskii, G.A. Isupov, V.A. Agranovskaya, N.N. Krainik, Soviet Physics Solid State 2, 2584 (1961).
5. R.R. Neurgaonkar, M.H. Kalisher, T.C. Linn, E.J. Staples, K.L. Keester, Mat. Res. Bull. 15 1235 (1980).
6. R.R. Neurgaonkar, W.K. Cary, J.R. Oliver, Ferroelectrics 35, 301 (1985).
7. R.R. Neurgaonkar, Prof. SPIE 465, 97 (1984).
8. Yao Xi, Chen Zhili, L.E. Cross, J. Appl. Phys. 54, 3399 (1984).
9. X.T. Chen, D.N. Huang, Z.W. Yin, Proc. 6th IEEE Int. Symp. on Ferroelectrics, June 8-11 1986, Lehigh University, pg. 62.
10. T.R. Shrout, L.E. Cross, P. Moses, H.A. McKinstry, R.R. Neurgaonkar, Proc. 1980 IEEE Symposium on Ultrasonics, Nov. 1980, pp. 414.
11. L.E. Cross, R. Betsch, H. McKinstry, T. Shrout, Proc. 34th Annual Freq. Control Symp., May 1980, pp. 82.

Ferroelectrics, 1987, Vol 76, pp. 479-487
Photocopying permitted by license only

GRAIN SIZE DEPENDENCE OF DIELECTRIC AND ELECTROSTRICTION OF $Pb(Mg_{1/3}Nb_{2/3})O_3$-BASED CERAMICS

THOMAS R. SHROUT, UMESH KUMAR, MOHAMMED MEGHERHI, NING YANG AND SEI-JOO JANG
Materials Research Laboratory, The Pennsylvania State University, University Park, PA 16802

Abstract. The dielectric and electrostrictive properties of relaxor ferroelectric $Pb(Mg_{1/3}Nb_{2/3})O_3$-based ceramics are strongly affected by the microstructure with emphasis on the grain size. Both the dielectric constant K and electrostrictive field coefficient (M) were found to increase with increasing grain size whereas the electrostrictive polarization coefficient Q was essentially independent of preparation. It was observed, however, that factors other than grain size, such as diffuseness of the phase transition, must also be taken into account to explain microstructural effects on various properties of relaxor dielectrics.

INTRODUCTION

It is documented and commercially realized that electrostrictive materials such as $Pb(Mg_{1/3}Nb_{2/3})O_3$-based ceramics (PMN) are suitable for application in ultra-precise position actuators, especially in the field of adaptive optics.[1] In such applications, the materials are required to deform up to 0.1% in strain without hysteresis and with displacement control in the range of ± 0.01 μm. Thus the material's dielectric and electrostrictive characteristics must be well understood. As in virtually all ceramics, and especially piezoelectrics, the desired properties vary with sample preparation and resultant microstructure with emphasis on grain size. It is believed that the properties of electrostrictive materials are also highly dependent on grain size.

Preliminary work by Uchino et al.[2] revealed a large deviation in the electrostrictive strain magnitude as well as the hysteresis strain level in PMN ceramics. Similar effects were also observed in PLZT ceramics.[1] In the case of PMN, however, Uchino only slightly modified the grain size and in the attempt had to modify the composition by going MgO deficient which resulted in a second phase, that being pyrochlore, which in itself is detrimental to dielectric and other properties.

It is the purpose of this paper to report the electrostrictive properties of stoichiometric single phase PMN-based ceramics exhibiting a wide range of grain sizes as well as their effect on dielectric and other properties.

EXPERIMENTAL

The electrostrictive material chosen for this study was a solid solution composition $0.93(Pb(Mg_{1/3}Nb_{2/3})O_3\text{-}0.07PbTiO_3$ (PMN-PT)). This composition was selected because its Curie temperature is near to that of room temperature. The PMN-PT powder was prepared by solid state reaction using the appropriate amount of reagent grade raw materials* of lead carbonate hydroxide $PbCO_3 \cdot Pb(OH)_2$**, magnesium carbonate hydroxide $MgCO_3 \cdot Pb(OH)_2$, titanium dioxide*** TiO_2 and niobium pentoxide**** Nb_2O_5. Since it is well known that the formation of perovskite PMN is difficult to fabricate in single phase form without the appearance of a parasitic pyrochlore phase ($Pb_3Nb_4O_{13}$), the columbite precursor method proposed by Swartz and Shrout[3] was used. The precursor method is as follows:

1100° C/4 hrs

$$0.93MgO+0.93Nb_2O_5+0.21TiO_2 \text{-----} > Mg_{0.93}Nb_{1.86}Ti_{0.21}O_6\text{-Columbite}$$

700° C/4 hrs

$$PbO+1/3Mg_{0.93}Nb_{1.86}Ti_{0.21}O_6 \text{-----} > 0.93PMN\text{-}0.07PT\text{-Perovskite}$$

In processing the columbite precursor, the poor dispersion characteristics of MgO powder can lead to insufficient mixing intimacy and thus incompletely reacted calcined powder. To insure proper mixing, both steric hinderance (polyelectrolyte dispersant) an electrostatic repulsion (pH adjustment by ammonia) dispersion mechanisms were required to prepare a 25 vol% slurry with deionized H_2O. The slurry was vibratory milled, followed by drying and calcination at 1100° C for 4 hrs. The calcined slug was pulverized using a hammermill and the appropriate amount of PbO was added. A 30 vol% slurry was prepared and vibratory milled followed by drying and calcination at 700° C for 4 hours. Both the columbite and subsequent PMN calcines were examined by X-ray diffraction to insure phase purity. No second phase pyrochlore, within the detection limits of the X-ray diffractometer, was observed. To obtain yet a more uniform and reactive powder, the calcined PMN-PT powder was milled as above, to a particle size of $\sim 0.9\ \mu$ (50%) as determined by a Microtract Particle Size Analyser.

---

*Hammond Lead Products, Inc., White Lead grade HLPA (99%).
**Fisher Scientific Co., Magnesium Carbonate purified grade.
***Fansteel Metals, Nb_2O_5 Tech. Grade (99.5%).
****Whittaker, Clark and Daniels, TiO_2 USP Grade (99%).

Disks were prepared using PVA binder followed by burnout prior to sintering. Sintering was performed over a temperature range of 950° C to 1300° C for various times. To prevent PbO volatilization, the disks were fired in a coarse PMN sand of the same composition. Generally a heating rate of 900° C/hr. was used to further help prevent PbO loss. Weight loss, geometrical density, and grain size were determined for all the various firings. The grain size was determined on fracture surfaces monitored by SEM. Samples having densities greater than 90% theoretical were surface ground and electroded using sputtered on gold.

The dielectric measurements were carried out on an automated system (described in Reference 4). Both the dielectric constant and dissipation factor were measured pseudo-continuously at various frequencies (100 Hz, 1 kHz 10 kHz, and 100 kHz) as the samples were cooled from 125° C to -55° C. Typically 3-4 samples from each thermal history were measured. The parameters used for analysis of the dielectric data were the maximum dielectric constant (1 kHz) and the temperature (T_C) at which this maximum occurred. Since most of the samples had approximately the same density, no correction for porosity was made.

The electric field (E) induced electrostriction strain (transverse) coefficient M_{12} expressed in the following equation,

$$S_2 = M_{12}E_1^2 \tag{1}$$

where S is the transverse strain, was determined using a resistive strain gauge technique, under an a.c. electric field of 0.1 Hz applied to the sample. In conjunction with a modified Sawyer-Tower system, the electrostrictive polarization Q_{12} coefficient as expressed by the following equation was also determined

$$S_2 = Q_{12}P_1^2 \tag{2}$$

RESULTS AND DISCUSSION

Physical and dielectric properties of PMN-PT samples as a function of thermal history are reported in Table 1. As tabulated, firing as low as 950° C for at least 4 hrs could result in densities greater than 95% theoretical ($\sim$ 8.11 g/cc). In general, the weight loss of PbO was maintained in the range of 0.5 to 1.5 wt% with slightly higher losses occurring at higher temperatures.

Also reported in Table 1, is a wide range in grain sizes ($\sim$ 1.5 μ to 9 μ) for the various firings. It is clearly evident that low temperature firings resulted in relatively small grain sizes (2-3 μ) with grain growth occurring at higher sintering temperatures. Even at sintering temperatures as high as 1300° C, which is near the melting point, however, individual grains larger than 15 μ could not be achieved whereas grains greater than 20 μ were reported in Uchino's work. Lack of large grains can be

attributed to the fine and uniform stoichiometric powder thus being less susceptible to abnormal grain growth. Also evident from Table 1 was the fact that sintering times had little affect on grain growth. Typical photomicrographs from fractured surfaces are shown in Figure 1. As observed in the case of most lead-based relaxor dielectrics, the fracture was intergranular believed to be the result of a weak amorphous PbO grain boundary phase.[5] However, for certain samples fired for extended periods of time, the fracture was transgranular. No explanation as to why both types of fracture occurs can be given at this time.

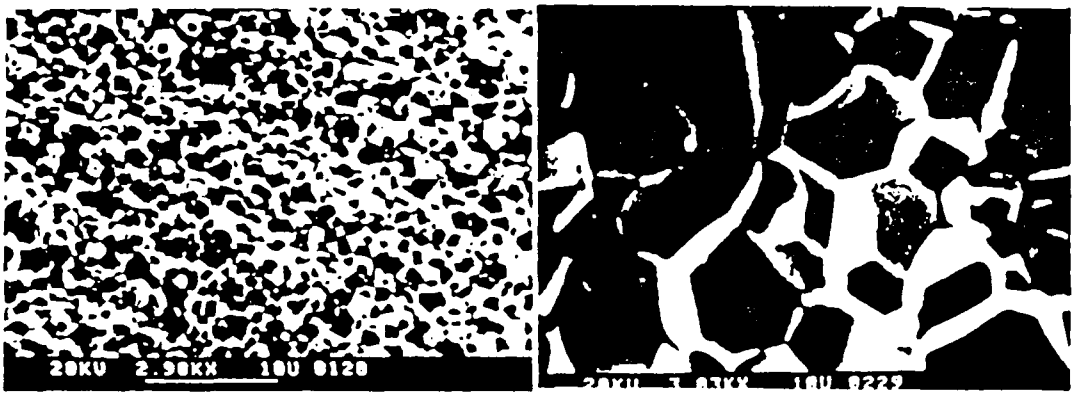

Figure 1. SEM photomicrographs of fractured surface of PMN-PT samples (left-1150° C/0.5 hrs.; right-1250° C/20 hrs.).

FIRING CONDITIONS	WT LOSS	ρ (g/cc)	GRAIN SIZE	k_{max}	T_c (°C)	δ (°C)	$^{**}M_{12}(x10^{-16}m^2v^{-2})$	$Q_{12}(x10^{-2}m^4c^{-2})$
950° C-0.5 hrs	0.5%	7.4	1.5 um	11,500	24	58	-0.60	-0.55
4 hrs	0.7	7.83	2	13,000	22.8	50	-0.74	0.47
48 hrs	0.6	7.88	2	20,300	---	39	-1.20	-0.59
1050° C-0.5 hrs	0.8	7.88	2	12,600	20.6	57	-0.47	-0.47
(zirconate sand)	(0.97)			(14,800)		(47)		
4 hrs	0.5	7.91	3	15,700	20.5	44	-1.31	---
20 hrs	1.1	7.89	3*	16,800	22.2	43	-1.38	-0.45
1150° C-0.5 hrs	0.7	7.87	3	13,500	19.7	48	-1.06	-0.59
(zirconate sand)	(0.87)			(15,100)		(47)		
4 hrs	1.0	7.88	3	17,800	---	43	-1.27	-0.56
1250° C-0.5 hrs	1.1	7.84	5*	17,5000	---	44	-1.45	-0.53
4 hrs	1.2	7.82	6.5*	20,800	18.4	42	-1.52	-0.60
20 hrs	1.45	7.76	9*	22,800	17.9	39	-1.59	-0.70
1300° C-0.5 hrs	1.1	7.82	6	21,000	18.7	41	-1.66	-0.49

*Transgranular fracture ooserved.

**Value determinal at E-field of $1\!1\!0^6$ v/m.

Table 1 Physical, Dielectrical, and Electrostrictive Properties of PMN-PT Ceramics.

Dielectric Properties

Characteristic of relaxor ferroelectrics, all the samples exhibited similar frequency dispersion behavior of both k and loss. Typical k vs T curves (@ 1kHz) for several samples fired at various temperatures with similar hold times and their corresponding grain sizes are shown in Figure 2. As clearly evident from Figure 2, there appears to be a significant dependence of k with grain size, with k increasing with grain size. Similar results were reported by Swartz et al.[4] The grain size dependency is believed to be attributed to low dielectric constant continuous or semi-continuous amorphous grain boundary phase ($\sim$ 5 to 10 nm) comprised primarily of PbO[5,6]. A plot of k_{max} as a function of grain size for all PMN-PT samples reported in Table 1 is shown in Figure 3. As evident from the figure, PMN-PT samples having similar grain sizes can have drastically different levels of k_{max}. This is especially observed for samples fired at lower temperatures (950 to 1050° C). One possible explanation could be related to the amount of the amorphous PbO grain boundary phase present. Empirically, samples with higher weight loss due to PbO volatility, have in general, higher levels of k_{max}. Further evidence of the effect of PbO weight loss on k_{max} was investigated by firing PMN-PT samples in a coarse zirconate sand, which promoted PbO weight loss during sintering. As expected, such samples had significantly higher k than their fired PMN-sand fired counterparts. As a note, such firings in the zirconate sand were only successful at the lower firing temperatures and short times where reactivity between the PMN-PT samples and the sand was minimal. PMN-PT samples with higher weight loss also had slightly shifted T_C (downward) also reported by Swartz.[4]

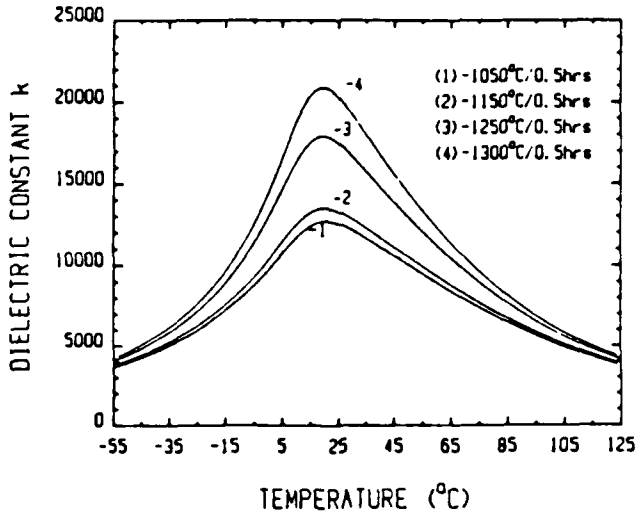

Figure 2. Dielectric constant k vs. temperature (@ 1 kHz) for PMN-PT samples fired at various temperatures with similar hold times.

The dielectric grain size dependency explanation presented above neglects the fact that the starting PMN-PT powder was stoichiometric and that all the samples had weight loss due to PbO volatilization. Thus the question arises, where did the amount of PbO grain boundary phase required to significantly vary the bulk dielectric constant come from? Perhaps phase(s) such as pyrochlore and thus free PbO are present but in quantities outside X-ray diffraction limits.

A further explanation of the wide range of k_{max}'s for similar grain sizes was believed to be related to the level of diffuseness of the phase transition. For ferroelectrics with diffused phase transitions, the law $1/k \sim (T-T_c)^2$, has been shown to hold over a wide temperature range instead of the normal Curie-Weiss Law[7,8]. Given that the local Curie temperature distribution is Gaussian in nature, a level of diffuseness (δ) can be determined from the plot of the reciprocal dielectric constant as a function of $(T-T_c)^2$ as given by the expression

$$\frac{1}{k} \sim \frac{1}{k_{max}} + \frac{(T-T_c)^2}{2k_m\delta^2} \qquad (3)$$

where T is a temperature above T_c, and k_{max} the y-axis intercept.

Figure 3 shows a plot of $1/k$ vs $(T-T_c)^2$ for various PMN-PT samples with various thermal histories. As shown, it is clear that samples fired at relatively low temperatures and short times had significantly higher slopes and thus larger diffuseness parameters (δ). The diffuseness parameter δ for all the samples can be found in Table 1, and when plotted as a function of k_{max}, as shown in Figure 4, a good correlation even for equivalent grain sizes was observed. The variation in diffuseness of the phase transition may be the result of defects produced during high energy milling which essentially anneal away during sintering. The less diffuse nature of PMN-PT samples fired at higher temperatures (or longer times at lower temperatures) could also be the result of short range ordering of Pb vacancies as proposed by Randall et al.[9], which would also correlate to the higher weight losses presented earlier.

Along these same lines, a model proposed to explain the grain size dependence of the dielectric constant in $(Pb,La)(Zr,Ti)O_3$ (PLZT) ceramics[10] was believed to be the result of steep compositional gradients near the grain boundary. This region being highly stressed and disordered affects the thermal reorientation of polar micro-regions and acts as a reduced dielectric constant boundary layer. Thus larger grain size samples exhibit higher dielectric constants. The above model works well to explain the grain size dependence of dielectric constant found in PMN-PT reported in this work. Perhaps a reduced polarizability boundary region is the result of the high energy milling of the

powder. For samples with small grains yet having large dielectric constants, such as the 950° C/48 hr samples, the long thermal treatment effectively anneals away the defective boundary region. Henceforth, if the degree of disorder (or order) can be maintained by proper thermal treatment, little if any grain size dependency on the dielectric properties will be observed. Clearly, however, an extensive amount of work is still required to quantify the above proposed model.

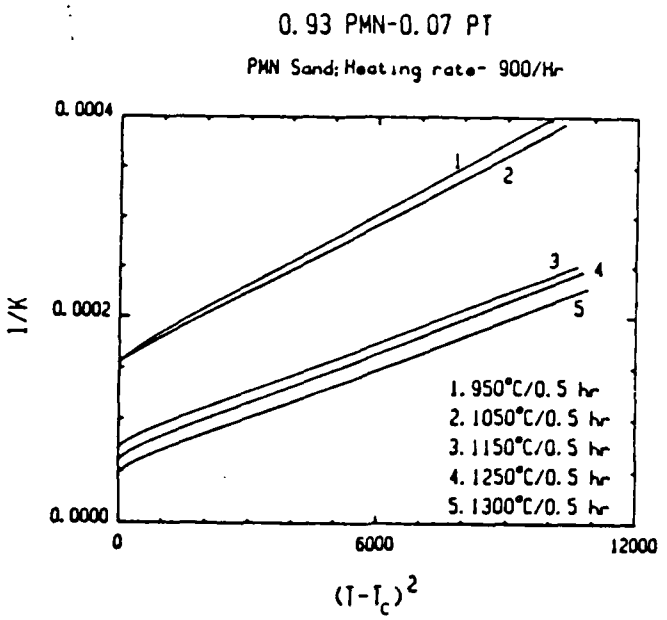

Figure 3. Reciprocal dielectric constant vs. $(T-T_c)^2$ for various PMN-PT samples.

Electrostriction

Typical strain-field curves for several PMN-PT samples of varying grain size are shown in Figure 6. Unlike the results by Uchino et al.[2], the level of strain hysteresis, the deviation of strain between rising and falling fields, was found to be very small for all PMN-PT samples regardless of their thermal history.

Both electrostrictive field (M_{12}) and polarization (Q_{12} coefficients determined for the PMN-PT samples are reported in Table II. As expected, samples with larger grain sizes, but more importantly higher dielectric constants, had the largest electrostrictive polarization strain levels, and thus the higher M_{12} values. The electrocstrictive polarization coefficient Q_{12}, however, was found to be virtually independent of thermal history whether it be grain size, weight loss, etc. Values of Q_{12} reported in this work were found to be similar to those reported

elsewhere.[11]

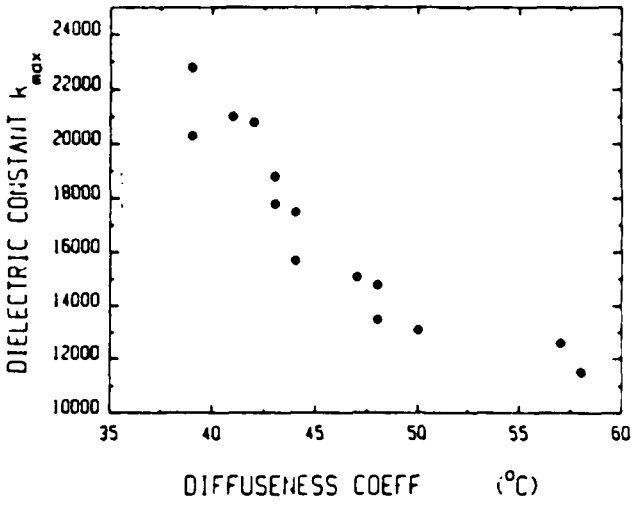

Figure 4. Dielectric constant k_{max} as function of disorder parameter δ.

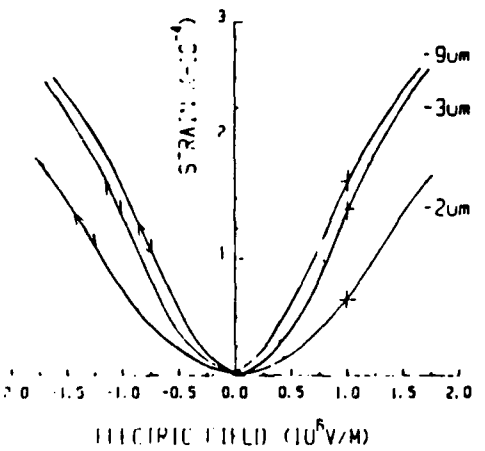

Figure 5. Electrostriction curves for PMN-PT samples of different thermal histories.

SUMMARY

The dielectric and electrostrictive behavior (M) of PMN-PT ceramics is strongly affected by preparation history. Both k and M_{12} were found to significantly increase with grain size. However, grain size alone could not explain all the results whereas the level of the diffuseness of the phase transition must also be taken into consideration. No significant affect of thermal history on the electrostrictive polarization coefficient (Q) was observed.

To further substantiate the origin of varying degrees of disorder (order), further work using pyroelectric measurements to investigate macro- and micro-polar behavior and TEM techniques must be employed.

In conclusion, to insure optimum properties for electrostrictive actuators, particularly if small grain size is desirable, as for the case of multilayer actuators, careful thermal preparation must be used.

REFERENCES

1. K. Uchino, Cer. Bull., 65, 647-652 (1986).
2. K. Uchino, M. Tatsumi, I. Hayashi, and T. Hayashi, Jpn. J. Appl. Phys., 24, 733-735 (1985).
3. S. Swartz and T. Shrout, Mat. Res. Bull., 17, 1245-1250 (1982).
4. S. Swartz, T.R. Shrout, W.A. Schulze, and L.E. Cross, J. Am. Cer. Soc., 67, 311-315 (1984).
5. E. Goo and G. Thomas, J. Am. Cer. Soc., 69, C-188-C-190 (1986).
6. A.J. Gorton, J. Chen, H. Chan, D. Smyth, and M.P. Harmer, Proc. Sixth IEEE Intl. Symp. Appl. Ferroelectrics, 150-153 (1986).
7. T. Yamada, J. Appl. Phys., 43, 328 (1972).
8. K. Uchino, S. Nomura, L.E. Cross, S.J. Jang, and R.E. Newnham, J. Appl. Phys., 51, 1142-1145 (1980).
9. C.A. Randall, D.J. Barber, R.W. Whatmore, and P. Groves, (to be published in Ferroelectrics).
10. D.N. Huang, Z.W. Yin, and L.E. Cross, Proc. Sixth IEEE Intl. Symp. Appl. Ferroelectrics, 159-164 (1986).
11. S.J. Jang, Ph.D. Thesis, The Pennsylvania State University (1980).

SOL-GEL PROCESSING OF $0.91Pb(Zn_{1/3}Nb_{2/3})O_3$-$0.09PbTiO_3$: STABILIZATION OF THE PEROVSKITE PHASE

J.M. HAYES, T.R. GURURAJA, Gregory L. GEOFFROY and L.E. CROSS
Materials Research Laboratory and Department of Chemistry, The Pennsylvania State University, University Park, PA 16802, USA

Received 18 May 1987

$0.91Pb(Zn_{1/3}Nb_{2/3})O_3$-$0.09PbTiO_3$ was prepared by a sol-gel route in which Zn and Nb were prereacted to form "$Zn[Nb(OEt)_6]_2$" in situ. Calcination conditions were varied to optimize the percentage of perovskite phase stabilized. The maximum amount of perovskite phase stabilized was 75%, which occurred at a calcination temperature of 1000°C.

1. Introduction

Much attention has been directed in the recent years towards lead-based ferroelectric compounds with a perovskite structure and a general formula $Pb(B'B'')O_3$ for capacitor and electrostrictive applications. Lead zinc niobate, $Pb(Zn_{1/3}Nb_{2/3})O_3$ (herein designated PZN), is such a ferroelectric which has a high dielectric constant and a diffuse phase transition. Single crystals of perovskite PZN have been synthesized by the flux method. These single crystals show excellent dielectric, optical and electrostrictive properties [1-3]. The solid solution between PZN with rhombohedral symmetry and $PbTiO_3$ (PT) with tetragonal symmetry has a morphotropic phase boundary (MPB) near 9 mol% of PT [4]. Single crystals grown by the flux method with compositions near the MPB show unusually large dielectric and piezoelectric constants and electromechanical coupling coefficients (92%) [5]. Conventional ceramic processing has remained unsuccessful in preparing perovskite-type PZN or PZN-PT ceramics. The product obtained by solid-state reaction at ≈ 1100°C is mainly the cubic pyrochlore phase, $Pb_3Nb_4O_{13}$, which of course is detrimental to both the dielectric and piezoelectric properties.

Sol-gel processing offers a number of advantages over conventional mixed-oxide processing. These include higher purity, molecular homogeneity, reduced firing temperatures and finer control of microstructure. It is feasible that these advantages could result in the ability to form new materials otherwise unobtainable. The present study was undertaken to determine if sol-gel technology could be utilized to stabilize the perovskite phase in PZN-PT ceramics at a composition near the MPB. The reduced firing temperatures required for sol-gel prepared materials may make this possible. The different reactivities of the species in solution as opposed to the reactivities of the oxides in the solid-state reaction may also be an important factor in determining if the perovskite phase can be stabilized.

2. Experimental

2.1. Sol-gel processing

A sol-gel process similar to that reported by Gurkovich and Blum [6,7] for the formation of $PbTiO_3$ monoliths was investigated for the formation of $0.91Pb(Zn_{1/3}Nb_{2/3})O_3$-$0.09PbTiO_3$.

The chemicals $Pb(OAc)_2 \cdot 3H_2O$ (Aldrich, 99+%), $Zn(OAc)_2 \cdot 2H_2O$ (Aldrich, 98+%), $Nb(OEt)_5$ (Alfa), $Ti(O\text{-}i\text{-}Pr)_4$ (Aldrich), $ZnCl_2$ (Aldrich, 99.999%), potassium (Aldrich, sticks in mineral oil) and 2-methoxyethanol (Aldrich, 99%, herein referred to as 2-MOE) were used as supplied. Anhydrous ethanol (Pharmco, 200 proof) was freeze-pump-

0167-577x/87/$ 03.50

thawed and stored over molecular sieves to be free of both H_2O and O_2. Manipulations with $ZnCl_2$ and the moisture sensitive $Nb(OEt)_5$, $Ti(OR)_4$ and potassium were done under anhydrous N_2 atmosphere. The reaction vessel employed for sol formations was a simple distillation assembly. This consisted of a three-neck round bottom flask equipped with a N_2 purge (to prevent moisture from entering the system during cooling cycles) and a thermometer to monitor solution temperature, a Claisen stillhead adapter (for sequential addition of reagents), a thermometer for monitoring the vapor temperature and a condenser.

This sol-gel route involves the reaction of the organometallic compound $Zn[Nb(OEt)_6]_2$, generated in situ, with a sol containing the appropriate amounts of Pb and Ti. While $Zn[Nb(OEt)_6]_2$ has not previously been synthesized and reported in the literature, Mehrotra and co-worker have reported the preparation of similar complexes, such as $Zn[Al(OR)_4]_2$ and $Ni[Nb(OR)_6]_2$ [8]. A reaction pathway similar to Mehrotra's [8] was chosen to generate $Zn[Nb(OEt)_6]_2$ in situ:

$$K \xrightarrow{EtOH} KOEt \xrightarrow[EtOH]{+Nb(OEt)_5} KNb(OEt)_6$$

$$\xrightarrow[EtOH]{+\frac{1}{2}ZnCl_2} \tfrac{1}{2}Zn[Nb(OEt)_6]_2 + KCl\,. \qquad (1)$$

As this compound was expected to be very moisture sensitive, all handlings were done in dry N_2 atmosphere and all flasks were flame-dried while under vacuum.

The synthesis of $KNb(OEt)_6$ was reported by Mehrotra et al. [9]. A 100 ml Schlenk flask was charged with 16 ml anhydrous EtOH, potassium (0.32 g, 8.2 mmol) and $Nb(OEt)_5$ (2.59 g, 8.14 mmol). This faint yellow solution was refluxed 2.5 h to give a colorless solution. To this was added a 13 ml EtOH solution of $ZnCl_2$ (0.56 g, 4.1 mmol) via canula and a precipitate (KCl) formed immediately. The reaction mixture was refluxed 1.5 h to be sure that reaction was complete. Toluene (10 ml, dry and degassed) was added to decrease the already slight solubility of KCl in EtOH. The resulting mixture was filtered (Schlenk frit, still in N_2 atmosphere) and the solvent was removed from the colorless solution in vacuo to give a white residue. This residue was not analyzed, but was assumed to be the desired $Zn[Nb(OEt)_6]_2$.

To prepare the Pb sol, a 250 ml flask was charged with $Pb(OAc)_2 \cdot 3H_2O$ (5.09 g, 13.4 mmol) and 2-MOE (100 ml). The solution was heated until the temperature of the condensing vapors reached that found for pure 2-MOE (122–123°C under our conditions). To this anhydrous Pb sol, maintained at ≈80°C, was added $Ti(O\text{-}i\text{-}Pr)_4$ (0.36 g, 1.2 mmol) and a 10 ml 2-MOE solution of the $Zn[Nb(OEt)_6]_2$ residue. This reaction solution was heated until the temperature of the condensing vapors reached 123°C. It was then immersed in a liquid N_2/i-PrOH bath (≈ −20°C) and a solution of distilled H_2O (0.97 g, 54 mmol) and 2 ml 2-MOE was added dropwise. Gelation occurred within 3 h to form a yellow gel. This gel was dried in vacuo to yield a white amorphous powder (5.3 g).

2.2. Heat treatments and measurements

The amorphous powders were heat treated under various firing conditions. Temperatures were varied from 325 to 1100°C, and were held for periods of time ranging from 15 min to 2 h. Samples were heated either at a slow temperature ramp (≈125°C/h) or by fast-fire (samples placed directly in furnace already at the desired temperature). Sample cooling was attained either by a slow cool process (samples cooled in the furnace with power off) or by a water quench method.

The relative amounts of perovskite and pyrochlore phases at room temperature were determined using powder X-ray diffraction patterns. Powder X-ray diffraction studies of these samples were performed using Cu $K\alpha_1$ ($\lambda = 1.54059$ Å) radiation with a SCINTAG PAD V diffractometer (SCINTAG Inc., Santa Clara, CA, USA) at 40 kV, 35 mV and scan 2 deg/min. The major X-ray peak intensities were measured for the perovskite and pyrochlore phases, i.e. (110) and (222), respectively. The percentage of perovskite phase was calculated using the following equation:

$$\%\ \text{perov} = 100\, I_{\text{perov}}/(I_{\text{pyro}} + I_{\text{perov}})\,. \qquad (2)$$

3. Results and discussion

To study the effect of calcination conditions on the stability of the perovskite phase, the sol-gel derived $0.91Pb(Zn_{1/3}Nb_{2/3})O_3$–$0.09PbTiO_3$ amorphous powder was calcined at different temperatures for varying periods of time with different heating and cooling ramps. Table 1 shows the results of this study in terms of the percentage of perovskite phase detected (eq. (2)). The formation of perovskite phase occurs within the temperature range from ≈900 to ≈1100°C. The maximum amount of perovskite phase stabilized was 75% at a calcination temperature of 1000°C. At temperatures <900°C, pyrochlore (P_3N_4) is the only phase observed (by X-ray diffraction). At temperatures >1000°C, the amount of perovskite phase decreases probably due to the loss of PbO at higher temperatures. It has been shown that the loss of PbO favors the formation of the pyrochlore phasse in PMN ceramics [12,13]. At calcination temperatures >1100°C, the perovskite phase is probably not stable at all and none was detected.

The time periods and/or the heating and cooling ramps show a peculiar behavior within this temperature rang (900 to 1100°C). At the 950 and 1000°C calcination temperatures, the materials that were slowly heated, calcined for 60 min and allowed to cool slowly were essentially the same % perovskite as those that were fast-fired, calcined 15 min and H_2O quenched. Contrarily, at calcination temperatures of 900 and 1100°C the materials that were slowly heated, calcined for 60 min and slowly cooled were very different in the % perovskite than those that were fast-fired, calcined only 15 min and H_2O quenched. For the 60 min calcination at 1100°C, varying the heating and cooling ramps produced no change in the amount of perovskite phase formed (see the last four entries in table 1). This suggests that it is the time period of the calcination that determines the % perovskite formed and not the heating or cooling ramps employed.

Fig. 1 shows the powder X-ray diffraction patterns of samples heat treated at various temperatures for 1 h periods (slow temperature ramp and slow cooling employed). It is apparent from fig. 1 and table

Table 1
Amount of perovskite phase formed as a function of heating and cooling ramps

Calcination temperature (°C)	Time (min)	Heating method	Cooling method	% perovskite
650	60	ramp	slow	0
750	60	ramp	slow	0
800	15	fast-fire	quench	0
850	60	ramp	slow	0
900	15	fast-fire	quench	55
900	60	ramp	slow	25
950	15	fast-fire	quench	63
950	60	ramp	slow	65
975	15	fast-fire	quench	66
1000	15	fast-fire	quench	73
1000	60	ramp	slow	75
1025	15	fast-fire	quench	61
1050	15	fast-fire	quench	65
1100	15	fast-fire	quench	63
1100	60	ramp	slow	29
1100	60	ramp	quench	33
1100	60	fast-fire	slow	30
1100	60	fast-fire	quench	30

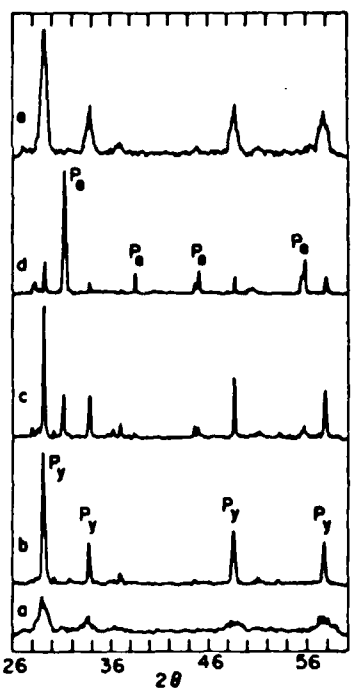

Fig. 1. Powder X-ray diffraction patterns of the sol-gel derived PZN–PT amorphous solid heated at various temperatures: (a) 440°C, (b) 850°C, (c) 900°C, (d) 1000°C and (e) 1125°C. P_y and P_p denote the pyrochlore and the perovskite phase, respectively.

1 that the pyrochlore (P_3N_4) phase is formed in the low-temperature region prior to perovskite phase formation. This pyrochlore phase was observed to be forming even at 325°C (not shown). As there were a few small X-ray peaks that could not be indexed, there may be a small amount of some unidentified phase(s) present.

Differential thermal analysis (DTA) curves of the amorphous solid show a large exothermic peak from 340 to 600°C attributed to burn-off of the organics, and an endothermic peak from 860 to 930°C, which we attributed to perovskite phase formation. This is consistent with the results of the heat treatments, as perovskite phase was not observed at temperatures below 900°C. As pyrochlore was observed even at temperatures as low as 325°C, the peak due to pyrochlore formation must be lost in the large organic burn-off peak.

To understand the causes for pyrochlore formation, the reaction kinetics and thermodynamics of the system must be considered. There have been relatively few studies concerning the formation mechanisms and kinetics of these ferroelectrics, with much attention directed at $Pb(Mg_{1/3}Nb_{2/3})O_3$ (PMN). Several studies indicate that the reactivity of the oxide MgO (or the oxide of the corresponding B' site cation in other such $Pb(B'B'')O_3$ ferroelectrics) is directly related to the formation of the perovskite phase. Variations in processing that improve the reactivity of MgO, such as finer raw materials [10], mixing/milling (improve dispersability [10], repeated calcinations [10], and the sol–gel technique [11], result in a significantly increased amount of perovskite PMN. No such variation in processing, however, has yielded a 100% perovskite PMN material.

Realizing the importance of the reactivity of MgO, Swartz and Shrout [12] devised a method for the preparation of pyrochlore-free PMN ceramics. This approach involves prereacting the B' and B'' site oxides, MgO and Nb_2O_5, to form $MgNb_2O_6$, which has the columbite structure. The $MgNb_2O_6$ is then reacted with PbO to form 100% pure perovskite PMN. The success of this method lies in the prereaction of MgO and Nb_2O_5. This eliminates the possibility of PbO preferentially reacting with Nb_2O_5 to form the pyrochlore P_3N_4 phase. Gururaja et al. [13] attempted to utilize this approach to prepare perovskite PZN ceramics. ZnO and Nb_2O_5 were prereacted to form $ZnNb_2O_6$, followed by subsequent reaction with PbO. The product of this reaction turned out to be pyrochlore, and the perovskite phase could not be stabilized in PZN ceramics by this method. This signifies that the reaction kinetics are not the only determining factor for pyrochlore formation in the PZN system. As this method has also failed to stabilize the perovskite phase in other cases (e.g. $Pn(Zn_{1/3}Ta_{2/3})O_3$ and $Pb(Cd_{1/3}Nb_{2/3})O_3$), it is apparent that the thermodynamics of these systems must also be considered.

The relative stabilities of the pervoskite and other possible structures for the ABO_3 family of ceramics has received a great deal of attention over the years. The two basic requirements for the stability of the perovskite structure are: (1) the ionic radii of the cations should be within proper limits and (2) the cations–anions should have a strong ionic bond. The first requirement refers to the size of the perovskite unit cell. Goldschmidt suggested the concept of a tolerance factor (t) to describe the stability limits of a crystal structure in terms of the ionic radii [14]. The perovskite structure was concluded to be expected within the limits $t = 0.88$ to 1.09 (when the ionic radii for the A site cations are corrected for coordination number 12). The second requirement concerns the ionic character in the bonds. The difference between the electronegativities of a cation and anion is proportional to the degree of ionicity within the bond. In an effort to understand the relationship of these two basic requirements in determining perovskite structure stability, Halliyal et al. [15] reported a plot of the tolerance factors and electronegativity differences for several known ABO_3-type perovskite compounds. An important trend becomes apparent as a result of this plot. Compounds that have both large tolerance factors and large electronegativity differences, e.g. $BaTiO_3$ (BT) and $KNbO_3$ (KN), have stable perovskite structures. For the $Pb(B'B'')O_3$ compounds, PMN, PZN, $Pb(Fe_{1/2}Nb_{1/2})O_3$ (PFN), $Pb(Fe_{2/3}W_{1/3})O_3$ (PFW), $Pb(Ni_{1/3}Nb_{2/3})O_3$ (PNN) and $Pb(In_{1/2}Nb_{1/2})O_3$ (PIN), the tolerance factors and electronegativity differences both are small, and the perovskite structure is not easily stabilized. Thus, in the case of these latter mentioned ferroelectrics, it appears that the thermodynamics of the system are

also important in determining the stability of the perovskite structure.

The results of the heat treatments of the sol-gel derived material are consistent with the postulation that perovskite is not the most thermodynamically stable phase in PZN. The perovskite phase in this material seems to be most stable at 1000°C. The finer particle size and higher degree of homogeneity of the sol-gel derived material (as opposed to the mixed-oxide derived material) and the prereaction of the Zn and Nb species were probably important factors in stabilizing the perovskite phase. This suggest that both the reaction kinetics and thermodynamics must be considered in determining the perovskite phase stability in PZN.

4. Summary

The use of sol-gel has afforded a 75% perovskite PZN-PT material. The perovskite phase in this material seems to be most stable at 1000°C.

These results are preliminary. The sol-gel process appears to be a promising route for the stabilization of the perovskite phase in such materials as PZN, and further work to exploit this may prove to be very beneficial.

References

[1] Y. Yokomizo, T. Takahashi and S. Nomura, J. Phys. Soc. Japan 28 (1970) 1278.
[2] S. Nomura and J. Kuwata, Mat. Res. Bull. 14 (1979) 769.
[3] J. Kuwata, K. Uchino and S. Nomura, Ferroelectrics 22 (1979) 863.
[4] J. Kuwata, K. Uchino and S. Nomura, Ferroelectrics 37 (1981) 579.
[5] J. Kuwata, K. Uchino and S. Nomura, Japan. J. Appl. Phys. 21 (1982) 1298.
[6] S.R. Gurkovich and J.B. Blum, in: Ultrastructure processing of ceramics, glasses and composites, eds. L.L. Hench and D.R. Ulrich (Wiley-Interscience, New York, 1984) ch. 12.
[7] J.B. Blum and S.R. Gurkovich, J. Mat. Sci. 20 (1985) 4479.
[8] M. Aggrawal, C.K. Sharma and R.C. Mehrotra, Synth. React. Met.-Org. Chem. 13 (1983) 571;
R. Jain, A.K. Rai and R.C. Mehrotra, Z. Naturforsch. 40b (1985) 1371.
[9] R.C. Mehrotra, M.M. Aggrawal and P.N. Kapoor, J. Chem. Soc. A (1968) 2673.
[10] M. Lejeune and J.P. Boilot, Ceram. Intern. 9 (1983) 119.
[11] T.W. Dekleva, unpublished work.
[12] S.L. Swartz and T.R. Shrout, Mat. Res. Bull. 17 (1982) 1245.
[13] T.R. Gururaja, A. Safari and A. Halliyal, Am. Ceram. Soc. Bull. 65 (1986) 1601.
[14] V.M. Goldschmidt, Skr. Norske Vidensk. Akad. Oslo, No. 2 (1926).
[15] A. Halliyal, U. Kumar, R.E. Newnham and L.E. Cross, Am. Ceram. Soc. Bull. 66 (1987) 671.

Am Ceram Soc Bull, 66 [4] 671-76 (1987)

Stabilization of the Perovskite Phase and Dielectric Properties of Ceramics in the $Pb(Zn_{1/3}Nb_{2/3})O_3$-$BaTiO_3$ System

ARVIND HALLIYAL,* UMESH KUMAR,* ROBERT E. NEWNHAM,* and LESLIE E. CROSS*

Pennsylvania State University, Materials Research Lab, University Park, PA 16802

The formation of a pyrochlore structure phase is a major problem in the preparation of $Pb(Zn_{1/3}Nb_{2/3})O_3$ (PZN)-based ceramics since its presence is detrimental to the dielectric and piezoelectric properties. An analysis of electronegativity difference and tolerance factor of several ABO_3 type of compounds shows that $BaTiO_3$ is an excellent additive to stabilize perovskite phase in PZN, and the present experiments show that 6 to 7 mol% of $BaTiO_3$ stabilizes perovskite structure in PZN. Phase relations, ceramic preparation procedure, and dielectric properties of compositions in the PZN-BT system are presented. Curie temperatures of the compositions in this system range between $-130°$ to 140°C. Compositions suitable for capacitor application have been identified.

Lead zinc niobate ($Pb(Zn_{1/3}Nb_{2/3})O_3$, hereafter designated PZN) is a ferroelectric with perovskite structure exhibiting a diffuse phase transition. It has a rhombohedral structure at room temperature and undergoes a phase transition at ≈140°C to cubic structure. Single crystals of PZN with perovskite structure can be synthesized using the flux method. Single crystals of PZN showing excellent dielectric, optical, and electrostrictive properties have been studied extensively.[1-3]

The solid solution between PZN with rhombohedral symmetry and $PbTiO_3$ (PT) with tetragonal symmetry has a morphotropic phase boundary (MPB) at room temperature for a composition near 9 mol% of PT.[4] Single crystals with composition near the MPB show unusually large dielectric and piezoelectric constants and higher electromechanical coupling coefficients (92%)[5] than those of the PZT family of ceramics. Single crystals of PZN-PT can also be grown by the flux method.[6]

It is very difficult to prepare pure PZN or PZN-PT ceramics with the perovskite structure by conventional ceramic processing. The product obtained by solid-state reaction at ≈1100°C is largely a cubic pyrochlore phase of the type $Pb_3Nb_4O_{13}$, which is detrimental to both dielectric and piezoelectric properties. The formation of pyrochlore phase has been observed in a number of lead-based $A(B'B'')O_3$ type ferroelectric compounds with perovskite structure.[6]

The problem of pyrochlore formation has been studied in $Pb(Mg_{1/3}Nb_{2/3})O_3$ (PMN) ceramics. By following a different processing scheme, Swartz and Shrout[6] were able to stabilize perovskite structure in PMN. The reaction sequence used by them is

$$MgO + Nb_2O_5 \xrightarrow{1000°C} MgNb_2O_6 \quad (1)$$

$$MgNb_2O_6 + 3PbO \xrightarrow{900°C} 3Pb(Mg_{1/3}Nb_{2/3})O_3 \quad (2)$$

In this method, MgO is prereacted with Nb_2O_5 to form $MgNb_2O_6$ which has columbite structure. The $MgNb_2O_6$ is then reacted with PbO to obtain 100% pure perovskite PMN ceramics. Since Mg^{+2} and Zn^{+2} have same charge and approximately similar ionic radii, it seems plausible to prepare perovskite PZN ceramics by first preparing $ZnNb_2O_6$ by reacting ZnO and Nb_2O_5 and subsequently reacting $ZnNb_2O_6$ with PbO. For reasons which are not clear, the reaction product obtained by this reaction sequence is pyrochlore.[7]

Recently, Furukawa *et al.*[8,9] have reported that the formation of the pyrochlore phase in PZN can be suppressed by adding 15 mol% of either $BaTiO_3$ or $SrTiO_3$. These ceramics show a maximum dielectric constant of ≈5000 which is much lower than that of PZN single crystals (≈60 000). The ceramics in the $(1-x)PZN-xPT$ system always yield a mixture of perovskite and pyrochlore phase when $x<0.75$.[7] The perovskite structure in PZN-PT ceramics can be further stabilized by the addition of $Ba(Zn_{1/3}Nb_{2/3})O_3$,[11] or by the partial substitution of PbO with K_2O.[12] These additions, however, dilute the dielectric and piezoelectric properties. Lastly, perovskite type PZN can be synthesized under high pressure at elevated temperature.[10]

The present study was undertaken to stabilize perovskite phase in PZN ceramics by adding only a small percentage of a second perovskite compound. If the perovskite phase can be stabilized by only a small amount of a second component, the properties of PZN probably will not be altered significantly. From the work of Furukawa *et al.*,[8] it is clear that the perovskite structure in PZN can be stabilized by the addition of a more ionic compound. In the present work, an analysis of the stability of several compounds having the perovskite structure is made by considering the structure field map and ionic nature of the chemical bonds. This analysis shows that $BaTiO_3$ (BT) is an excellent additive for stabilizing the perovskite structure in PZN. The present preparation studies confirmed that BT is very effective in suppressing the formation of pyrochlore phase in PZN. In the present paper the preparation procedure, phase relations, and dielectric properties of several compositions in PZN-BT binary system are reported.

Stability of Perovskite Structure

The stability of different crystal structures belonging to a particular class of compounds can be studied by structure field

*Member, the American Ceramic Society

Received July 14, 1986, revised copy received September 29, 1986, approved December 5, 1986

Peer Reviewed Contribution

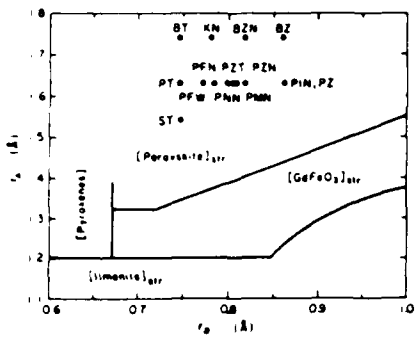

Fig. 1. Structure field map of ABO_3 [perovskites]—BT: $BaTiO_3$; ST: $SrTiO_3$; PT: $PbTiO_3$; KN: $KNbO_3$; BZ: $BaZrO_3$; PZ: $PbZrO_3$, PZT: $Pb(Zr_{1-2}Ti_{1-2})O_3$; PMN: $Pb(Mg_{1-3}Nb_{2-3})O_3$; PZN: $Pb(Zn_{2-3}Nb_{2-3})O_3$; PFN: $Pb(Fe_{1-2}Nb_{1-2})O_3$, PFW: $Pb(Fe_{2-3}W_{1-3})O_3$; PNN: $Pb(Ni_{1-3}Nb_{2-3})O_3$, PIN: $Pb(In_{1-2}Nb_{1-2})O_3$; BZN: $Ba(Zn_{2-3}Nb_{2-3})O_3$

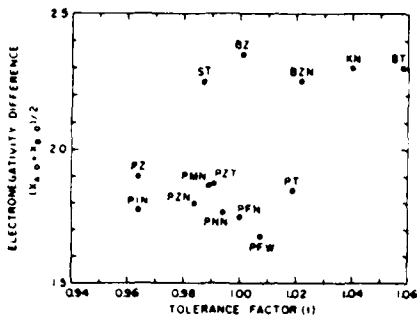

Fig. 2. Plot of electronegativity difference vs tolerance factor.

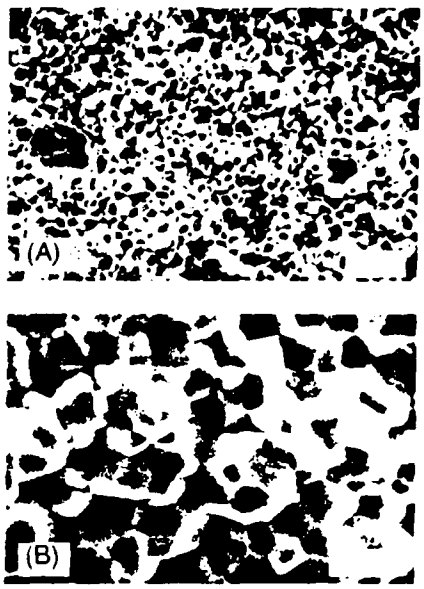

Fig. 3. Microstructure of (A) 0.9PZN–0.1BT (bar = 10 μm) and (B) 0.85PZN–0.15BT (bar = 5 μm). Both were sintered at 1150°C for 1 h.

maps.[13] Structure field maps provide a useful way of correlating ionic radii with structure types. A structure field map of ABO_3 compounds near the perovskite region is shown in Fig. 1. Here r_A is the radius of the larger cation and r_B is the radius of the smaller cation. Several ABO_3 type ferroelectric oxides are marked in this diagram. It is clear that all the compounds under consideration fall well within the ideal perovskite region of the structure field map. However, it is difficult to prepare several $A(B'B'')O_3$ lead-based compounds such as PMN, PZN, PFN, PFW, PNN, and PIN in perovskite form by the usual ceramic processing techniques. Such mixed oxide methods yield a mixture of perovskite and pyrochlore phases. The occurrence of pyrochlore structure can be explained by considering the ionic nature of the chemical bonds in these compounds.

Oxide perovskites are basically ionic compounds. For an ABO_3 compound to form a stable perovskite structure, the ionic radii of the cations should be within proper limits and the elements should form strong mutual ionic bond. Goldschmidt has proposed the concept of tolerance factor to describe the stability limits of a crystal structure in terms of the ionic radii.[14] For the perovskite structure, the tolerance factor, t, is given by

$$t = \frac{r_A + r_O}{\sqrt{2}(r_B + r_O)} \tag{3}$$

Here r_A and r_B are the ionic radii of cations A and B and r_O is the ionic radius of oxygen. The perovskite structure is stable if t is large.[14]

The second factor to be considered in determining the stability of perovskite structure is the degree of ionic character of the chemical bonds in the compound. The percentage of ionic character of the bonds is proportional to the electronegativity difference between cations and anions.

For several ABO_3 compounds with perovskite structure, the tolerance factors were calculated using Eq. (3) and the ionic radii proposed by Shannon and Prewitt.[15,16] The electronegativity differences of cation A and oxygen (χ_{A-O}) and cation B and oxygen (χ_{B-O}) were calculated using Pauling's electronegativity scale.[17] For $A(B'B'')O_3$ type perovskites, a weighted average value was used for calculating r_B and χ_{B-O}. A plot of average electronegativity differences $(\chi_{A-O} + \chi_{B-O})/2$ vs the tolerance factor is shown in Fig. 2.

A few interesting observations can be made from Fig. 2. Barium titanate and $KNbO_3$ have both large tolerance factor and large electronegativity difference, and hence these compounds should have stable perovskite structure. For PbO-based perovskite $A(B'B'')O_3$ compounds, PMN, PZN, PFN, PFW, PNN, and PIN, both the tolerance factor and electronegativity difference are small, and hence they may not form perovskite structure easily. However, there are certain exceptions, such as $PbZrO_3$ which has a low tolerance factor and low electronegativity difference but never shows the formation of a phase with pyrochlore structure. Probably for these compounds, other factors, such as electron configuration, cation valence stability, ordering parameters, etc., should also be considered.

Figure 2 also shows that it should be more difficult to stabilize PZN in perovskite form than PMN which is in accordance with experimental results. PMN can be prepared in perovskite form by repeated calcination or by the reaction sequence proposed by Swartz and Shrout.[6] It is not possible to stabilize PZN in perovskite form by these techniques. The figure also reveals why the solid solution system $(1-x)$ PZN$-x$PT can be stabilized in perovskite form if $x > 0.25$. The addition of PT to PZN increases both the net tolerance factor and the electronegativity difference. Since $BaTiO_3$ has the largest electronegativity difference and tolerance factor it should be possible to stabilize PZN or PMN in perovskite form by adding a smaller percentage of $BaTiO_3$ than $PbTiO_3$. Present studies indicated that the addition of 6 to 7 mol% of $BaTiO_3$ is sufficient to stabilize perovskite structure in PZN. It should be noted, however, that the analysis presented here is one of quasithermodynamic equilibrium. Previous studies have shown that PZN single crystals can be prepared in perovskite form by the flux method either by slow cooling of the melt or by water quenching.[18] On reheating the crystals, the perovskite structure converts to pyrochlore structure at ≈ 600°C, indicating that the perovskite structure in PZN is in metastable condition for the above preparation procedure. Reaction kinetics also play a major role in the stability of perovskite structure in ferroelectric relaxors such as PMN or PZN. In PMN, the perovskite structure can be stabilized either by repeated calcination or by the columbite precursor method, as described earlier.[6] For a better understanding of the stability of perovskite structure in lead-based ferroelectric relaxors, one should consider reaction kinetics also. The kinetics of the reaction would depend to a large extent on the purity,

Table I. Calcination and Sintering Temperatures for $(1-x)PZN-xBT$

x	Calcination temperature (°C)	Sintering temperature (°C)	Time (h)	Perovskite phase (%)	Percentage of theoretical density (%)
0	900	1000	4	0	
0.02	900	1000	3	35	
0.05	900	1075	1	85	90–92
0.07	900	1100	1	100	94–97
0.08	900	1100	1	100	94–97
0.09	900	1100	1	100	94–97
0.10	900	1150	1	100	95–97
0.15	900	1150	1	100	95–97
0.20	900	1150	1	100	95–97
0.30	900	1175	1	100	94–96
0.40	900	1175	1	100	94–96
0.50	900	1250	1	100	94–96
0.60	900	1275	1	100	94–96
0.70	1150	1325	1	100	94–96
0.80	1150	1325	2	100	92–95
0.85	1150	1325	2	100	92–95
0.90	1150	1350	2	100	90–92
1.00		1350	2	100	92–94

particle size, and surface area of the starting materials used, and on the details of ceramic processing. The minimum amount of second perovskite compound needed to stabilize perovskite phase may vary slightly depending on reaction kinetics.

Sample Preparation and Measurements

In the binary system $(1-x)PZN-xBT$, compositions were prepared at 10 mol% intervals of $BaTiO_3$. Near PZN, compositions were prepared at 1 mol% intervals to determine the minimum amount of $BaTiO_3$ needed to obtain ceramics with 100% perovskite phase.

For compositions with $x \leq 0.8$, reagent grade PbO,* ZnO,† Nb_2O_5,‡ TiO_2,§ and $BaCO_3$§ were used as starting materials. Excess PbO amounting to 0.5 wt% was added to compensate for PbO loss during firing. The mixtures were ball milled in polyethylene jars using C_2H_5OH for 12 to 16 h using ZrO_2 grinding media. The slurry was dried and calcined for 4 to 10 h at temperatures ranging from 900° to 1150°C. The calcined powder was ball milled and dried again to obtain homogeneous powder. Pellets 12 mm in diameter and 2–3 mm thick were pressed using PVA binder, and the binder was burnt out by a slow heating at 500°C for 1 h. Samples were sintered in a sealed Al_2O_3 crucible at temperatures ranging from 1000° to 1350°C using a heating rate of 200°C/h in an SiC resistance furnace. To limit PbO loss from the pellets, a PbO-rich atmosphere was maintained by placing an equimolar mixture of PbO and ZrO_2 inside the crucible. Weight loss on sintering was held to <1 wt% for all the compositions. The conditions for calcination and sintering for different compositions are given in Table I.

For compositions with $0.8 < x \leq 1$, prereacted $ZnNb_2O_6$ and high purity $BaTiO_3$ powder‖ were used as precursor materials to increase the reactivity of the powders during calcination. First, reagent grade ZnO and Nb_2O_5 were mixed by ball milling and calcined at 1000°C for 4 h to obtain $ZnNb_2O_6$. Lead oxide, $ZnNb_2O_6$, and $BaTiO_3$ were then mixed and ball milled. The rest of the procedure for preparing ceramics is the same as described above. Selected compositions containing 0.1 to 0.4 wt% of MnO_2 were prepared to determine the effect of MnO_2 on dielectric properties.

The relative amounts of pyrochlore and perovskite phases were determined using powder X-ray diffraction patterns of sintered samples by measuring the major X-ray peak intensities for the perovskite and pyrochlore phases, i.e. (110) and (222), respectively. The percentage of perovskite phase was calculated using the following equation

$$\% \ perov = \frac{100 x I_{perov}}{(I_{perov} + I_{pyro})} \quad (4)$$

Theoretical densities were calculated from lattice parameter measurements, and bulk densities were geometrically determined.

For dielectric measurements, gold electrodes were sputtered and air-dry silver paint was applied over gold electrodes. Dielectric measurements were performed on an automated system, wherein a temperature control box** and LCR meters†† were controlled by a desktop computer.‡‡ Dielectric constant and dissipation factors were measured between 100 Hz and 100 kHz, as the samples were cooled at a rate of 3° to 4°C/min. The temperature range covered was 250° to −150°C.

The electrical resistivity was determined by applying a voltage of 10 V across the samples at room temperature using a picoampmeter,§§ with the current value recorded after 10 min.

Table II. Amount of Additives Needed to Stabilize Perovskite Phase in PZN

Additive	Amount (mol%)
$BaTiO_3$	6–7*
$SrTiO_3$	9–10[19]
$PbTiO_3$	25–30[7]
$BaZrO_3$	15–18*
$Ba(Zn_{1/3}Nb_{2/3})O_3$	15[11]
Replacing Pb with K	10[12]
$PbZrO_3$	55–60[20]

*From present work.

Results and Discussion

Calcination and Sintering

The calcination and sintering conditions, fired densities, and percent perovskite phase for all the compositions are given in Table I. Higher calcination and sintering temperatures were necessary for compositions containing a large fraction of $BaTiO_3$. Compositions with x in the range $0.9 < x < 1$ could not be sintered to sufficient densities. Probably evaporation of PbO during firing is the primary reason for the failure in preparing dense ceramics in this composition range. Lead zinc niobate ceramic containing no BT additive was completely pyrochlore in structure. The percentage of perovskite phase increased by the addition of $BaTiO_3$ as shown in Table I. Compositions containing >7 mol% $BaTiO_3$ did not have any pyrochlore phase. It is clear that the formation of pyrochlore phase in PZN can be completely avoided by adding 6 to 7 mol% $BaTiO_3$. The perovskite phase in PZN can be stabilized by the addition of other perovskite compounds such as $SrTiO_3$, $PbZrO_3$, or $BaZrO_3$.[18] The minimum amount of different oxides or perovskite compounds needed to stabilize the perovskite structure in PZN by conventional ceramic processing is given in Table II. The percentage of theoretical density was in the range of 94% to 96% for most of the compositions. Typical SEMs of fractured ceramics are shown in Fig. 3. The grain size was in the range 2–5 μm.

*Supplied by Hammond Lead Products, Inc., Pottstown, PA.
†Supplied by NJ Zinc Co., Palmerton, PA.
‡Supplied by Teledyne Wah Chang Albany, Albany, OR
§Supplied by J. T. Baker Chemical Co., Philipsburg, NJ
‖Grade HPB, TAM Ceramics, Inc., Niagara Falls, NY
**Model 2300, Delta Design, Inc., San Diego, CA.
††Model 4274A and 4275A LCR meters, Hewlett Packard, Inc., Palo Alto, CA
‡‡Model 9816, Hewlett Packard, Inc., Palo Alto, CA
§§Model 4140B pA meter, Hewlett Packard, Inc., Palo Alto, CA

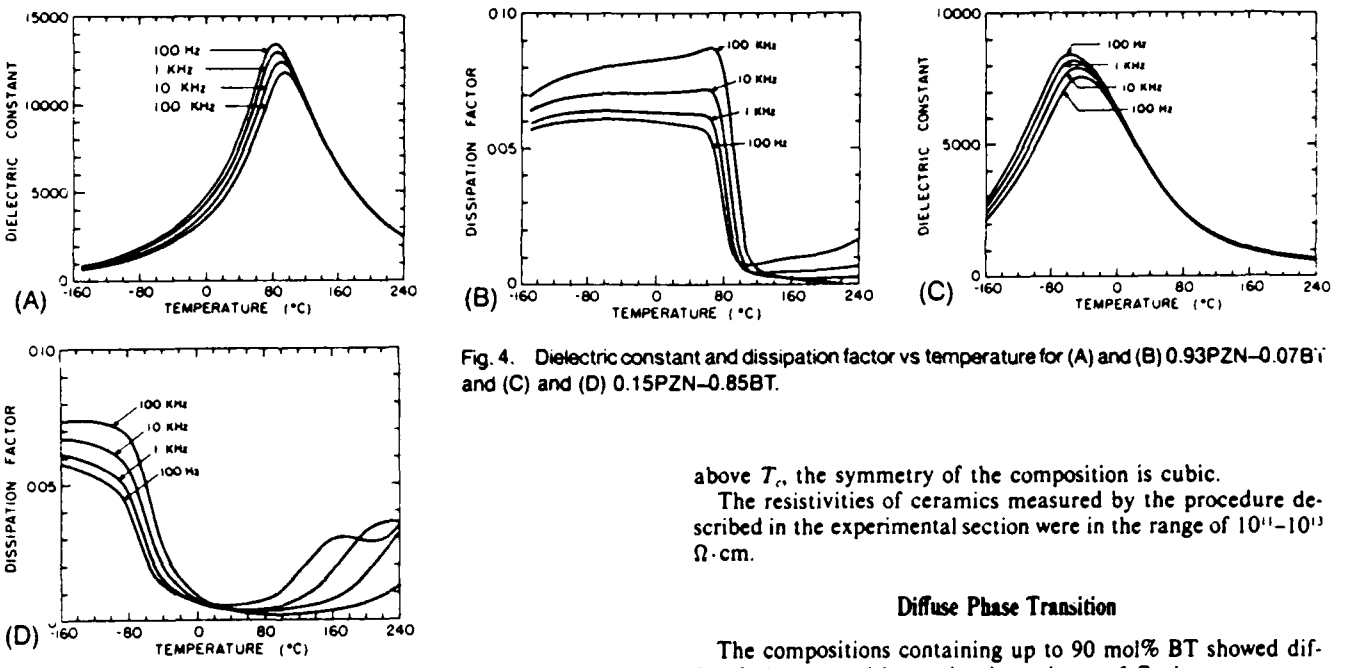

Fig. 4. Dielectric constant and dissipation factor vs temperature for (A) and (B) 0.93PZN–0.07BT and (C) and (D) 0.15PZN–0.85BT.

Dielectric Measurements

Figure 4 shows the temperature dependencies of dielectric constant and dissipation factor at various frequencies for compositions containing 7 and 85 mol% $BaTiO_3$. All the compositions up to 90 mol% $BaTiO_3$ showed broad maxima of dielectric constant and an increase in Curie temperature (T_c) with increasing frequency characteristic of relaxor ferroelectrics. Corresponding frequency dispersion of the dissipation factor was also observed.

The temperature dependence of dielectric constant (at 1 kHz) for a range of compositions are shown in Figs. 5–7. The variation of Curie temperature with composition is shown in Fig. 8. The Curie temperature decreases sharply with the addition of $BaTiO_3$. For compositions containing 70 to 80 mol% $BaTiO_3$, T_c is approximately -130°C. When the amount of $BaTiO_3$ is >80 mol%, T_c increases sharply. The magnitude of the dielectric constant maximum increases with the addition of up to 7 mol% $BaTiO_3$ and decreases sharply with further addition of $BaTiO_3$ as shown in Fig. 9. It increases again for compositions containing >70 mol% $BaTiO_3$. From the X-ray diffraction pattern and the temperature of dielectric maximum data, the phase diagram of PZN-BT system is as shown in Fig. 10. Here it is assumed that above T_c, the symmetry of the composition is cubic.

The resistivities of ceramics measured by the procedure described in the experimental section were in the range of 10^{11}–10^{13} Ω·cm.

Diffuse Phase Transition

The compositions containing up to 90 mol% BT showed diffused phase transition and a dependence of Curie temperature on frequency. The temperature difference between the T_c's measured at 0.1 and 100 kHz (ΔT_c) gives an estimation of the relaxor characteristic of the transition. The values of ΔT_c are listed in Table III. Compositions containing 20 to 40 mol% BT showed the strongest frequency dispersion.

For ferroelectrics with a diffused phase transition, the law $1/\epsilon \approx (T-T_0)^2$ has been shown to hold over a wide temperature range instead of the normal Curie Weiss law.[15] If the local Curie temperature distribution is Gaussian, the reciprocal permittivity can be written in the form

$$\frac{1}{\epsilon} = \frac{1}{\epsilon_m} + \frac{(T-T_0)^2}{2\epsilon_m \delta^2} \tag{5}$$

Here δ is diffuseness parameter. For PZN-PT compositions, from the slope of plots of $1/\epsilon$ vs $(T-T_0)^2$, the values of δ were calculated (Table III). The value of δ showed an increase with the amount of BT and was highest for compositions with 40 to 50 mol% of BT, indicating a broadened phase transition for these compositions.

Compositions for Capacitors

There is a growing need for ceramic materials for multilayer capacitors[21] with high dielectric constant and low temperature

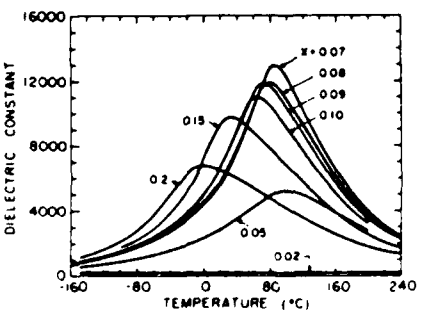

Fig. 5. Variation of dielectric constant (1 kHz) with temperature for $(1-x)$PZN – xBT compositions, $x=0$ to 0.2.

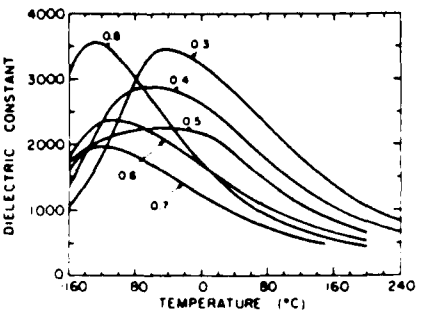

Fig. 6. Variation of dielectric constant (1 kHz) with temperature for $(1-x)$PZN – xBT compositions, $x=0.3$ to 0.8.

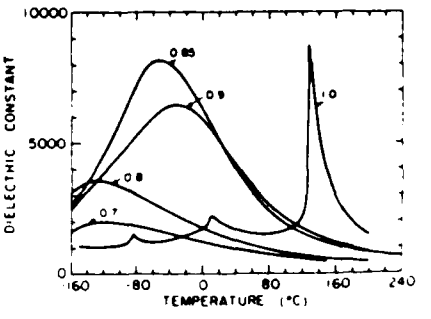

Fig. 7. Dielectric constant (1 kHz) vs temperature for $(1-x)$PZN – xBT compositions, $x=0.7$ to 1.0.

Arvind Halliyal

Umesh Kumar

Robert E. Newnham

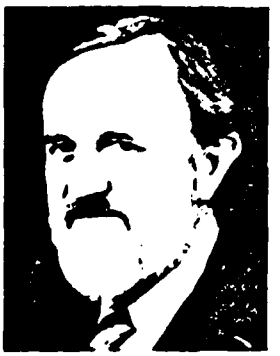

Leslie E. Cross

Arvind Halliyal is a research associate with the Materials Research Lab at Pennsylvania State University, University Park, PA. He received his B.Sc. in physics from Bangalore University, India, in 1972 and an M.Tech. in materials science from Indian Institute of Technology, Kanpur, India, in 1976. He obtained his M.S. in materials science from the University of Southern California in 1978 and a Ph.D. in solid-state science from Penn State in 1984. Prior to joining Penn State he was with Bharat Electronics Ltd., India. Dr. Halliyal's current research interests are in the areas of ferroelectric relaxors, dielectric and piezoelectric ceramics and composites, glass-ceramics, pyroelectric materials, thermistors, and sensors.

Umesh Kumar is a graduate student at the Materials Research Lab at Pennsylvania State University. He earned his B.Sc. and M.Sc., both in applied sciences, from Madras University, India. He received an M.Tech. in materials science from Indian Institute of Technology, Kanpur, India. His current research is concerned with the preparation and characterization of PZN- and PMN-based ceramics.

Robert E. Newnham is professor of solid-state science at Pennsylvania State University. He received his B.S. from Hartwick College, Oneonta, NY, in 1950; M.S. from Colorado State University, Fort Collins, in 1952; Ph.D. in physics from Penn State in 1956; and Ph.D. in crystallography from Cambridge University, Cambridge, United Kingdom, in 1960. Before joining Penn State, Dr. Newnham was an associate professor of electrical engineering at the Massachusetts Institute of Technology from 1958 to 1966. His research interests include crystal physics and structure-property relationships; phase transitions in ferroic materials; piezoelectric, pyroelectric, and electrostrictive phenomena; composite materials for transducer applications; and sensors.

Leslie E. Cross is professor of electrical engineering and director of the Materials Research Lab at Pennsylvania State University. He received his B.Sc. and Ph.D. in physics from Leeds University, Leeds, United Kingdom, in 1948 and 1952, respectively. Prior to joining Penn State in 1961, Dr. Cross was at Leeds University as a lecturer during 1948–51 and research associate during 1954–61. His research interests include ferroelectric materials and ferroic phenomena; dielectric, piezoelectric, and pyroelectric crystals, ceramics, and composites; electronic ceramics and their applications; electrostriction; electrooptics; sensors; and phase transitions.

x in the range $0 < x \leq 0.9$ showed diffuse phase transition with Curie temperature between $-130°$ to 140°C.

Acknowledgements

The authors are thankful to Prof. Rustum Roy for helpful suggestions. This work was made possible by the financial support from the Office of Naval Research (Contract No. N00014-82-K-0339).

References

Y. Yokomizo, T. Takahashi, and S. Nomura, "Ferroelectric Properties of $Pb(Zn_{1/3}Nb_{2/3})O_3$," *J. Phys. Soc. Jpn.*, **28** [5] 1278–84 (1970).

[2]S. Nomura and J. Kuwata, "Electrostriction in $Pb(Zn_{1/3}Nb_{2/3})O_3$," *Mater. Res. Bull.*, **14**, 769–74 (1979).

[3]J. Kuwata, K. Uchino, and S. Nomura, "Diffuse Phase Transitions in Lead Zinc Niobate," *Ferroelectrics*, **22**, 863–67 (1979).

[4]J. Kuwata, K. Uchino, and S. Nomura, "Phase Transitions in the $Pb(Zn_{1/3}Nb_{2/3})O_3$–$PbTiO_3$ System," *Ferroelectrics*, **37**, 579–87 (1981).

[5]J. Kuwata, K. Uchino, and S. Nomura, "Dielectric and Piezoelectric Properties of $0.91Pb(Zn_{1/3}Nb_{2/3})O_3$–$0.09PbTiO_3$ Single Crystals," *Jpn. J. Appl. Phys.*, **21** [9] 1298–1302 (1982).

[6]S. L. Swartz and T. R. Shrout, "Fabrication of Perovskite Lead Magnesium Niobate," *Mater. Res. Bull.*, **17** [10] 1245–50 (1982).

[7]T. R. Gururaja, A. Safari, and A. Halliyal, "Preparation of Perovskite PZN-PT Ceramic Powder near the Morphotropic Phase Boundary," *Am. Ceram. Soc. Bull.*, **65** [12] 1601–03 (1986).

[8]O. Furukawa, Y. Yamashita, M. Harata, T. Takahashi, and K. Inagaki, "Dielectric Properties of Modified Lead Zinc Niobate Ceramic," *Jpn. J. Appl. Phys.*, **24** [Supp. 24-3] 96–99 (1985).

[9]Y. Yamashita, O. Furukawa, M. Harata, T. Takahashi, and K. Inagaki, "A New Lead Perovskite Y5S Dielectric for Multilayer Ceramic Capacitor," *Jpn. J. Appl. Phys.*, **24** [Suppl. 24-2] 1027–29 (1985).

[10]Y. Matsuo, H. Sasaki, S. Hayakawa, F. Kanamaru, and M. Koizumi, "High-Pressure Synthesis of Perovskite-Type $Pb(Zn_{1/3}Nb_{2/3})O_3$," *J. Am. Cer. Soc.*, **52** [9] 516–17 (1969).

[11]S. Nomura and H. Arima, "Dielectric and Piezoelectric Properties in the Ternary System of $Pb(Zn_{1/3}Nb_{2/3})O_3$–$Ba(Zn_{1/3}Nb_{2/3})O_3$–$PbTiO_3$," *Jpn. J. Appl. Phys.*, **11** [3] 358 (1972).

[12]L. Hanh and S. Nomura, "Ferroelectric and Piezoelectric Properties of $xPb_{...}Ky(Zn_{1/3}Nb_{2/3})O_{...}-(1-x)PbTiO_3$ Solid Solutions," *Jpn. J. Appl. Phys.*, **15** [6] 1059 (1976).

[13]O. Muller and R. Roy; in Crystal Chemistry of Nonmetallic Materials. Springer-Verlag, New York, 1974.

[14]V. M. Goldschmidt, Geochemische Verteilungsgesetze der elemente I-IX, Skrift. Norske, Vid. Akad. Oslo, I. Mat.-Naturv. K1.

[15]R. D. Shannon and C. T. Prewett, "Atomic Radii in Oxides and Fluorides," *Acta Crystallogr. Sect. B Struct. Crystallogr. Cryst. Chem.*, **25**, 925–45 (1969).

[16]R. D. Shannon and C. T. Prewitt, "Revised Values of Effective Ionic Radii," *ibid.*, **26**, 1046–48 (1970).

[17]L. Pauling; in The Nature of Chemical Bonds. Cornell University Press, Cornell, NY, 1960.

[18]A. Halliyal, T. R. Gururaja, U. Kumar, and A. Safari, "Stability of Perovskite Phase in $Pb(Zn_{1/3}Nb_{2/3})O_3$ and Other $A(B'B'')O_3$ Perovskites," IEEE Ultrasonic Symposium on Application of Ferroelectrics, Lehigh University (1986) (in press).

[19]J. Belsick, "Phase Relations and Dielectric Properties in the $Pb(Zn_{1/3}Nb_{2/3})O_3$–$SrTiO_3$–$PbTiO_3$ System", B.S. Thesis, Pennsylvania State University, University Park, PA, 1986.

[20]M. Lanagan and D. Anderson; private communication.

[21]J. M. Herbert, in Ceramic Dielectrics and Capacitors. Gordon and Breach Science Publishers, New York, 1985.

[22]M. Yonezawa, "Low-Firing Multilayer Capacitor Materials," *Am. Ceram. Soc. Bull.*, **62** [12] 1375–78, 1383 (1983).

[23]W. Pan, G. O. Dayton, and L. E. Cross, "Dielectric Aging Effects in Doped Lead Magnesium Niobate Lead Titanate Relaxor Ferroelectric Ceramics," IEEE Proc. of Symp. on Application of Ferroelectrics, Lehigh University (1986) (in press). ■

Am. Ceram. Soc. Bull., 66 [4] 664–67 (1987)

Phase Relations and Dielectric Properties of Ceramics in the System $Pb(Zn_{1/3}Nb_{2/3})O_3$-$SrTiO_3$-$PbTiO_3$

JOHN R. BELSICK,* ARVIND HALLIYAL,* UMESH KUMAR, and ROBERT E. NEWNHAM*

Pennsylvania State University, University Park, PA 16802

Lead-zinc-niobate-based ceramics $Pb(Zn_{1/3}Nb_{2/3})O_3$ (PZN), are difficult to prepare because of the formation of a pyrochlore phase which is detrimental to both the dielectric and piezoelectric properties. The addition of 9 to 10 mol% $SrTiO_3$(ST) stabilizes the perovskite phase in PZN. Phase relations and dielectric properties of ceramics in the system PZN-ST-$PbTiO_3$ were investigated. The stability of the perovskite phase was studied as a function of calcination temperature and time. Compositions in this system with high dielectric constant and low temperature coefficient of capacitance have been identified.

Lead zinc niobate [$Pb(Zn_{1/3}Nb_{2/3})O_3$—herein designated PZN] is a ferroelectric material with a partially disordered perovskite structure. It undergoes a diffuse phase transition near 140°C. The crystal symmetry is rhombohedral (ferroelectric) at room temperature and cubic (paraelectric) above 140°C.[1-3] The solid solution between PZN with rhombohedral symmetry and $PbTiO_3$(PT) with tetragonal symmetry has a morphotropic phase boundry (MPB) near 9 mol% PT. Single crystals with compositions near the MPB show extremely large dielectric and piezoelectric coefficients, much larger than those of PZT ceramics.[3] PZN and PZN-PT single crystals can be grown rather easily by a flux method and their properties have been reported.[4] PZN is also a promising candidate material for electrostrictive micropositioners.[5]

Unfortunately, it is very difficult to synthesize pure PZN or PZN-PT ceramics with the perovskite structure near the MPB by the usual solid-state reaction. The product obtained by solid-state reaction at ≈1100°C is a mixture containing a stable, cubic $Pb_3Nb_4O_{13}$-type pyrochlore phase. The formation of the pyrochlore phase is detrimental to both the dielectric and piezoelectric properties. In the system PZN-PT, the perovskite phase is stable only when the PT content exceeds 25 mol%. PZN ceramics with the perovskite structure can be prepared under high pressure and temperature conditions (25 kbars, 800° to 1000°C).[6] The perovskite structure in PZN can also be stabilized by the addition of $Ba(Zn_{1/3}Nb_{2/3})O_3$ (BZN)[7] as a third component or by the partial replacement of PbO by K_2O.[8] However, BZN or K_2O additions dilute the dielectric and piezoelectric properties. The peak dielectric constant reported in these ceramics is ≈7000, which is low compared to the extremely large values observed in PZN-PT single crystals. A similar reduction in piezoelectric properties has also been observed.

The problem of pyrochlore formation has been studied extensively in $Pb(Mg_{1/3}Nb_{2/3})O_3$ (PMN) ceramics.[9,10] By following a different processing scheme, Swartz and Shrout were able to stabilize the perovskite structure in PMN. They adopted the following reaction sequence:

$$MgO + Nb_2O_5 \xrightarrow{1000°C} MgNb_2O_6 \quad (1)$$

$$MgNb_2O_6 + 3PbO \xrightarrow{900°C} 3Pb(Mg_{1/3}Nb_{2/3})O_3 \quad (2)$$

In this method, MgO is prereacted with Nb_2O_5 to form $MgNb_2O_6$ which has the columbite structure. $MgNb_2O_6$ is then reacted with PbO to obtain 100% pure perovskite PMN ceramics. For reasons which are not clear, we were unsuccessful in preparing perovskite PZN by this processing scheme (by reacting $ZnNb_2O_6$ with PbO).

The stability of several ABO_3 perovskite compounds has been examined by considering their electronegativity difference and tolerance factor.[11] The analysis showed that $BaTiO_3$ (BT) and $SrTiO_3$ (ST) are ideal additives for stabilizing the perovskite structure in PZN. PZN ceramics with 100% perovskite structure can be prepared by adding only 6 to 7 mol% of BT and ≈10 mol% ST.[11] Phase relations and dielectric properties of compositions in the PZN-BT system have been reported,[11] and compositions useful for capacitors have been identified.[12]

The dielectric properties of several compositions in the system PZN-PT-ST have been studied by Yamashita *et al.*[13] for possible use in multilayer capacitors. Their study indicates that the pyrochlore phase can be eliminated by adding 20 mol% ST together with 20 mol% PT to PZN. In compositions containing only ST, pyrochlore phase cannot be eliminated completely. In their study, the composition 0.8 PZN-0.2 ST showed ≈90% of perovskite phase. However, our preliminary studies indicated that it is possible to stabilize the perovskite structure in PZN by adding only 10 mol% ST. The reason for the large amount of pyrochlore phase observed by Yamashita *et al.*[13] seems to be low calcination temperature (780°C). The present work was undertaken to investigate systematically the effect of calcination temperature and time on the stability of the perovskite structure in the system PZN-ST-PT and to prepare pyrochlore-free ceramics with large dielectric constants by optimizing the calcining and sintering conditions.

Experimental Procedure

The compositions selected for the present study were of the type (1-*x*-*y*) PZN-*x*ST-*y*PT, with *x* and *y* varying between 0 and 0.2. The columbite precursor method was used to reduce the formation of pyrochlore phase. ZnO and Nb_2O_5 were batched in the proper ratio to first prepare the columbite phase $ZnNb_2O_6$.

*Member, the American Ceramic Society

Received January 13, 1987, approved February 5, 1987

Supported by the Office of Naval Research under Contract No N00014-82-K-0339

Peer Reviewed Contribution

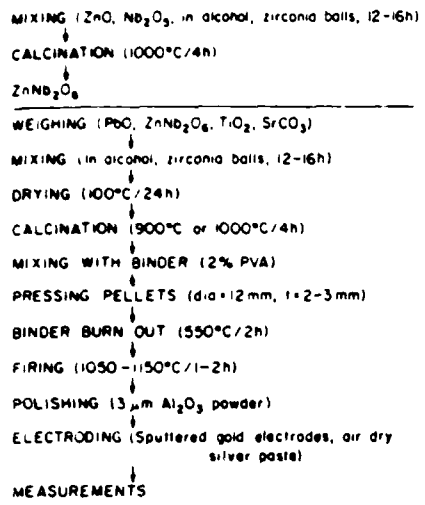

Fig. 1. Procedure for sample preparation.

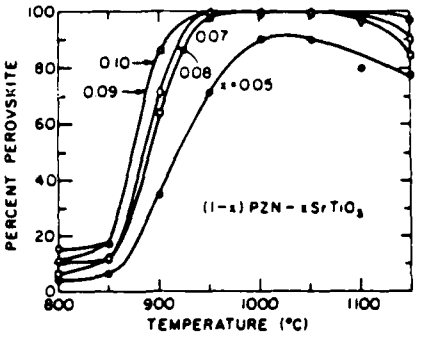

Fig. 2. Percentage of perovskite phase vs calcination temperature for $(1-x)$ PZN-xST ceramics.

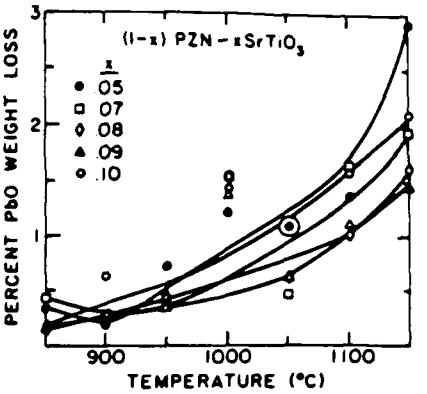

Fig. 3. Percentage PbO loss vs calcination temperature for $(1-x)$ PZN-xST ceramics.

The precursor was then mixed in stoichiometric ratio with PbO, $SrCO_3$, and TiO_2, and the ceramics were prepared by the procedure outlined in Fig. 1. Half a weight percent of excess PbO was added in all the compositions to compensate for PbO loss during calcination and sintering. The powders were calcined at 900°C for 4 h and a second calcination was conducted at 1000° for 4 h if the calcined powder contained any pyrochlore phase. The calcined powders were crushed and ball-milled and pellets ≈12 mm in diameter and 2 to 3 mm thick were pressed using PVA binder.

The pellets were then fired between 1050° and 1175°C for 1 to 2 h in sealed alumina crucibles. To compensate for the PbO weight loss, a PbO-rich atmosphere was maintained by placing an equimolar mixture of PbO and ZrO_2 inside the crucible.

The percentage of perovskite phase and lattice constants were determined by powder X-ray diffraction (XRD) patterns of calcined powder and fired ceramics. The relative amounts of the pyrochlore and perovskite phases were determined by measuring the major X-ray peak intensities for the perovskite and pyrochlore phases [(110) and (222) respectively]. The percentage of perovskite phase was calculated using the following equation:

$$\%perov = \frac{100 \times I_{perov}}{(I_{perov} + I_{pyro})} \quad (3)$$

Theoretical densities were calculated from lattice parameter measurements and bulk densities were determined geometrically.

For dielectric measurements, gold electrodes were sputtered, and air-dry silver paint was applied over the gold electrodes. Dielectric measurements were conducted on an automated system, wherein a temperature control box* and LCR bridge† were controlled by a desktop computer.‡ Dielectric constant and dissipation factors were measured between 100 Hz and 100 KHz, as the samples were cooled at a rate of 3° to 4°/min. The temperature range was −100 to 200°C.

Results and Discussion

Calcination and Sintering

Several compositions in the $(1-x)$PZN system (with $x=0.05$ to 0.20) were calcinated at different temperatures for varying time periods to study the effect of calcination conditions on the amount of perovskite phase. Separate mixtures were calcined for 4 h at each calcination temperature and the amount of perovskite phase was determined from powder XRD patterns. Figure 2 shows a plot of the percentage of perovskite phase in each composition as a function of calcination temperature. Figure 3 shows a plot of percentage PbO loss during calcination. For all the compositions the amount of perovskite phase is <20% for calcination temperatures below 850°C. For calcination temperatures higher than 850°C, the amount of perovskite phase increased sharply. Compositions with 9 to 10 mol% of ST, calcined at 950° to 1050°C showed 100% perovskite phase. In all the compositions, a small fraction of pyrochlore phase was observed for calcinations above 1050°C. This behavior is probably due to the loss of PbO at high temperatures (Fig. 3). It has been known that loss of PbO favors the formation of pyrochlore phase in lead-based relaxor compounds such as $Pb(Mg_{1/3}Nb_{2/3})O_3$.[9] The reason for the observation of a large fraction of pyrochlore phase in PZN-ST system by Yamashita *et al.*[1] is clear. In their study the calcination was conducted at a low temperature (780°C). From the present work it can be seen that the calcination temperature should be higher than 950°C to obtain pyrochlore-free PZN ceramics. The effect of calcination time on the amount of perovskite phase is shown in Fig. 4. Initially the amount of perovskite phase increases sharply with calcination time and then decreases slowly for longer periods of cal-

*Model 2300, Delta Design, Inc., San Diego, CA.
†Model 4274A and 4275A LCR meters, Hewlett-Packard, Inc., Palo Alto, CA.
‡Model 9816, Hewlett-Packard, Inc., Palo Alto, CA.

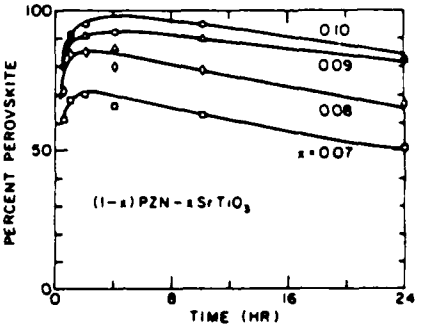

Fig. 4. Percentage of perovskite phase vs calcination time at 900°C for $(1-x)$ PZN-xST ceramics.

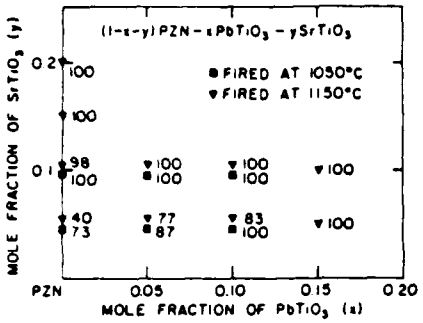

Fig. 5. Percentage perovskite phase in ceramic samples fired at 1050° and 1150°C.

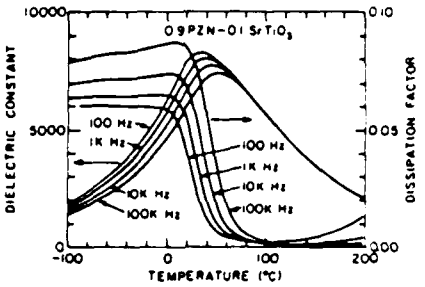

Fig. 6. Dielectric constant and dissipation factor vs temperature for 0.9 PZN-0.1 ST ceramics.

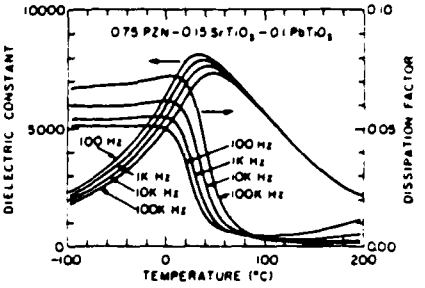

Fig. 7. Dielectric constant and dissipation factor vs temperature for 0.75 PZN-0.15 ST-0.1 PT ceramics.

cination, probably because of the loss of PbO. From the present study the optimum calcination conditions to obtain PZN ceramics with minimum amount of pyrochlore phase are 950° to 1000°C and 2 to 4 h.

It should be noted that, for calcination or firing done at temperatures >1050°C, there is a slight formation of pyrochlore phase. The firing schedule, percentage theoretical density, and percentage perovskite phase in fired ceramics are listed in Table I. Samples sintered at 1150°C contained a slightly larger fraction of pyrochlore phase than the samples sintered at 1050° to 1100°C. In the system PZN-ST-PT, the PT helps in further reducing the amount of pyrochlore phase. Figure 5 shows the amount of perovskite phase in ceramic samples fired at 1050° and 1150°C. The grain size in the ceramics, determined by SEM micrographs of fractured ceramics, ranged from 2 to 5 μm.

Dielectric Properties

Plots of dielectric constant and dissipation factor versus temperature for 0.9 PZN-0.1 ST and 0.75 PZN-0.15 ST-0.1 PT are shown in Figs. 6 and 7. All compositions showed a broad maxima of dielectric constant and an increase in Curie temperature (T_c) with increasing frequency, characteristic of relaxor ferroelectrics. A corresponding frequency dispersion of the dissipation factor was also observed.

The dielectric constant at T_c increases with additions of ST up to 10 mol% and then decreases with further additions of ST (Fig. 8). The dielectric constant initially increases with the addition of ST resulting from the increase in the amount of perovskite phase in the ceramics. The dielectric constants at T_c are between 4000 and 8000 in the PZN-ST binary system and between 6000 and 8000 in the PZN-ST-PT ternary system.

In the system PZN-ST, the variation of T_c with the mole fraction of ST is shown in Fig. 9. The T_c decreases sharply with increasing ST. The compositions 0.9 PZN-0.1 ST and 0.75 PZN-0.15 ST-0.1 PT have their T_c values near room temperature.

The difference between the Curie temperatures measured at 100 Hz and 100 KHz (ΔT_c) gives an estimate of the relaxor nature of the material. The larger the ΔT_c values, the greater the frequency dispersion of the maximum dielectric constant.

Table I. Sintering Data for PZN-ST-PT Ceramics

Composition			Sintering temperature (°C)	Time (hr)	% Theoretical density	Perovskite (%)
PZN	ST	PT				
0.95	0.05		1050	2	89.8	73
			1075	2	89.3	75
			1125	2	86.5	63
			1150	1	70.9	40
			1150	2	76.9	41
			1175	1	66.4	35
0.93	0.07		1050	2	93.5	94
			1150	1	91.1	79
0.92	0.08		1050	2	92.6	97
			1150	1	90.0	86
0.9	0.1		1150	1	94.4	100
0.85	0.15		1150	1	94.7	100
0.8	0.2		1150	1	93.6	100
0.9	0.05	0.05	1050	2	92.1	87
			1150	1	88.6	77
0.85	0.05	0.1	1050	2	91.0	100
			1150	1	85.3	83
0.85	0.1	0.05	1075	2	93.5	100
			1150	1	91.1	100
0.8	0.1	0.1	1075	2	92.6	100
			1150	1	90.5	100
0.8	0.15	0.05	1150	1	92.7	100
0.75	0.15	0.1	1150	1	93.7	100

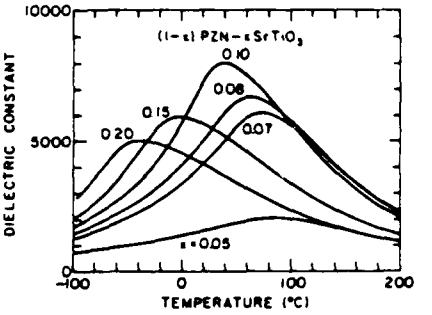

Fig. 8. Dielectric constant vs temperature for $(1-x)$ PZN-xST ceramics.

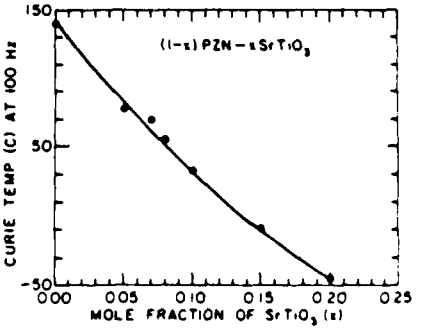

Fig. 9. Curie temperature vs mole fraction of ST for $(1-x)$ PZN-xST ceramics.

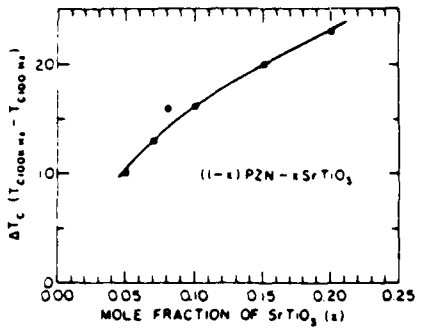

Fig. 10. ΔT_c vs mole fraction of ST for $(1-x)$ PZN-xST ceramics.

A plot of ΔT_c as a function of mole fraction of ST is shown in Fig. 10. A summary of the dielectric data can be found in Table II. Plots of temperature coefficient of capacitance (TCC) for selected compositions are shown in Fig. 11. Compositions 0.9 PZN-0.1 ST, 0.85 PZN-0.15 ST, 0.8 PZN-0.15 ST-0.05 PT, and 0.75 PZN-0.15 ST-0.1 PT satisfy Z5U and Y5U TCC specifications for capacitors.

Summary

Ceramics in the $(1-x-y)$ PZN-xST-yPT system having the perovskite structure can be prepared if the mole fraction of ST is $x \geq 0.1$. The calcination and sintering conditions were found to be very critical in obtaining pyrochlore-free ceramics. All compositions studied showed a broad diffuse phase transition with a shift in Curie temperature with frequency. Compositions with high dielectric constant and low values of temperature coefficient of capacitance have been identified.

References

[1]Y. Yokomizo, T. Takahashi, and S. Nomura, "Ferroelectric Properties of $Pb(Zn_{1/3}Nb_{2/3})O_3$," *J. Phys. Soc. Jpn.*, **28** [5] 1278–84 (1970).
[2]J. Kuwata, K. Uchino, and S. Nomura, "Diffuse Phase Transition in Lead Zinc Niobate," *Ferroelectrics*, **22**, 863–67 (1979).
[3]J. Kuwata, K. Uchino, and S. Nomura, "Dielectric and Piezoelectric Properties of 0.91 $Pb(Zn_{1/3}Nb_{2/3})O_3$-0.09 $PbTiO_3$ Single Crystals," *Jpn. J. Appl. Phys.*, **21** [8] 1298–1302 (1982).
[4]J. Kuwata, K. Uchino, and S. Nomura, "Phase Relations in the $Pb(Zn_{1/3}Nb_{2/3})O_3$-$PbTiO_3$ System," *Ferroelectrics*, **37**, 579–82 (1981).
[5]S. Nomura and J. Kuwata, "Electrostriction in $Pb(Zn_{1/3}Nb_{2/3})O_3$," *Mater. Res. Bull.*, **14**, 769–74 (1979).
[6]Y. Matsuo, H. Sasaki, S. Hayakawa, F. Kanamura, and M. Koizumi, "High Pressure Synthesis of Perovskite Type $Pb(Zn_{1/3}Nb_{2/3})O_3$," *J. Am. Ceram. Soc.*, **52** [9] 516–17 (1969).
[7]S. Nomura and H. Arima, "Dielectric and Piezoelectric Properties in the Ternary System of $Pb(Zn_{1/3}Nb_{2/3})O_3$-$Ba(Zn_{1/3}Nb_{2/3})O_3$," *Jpn. J. Appl. Phys.*, **11** [3] 358 (1972).
[8]L. Hanh and S. Nomura, "Ferroelectric and Piezoelectric Properties of $xPb_{1-y}K_y(Zn_{1/3}Nb_{2/3})O_{3-y/2}-(1-x)PbTiO_3$ Solid Solutions," *Jpn. J. Appl. Phys.*, **15** [6] 1059 (1976).
[9]S. L. Swartz and T. R. Shrout, "Fabrication of Perovskite Lead Magnesium Nobate," *Mater. Res. Bull.*, **17**, 1245–50 (1982).
[10]S. L. Swartz, T. R. Shrout, W. A. Schulze, and L. E. Cross, "Dielectric Properties of Lead-Magnesium Niobate Ceramics," *J. Am. Ceram. Soc.*, **67**, 311–15 (1984).
[11]A. Halliyal, U. Kumar, and R. E. Newnham, "Stabilization of Perovskite Phase and Dielectric Properties of Ceramics in the $Pb(Zn_{1/3}Nb_{2/3})O_3$-$BaTiO_3$ System"; to be published in the *American Ceramic Society Bulletin*.
[12]O. Furukawa, Y. Yamashita, M. Harata, T. Takahashi, and K. Inagaki, "Dielectric Properties of Modified Lead Zinc Niobate Ceramics," *Jpn. J. Appl. Phys.*, **24**, Suppl. 24–3, 96–99 (1985).
[13]Y. Yamashita, O. Furukawa, M. Harata, T. Takahashi, and K. Inagaki, "A New Lead Perovskite Y5S Dielectric for Multilayer Ceramic Capacitor," *Jap. J. Appl. Phys.*, **24**, 1027–29 (1985). ■

Table II. Dielectric Properties of PZN-ST-PT Ceramics

Composition			Sintering temperature	T_c at 100 Hz		K	
PZN	ST	PT	(°C)	(°C)	ΔT_c	(T_c (100 Hz))	(RT(100 Hz))*
0.95	0.05		1050	77	10	2130	1280
0.93	0.07		1050	69	13	6450	2780
0.92	0.08		1050	54	16	6810	3990
0.9	0.1		1150	32	16	7990	5170
0.85	0.15		1150	−10	20	5970	2900
0.8	0.2		1150	−45	23	4820	2490
0.9	0.05	0.05	1050	110	8	6590	2110
0.85	0.05	0.1	1050	137	5	8330	2090
0.85	0.1	0.05	1075	58	15	7860	4570
0.8	0.1	0.1	1075	81	13	7610	2810
0.8	0.15	0.05	1150	10	17	7040	4420
0.75	0.15	0.1	1150	34	15	7980	5610

*Room temperature dielectric constant.

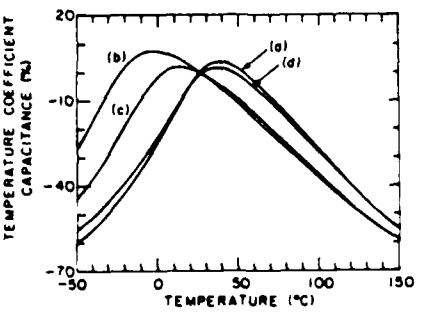

Fig. 11. TCC vs temperature for (*A*) 0.9 PZN-0.1 ST, (*B*) 0.85 PZN-0.15 ST, (*C*) 0.8 PZN-0.15 ST-0.05 PT, and (*D*) 0.75 PZN-0.15 ST-0.1 PT.

John R. Belsick

John R. Belsick is a graduate student in solid-state science at the Pennsylvania State University, University Park, PA. He earned a B.S. in ceramic science and engineering from Pennsylvania State University in 1986. His current research interests are ceramic piezoelectric materials.

Arvind Halliyal is a research associate with the Materials Research Lab at Pennsylvania State University. His photograph and biographical sketch appear on page 676.

Umesh Kumar is a graduate student at the Materials Research Lab at Pennsylvania State University. His photograph and biographical sketch appear on page 676.

Robert E. Newnham is professor of solid-state science at Pennsylvania State University. His photograph and biographical sketch appear on page 676.

Dielectric and Ferroelectric Properties of Ceramics in the $Pb(Zn_{1/3}Nb_{2/3})O_3$-$BaTiO_3$-$PbTiO_3$ System

A. HALLIYAL,* U. KUMAR,* R. E. NEWNHAM,* and L. E. CROSS*

Materials Research Laboratory, The Pennsylvania State University, University Park, Pennsylvania 16802

The use of $Pb(Zn_{1/3}Nb_{2/3})O_3$ ceramics is restricted by the formation of a pyrochlore phase detrimental to both dielectric and piezoelectric properties. Recently it has been shown that a 6 mol% addition of $BaTiO_3$ to PZN suppresses the formation of pyrochlore phase. Phase relations and dielectric properties of ceramics in the PZN-BT-PT system are reported here. Compositions with the perovskite structure, having high dielectric constant and low temperature coefficient of capacitance, have been identified.

I. Introduction

LEAD ZINC NIOBATE [$Pb(Zn_{1/3}Nb_{2/3})O_3$, hereafter designated PZN] is a ferroelectric material with a partially disordered perovskite structure. It undergoes a diffuse phase transition near 140°C. The crystal symmetry is rhombohedral (ferroelectric) at room temperature and cubic (paraelectric) above 140°C.[1-3] In the $Pb(Zn_{1/3}Nb_{2/3})O_3$-$PbTiO_3$ (PZN-PT) system, a morphotropic phase boundary (MPB) exists between the rhombohedral PZN and tetragonal PT phases, near 9 mol% of PT. Single crystals with compositions near MPB show extremely large dielectric and piezoelectric coefficients, much larger than those of PZT ceramics.[3] PZN and PZN-PT single crystals can be grown rather easily by a flux method and their properties have been reported.[4] PZN is also a promising candidate material for electrostrictive micropositioners.[5]

Unfortunately, it is very difficult to synthesize perovskite PZN or PZN-PT ceramics near MPB by the usual solid-state reaction. The product obtained by solid-state reaction at ≈1100°C is a mixture containing a stable cubic-type pyrochlore phase. The formation of pyrochlore phase is detrimental to both the dielectric and piezoelectric properties. In the PZN-PT system, the perovskite phase is stable only when the PT content exceeds 25 mol%. PZN ceramics with perovskite structure can be prepared under high pressure and temperature conditions (2.2 GPa, 800° to 1000°C). The perovskite structure in PZN can also be stabilized by the addition of $Ba(Zn_{1/3}Nb_{2/3})O_3$ (BZN)[7] as a third component or by the partial replacement of PbO by K_2O.[8] However, BZN or K_2O additions dilute both the dielectric and piezoelectric properties. The peak dielectric constant reported in these ceramics is ≈7000, which is very low compared to the extremely large values observed in PZN-PT single crystals. A similar reduction in piezoelectric properties is also observed.

In a previous paper,[9] we examined the stability of several ABO_3 perovskite compounds by considering their electronegativity difference and tolerance factor. The analysis showed that $BaTiO_3$ (BT) is an ideal additive for stabilizing the perovskite phase. We were able to prepare PZN ceramics with 100% perovskite structure by the addition of only 6 to 7 mol% of BT. Phase relations and dielectric properties of compositions in the PZN-BT system have been reported,[9] and compositions useful for capacitors have been identified.[10]

The present work was undertaken to investigate the stability of perovskite phase in the PZN-PT-BT ternary system and to examine the dielectric and piezoelectric properties of ceramics with perovskite structure. Phase relations and dielectric properties are presented in this paper. The piezoelectric properties will be reported in a subsequent paper.

II. Sample Preparation

The compositions selected for the present study were of the type $(1 - x - y)$PZN-xPT-yBT with x varying between 0 and 0.20, and y varying between 0.05 to 0.20. The method of sample preparation is shown in Fig. 1 and has been described in detail in Ref. 9. Samples were sintered in a sealed alumina crucible by heating at a rate of 200°C/h. To limit the loss of PbO from the pellets, a PbO-rich atmosphere was maintained by placing an equimolar mixture of PbO and ZrO_2 inside the crucible. Weight loss on sintering was held to <0.5%. Details concerning the procedure followed for X-ray analysis, determination of percentage of pyrochlore phase, and dielectric measurement can be found in Ref. 9. To distinguish rhombohedral and tetragonal crystalline phases in sintered ceramics, X-ray powder diffraction patterns of the 002 peak were taken at a slow scanning rate (⅛°/min).

III. Results and Discussion

(1) Formation of the Pyrochlore Phase

Powder X-ray diffraction patterns of ceramics were used to

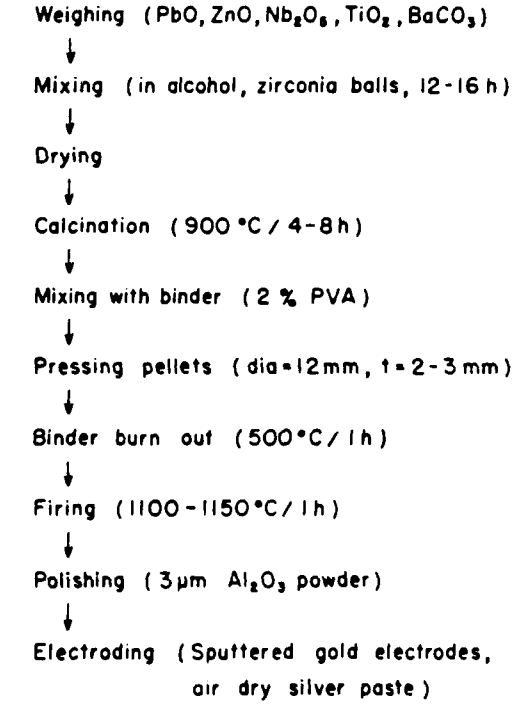

Fig. 1. Procedure for sample preparation.

Received June 20, 1986; revised copy received July 25, 1986; approved September 5, 1986
Supported by the Office of Naval Research
*Member, the American Ceramic Society

Table I. Dielectric Properties of PZN-PT-BT Ceramics

Composition			Crystal symmetry*	Lattice constants†		K_{max} (100 Hz)	ΔT_c‡	δ
PZN	BT	PT		a (nm)	c (nm)			
0.95	0.05		R			5400§		75
0.90	0.05	0.05	T	0.4056		15000	8	50
0.85	0.05	0.10	T	0.4034	0.4081	15000	7	45
0.80	0.05	0.15	T	0.4021	0.4089	14500	4	43
0.75	0.05	0.20	T	0.4019	0.4105	14000	1	40
0.90	0.10		R	0.4059		11400	16	63
0.85	0.10	0.05	R	0.4050		13100	15	56
0.80	0.10	0.10	T	0.4038	0.4072	13800	14	53
0.75	0.10	0.15	T	0.4024	0.4083	12600	6	52
0.70	0.10	0.20	T	0.4019	0.4091	10000	4	50
0.85	0.15		R	0.4056		9950	16	68
0.80	0.15	0.05	R	0.4050		11000	18	67
0.75	0.15	0.10	R	0.4042		12100	15	61
0.70	0.15	0.15	T	0.4020	0.4065	12100	11	57
0.65	0.15	0.20	T	0.4013	0.4077	11800	3	51
0.80	0.20		C	0.4057		7150	25	85
0.75	0.20	0.05	C	0.4044		8600	22	80
0.70	0.20	0.10	T	0.4036	0.4042	10600	18	70
0.65	0.20	0.15	T	0.4024	0.4046	10000	10	66

*R rhombohedral, T tetragonal, C cubic. †$\Delta T_c = T_c$(100 kHz) − T_c(100 Hz) ‡Low dielectric constant because of pyrochlore phase. §At 25°C.

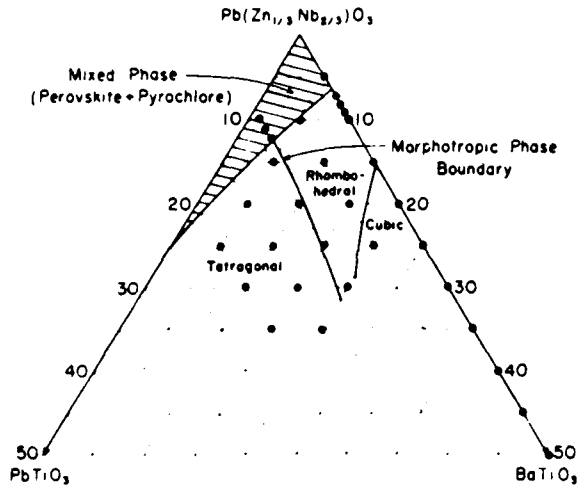

Fig. 2. Phase diagram of $Pb(Zn_{1/3}Nb_{2/3})O_3$-$BaTiO_3$-$PbTiO_3$ system. Circles show the composition of the samples studied.

determine the percentage of pyrochlore phase. About 15% of pyrochlore phase was detected in 0.95PZN-0.05BT ceramics. There was ≈2% to 3% of pyrochlore phase in composition 0.9PZN-0.05BT-0.05PT in the calcined powder (900°C/6 h), but no pyrochlore phase was detected in sintered samples (1100°C/1 h). The remainder of the compositions did not show a pyrochlore phase after calcination at 900°C for 4 to 6 h. The densities of the ceramic samples were in the range 93% to 97% of their respective theoretical densities.

In the PZN-BT binary system, it has been observed that 6 to 7 mol% of BT stabilizes the perovskite phase in PZN. It is clear that in the PZN-PT-BT ternary system, BT narrows the pyrochlore formation region. The lattice constants are tabulated in Table I. The compositions containing >15 mol% of PT are tetragonal. The morphotropic phase boundary (MPB) between the rhombohedral and tetragonal phases occurs between 5 to 15 mol% of PT. The phase diagram of the PZN-PT-BT systems is shown in Fig. 2, in which the region where a perovskite pyrochlore mixed phase occurs is also indicated. An approximate MPB is also marked. In the $(1 - x)$PZN-xBT system, compositions with $0.2 < x < 0.9$ are cubic at room temperature. Typical scanning electron micrographs

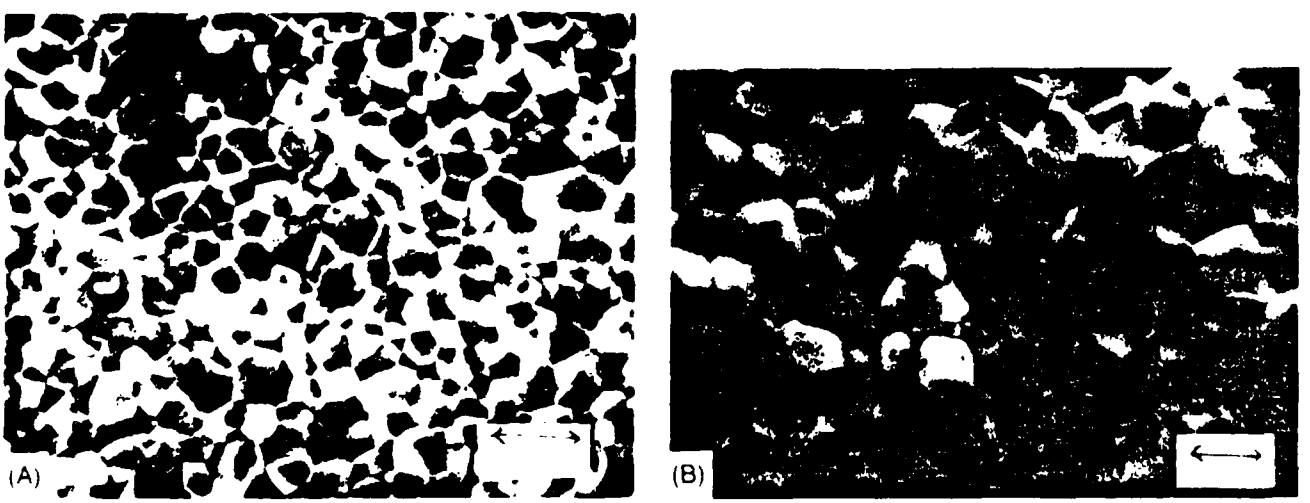

Fig. 3. Microstructure of (*A*) 0.9PZN-0.1BT and (*B*) 0.85PZN-0.05BT-0.1PT

of ceramics are shown in Fig. 3. The grain size was in the range of 2 to 5 μm.

(2) Dielectric Properties

The variation of dielectric constant and dissipation factor (1 kHz) with temperature is shown in Figs. 4 to 7. The following generalizations can be made about the dielectric properties

(1) The peak dielectric constants are in the range of 6000 to 15 000. The compositions near MPB (10 to 15 mol% of PT) show the highest peak dielectric constants.

(2) Most of the compositions show a diffuse phase transition with a strong frequency dispersion. The frequency dispersion and diffuseness of the transition decrease as the amount of PT in the composition increases. This can be seen in Fig. 8, where the temperature and frequency dependence of two compositions, 0.9PZN-0.05BT-0.05PT and 0.75PZN-0.05BT-0.20PT, are compared. This trend is evident in all the compositions.

(3) The Curie temperature (T_c) increases with increasing frequency, which is characteristic of relaxor ferroelectric materials. The difference between the Curie temperatures measured at 0.1 and 100 kHz (ΔT_c) gives an estimation of the relaxor nature of the transition. The Curie temperatures at different frequencies are plotted in Fig. 9 as a function of mole fraction of PT. It is clear that both the diffuseness and frequency dependence of T_c become less prominent as the amount of PT increases. In compositions with the same percentage of PT, ΔT_c increases with the amount of BT. In relaxor ferroelectrics if the local Curie temperature distribution is Gaussian, the diffuseness of the transition can be described by diffuseness parameters δ, defined in Ref. 9. If the value of δ is large, it indicates a broader dielectric curve. The values of ΔT_c, peak dielectric constant (100 Hz), and δ are listed in Table I. The value of δ decreases with the amount of PT, indicating a less broad phase transition. The value of δ increases with the amount of BT, in agreement with earlier observation.

(3) Temperature Coefficient of Capacitance

There is a need for high dielectric constant capacitor materials which can be sintered at temperatures of <1000°C, with low temperature dependence of capacitance. The temperature coefficient of capacitance (TCC) is defined as

$$\text{TCC} = 100\left(\frac{C_T - C_{25°C}}{C_{25°C}}\right) \tag{1}$$

The values of TCC for a few compositions which have Curie temperature around room temperature are shown in Fig. 10. For all five compositions shown in Fig. 10, the TCC values are within the limits of Z5U and Y5U capacitor specifications.

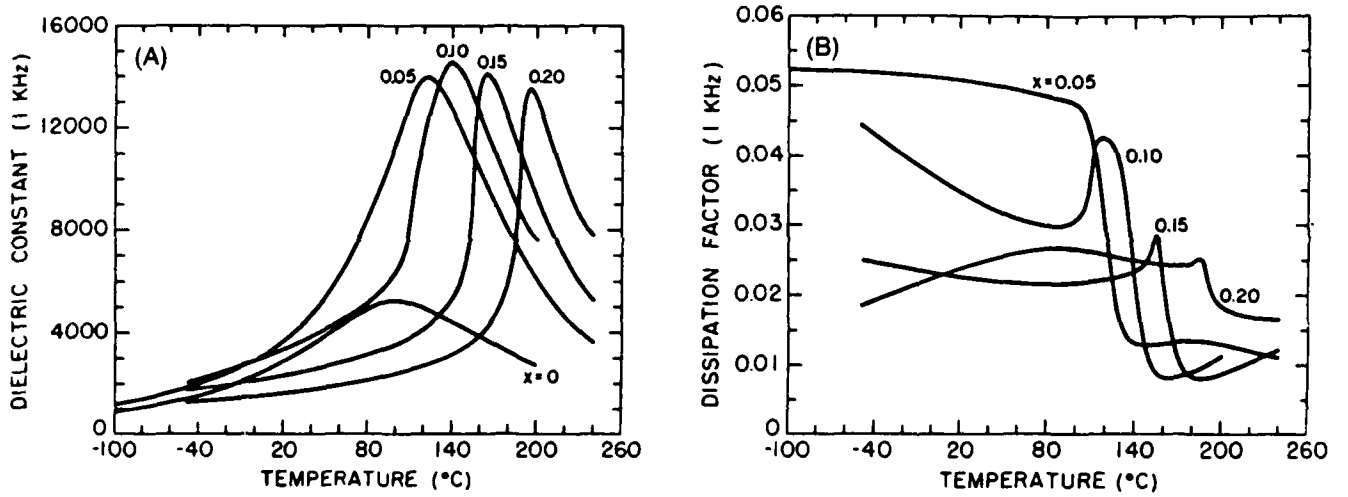

Fig. 4. (*A*) Dielectric constant and (*B*) dissipation factor (1 kHz) vs temperature for $(1-x)$PZN-0.05BT-xPT ceramics.

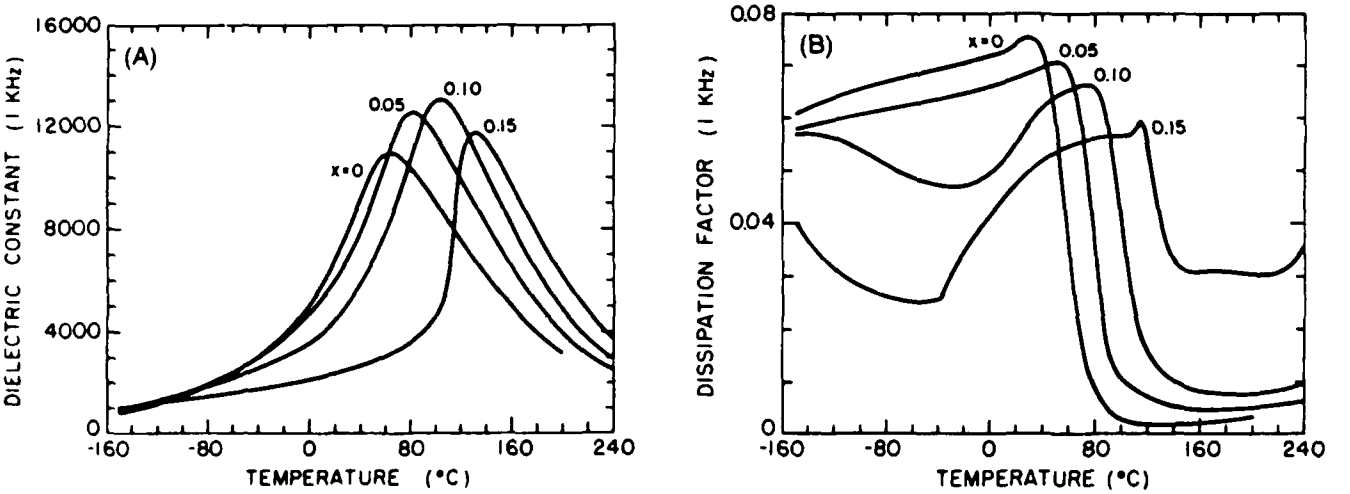

Fig. 5. (*A*) Dielectric constant and (*B*) dissipation factor (1 kHz) vs temperature for $(1-x)$PZN-0.10BT-xPT ceramics.

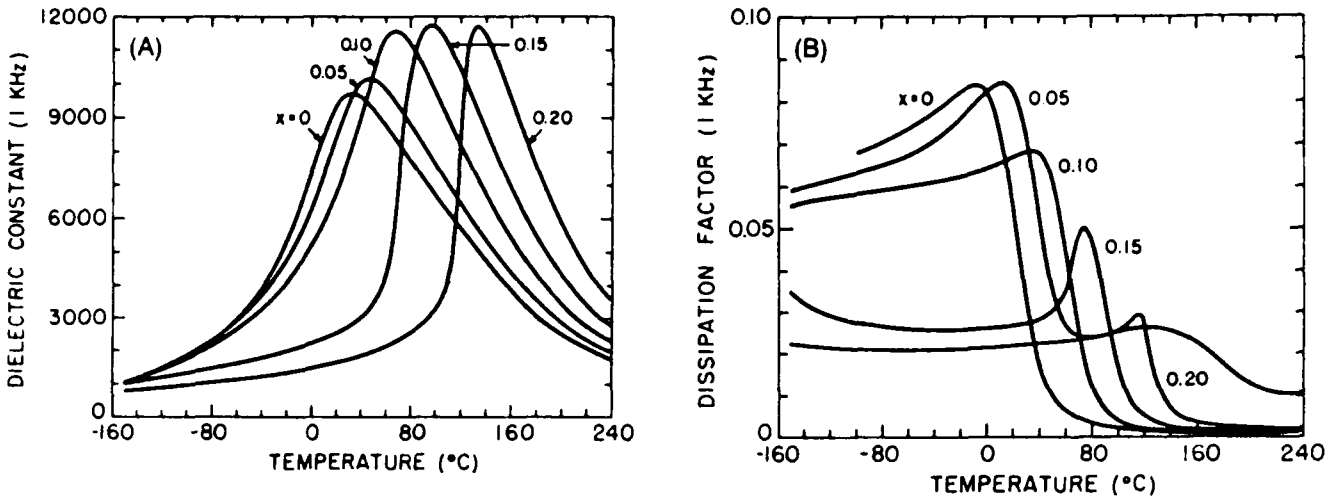

Fig. 6. (*A*) Dielectric constant and (*B*) dissipation factor (1 kHz) vs temperature for (1 − *x*)PZN-0.15BT-*x*PT ceramics.

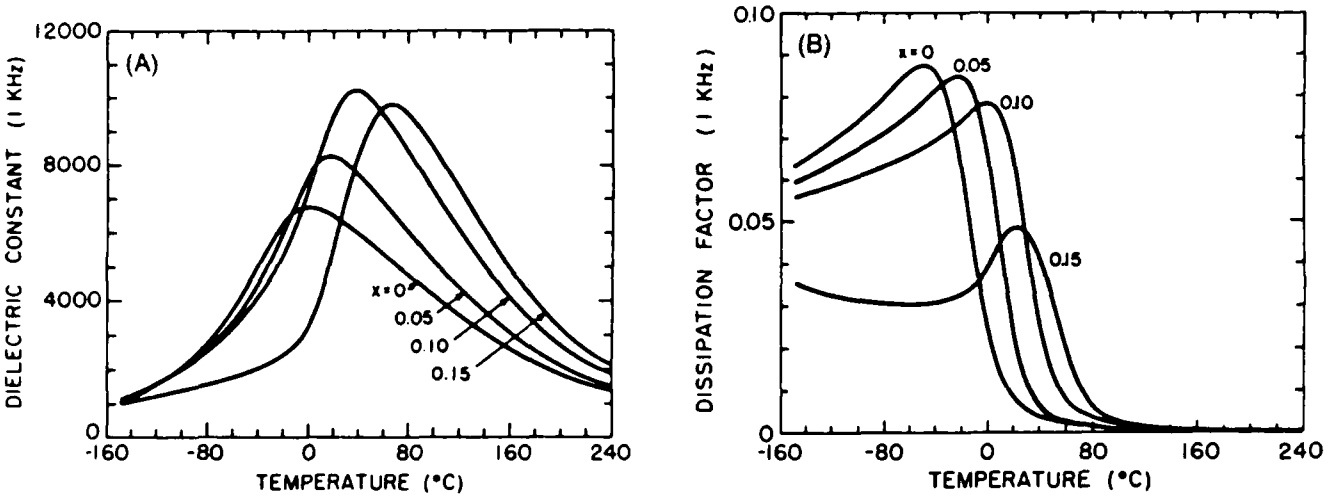

Fig. 7. (*A*) Dielectric constant and (*B*) dissipation factor (1 kHz) vs temperature for (1 − *x*)PZN-0.20BT-*x*PT ceramics.

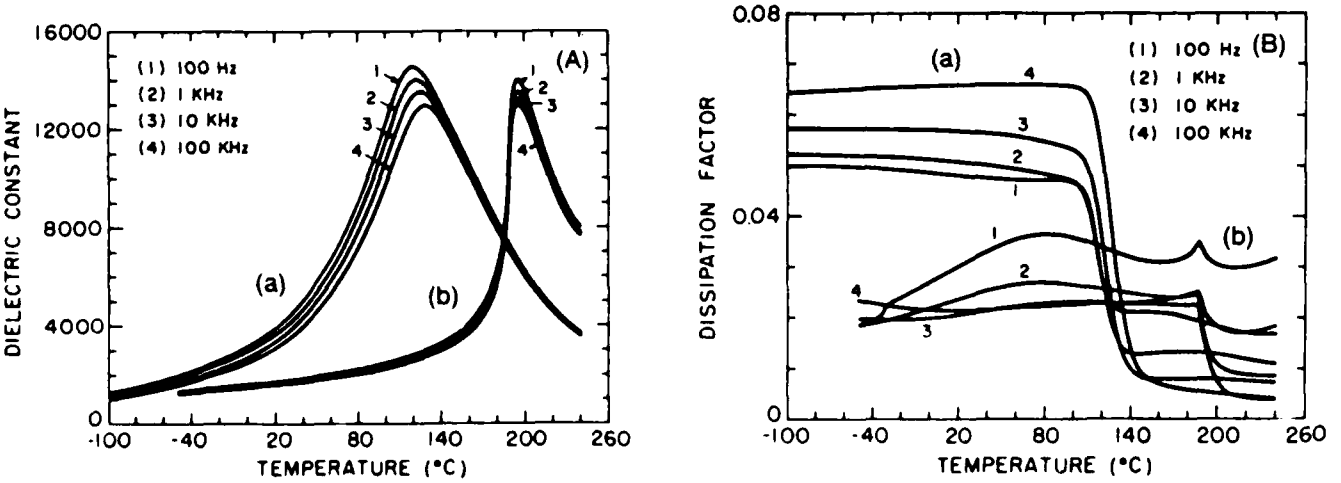

Fig. 8. Variation of (*A*) dielectric constant and (*B*) dissipation factor with temperature and frequency for (*a*) 0.90PZN-0.05BT-0.05PT and (*b*) 0.75PZN-0.05BT-0.20PT ceramics.

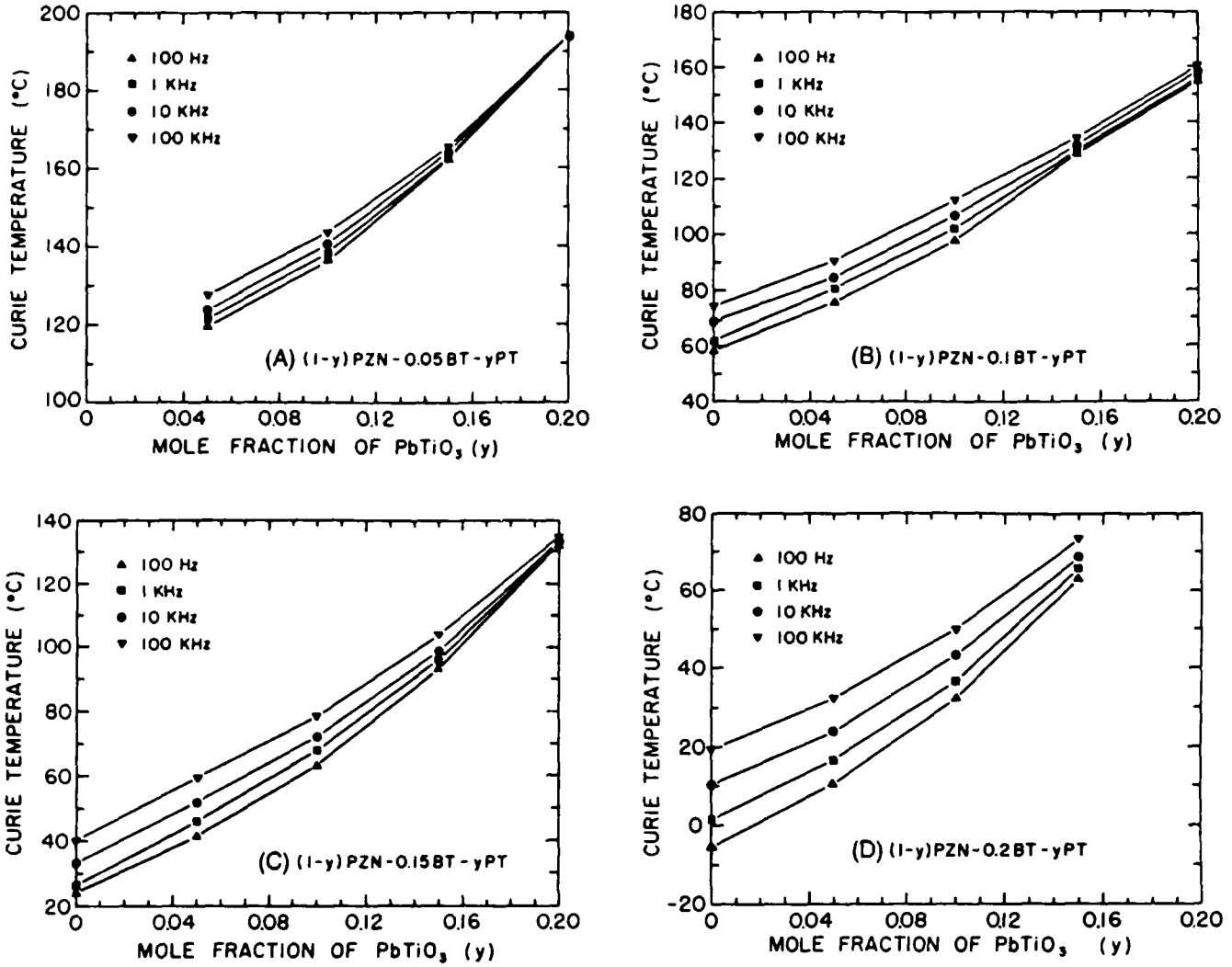

Fig. 9. Variation of Curie temperature with mole fraction of PT in $(1 - x - y)$PZN-xBT-yPT system, showing the frequency dispersion for (*A*) $x = 0.05$, (*B*) $x = 0.10$, (*C*) $x = 0.15$, (*D*) $x = 0.20$.

IV. Summary

Ceramics in the $(1 - x - y)$PZN-xBT-yPT system having the perovskite structure can be prepared if the mole fraction of $x > 0.05$. The addition of BT to PZN-PT completely suppresses the formation of the pyrochlore phase. The phase relations and dielectric properties of ceramics with $0.05 \leq x \leq 0.2$ and $0 \leq y \leq 0.2$ have been investigated. The approximate location of the morphotropic phase boundary has been identified. Many of the compositions show a diffuse phase transition with a shift in the Curie temperature with frequency. The relaxor characteristics of the transition have been discussed. Compositions with high dielectric constant near room temperature and low values of temperature coefficient of capacitance have been identified.

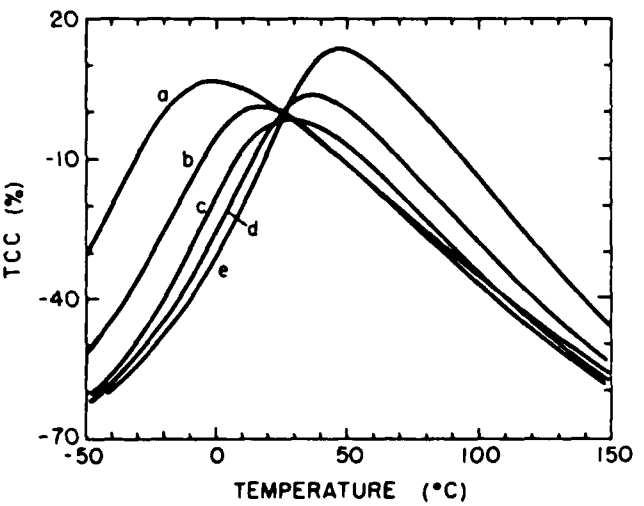

Fig. 10. Temperature coefficient of capacitance (1 kHz) of (*a*) 0.8PZN-0.2BT, (*b*) 0.75PZN-0.20BT-0.05PT, (*c*) 0.85PZN-0.15BT, (*d*) 0.7PZN-0.2BT-0.1PT, (*e*) 0.8PZN-0.15BT-0.05PT.

References

[1] Y. Yokomizo, T. Takahashi, and S. Nomura, "Ferroelectric Properties of $Pb(Zn_{1/3}Nb_{2/3})O_3$," *J. Phys. Soc. Jpn.* **28** [5] 1278-84 (1970).
[2] J. Kuwata, K. Uchino, and S. Nomura, "Diffuse Phase Transitions in Lead Zinc Niobate," *Ferroelectrics* **22**, 863-67 (1979).
[3] J. Kuwata, K. Uchino, and S. Nomura, "Dielectric and Piezoelectric Properties of $0.91Pb(Zn_{1/3}Nb_{2/3})O_3$-$0.09PbTiO_3$ Single Crystals," *Jpn. J. Appl. Phys.* **21** [9] 1298-302 (1982).
[4] J. Kuwata, K. Uchino, and S. Nomura, "Phase Relations in the

$Pb(Zn_{1/3}Nb_{2/3})O_3$-$PbTiO_3$ System," *Ferroelectrics*, **37**, 579–82 (1981).
[5]S. Nomura and J. Kuwata, "Electrostriction in $Pb(Zn_{1/3}Nb_{2/3})O_3$," *Mater. Res. Bull.*, **14**, 769–74 (1979).
[6]Y. Matsuo, H. Sasaki, S. Hayakawa, F. Kanamura, and M. Koizumi, "High Pressure Synthesis of Perovskite Type $Pb(Zn_{1/3}Nb_{2/3})O_3$," *J. Am. Ceram. Soc.*, **52** [9] 516–17 (1969).
[7]S. Nomura and H. Arima, "Dielectric and Piezoelectric Properties in the Ternary System of $Pb(Zn_{1/3}Nb_{2/3})O_3$-$Ba(Zn_{1/3}Nb_{2/3})O_3$-$PbTiO_3$," *Jpn. J. Appl. Phys.*, **11** [3] 358 (1972).
[8]L. Hanh and S. Nomura, "Ferroelectric and Piezoelectric Properties of $xPb_{1-x}K_x(Zn_{1/3}Nb_{2/3})O_{3-x/2}$-$(1-x)PbTiO_3$ Solid Solutions," *Jpn. J. Appl. Phys.*, **15** [6] 1059 (1976).
[9]A. Halliyal, U. Kumar, R. E. Newnham, and L. E. Cross, "Stabilization of Perovskite Phase and Dielectric Properties of Ceramics in the $Pb(Zn_{1/3}Nb_{2/3})O_3$-$BaTiO_3$ System", to be published in *Am. Ceram. Soc. Bull.*
[10]O. Furukawa, Y. Yamashita, M. Harata, T. Takahashi, and K. Inagaki, "Dielectric Properties of Modified Lead Zinc Niobate Ceramic," *Jpn. J. Appl. Phys.*, **24**, Suppl. 24-3, 96–99 (1985).

Measurements of strain and the optical indices in the ferroelectric $Ba_{0.4}Sr_{0.6}Nb_2O_6$: Polarization effects

A. S. Bhalla, R. Guo, and L. E. Cross
Materials Research Laboratory, The Pennsylvania State University, University Park, Pennsylvania 16802

Gerald Burns and F. H. Dacol
IBM Thomas J. Watson Research Center, P.O. Box 218, Yorktown Heights, New York 10598

Ratnakar R. Neurgaonkar
Rockwell International Science Center, Thousand Oaks, California 91360

(Received 17 November 1986)

We report accurate temperature-dependent measurements of the optic index of refraction, the birefringence, and the strain in the ferroelectric, tungsten-bronze crystal $Ba_{0.4}Sr_{0.6}Nb_2O_6$. This composition congruently melts, so large homogeneous high-quality crystals can be grown. From the experimental data, it appears that far above the ferroelectric phase transition temperature ($T_c \approx 88$ °C), up to a temperature T_d (≈ 300 °C), the crystals appear to possess a local, randomly oriented (up or down), polarization P_d. The values of T_d obtained from the index and completely independent strain measurements are in very good agreement with each other, as are the values of P_d. Various aspects of our understanding of the polarization behavior and other effects in this ferroelectric system are discussed.

INTRODUCTION

There is a great deal of interest in ferroelectric materials that have the tungsten-bronze crystal structure.[1] Above the ferroelectric transition temperature T_c, the structure is tetragonal and has a center of symmetry (space group D_{4h}^5-$P_{4/mbm}$).[2] Below T_c it remains tetragonal (C_{4v}^2-P_{4bm}) with a reversible spontaneous polarization P_r, along the tetragonal or c axis. These space groups refer to the average crystal structure (these are defect structures[2,3]) and will be discussed below; none of the tungsten-bronze ferroelectrics actually are ordered compounds.[4]

In this paper the properties of the tungsten-bronze ferroelectric $Ba_{1-x}Sr_xNb_2O_6$ (BSN) are discussed. It has been shown that for $x \approx 0.6$ the material is congruently melting[5] and, hence, large crystals of high optical quality can be grown,[6] which have found many applications.[7] The primitive unit cell of this material is shown in Fig. 1. The chemical formula can be usefully thought of as $(Ba_{1-x}Sr_x)_5(NbO_3)_{10}$ since there are ten niobium octahedra in this unit cell and the Ba and Sr atoms occupy the α and β positions randomly. However, there are six such positions and only five Ba+Sr atoms; thus the structure has built-in defects.

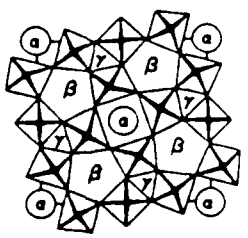

FIG. 1. The unit cell of the tungsten bronze $(Ba,Sr)_5(NbO_3)_{10}$ looking down the c axis.

Recently, there has been considerable discussion of "crystalline ferroelectrics [specifically the tungsten-bronze ferroelectric $K_2Sr_4(NbO_3)_{10}$] with a glassy polarization phase."[8-10] These are materials in which there is evidence for regions of local, randomly oriented, polarization far above the ferroelectric transition temperature T_c, up to a temperature T_d. The principal evidence for this behavior comes from the temperature dependence of the index of refraction, $n(T)$. However, there is now evidence from low-temperature thermal-conductivity and specific-heat measurements,[11] Raman measurements of the phonon spectra,[12] and second-harmonic-generation measurements[13] for the existence of such polarization behavior. Some aspects of this work have been reviewed.[14]

In this paper, for BSN we show that measurements of the temperature dependence of the length, that is, strain, $x(T)$, also gives strong evidence for a polarization far above T_c. Further, the strain and index measurements, on the same samples, lead to consistent results. In a discussion, at the end of the paper, we relate these crystalline ferroelectrics that have an extended polarization behavior above the dielectric maximum to ferroelectrics with a diffuse phase transition.

EXPERIMENTAL

Large, clear optical-quality BSN crystals were pulled from the melt by the Czochralski technique in a manner

described previously.[6] The earlier problems of coring and striations in growing tungsten-bronze ferroelectrics have been eliminated by using very pure starting materials and pulling at the congruent melting composition.[5,6] Before use, all samples were annealed overnight at 500 °C in order to remove internal stresses and possible bias effects.

The remanent polarization P_r was obtained by the integration of the pyroelectric-coefficient–versus–temperature method.[15] Thin, sputtered gold c plates were used, and the samples were cooled through the transition temperature ($T_c \approx 88$ °C) with a dc field of 10 kV/cm. The dielectric constant was measured by standard techniques.

The index of refraction parallel to P_r (n_3) and perpendicular to P_r (n_1) were measured by the minimum-deviation technique.[8] Oriented BSN prisms were used in an oven in conjunction with various lasers as light sources.

The birefringence, Δn_{31}, was also directly measured. An a-cut plate (i.e., the a axis perpendicular to the plate) was polished into a wedge shape with a known wedge angle (5°–7°). Δn_{31} was measured using a polarizing microscope with a hot stage and the sodium D lines as a light source ($\lambda = 5893$ Å). The birefringence was determined by

$$\Delta n_{31} = \lambda / d \sin\theta \ , \tag{1}$$

where θ is the wedge angle and d is the separation between the interference fringes resulting from the varying thickness of the wedge.

The length measurements were made from room temperature to 500 °C under a heating rate of 1 °C/min on rectangular bar BSN samples cut normal to the c axis to give $x_3(T)$, or the a axis, to give $x_1(T)$, typically 8 mm × 1 mm × 1 mm. The strains were measured as a function of temperature using a linear voltage-differential transformer (LVDT) dilatometer (model 24DCDT-250 or model 24DCDT-050) from the Schwartz Co., N.J.

RESULTS

Polarization

The temperature dependence of the dielectric constant along the ferroelectric axis, $\epsilon_3(T)$, the reversible spontaneous polarization P_r, and the pyroelectric coefficient are plotted in Fig. 2. The results are in reasonable agreement with earlier published data on these materials.[1,16] From $\epsilon_3(T)$ we see that $T_c \approx 88$ °C and note that P_r is down to zero by ≈ 100 °C. This behavior is in sharp contrast to the fluctuating polarization behavior that will be discussed later.

$n(T)$ and $x(T)$ theory

We consider the macroscopic quantities, the change of the optic index of refraction, $n(T)$, and the strain, $x(T)$, which is the fractional change of length. In a centrosymmetric crystal, by symmetry both of these quantities depend on the square of the polarization in the same way:

$$\Delta(n^{-2})_{ij} = \sum_{k,l} g_{ijkl} P_k P_l \ , \tag{2}$$

$$x_{ij} = \sum_{k,l} Q_{ijkl} P_k P_l \ , \tag{3}$$

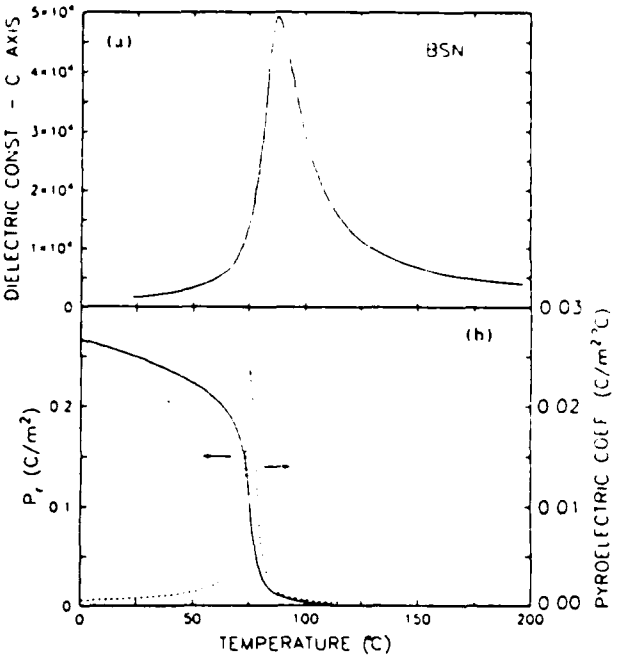

FIG. 2. The measured temperature dependence of the dielectric constant (ϵ), reversible spontaneous polarization (P_r), and the pyroelectric coefficient.

where g and Q are the quadratic electro-optic and electrostrictive coefficients, respectively (both fourth-rank tensors). The subscripts can have values 1, 2, or 3 for the three directions (x, y, and z), and P is the polarization. Since BSN is tetragonal, both above and below T_c it is easy to write the tensor effects parallel (3 component) and perpendicular (1 component) to the tetragonal axis (3 axis or z axis). Assuming that all polarization must occur along the ferroelectric (3) axis, then in contracted notation[3,17] we have, for the indices of refraction,

$$\Delta n_3 = -g_{33}(n_3^0)^3 P_3^2/2 \ , \tag{4a}$$

$$\Delta n_1 = -g_{13}(n_1^0)^3 P_3^2/2 \ , \tag{4b}$$

and for the birefringence,

$$\delta(\Delta n_{31}) \equiv \Delta n_3 - \Delta n_1 = -\tfrac{1}{2}(n_3^0)^3 \left[g_{33} - g_{13} \left[\frac{n_1^0}{n_3^0} \right]^3 \right] P_3^2 \ , \tag{4c}$$

where n^0 is the index of refraction if there were no polarization of any sort present, whether along the 3 axis (n_3^0) or perpendicular to it (n_1^0).

For the strains the expression are

$$\Delta c/c_0 = Q_{33} P_3^2 \ , \tag{5a}$$

$$\Delta a/a_0 = Q_{13} P_3^2 \ . \tag{5b}$$

An important aspect of Eqs. (4) and (5) is that they depend quadratically on the polarization. Thus, if P_3 is randomly, spatially directed up and down, the effects will

add, not cancel. The second important point to appreciate is that P_3 can be spatially inhomogeneous, but still the effects will add. For measurements of the crystal lengths this is clear. For $n(T)$ measurements the spatial resolution is of the order of the wavelength of light; thus local polarization regions that can be several thousand angstroms apart will be effectively averaged.

$n(T)$ data

Figure 3(a) shows the indices of refraction both parallel and perpendicular to the tetragonal c axis at 6328 Å. As can be seen, the changes in n_3 are considerably larger than those perpendicular to the tetragonal axis (n_1), which is shown in Fig. 3(b) on a considerably expanded scale. These data are similar to those published previously.[18,10] The most noticeable difference between these results and the earlier data[18] is the lack of thermal hysteresis near T_c. The reason for this is not totally clear; however, the crystals reported on here are very pure, annealed, and were grown at the congruent point in the phase diagram, which results in striation-free crystals. Thus we believe that these crystals represent the ture behavior.

Measurements taken at 6328 and 4880 Å for n_3 are plotted in Fig. 4, where a constant has been subtracted from the latter results so that both can be presented on the same expanded scale.

The data for n_3 at 6328 Å are the same as shown in Fig. 3. Classical, soft-mode ferroelectrics have an index of refraction that is approximately linear with temperature

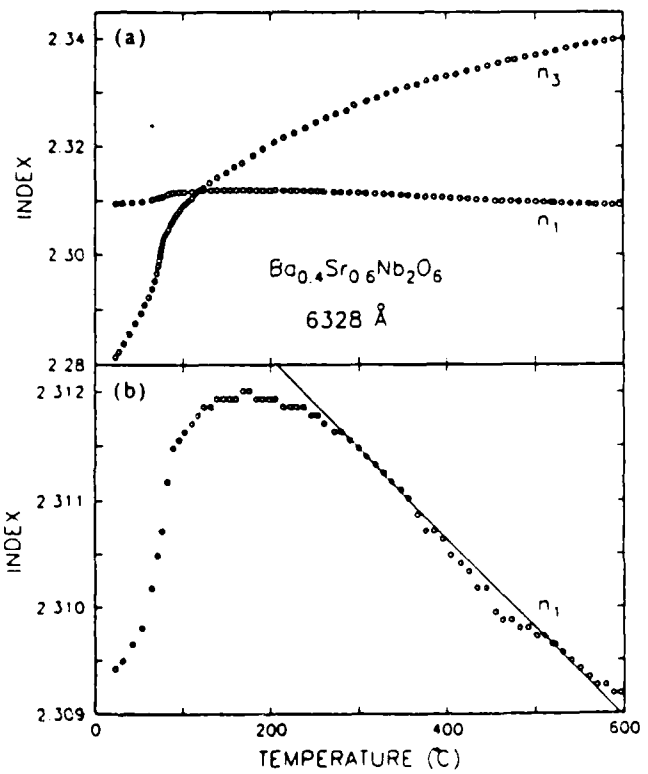

FIG. 3. (a) The measured n_3 and n_1 at 6328 Å. (b) The same n_1 shown on an expanded scale.

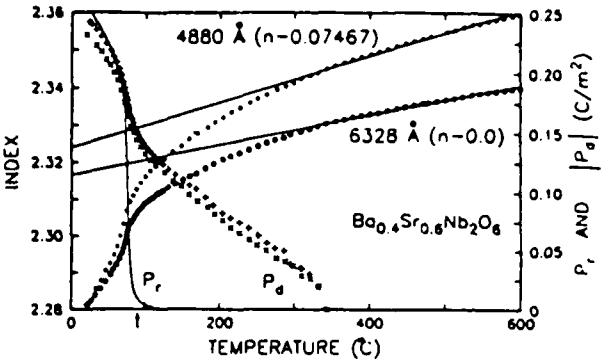

FIG. 4. The temperature dependence of n_3 at two wavelengths as indicated. P_d obtained, as described in the text, is shown. Also shown in P_r obtained from Fig. 2.

above T_c; then below T_c, $n(T)$ reflects the spontaneous polarization via Eq. 4(a). Such behavior has been reported in several systems.[19] However, the data in Fig. 4 behave quite differently. There is no linear behavior just above T_c; instead, there appears to be considerable curvature in n_3 above T_c.

The two straight lines in Fig. 4 approximately represent the high-temperature linear behavior of $n_3(T)$. T_d is functionally defined as the temperature at which the straight line deviates from the measured data. As can be seen, for the data taken at both wavelengths, approximately the same values of T_d are found. Assuming that the deviations from the straight-line behavior are due to local polarization regions, the data can be analyzed via Eq. 4(a) to yield a polarization, which is called P_d. This procedure has been used before.[7-10]. To analyze the data in this manner [via Eq. 4(a)], for each wavelength the straight line is taken as n^0, Δn is the difference between the straight line and the measured values (Δn is zero at T_d), and, as used before,[10] we take $g_{33}=0.10$ and 0.12 m^4/C^2 at 6328 and 4880 Å, respectively.[20-22] The resultant values of P_d at the two wavelengths are plotted in Fig. 4. The use of the small wavelength dependence[21] of g_{33} improves the agreement between the two sets of data, which gives some indication that the ideas in this approach of analysis is correct. Also shown in Fig. 4 is the reversible polarization from Fig. 2. As can be seen, P_r and P_d are in reasonable agreement at room temperature, which again indicates that our understanding, via the quadratic electro-optic effects, is appropriate.

Figure 5 shows birefringence, Δn_{31}, as a function of temperature. BSN is an optically negative crystal. As is evident from Fig. 5, Δn_{31} decreases with temperature and goes through zero above T_c and the crystal becomes optically positive. Similar to the n_3 and n_1-versus-T data [Fig. 3(a)], there is no thermal hysteresis noticed in the Δn_{31}-versus-T data. Also shown in this figure is n_3-n_1 obtained (via Fig. 3) at 6328 Å. The results are in very good agreement with Δn_{31}, which was measured at 5893 Å. From these data, P_d can be obtained as has been discussed above with respect to $n_3(T)$. To do this, we used a value of 0.09 m^4/C^2 for the average value of g_{ij}, the term

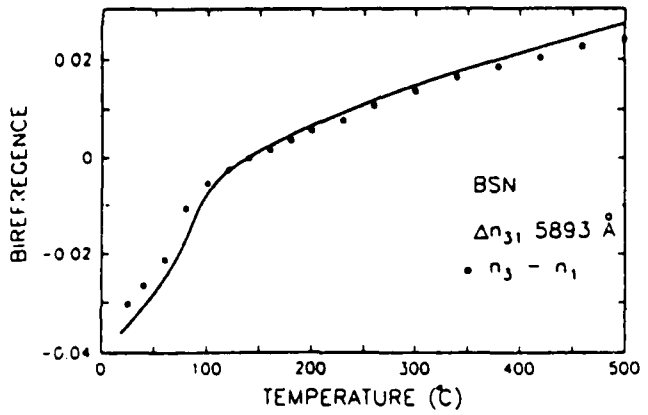

FIG. 5. The solid line is the birefringence (Δn_{31}) measured with the sodium D lines. The results for heating and cooling overlap each other. The open circles are $n_3 - n_1$ obtained from the measurements in Fig. 3.

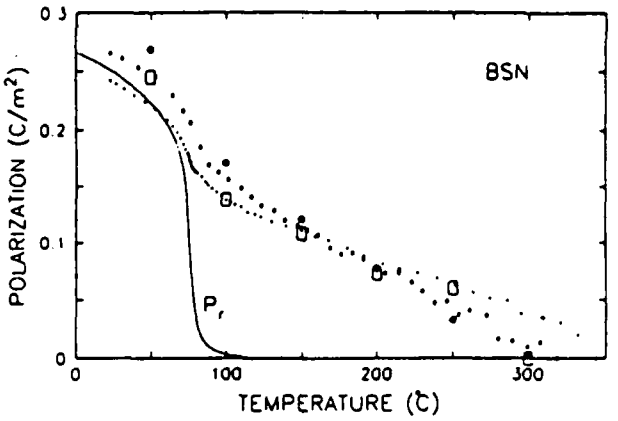

FIG. 7. Values of P_d, obtained by the different methods are summarized in this figure. Also, the reversible, spontaneous polarization P_r is shown as the solid line. P_d obtained from n_3 are given by the small circles, values from n_1 are given by the small open rectangles, values from the birefringence n_{31} are given by the large open rectangles, and values from $\Delta c/c$ are given by the large solid circles.

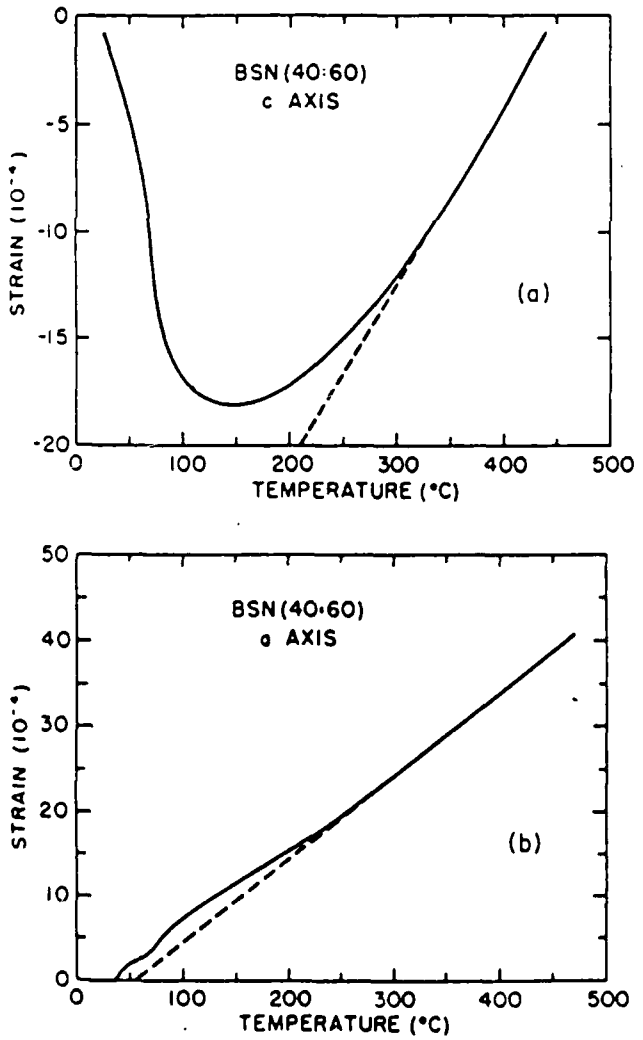

FIG. 6. (a) The measured strain along the c axis obtained as described in the text. (b) The same, but perpendicular to the c axis.

in large square brackets in Fig. 4(c). These results will be presented and discussed in connection with the last figure.

$x(T)$ data

The thermal strain parallel ($\Delta c/c$) and perpendicular ($\Delta a/a$) to the ferroelectric c axis have been measured by a high-sensitivity dilatometer. The results are shown in Figs. 6(a) and 6(b), respectively. The highest-temperature data, far above T_c, can be approximated by a straight line, along both axes, as can be seen in the figures. The deviation from this linear high-temperature behavior occurs at approximately the same temperature (≈ 300 °C). However, due to the much larger strain along the c axis, we place more emphasis on these data than those perpendicular to the c axis. (The same situation occurs for index data, see Figs. 3 and 4.)

We analyze the deviation of the strain from the high-temperature linear behavior via Eq. 5(a) to obtain P_d. Using the measured $\Delta c/c$ and a value[23] of $Q_{33} = 3 \times 10^{-2}$ m^4/C^2, then P_d can be calculated. The results are plotted in Fig. 7.

DISCUSSION

In Fig. 7 we summarize the P_d, really $(\bar{P}_d^2)^{1/2}$, values obtained from n_3, Δn_{31}, $\Delta c/c$, and even n_1, which was not discussed as yet. Also plotted is the normal reversible polarization data, P_r, from Fig. 2.

Considering the differences between the physical quantities that are measured (various aspects of the optic index of refraction and strain), the agreement in the P_d values in Fig. 7 is excellent. The values are in good agreement not only in magnitude but also in the T_d values (the temperature at which P_d differs from zero).

Good agreement would be expected for P_d obtained from $n_3(T)$ and $\Delta n_{31}(T)$ since the largest variations with

temperature come from n_3 (Fig. 2). However, it is reassuring to see that this is the case, remembering that the measuring techniques are quite different. Also plotted in Fig. 7 is P_d obtained from $n_1(T)$. As can be seen in Fig. 3(a), the temperature variation of n_1 is small compared to n_3, yet the data are sufficiently accurate so that a reasonable high-temperature linear region can be delineated [the straight line in Fig. 3(b)] and P_d can be calculated [via Eq. 4(b)] using $g_{13} \approx 0.01$ m^4/C^2, as discussed. The results are quite consistent with P_d obtained by the other methods.

The strain measurements reported here are qualitatively similar to those reported in the ceramic[24] 90% $Pb(Mg_{1/3}Nb_{2/3})O_3$–10% $PbTiO_3$. In this ceramic material, the high-temperature region (above ≈ 300 °C) can be approximated by linear behavior and very little happens at T_c (≈ 50 °C).

In two ferroelectric systems that show a higher-temperature polarization phase similar to that discussed here, the values of T_d could be quantitatively understood in terms of T_c of the end member. For example, T_d of La doped lead zirconate titanate (PLZT) is approximately equal to T_c of lead zirconate titanate (PZT) (Ref. 8) (i.e., La-free material). Similarly, T_d of $Pb(Ti_{1-x}Sn_x)O_3$ is found[12] to be equal to T_c of $PbTiO_3$. For BSN crystals there is no end member for which an estimate of T_d can be made. However, we emphasize that the difference between T_d and T_c is large (> 200 °C).

Thus, it seems that at $\approx T_d$ small local regions of the crystal begin to show a polarization due to a favorable arrangement of the atoms (presumably the Ba and Sr atoms). The macroscopic index of refraction and strain measurements can detect this effect because P_d^2 rather than P_d contributes to these terms. These macroscopic measurements average the inhomogeneous contributions, as discussed. Once local regions of polarization occur, the cooperative effect that occurs at T_c can be understood.[12]

A critical question which must be addressed, using supplemental data and experiments, is whether the polarization observed here at temperatures above the weak-field dielectric maximum (T_c) is static, or whether the vector direction in each polar region is suffering dynamical inversions over time. Since both the optical and the dilatometric measurements discussed in this paper measure the rms polarization, either model would give equivalent values for P_d. In general, one would expect that dynamical inversion of P_d in polar micro regions would be modulated by a weak external E_3 field so as to change the fraction of up and down polarizations and thus contribute a significant component to the dielectric polarizability. On the dynamical model, the dielectric peak at T_c in BSN could occur either due to cooperative ordering of the polar microregions, or to a critical slowing down of the dipolar component of the polarizability and a freezing in of the dipoles to a glass state.

In the static model the dipolar component which appears at temperatures well above T_c is already frozen. Polarizability would now be contributed by expansion and contraction of the dipolar region and the maximum in ϵ_3 and T_c would be essentially due to cooperative ordering.

Lead magnesium niobate ($PbMg_{1/3}Nb_{2/3}O_3$) and lead lanthanum zirconate titanate (PLZT) compositions such as the 8:65:35 show very strong dielectric relaxation for temperatures at and below the weak-field dielectric peak.[23,24] These materials show a remanent polar state that is only stable at temperatures much below the dielectric peak (the so-called β-α transition in PLZT). In these materials there is rather strong ancilliary evidence for the dynamical model.

In BSN 40:60 there is clearly a highly dispersive microdomain state in virgin crystals cooled below 88 °C, but, upon poling, stable macrodomains are retained up to 88 °C.[25] Some evidence for the dynamical model may be adduced from the work of Sundius,[26] who measured the electrostrictive Q_{33}, Q_{13}, and Q_{11} constants under alternating field. She finds that Q_{11} is essentially independent of temperature to T_c, but Q_{33} and Q_{31} are markedly temperature dependent and approach zero near T_c. If, as suggested above, a major component of polarizability comes from the flipping of already polar regions, as is evidenced from the dilatometric studies, the lattice has already adjusted dimension for these polar regions and the phenomenon of electrostriction (which is quadratic inversion of P) will not change the crystal shape at all, so that if polar flipping is the major contributor to dielectric polarizability at T_c, Q_{33} and Q_{31} must go to zero at that temperature. For a field E, on the other hand, the up and down states of P_3 will not be affected and "normal" electrostriction constants should be observed.

Another critical experiment which should be attempted is measurement of the quadratic electro-optic constants g_{33}, g_{13}, and g_{11}. If g_{33} and g_{13} approach zero near T_c with the same shape as Q_{33} and Q_{13}, and g_{11} is also temperature independent, further strong support would be provided for the dynamical model.

Perhaps the final key to understanding these fascinating materials will be the identification of the size, shape, and nature of the polar nanostructure using high-resolution transmission-electron microscopy (TEM). Such evidence is now appearing for PLZT's, $PbMg_{1/3}Nb_{2/3}O_3$, and $PbSc_{1/2}Ta_{1/2}O_3$ relaxor ferroelectrics,[27–29] and will certainly also be important in the BSN compositions.

[1] M. E. Lines and A. M. Glass, *Principles and Applications of Ferroelectrics and Related Materials* (Clarendon, Oxford, 1977); F. Jona and G. Shirane, *Ferroelectric Crystals* (Pergamon, New York, 1962).

[2] S. C. Abrahams, P. B. Jamieson, and J. L. Bernstein, J. Chem. Phys. 54, 2355 (1971), and the references quoted there to their earlier papers.

[3] G. Burns, *Solid State Physics* (Academic, New York, 1985).

[4] B. A. Scott, E. A. Giess, B. L. Olson, G. Burns, A. W. Smith, and D. F. O'Kane, Mater. Res. Bull. 5, 47 (1970).

[5] K. Megumi, N. Nagatsuma, K. Kashiwada, and Y. Furuhata, Mater. Sci. 11, 1583 (1976).

[6] R. R. Neurgaonkar, M. H. Kalisher, T. C. Lim, E. J. Staples, and K. K. Keester, Mater. Res. Bull. 15, 1235 (1980); R. R.

Neurgaonkar, W. K. Cory, and J. R. Oliver, Ferroelectrics 15, 3 (1983).
[7]R. R. Neurgaonkar and W. K. Cory, J. Opt. Soc. Am. 3, 274 (1986).
[8]G. Burns and F. H. Dacol, Jpn. J. Appl. Phys. 24, Suppl. 24-2, 85 (1986).
[9]G. Burns and F. H. Dacol, Solid State Commun. 48, 853 (1983); G. Burns and B. A. Scott, *ibid.* 13, 423 (1973).
[10]G. Burns and F. H. Dacol, Phys. Rev. B. 30, 4012 (1984); G. Burns, *ibid.* 13, 215 (1976).
[11]J. J. DeYoreo, R. O. Pohl, and G. Burns, Phys. Rev. B 32, 5780 (1985). Rather complete references to earlier work are given here. Also see Jpn. J. Appl. Phys. 24, Suppl. 24-2, 975 (1986).
[12]G. Burns and F. H. Dacol, Solid State Commun. 58, 567 (1986).
[13]T. Heinz, G. Burns, and N. Halas, Bull. Am. Phys. Soc. 31, 603 (1986).
[14]G. Burns, Phase Transitions 5, 261 (1985); G. Burns and F. H. Dacol, Ferroelectrics 52, 103 (1983).
[15]R. L. Byer and C. B. Roundy, Ferroelectrics 3, 333 (1972).
[16]A. M. Glass, J. Appl. Phys. 40, 4699 (1969).
[17]J. F. Nye, *Physical Properties of Crystals* (Clarendon, Oxford, 1957).
[18]E. L. Venturini, E. G. Spenger, P. V. Lenzo, and A. A. Ballman, J. Appl. Phys. 39, 343 (1968).
[19]G. Burns, F. H. Dacol, J. P. Remeika, and W. Taylor, Phys Rev. B 26, 2702 (1982); G. Burns and F. H. Dacol, Jpn. J. Appl. Phys. 24, Suppl. 24-2, 649 (1986).
[20]G. Burns and A. W. Smith, IEEE J. Quantum Electron. QE-4, 584 (1968).
[21]J. E. Geusic, S. K. Kurtz, L. G. Van Uitert, and S. H. Wemple, Appl. Phys. Lett. 4, 141 (1964).
[22]M. DiDomenico and S. H. Wemple, J. Appl. Phys. 40, 720 (1969).
[23]L. E. Cross, S. J. Jang, R. E. Newnham, S. Nomura, and K. Uchino, Ferroelectrics 23, 187 (1980).
[24]Y. Xi, C. Z. Li, and L. E. Cross, J. Appl. Phys. 54, 3399 (1983).
[25]T. W. Cline, Ph.D. thesis, The Pennsylvania State University, 1977.
[26]C. Sundius, M. Sc. thesis, The Pennsylvania State University, 1983.
[27]M. P. Harmer, A. S. Bhalla, B. H. Fox, and L. E. Cross, Mater. Lett. 2, 278 (1984).
[28]H. M. Chan, M. P. Harmer, A. S. Bhalla, and L. E. Cross, Jpn. J. Appl. Phys. 24, 550 (1985).
[29]H. M. Chan, M. P. Harmer, A. S. Bhalla, and L. E. Cross, Am. Ceram. Soc. Bull. 65, 517 (1986).

Phenomenology and Properties of Conventional Ceramic Piezoelectrics

Thermodynamic theory of $PbTiO_3$

M. J. Haun, E. Furman, S. J. Jang, H. A. McKinstry, and L. E. Cross
Materials Research Laboratory, The Pennsylvania State University, University Park, Pennsylvania 16802

(Received 30 March 1987; accepted for publication 2 July 1987)

A phenomenological thermodynamic theory of $PbTiO_3$ was developed using a modified Devonshire form of the elastic Gibbs free energy. The spontaneous strain as a function of temperature was determined from pure sol-gel derived $PbTiO_3$ powder and used with selected data from the literature to determine the coefficients of the energy function. The theoretical prediction of the phase stability, spontaneous polarization and strains, and dielectric and piezoelectric properties agree well with experimental data. This theory provides a way of predicting the intrinsic single domain dielectric and piezoelectric properties of $PbTiO_3$, which have not been completely determined from experimental measurements.

I. INTRODUCTION

Lead titanate has been extensively used in ceramics as an end member of solid solution systems that have important technological applications.[1] However, the properties of pure ceramic and single-crystal $PbTiO_3$ have been difficult to study because of the high electrical conductivity and large tetragonal distortion that occurs at the ferroelectric to paraelectric transition at $\simeq 492$ °C.

Pure, dense ceramic samples will break up into powder when cooled through this transition. Small amounts of dopants have been added to $PbTiO_3$ to produce dense ceramics with large electromechanical anisotropy.[2,3] These materials are of interest in high-frequency ultrasonic transducer applications,[4-6] but still do not provide data on the properties of pure ceramic $PbTiO_3$.

Small amounts of dopants have also been added to single-crystal $PbTiO_3$ to increase the electrical resistivity and allow dielectric measurements to be made. Even so, considerable discrepancies exist in the published data because of the differences in crystal quality and measuring techniques that were used. Values of the Curie–Weiss constant and Curie temperature have varied from 1.1 to 4.1 ($\times 10^5$ °C) and from 449 to 485 °C, respectively.[7,8] In addition, very little data exists on the temperature dependence of the dielectric and piezoelectric properties measured on good-quality single domain single crystals.

The development of a Landau–Ginsburg–Devonshire[9] type thermodynamic theory of $PbTiO_3$ would be a particularly useful method of providing a more complete description of the intrinsic single domain properties of this material. Remeika and Glass[8] determined some of the coefficients of the elastic Gibbs free-energy function, but were unable to separate the fourth- and sixth-order dielectric stiffness coefficients, because the spontaneous polarization (P_s) at the Curie point (T_c) was unknown.

Gavrilyachenko *et al.*[10] measured P_s at 20 °C from a dielectric hysteresis loop, and used this value to determine the electrostrictive constant from the uniform deformation parameter[11] (spontaneous strain). The temperature dependence of P_s was then calculated from the temperature dependence of the uniform deformation parameter[12] by assuming the electrostrictive constant to be independent of temperature. The value of P_s at T_C was then used to calculate the fourth- and sixth-order dielectric stiffness coefficients in the energy function.[13] However, the coefficients of the polarization interaction terms in a three-dimensional energy function had still not been determined for $PbTiO_3$.

Amin *et al.*[14] determined all of the coefficients of a three-dimensional energy function, including all of the fourth- and sixth-order polarization interaction terms, for the single-cell region of the $PbZrO_3$: $PbTiO_3$ solid solution system. The coefficients of the polarization interaction terms were determined by fitting the morphotropic phase boundary between the tetragonal and rhombohedral states. These coefficients were then extrapolated across the tetragonal phase field to $PbTiO_3$. This resulted in a larger dielectric susceptibility parallel to the polar axis compared to that perpendicular to polar axis, which does not agree with single-crystal data.[13]

The purpose of this study is to develop a more complete phenomenological theory of $PbTiO_3$ that will better represent the intrinsic single domain behavior of this material. The temperature dependence of the dielectric and piezoelectric properties of $PbTiO_3$ could then be calculated. This theory could also be useful in investigating solid solution systems, where the coefficients of the energy function and properties of the end member $PbTiO_3$ are required.

Indirect methods were used to determine the coefficients of the energy function due to the lack of good single domain single-crystal data. A sol-gel technique was used to produce a pure and fine powder of $PbTiO_3$. Using high-temperature x-ray diffraction the spontaneous strain was determined from the temperature dependence of the cell parameters. These data were used with selected data from the literature to determine the coefficients of the energy function.

In the next section the elastic Gibbs free-energy expansion and the equations used to calculate the spontaneous polarization and strain, and the dielectric and piezoelectric properties will be presented. The experimental high-temperature x-ray diffraction measurements and results will

 0021-8979/87/203331-08$02.40

then be discussed in Sec. III, followed by a description of the procedure used to determine the coefficients of the energy function in Sec. IV. Theoretical calculations using these values of the coefficients will be discussed and compared with experimental data in Sec. V. Finally, a summary of this study and future applications of the results will be presented in Sec. VI.

II. PHENOMENOLOGICAL THERMODYNAMIC THEORY

Using the Landau–Ginsburg–Devonshire formalism the elastic Gibbs free energy was expanded in a power series of the polarization assuming isothermal conditions. The nonzero coefficients of the energy function were limited by the symmetry of the paraelectric phase: $m3m$ for $PbTiO_3$. Using reduced notation,

$$\begin{aligned}\Delta G = {} & \alpha_1(P_1^2+P_2^2+P_3^2)+\alpha_{11}(P_1^4+P_2^4+P_3^4)+\alpha_{12}(P_1^2P_2^2+P_2^2P_3^2+P_3^2P_1^2)+\alpha_{111}(P_1^6+P_2^6+P_3^6)\\ & +\alpha_{112}[P_1^4(P_2^2+P_3^2)+P_2^4(P_1^2+P_3^2)+P_3^4(P_1^2+P_2^2)]+\alpha_{123}P_1^2P_2^2P_3^2-\tfrac{1}{2}s_{11}(X_1^2+X_2^2+X_3^2)\\ & -s_{12}(X_1X_2+X_2X_3+X_3X_1)-\tfrac{1}{2}s_{44}(X_4^2+X_5^2+X_6^2)-Q_{11}(X_1P_1^2+X_2P_2^2+X_3P_3^2)\\ & -Q_{12}[X_1(P_2^2+P_3^2)+X_2(P_1^2+P_3^2)+X_3(P_1^2+P_2^2)]-Q_{44}(X_4P_2P_3+X_5P_1P_3+X_6P_1P_2),\end{aligned} \tag{1}$$

where P_i and X_i are the polarization and stress; α_i, α_{ij}, and α_{ijk} are the dielectric stiffness and higher-order stiffness coefficients at constant stress; s_{ij} is the elastic compliance coefficient at constant polarization; and Q_{ij} is the cubic electrostrictive constant in polarization notation.

There are four possible solutions to Eq. (1) corresponding to the cubic, tetragonal, orthohombic, and rhombohedral structures:

Cubic:	$P_1^2=P_2^2=P_3^2=0;$	(2)
Tetragonal:	$P_1^2=P_2^2=0, \quad P_3^2\neq 0;$	(3)
Orthorhombic:	$P_1^2=P_2^2\neq 0, \quad P_3^2=0;$	(4)
Rhombohedral:	$P_1^2=P_2^2=P_3^2\neq 0.$	(5)

The resulting energy functions and spontaneous polarization relations for these solutions have been reported in Ref. 14, along with equations for the spontaneous elastic strains (x_i), dielectric susceptibilities (η_i), and piezoelectric constants (d_{ij} and g_{ij}).

The cubic and tetragonal phases are stable in $PbTiO_3$, and the orthorhombic and rhombohedral phases are metastable. The cubic paraelectric phase is taken as the reference state with an energy of zero. The spontaneous polarization and strain, and piezoelectric constants in the cubic state are also equal to zero. The relative dielectric susceptibility coefficients (η_{ij}) of the cubic phase are

$$\eta_{11}=\eta_{22}=\eta_{33}=(2\alpha_1\epsilon_0)^{-1}, \quad \eta_{12}=\eta_{23}=\eta_{31}=0. \tag{6}$$

The equations for the tetragonal state will also be repeated here for convenience.

Tetragonal solution of the energy function (ΔG):

$$\Delta G=\alpha_1P_3^2+\alpha_{11}P_3^4+\alpha_{111}P_3^6. \tag{7}$$

Spontaneous polarization (P_i):

$$P_1^2=P_2^2=0, \quad P_3^2=\frac{-\alpha_{11}+(\alpha_{11}^2-3\alpha_1\alpha_{111})^{1/2}}{3\alpha_{111}}. \tag{8}$$

Spontaneous elastic strains (x_i):

$$x_1=x_2=Q_{12}P_3^2, \quad x_3=Q_{11}P_3^2, \quad x_4=x_5=x_6=0. \tag{9}$$

Relative dielectric susceptibility coefficients (η_{ij}):

$$\begin{aligned}&\eta_{11}=\eta_{22}=[(2\alpha_1+2\alpha_{12}P_3^2+2\alpha_{112}P_3^4)\epsilon_0]^{-1},\\ &\eta_{33}=[(2\alpha_1+12\alpha_{11}P_3^2+30\alpha_{111}P_3^4)\epsilon_0]^{-1},\\ &\eta_{12}=\eta_{23}=\eta_{31}=0.\end{aligned} \tag{10}$$

Piezoelectric voltage coefficients (g_{ij}):

$$g_{33}\approx 2Q_{11}P_3, \quad g_{31}\approx 2Q_{12}P_3, \quad g_{15}\approx Q_{44}P_3. \tag{11}$$

Piezoelectric charge coefficients (d_{ij}):

$$\begin{aligned}&d_{33}=2\epsilon_0\eta_{33}Q_{11}P_3, \quad d_{31}=2\epsilon_0\eta_{33}Q_{12}P_3,\\ &d_{15}=\epsilon_0\eta_{11}Q_{44}P_3.\end{aligned} \tag{12}$$

The above equations can be used to calculate the spontaneous polarization and strain, and dielectric and piezoelectric properties from the dielectric stiffness, higher-order stiffness, and electrostrictive constants.

III. HIGH-TEMPERATURE X-RAY DIFFRACTION

High-temperature x-ray diffraction was used to determine the cell parameters of pure homogeneous sol-gel derived $PbTiO_3$ powder as a function of temperature. The spontaneous strain was calculated from the cell parameters and used to determine the spontaneous polarization through the electrostrictive constants.

A sol-gel method, using lead acetate and titanium isopropoxide, was used to prepare $PbTiO_3$ powder. To control the lead stoichiometry during calcining, excess lead oxide was included in the powder by starting with additional lead acetate during the sol-gel procedure. After calcining the dried gel at 800 °C for 24 h, the excess lead oxide was washed out with acetic acid. The purity of the $PbTiO_3$ powder was found to be greater than 99.987% from semiquantitative spectrographic analysis. Trace elements of less than 0.005% Si and Mg, and less than 0.003% Ca were found. No other elements could be detected. A more complete description of the sol-gel method used is given in Ref. 15.

A microcomputer automated Picker x-ray diffractometer was used to collect the x-ray diffraction patterns using Cu$K\alpha$ radiation. The microcomputer was used to control the stepping motor of the diffractometer and to collect and store the data. Using this system the reproducibility of the position of the 001 and 234 peaks of quartz was less than 0.0007 and approximately 0.005° 2θ, respectively.[16]

A low thermal gradient high-temperature furnace, simi-

lar in design to the furnace described in Ref. 17, was attached to the diffractometer. One of the main advantages of this type of furnace design is that the support of the sample is independent of the body of the heating chamber. Thus the initial alignment of the sample will not be affected by a change in temperature.

A computer program was used to determine the angle, intensity, and width of the diffraction peaks using a Cauchy fitting by nonlinear least squares, as described in Ref. 16. The peak angles were used to calculate the cell constants and sample displacement using the Cohen least-squares refinement method.[18] This procedure corrected the cell constants due to the sample displacement error. The sample displacement was less than 2 μm throughout the measurements.

The cell parameters at 24 °C were calculated using diffractions peaks from 001 to 422 (21.365 to 146.7° 2θ). These values are shown in Table I along with the c/a ratio, unit cell volume, and theoretical density.

The 002/200 and 233/332 diffraction peaks were measured as a function of temperature, and the peak angles are plotted in Fig. 1. These data were used to calculate the cell parameters as shown in Fig. 2. The extrapolation of the cubic cell length (a_c') will be described in the next section. The c/a ratio and unit cell volume are plotted in Fig. 3 versus temperature.

The square root of the average of the sum of the squares of the differences between the measured angles and calculated angles from the cell constants gave a measure of the precision of the data. This value was 0.006° 2θ for the room-temperature measurements shown in Table I, and less than 0.03° 2θ for the high-temperature measurements. The standard deviations of the cell constant values at room temperature were calculated to be $\pm$ 0.0001 Å (see Table I).

IV. EVALUATION OF THE COEFFICIENTS OF THE ENERGY FUNCTION

The spontaneous polarization and strain, and dielectric and piezoelectric properties of $PbTiO_3$ can be calculated from the coefficients of the energy function as shown in Sec. II. The coefficients needed for these calculations are the dielectric stiffness (α_1), higher-order dielectric stiffnesses (α_{11}, α_{12}, α_{111}, and α_{112}), and electrostrictive constants (Q_{11}, Q_{12}, and Q_{44}). These coefficients will be determined from experimental data in this section.

All of the coefficients were assumed to be independent of temperature, except the dielectric stiffness constant α_1, which was given a linear temperature dependence based on the Curie–Weiss law:

$$\alpha_1 = (T - \theta)/2\epsilon_0 C. \tag{13}$$

TABLE I. Cell parameters and related constants of $PbTiO_3$ at 24 °C.

Cell constant a(Å)	3.8995 ± 0.0001*
Cell constant c(Å)	4.1552 ± 0.0001*
c/a ratio	1.066
Unit cell volume (Å^3)	63.18
Theoretical density (g/cm^3)	7.966

*The standard deviation of the least-squares cell constant calculations.

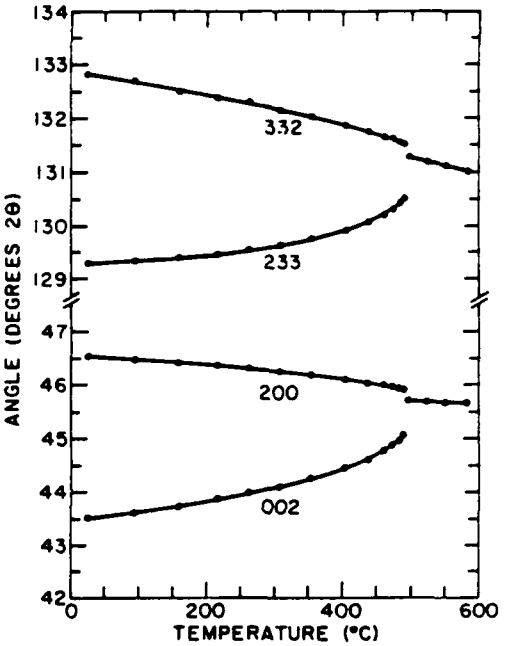

FIG. 1. Angles of the 002/200 and 233/332 diffraction peaks of $PbTiO_3$ plotted vs temperature.

C is the Curie constant, ϵ_0 is the permittivity of the free space, and θ is the Curie–Weiss temperature.

As described in the Introduction, a wide range of values of the Curie constant (C) and Curie–Weiss temperature (θ) have been reported in the literature. Due to these discrepancies indirect methods were used to determine C and θ. Amin, Cross, and Newnham[19] calculated the Curie constant from a combination of calorimetric and pheonomenological data. The same method was used to determine the Curie constant of the sol-gel derived $PbTiO_3$ powder prepared in this study. In both cases a Curie constant of 1.5×10^5 °C resulted. The Curie–Weiss temperature was determined indirectly from spontaneous strain data as described in the following paragraphs.

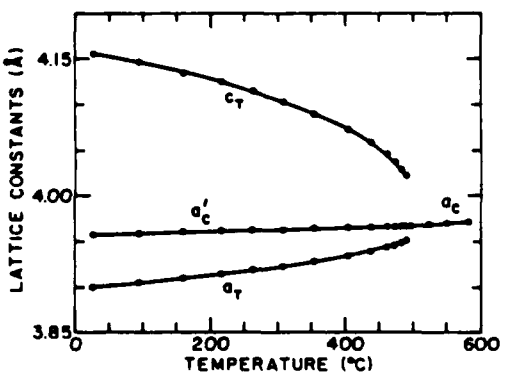

FIG. 2. Lattice constants of $PbTiO_3$ plotted vs temperature. a_T and c_T are the lattice constants of the tetragonal structure. a_c and a_c' are the lattice constants of the cubic structure above T_C and extrapolated into the tetragonal region, respectively. a_c' was calculated from the tetragonal cell constant data using Eq. (19) with the assumption that the x_3/x_1 ratio was − 3.455 at any temperature.

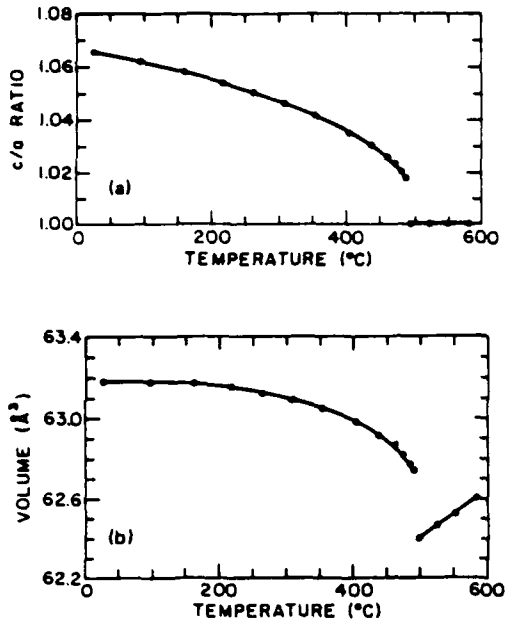

FIG. 3. (a) c/a ratio and (b) unit cell volume of $PbTiO_3$ plotted vs temperature.

The higher-order dielectric stiffness coefficients α_{11} and α_{111} were determined at the transition temperature (T_C) by equating the energies of the cubic and tetragonal states and combining this equation with the first partial derivative equilibrium condition $\partial G/\partial P_3 = 0$:

$$\alpha_{11} = [-(T_C - \theta)]/\epsilon_0 C P_0^2, \tag{14}$$

$$\alpha_{111} = (T_C - \theta)/2\epsilon_0 C P_0^4. \tag{15}$$

With these equations the $T_C - \theta$ difference and the spontaneous polarization at the transition (P_0) can be used to determine α_{11} and α_{111}.

By substituting Eqs. (13)–(15) into Eq. (8) the following relation results:

$$P_3^2 = \psi P_0^2,$$

where

$$\psi = \frac{2}{3}\left[1 + \left(1 - \frac{3(T-\theta)}{4(T_C - \theta)}\right)^{1/2}\right]. \tag{16}$$

Equation (16) can be used to calculate the spontaneous polarization from P_0, θ, and $T_C - \theta$, independently of the Curie constant.

Similar relations can be derived for the spontaneous strains x_1 and x_3 by substituting Eq. (16) into Eq. (9):

$$x_1 = \psi x_{10}, \quad \text{where} \quad x_{10} = Q_{12} P_0^2, \tag{17}$$

$$x_3 = \psi x_{30}, \quad \text{where} \quad x_{30} = Q_{11} P_0^2. \tag{18}$$

x_{10} and x_{30} are the spontaneous strains at the transition temperature T_C.

The spontaneous strains x_1 and x_3 can be calculated from the cell constants using the following relations:

$$x_1 = (a_T - a_C)/a_C', \quad x_3 = (c_T - a_C')/a_C'. \tag{19}$$

a_T and c_T are the cell constants of the tetragonal structure, and a_C' is the cell length of the cubic structure extrapolated into the tetragonal region.

When calculating the spontaneous strains of the tetragonal structure at a particular temperature, the cubic cell constant should be extrapolated to that temperature accounting for the thermal expansion. A linear extrapolation of the cell constant from above the transition can be made over a narrow temperature range with fairly good accuracy. However, a linear extrapolation of the cubic cell constant of $PbTiO_3$ of almost 500 °C to room temperature may cause erroneous results. The linear thermal expansion coefficient of many oxides changes significantly over a wide temperature range,[20] and thus would also contribute to this error.

Previously[11,14] the cubed root of the tetragonal volume $(a_T^2 c_T)^{1/3}$ was used as a_C'. Using this method there is no volumetric strain in the tetragonal state, resulting in a hydrostatic electrostrictive coefficient (Q_h) of zero. Thus an alternative procedure should be used to better estimate the spontaneous strain.

The ratio of the electrostrictive coefficients Q_{11} and Q_{12} can be determined from the ratio of the spontaneous strains x_1 and x_3 from Eq. (9):

$$x_3/x_1 = Q_{11}/Q_{12}. \tag{20}$$

The linear thermal expansion coefficient of the cubic cell constant data (a_C) shown in Fig. 2 was calculated from a linear least-squares fit to be $12.6 \times 10^{-6}\,°C^{-1}$. Using this thermal expansion coefficient, a_C was extrapolated a few degrees to the first set of tetragonal cell parameter data at 489 °C and used as a_C' to calculate the spontaneous strains x_1 and x_3. The resulting x_3/x_1 ratio and thus Q_{11}/Q_{12} ratio was -3.455.

The electrostrictive coefficients of perovskite ferroelectrics have been experimentally shown to be only slightly temperature dependent.[21,22] Thus the Q_{11}/Q_{12} ratio was assumed to be independent of temperature. a_C' was then calculated from the tetragonal cell constant data using Eq. (19) with the assumption that the x_3/x_1 ratio was -3.455 at any temperature. The a_C' data calculated using this procedure are plotted in Fig. 2.

The spontaneous strains x_1 and x_3 were calculated from the cell parameter data shown in Fig. 2 using Eq. (19) and were plotted in Fig. 4. A computer program was used to determine the values of x_{10}, x_{30}, and θ that gave the best least-squares fit of the experimental strain data using Eqs. (17) and (18) with T_C equal to 492.2 °C. This value of T_C was determined from a polynomial fit of the PZT phase diagram,[14] and agrees with x-ray and DTA data of the sol-gel derived $PbTiO_3$ powder used in this study. The theoretical fit of the strain data is shown in Fig. 4 by the solid curves, and the constants used in the calculations are given in Table II.

Using Eqs. (16)–(18) the spontaneous polarization can be calculated from the electrostrictive coefficients and the constants determined above. The electrostrictive coefficients have not been directly measured on $PbTiO_3$, but can be calculated from experimental spontaneous polarization and strain data. Using the room-temperature P_s value of 0.75 C/m^2 from Ref. 10 the Q_{11} and Q_{12} constants were calculated from the spontaneous strain data as listed in Table II. The

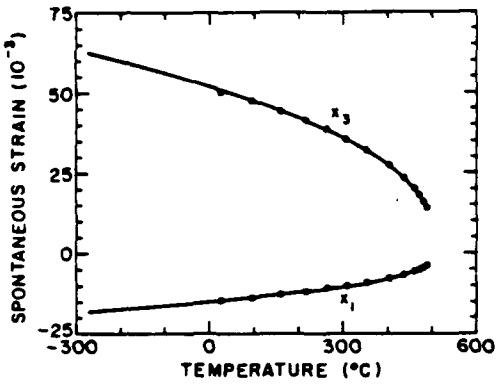

FIG. 4. Spontaneous strains x_1 and x_3 plotted vs temperature. The data points were calculated from the lattice parameter data shown in Fig. 2 using Eq. (19). The solid curves were calculated from the theory using Eq. (9) and the constants listed in Table II.

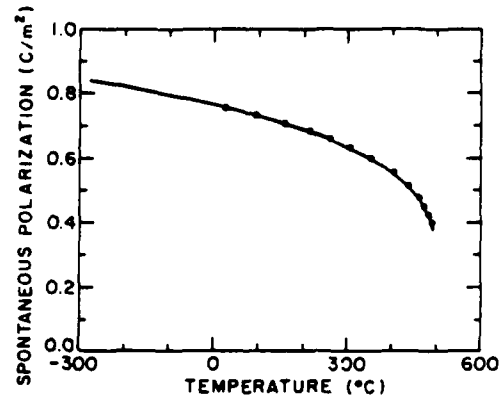

FIG. 5. Spontaneous polarization P_3 plotted vs temperature. The data points were calculated from the experimental spontaneous strain data shown in Fig. 4 using Eq. (9) and the electrostrictive constants listed in Table II. The solid curve was calculated from the theory using Eq. (16) and the constants listed in Table II.

Q_{44} constant listed in this table was estimated in Ref. 23 from η_{11}, d_{15}, and P_s data using Eq. (12).

The spontaneous polarization at the transition (P_0) was calculated from x_{10} and x_{30} using Eqs. (17) and (18) by assuming temperature-independent electrostrictive constants. P_0 was used with the other constants listed in Table II to calculate P_s as a function of temperature from Eq. (16) as shown in Fig. 5 by the solid curve. The data points in this figure were calculated from the experimental spontaneous strain data using Eq. (9).

The dielectric stiffness coefficients α_1, α_{11}, and α_{111} were calculated from Eqs. (13)–(15) using the values of C, T_C, θ, and P_0 listed in Table II. Using these coefficients the dielectric susceptibility coefficient η_{33} was calculated as a function of temperature from Eq. (10) as shown in Fig. 6 by the dashed curve. The data points and solid curves of the η_{33} and η_{11} coefficients in this figure are experimental dielectric constant measurements on crystals of $PbTiO_3$ by Fesenko, Gavrilyachenko, and Zarochentsev.[13] The decrease in dielectric constants from 0 to -100 °C was reported as being due to the relaxation of the defect contribution present in these crystals. The values of the dielectric constants at temperatures below -100 °C, where the defect contribution has "frozen out," may represent the intrinsic dielectric constants if no further relaxations occur at lower temperatures. The agreement between the experimental and theoretical values of η_{33} at low temperatures is fairly good considering the constants used in the calculations were determined independently of any dielectric data and the electrostrictive constants and higher-order dielectric stiffness coefficients were assumed to be independent of temperature.

To calculate the dielectric susceptibility coefficient η_{11} using Eq. (10) the dielectric stiffness coefficients α_{12} and α_{112} must be determined. These two coefficients are not present in the energy function for the tetragonal state [Eq. (7)] or in the first derivative quantities [Eqs. (8) and (9)], but do arise in the second derivative dielectric properties [Eq. (10)]. Thus experimental η_{11} data are needed to determine α_{12} and α_{112}. The low-temperature η_{11} data shown in Fig. 6 were used to determine temperature-independent α_{12} and α_{112} coefficients that gave the best least-squares fit of these data with Eq. (10). η_{11} was then calculated as a function of temperature as shown by the dashed curve in Fig. 6.

TABLE II. Constants used in the theoretical calculations.

T_C(°C)	492.2
θ(°C)	478.8
$T_C - \theta$(°C)	13.4
$C(10^5$ °C)	1.5
$x_{10}(10^{-2})$	−0.362
$x_{30}(10^{-2})$	1.24
P_0(C/m^2)	0.373
$Q_{11}(10^{-2}$ m^4/C^2)	8.9
$Q_{12}(10^{-2}$ m^4/C^2)	−2.6
$Q_{44}(10^{-2}$ m^4/C^2)	6.75[a]
$\alpha_1(10^6$ m/F) at T_C	5.045
$\alpha_1(10^6$ m/F) at 25 °C	−1.708
$\alpha_{11}(10^7$ m^5/C^2 F)	−7.252
$\alpha_{12}(10^8$ m^5/C^2 F)	7.5
$\alpha_{111}(10^8$ m^9/C^4 F)	2.606
$\alpha_{112}(10^8$ m^9/C^4 F)	6.1

[a] From Ref. 23.

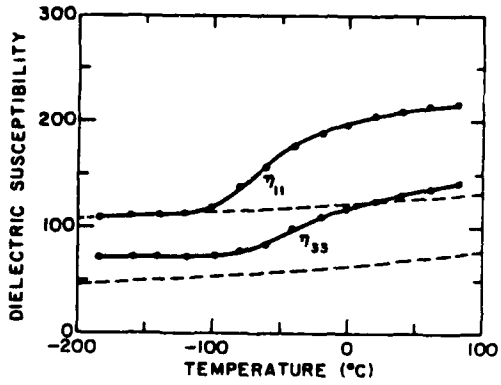

FIG. 6. Dielectric susceptibility coefficients η_{11} and η_{33} plotted vs temperature. The data points and solid curves are experimental measurements on single crystals from Ref. 13. The dashed curves are theoretical calculations using Eq. (10) and the constants from Table II. The experimental η_{11} data was used to determine the α_{12} and α_{112} dielectric stiffness coefficients.

V. THEORETICAL CALCULATIONS

The tetragonal and orthorhombic solutions to the elastic Gibbs free energy, and the dielectric and piezoelectric properties of $PbTiO_3$ will be calculated in this section using the equations from Sec. II and the constants from Table II. Comparisons will then be made with experimental results.

The tetragonal and orthorhombic solutions to the elastic Gibbs free energy are plotted versus temperature in Fig. 7. The tetragonal solution was calculated from Eq. (7), and the equation used for the orthorhombic solution is given in Ref. 14. Above T_C (492.2 °C) the energy of the tetragonal state is positive, and thus the cubic state with the reference energy set to zero is stable. At T_C the tetragonal energy decreases to zero, and then becomes negative below T_C causing the tetragonal phase to become stable.

As shown in Fig. 7 the energy of the tetragonal state is always lower than that of the orthorhombic state, and thus $PbTiO_3$ does not transform to orthorhombic as occurs in $BaTiO_3$. This is due to the larger value of the ϕ ratio ($= -\alpha_{12}/\alpha_{11}$) in $PbTiO_3$ compared to that in $BaTiO_3$. The value of ϕ controls the transition temperatures to lower symmetry phases. The value of ϕ in $PbTiO_3$ is large enough to keep the tetragonal phase stable down to 0 K. A lower value of ϕ in $BaTiO_3$ causes the tetragonal to orthorhombic and orthorhombic to rhombohedral transitions to occur.[9]

The higher-order dielectric stiffness coefficient α_{123} is needed to calculate the energy of the rhombohedral state.[14] This coefficient can be determined in the $PbZrO_3$:$PbTiO_3$ solid solution system where the rhombohedral phase is stable, and then extrapolated to $PbTiO_3$. Using this procedure the energy of the rhombohedral state was calculated and found to be greater than the energy of the tetragonal state.

The dielectric susceptibility coefficients in the cubic and tetragonal phases were calculated from Eqs. (6) and (10) and were plotted versus temperature in Fig. 8. In the tetragonal state close to T_C the dielectric susceptibility perpendicular to the polar axis (η_{11}) is less than the susceptibility parallel to the polar axis (η_{33}). At a lower temperature the values of these coefficients cross, and then η_{11} becomes greater than η_{33}. This same effect was theoretically[9] and experimentally[24] found to occur in $BaTiO_3$, except that the anisotropy (η_{11}/η_{33}) at room temperature was more than an order of magnitude greater than in $PbTiO_3$.

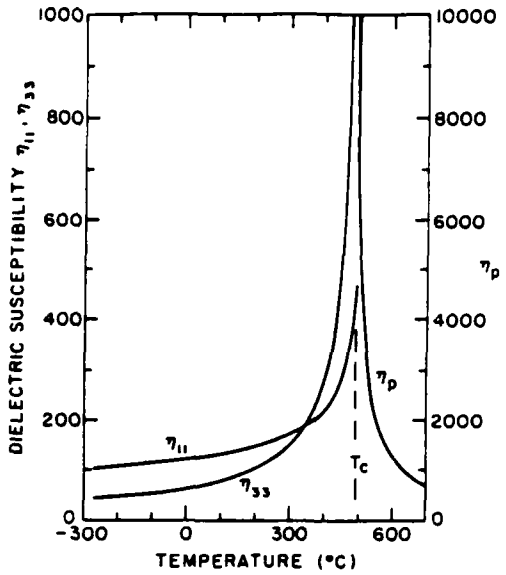

FIG. 8. Dielectric susceptibility coefficients of the tetragonal (η_{11} and η_{33}) and cubic (η_p) phases plotted vs temperature.

In addition to controlling the phase stability as described above, the value of ϕ also controls the dielectric anisotropy. The larger value of ϕ in $PbTiO_3$ causes the anisotropy to be smaller than in $BaTiO_3$. If the value of ϕ is increased, the anisotropy (η_{11}/η_{33}) will decrease and eventually η_{11} will be less than η_{33} at all temperatures.

The ratio of the sixth-order dielectric stiffness coefficients $\alpha_{112}/\alpha_{111}$ and $\alpha_{123}/\alpha_{111}$ controls the dielectric anisotropy and phase stability in addition to the ϕ ratio. Isupov[25] has studied the effect of the α_{12}, α_{112}, and α_{123} coefficients on the phase stability of perovskite ferroelectrics.

The piezoelectric voltage and charge coefficients (g_{ij} and d_{ij}) were calculated as a function of temperature using Eqs. (11) and (12) as shown in Figs. 9 and 10, respectively.

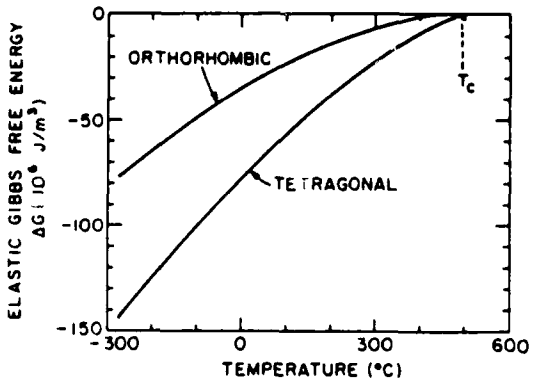

FIG. 7. Elastic Gibbs free energy for the tetragonal and orthohombic states plotted vs temperature.

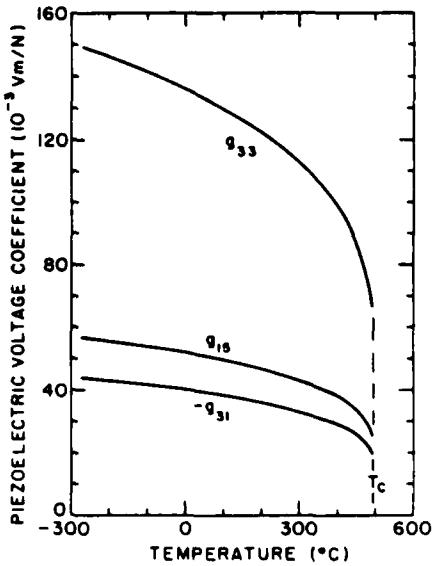

FIG. 9. Piezoelectric voltage coefficients (g_{ij}) plotted vs temperature.

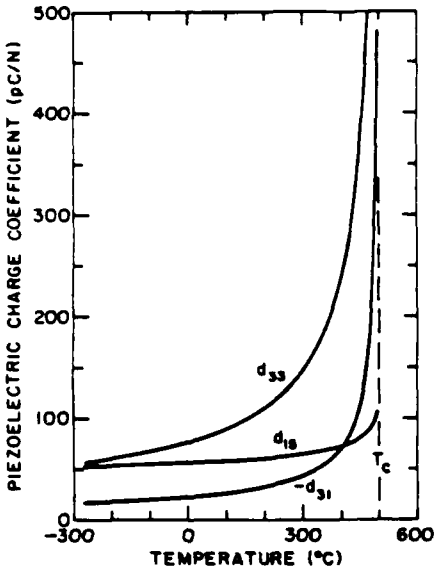

FIG. 10. Piezoelectric charge coefficients (d_{ij}) plotted vs temperature.

The negative temperature dependence of the g_{ij} coefficients was caused by the temperature dependence of the spontaneous polarization. The positive temperature dependence of the d_{33} and d_{31} coefficients was caused by the strong temperature dependence of the dielectric susceptibility coefficient η_{33}, which dominated the temperature dependence of the polarization. The smaller temperature dependence of η_{11}, compared to η_{33}, caused the d_{15} coefficient to increase only slightly over a wide temperature range.

Table III shows the theoretical single-crystal spontaneous polarization, ΔG's of the tetragonal and orthorhombic states, and dielectric and piezoelectric properties of $PbTiO_3$ at 25 °C. The calculated values of the dielectric susceptibilities η_{11} and η_{33} shown in this table are considerably less than the experimentally measured values at room temperature from Ref. 13. However, as previously shown in Fig. 6, good agreement was found at low temperatures where the defect contribution to the susceptibility had "frozen out."

The value of the calculated piezoelectric d_{33} coefficient shown in Table III is less than the experimentally measured values of 117 pC/N (measured by a dynamic method) and 193 pC/N (measured by a static method).[26] The larger experimental values may be due to the defect contribution to the dielectric constant as previously described. An experimental value of -25 pC/N was reported for the d_{31} coefficient.[26] This value is in good agreement with the calculated d_{31} shown in Table III. The temperature dependence of the d_{31} coefficient was also reported in Ref. 26, and is plotted in Fig. 11 along with the theoretical temperature dependence. The d_{15} coefficient was experimentally found to be 65 pC/N,[26] compared to the theoretical value of 56 pC/N shown in Table III.

TABLE III. Calculated single-crystal properties of $PbTiO_3$ at 25 °C.

P_s (C/m^2)	0.75
ΔG_T (10^6 J/m^3)	-72.7
ΔG_o (10^6 J/m^3)	-32.1
η_{11}	66.6
η_{33}	124.4
g_{33} (10^{-3} V m/N)	134.3
g_{31} (10^{-3} V m/N)	-39.2
g_{15} (10^{-3} V m/N)	50.9
d_{33} (10^{-12} C/N)	79.1
d_{31} (10^{-12} C/N)	-23.1
d_{15} (10^{-12} C/N)	56.1

VI. SUMMARY

High-temperature x-ray diffraction was used to determine the cell parameters of pure sol-gel derived $PbTiO_3$ powder. The spontaneous strain was calculated from these data and used with the electrostrictive contants to calculate the temperature dependence of the spontaneous polarization. All of the coefficients of the energy function were assumed to be independent of temperature, except the dielectric stiffness coefficient which was given a linear temperature dependence based on the Curie–Weiss law. These coefficients were determined from the experimental data collected in this study and from selected data from the literature. The theory was found to predict the spontaneous polarization and strains very well.

The calculated phase stability was found to agree with the experimental phase diagram by predicting a cubic to tetragonal phase transition without any other transitions to lower symmetry phases. The theoretical dielectric susceptibility coefficients and anisotropy of these coefficients were in good agreement with experimental dielectric data at low temperatures where the defect contributions had "frozen out." The calculated piezoelectric d_{31} coefficient was also found to agree quite well with low-temperature experimental data.

The energy function developed in this study provides a way of preceding the intrinsic single domain dielectric and piezoelectric properties of $PbTiO_3$, which had not been completely determined from experimental measurements. This

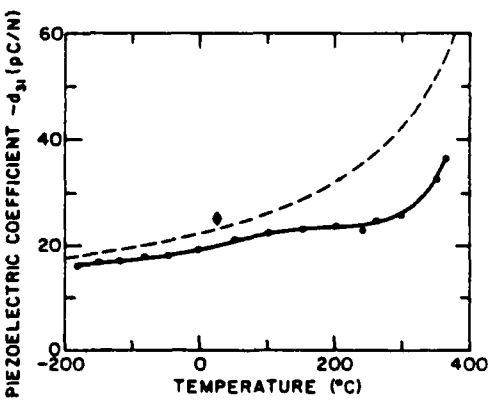

FIG. 11. Piezoelectric charge coefficient d_{31} plotted vs temperature. The diamond-shaped data point is an experimental room-temperature value of d_{31} from Ref. 26. The circular data points and solid curve are the experimentally measured temperature dependence of d_{31} from Ref. 26. The dashed curve is the theoretical calculation.

theory will also be useful in investigating solid solution systems, where the coefficients of the energy function and properties of the end member $PbTiO_3$ are required. A phenomenological theory of the $PbZrO_3$:$PbTiO_3$ solid solution system, which accounts for the oxygen octahedral tilting and second-order transition region,[27] is presently being developed using the results of this study.

The properties of pure ceramic $PbTiO_3$ can be estimated from the results of this theory using ceramic averaging techniques. Upper and lower limits of the dielectric and piezoelectric properties of ceramic $PbTiO_3$ have been approximated using a simple averaging procedure and the results of this study.[28] The calculated ceramic properties have been used to help understand the dielectric and piezoelectric behavior of modified $PbTiO_3$ ceramics.[29]

[1]B. Jaffe, W. J. Cook, and H. Jaffe, *Piezoelectric Ceramics* (Academic, London, 1971), p. 115.
[2]S. Ikegami, I. Ueda, and T. Nagata, J. Acoust. Soc. Am. **50**, 1060 (1971).
[3]I. Ueda, Jpn. J. Appl. Phys. **11**, 450 (1972).
[4]H. Takeuchi, S. Jyomura, and C. Nakaya, Jpn. J. Appl. Phys. **24** (Suppl. 24-2), 36 (1985).
[5]W. R. Xue, J. N. Kim, S. J. Jang, L. E. Cross, and R. E. Newnham, Jpn. J. Appl. Phys. **24** (Suppl. 24-2), 718 (1985).
[6]D. Damjanovic, T. R. Gururaja, S. J. Jang, and L. E. Cross, Mater. Lett. **4**, 414 (1986).
[7]V. G. Bhide, K. G. Deshmukh, and M. S. Hedge, Physica **28**, 871 (1962).
[8]J. P. Remeika and A. M. Glass, Mater. Res. Bull. **5**, 37 (1970).
[9]A. F. Devonshire, Philos. Mag. **40**, 1040 (1949).
[10]V. G. Gavrilyachenko, R. I. Spinko, M. A. Martynenko, and E. G. Fesenko, Fiz. Tverd. Tela **12**, 1532 (1970) [Sov. Phys.—Solid State **12**, 1203 (1970)].
[11]E. G. Fesenko, V. S. Filip'ev, and M. F. Kupriyanov, Fiz. Tverd. Tela **11**, 466 (1969) [Sov. Phys.—Solid State **11**, 366 (1969)].
[12]E. G. Fesenko, O. P. Kramarov, A. L. Khodakov, and M. L. Sholokhovich, Izv. Akad. Nauk SSSR Ser. Fiz. **21**, 305 (1957) [Bull. Acad. Sci. USSR **21**, 314 (1957)].
[13]E. G. Fesenko, V. G. Gavrilyachenko, and E. V. Zarochentsev, Izv. Akad. Nauk SSSR Ser. Fiz. **34**, 2541 (1970) [Bull. Acad. Sci. USSR **34**, 2262 (1970)].
[14]A. Amin, M. J. Haun, B. Badger, H. A. McKinstry, and L. E. Cross, Ferroelectrics **65**, 107 (1985).
[15]Z. Q. Zhuang, M. J. Haun, S. J. Jang, and L. E. Cross, in *Proceedings of the 6th IEEE International Symposium on Applications of Ferroelectrics*, Lehigh, PA, edited by Van Wood (IEEE, New York, 1986), pp. 394–397.
[16]G. E. Lenain, H. A. McKinstry, and S. Y. Limaye, in *Advances in X-Ray Analysis*, edited by C. S. Barrett, P. K. Predecki, and D. E. Leyden (Plenum, New York, 1985), Vol. 28, pp. 345–352.
[17]H. A. McKinstry, J. Appl. Phys. **41**, 5074 (1970).
[18]B. Cullity, *Elements of X-Ray Diffraction Second Edition* (Addison-Wesley, Reading, MA, 1978), pp. 350–368.
[19]A. Amin, L. E. Cross, and R. E. Newnham, Ferroelectrics **37**, 647 (1981).
[20]W. D. Kingery, H. K. Bowen, and D. R. Uhlmann, *Introduction to Ceramics*, 2nd ed. (Wiley, New York, 1976), p. 591–595.
[21]S. J. Jang, Ph.D. thesis, The Pennsylvania State University, 1979. K. Uchino, S. Nomura, L. E. Cross, S. J. Jang, and R. E. Newnham, J. Appl. Phys. **51**, 1142 (1980).
[22]G. Zorn, W. Wersing, and H. Gobel, Jpn. J. Appl. Phys. **24** (Suppl. 24-2), 721 (1985).
[23]A. V. Turik, E. G. Fesenko, V. G. Gavrilyachenko, and G. I. Khasabova, Kristallografiya **19**, 1095 (1974) [Sov. Phys.—Crystallogr. **19**, 677 (1974)].
[24]D. Meyerhofer, Phys. Rev. **112**, 413 (1958).
[25]V. A. Isupov, Fiz. Tverd. Tela **19**, 1347 (1977) [Sov. Phys.—Solid State **19**, 783 (1977)].
[26]V. G. Gavrilyachenko and E. G. Fesenko, Kristallografiya **16**, 640 (1971) [Sov. Phys.—Crystallogr. **16**, 549 (1971)].
[27]M. J. Haun, Z. Q. Zhuang, S. J. Jang, H. A. McKinstry, and L. E. Cross, in *Proceedings of the 6th IEEE International Symposium on Applications of Ferroelectrics*, Lehigh, PA, edited by Van Wood (IEEE, New York, 1986), pp. 398–401.
[28]M. J. Haun, E. Furman, S. J. Jang, and L. E. Cross, Trans. IEEE Ultrason. Ferroelectrics Frequency Control Soc. (to be published).
[29]J. N. Kim, M. J. Haun, S. J. Jang, L. E. Cross, and W. R. Xue, Trans. IEEE Ultrason. Ferroelectrics Frequency Control Soc. (to be published).

From: ADVANCES IN X-RAY ANALYSIS, Vol. 30
Edited by Charles S. Barrett, John V. Gilfrich, Ron Jenkins,
Donald E. Leyden, John C. Russ and Paul K. Predecki
(Plenum Publishing Corporation, 1987)

HIGH TEMPERATURE X-RAY DIFFRACTION STUDY OF SOL-GEL DERIVED $Pb(Zr_xTi_{1-x})O_3$ POWDERS

M.J. Haun, Y.H. Lee, H.A. McKinstry, and L.E. Cross

Materials Research Laboratory
The Pennsylvania State University
University Park, PA 16802

ABSTRACT

The lattice parameters of sol-gel derived $Pb(Zr_xTi_{1-x})O_3$ powders were determined as a function of temperature using a microcomputer automated Picker x-ray diffractometer. The spontaneous strain was calculated from the lattice parameters, and used with other experimental data to develop a thermodynamic phenomenological theory for the PZT solid solution system. A second tricritical point, where the transition changes from first to second order, was found to occur near or possibly at the morphotropic phase boundary between the tetragonal and high temperature rhombohedral phases. Using an equation derived from the theory, the spontaneous tilt angle of the oxygen octahedra in the low temperature rhombohedral phase was calculated from the experimental spontaneous strain data.

INTRODUCTION

Ceramics of lead zirconate:lead titanate (PZT) solid solutions have been widely used for piezoelectric transducer applications, because of their superior properties[1]. Compositions of PZT have also been used in pyroelectric detectors[2].

The PZT phase diagram is shown in Figure 1. A cubic paraelectric phase (P_C) occurs at high temperatures and has the perovskite crystal structure ABO_3. On the $PbTiO_3$ side of the phase diagram, a ferroelectric tetragonal phase (F_T) exists with a spontaneous polarization along the pseudocubic [001] direction. A morphotropic boundary separates the tetragonal phase from a ferroelectric high temperature rhombohedral phase ($F_{R(HT)}$).

Another ferroelectric to ferroelectric phase transition occurs between the high and low temperature rhombohedral phases. Both of these rhombohedral phases have a spontaneous polarization that occurs along the [111] direction. The low temperature rhombohedral phase has a tilting or rotation of the oxygen octahedra about the [111] axis, which does not occur in the high temperature phase.

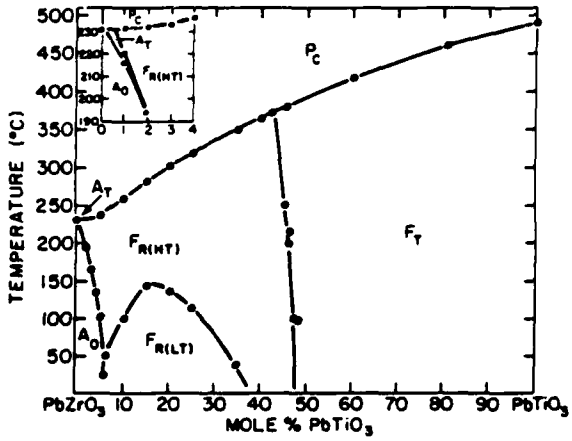

Figure 1. The $PbZrO_3$:$PbTiO_3$ phase diagram[1].

On the $PbZrO_3$ side of the phase diagram antiferroelectric tetragonal (A_T) and orthorhombic (A_O) phases are present. These antiferroelectric phases are composed of two sublattices with equal and opposite polarization, resulting in zero net polarization.

A phenomenological thermodynamic theory using the Landau:Ginsburg: Devonshire formalism has been a useful method of correlating the dielectric, piezoelectric, elastic, and thermal properties of many ferroelectric materials. When good quality single domain single crystals of the material are available, the unknown coefficients of the energy function can be directly determined.

Unfortunately, good quality single crystals are not available for the PZT system, and thus the procedure used to determine the coefficients of the energy function must be indirect. One indirect method is to use x-ray powder diffraction to determine the cell parameters as a function of temperature. The spontaneous strain can then be calculated and related through the electrostriction coefficients to the intrinsic spontaneous polarization, which can be used to determine coefficients in the energy function.

A phenomenological theory has been developed for the single cell region (cubic, tetragonal, and high temperature rhombohedral phases) of the PZT solid solution system using spontaneous strain data determined from x-ray diffraction[3]. The theory was then extended to include the low temperature rhombohedral phase by including the oxygen octahedral tilt angle as an additional order parameter[4,5]. First order phase transitions were assumed in this theory, where a discontinuous change occurs in the lattice parameters and spontaneous polarization at the transition.

However, at the cubic-rhombohedral boundary, a tricritical point has been shown to exist at the $Pb(Zr_{0.94}Ti_{0.6})O_3$ composition, where the transition changes from first to second order. At a second order phase transition, the lattice parameters and spontaneous polarization change continuously, and thus a change from discontinuous to continuous behavior occurs at a tricritical point.

From $PbZrO_3$ to the tricritical point, the transition was shown to be of first order, and a region of second order behavior occurs from the tricritical point over to at least the $Pb(Zr_{0.88}Ti_{0.12})O_3$ composition[2]. Experimental spontaneous strain data for $PbTiO_3$ and several PZT compositions in the tetragonal phase field over to the morphotropic phase boundary indicate that the cubic-tetragonal phase transition is first order. A second tricritical point should therefore occur between $Pb(Zr_{0.88}Ti_{0.12})O_3$ and the morphotropic boundary.

To find the second tricritical point, sol-gel derived PZT powders were prepared for several compositions in the rhombohedral phase field. The lattice parameters were determined as a function of temperature from high temperature x-ray diffraction and were used to calculate the spontaneous strain. Using this data with the phenomenological theory, the second tricritical point was found to occur near or possibly at the morphotropic boundary. A theory was developed for the second order transition region between the two tricritical points, and the details of this theory are presented in Reference 6.

The purpose of this paper is to describe the x-ray measurements and analysis, and the application of the x-ray data to the development of a phenomenological theory of PZT.

HIGH TEMPERATURE X-RAY DIFFRACTOMETER

A microcomputer automated Picker x-ray diffractometer was used to collect the x-ray diffraction patterns. The stepping motor was controlled by the microcomputer, which was also used to collect and store the data. Using this system the reproducibility of the position of the 001 and 234 peaks of quartz was less than 0.0007 and approximately 0.005 degrees two-theta, respectively[7].

A low thermal gradient high temperature furnace, similar in design to the furnace described in Reference 8, was attached to the diffractometer. One of the main advantages of this type of furnace design is that the support of the sample is independent of the body of the heating chamber. Thus the initial alignment of the sample will not be affected by a change in temperature.

X-RAY MEASUREMENTS AND ANALYSIS

Four compositions of $Pb(Zr_xTi_{1-x})O_3$ with x equal to 0.6, 0.7, 0.8, and 0.9 with excess lead oxide were prepared using a sol-gel method, as described in Reference 9. The dried gels were calcined at 800°C for 24 hours. The excess PbO was then removed by washing the powder with a 50/50 acetic acid/H_2O solution.

The x-ray diffraction patterns of the four PZT powders were measured using the system described above. The step size and count times used varied from 0.02-0.05 degrees two-theta and 2-15 seconds depending on the temperature and angle of the peak being measured. Larger step sizes and longer count times were used as the peak angle increased. The count times were also increased as the temperature was increased.

The high temperature cubic structure distorts to a lower symmetry when transforming to the tetragonal or rhombohedral phases, and many of the

diffraction peaks split into multiple peaks. The lattice parameters of the structure determine the angles of these multiple peaks. At the second order cubic to rhombohedral transition the lattice parameters change continuously, and thus the splitting of the peaks from single to multiple peaks also occurs continuously.

Figure 2 show the splitting of the cubic 220 peak to form the rhombohedral 220 and $\bar{2}20$ peaks for the $Pb(Zr_{0.8}Ti_{0.2})O_3$ composition. According to the phase diagram, the cubic to rhombohedral phase transition occurs at 298°C for this composition. Above the transition at 308°C, the cubic 220 peak displays the $K\alpha_1$ and $K\alpha_2$ radiation since the overlap has been eliminated. Below the transition two peaks occur corresponding to the rhombohedral 220 and $\bar{2}20$, each with a contribution from $K\alpha_1$ and $K\alpha_2$.

A computer program was used to determine the angle, intensity, and width of the diffraction peaks using a Cauchy fitting by nonlinear least squares, as described in Reference 7. On the right side of Figure 2, the computer fitting of the peaks was superimposed over the measured peaks. The $K\alpha_1$ an $K\alpha_2$ peaks were accounted for in the fitting, as can be seen by the fit of the single 220 cubic peak at 308°C.

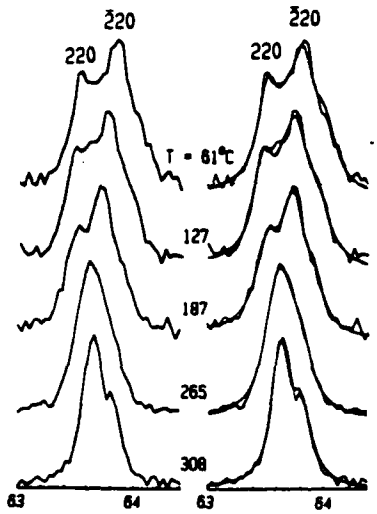

Figure 2. The x-ray diffraction pattern of the $Pb(Zr_{0.8}Ti_{0.2})O_3$ composition showing the splitting of the cubic 220 peak into the rhombohedral 220 and $\bar{2}20$ peaks. The measured peaks are shown on the left side of the figure, and the computer fitting of the peaks superimposed over the measured peaks is shown on the right.

The rhombohedral 220 and $\bar{2}20$ peaks could be separated up to 265°C by keeping the width of the peaks constant. Above this temperature the splitting became too small to distinguish the two peaks.

In Figure 3 the angle of the peaks determined from the computer program are plotted versus temperature. Between 265°C and the phase transition, where double peaks could not be fit, a single peak angle was determined. The dashed lines refer to the transition temperatures determined from the phase diagram.

CELL PARAMETERS AND SPONTANEOUS STRAIN

Four sets of rhombohedral double peaks (111, $\bar{1}11$; 220, $\bar{2}20$; 222, $\bar{2}22$; and 420, $\bar{4}20$) were used to calculate the cell parameters using the Cohen least squares refinement method[10]. This procedure also allowed for a correction due to the sample displacement, which was usually less than 0.03 mm. The square root of the average of the sum of the squares of the differences between the measured angles and calculated angles from the cell parameters gave a measure of the precision of the fit. These values were usually less than 0.02 degrees two-theta and often less than 0.005 degrees two-theta.

The rhombohedral angle is plotted versus temperature in Figure 4a for the for the four rhombohedral compositions. The spontaneous strain x_4 was calculated from the rhombohedral angle α using the relation $x_4 = (90°-\alpha)/90°$, and is plotted in Figure 4b.

The spontaneous strain x_4 in the high temperature rhombohedral state was related to the spontaneous polarization P_3 through the electrostriction constant Q_{44} by

$$x_4 = Q_{44}P_3^2 \qquad (1)$$

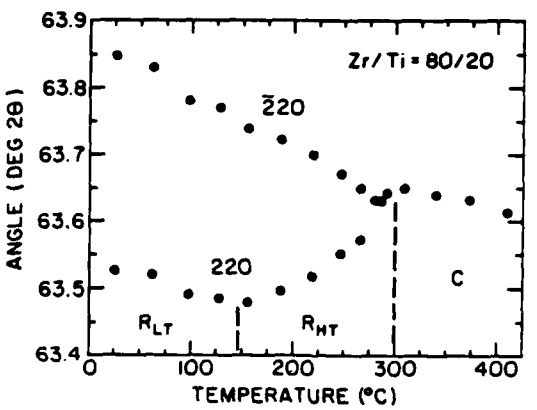

Figure 3. The angle of the cubic 220 peak and the rhombohedral 220 and $\bar{2}20$ peaks plotted versus temperature for the $Pb(Zr_{0.8}Ti_{0.2})O_3$ composition.

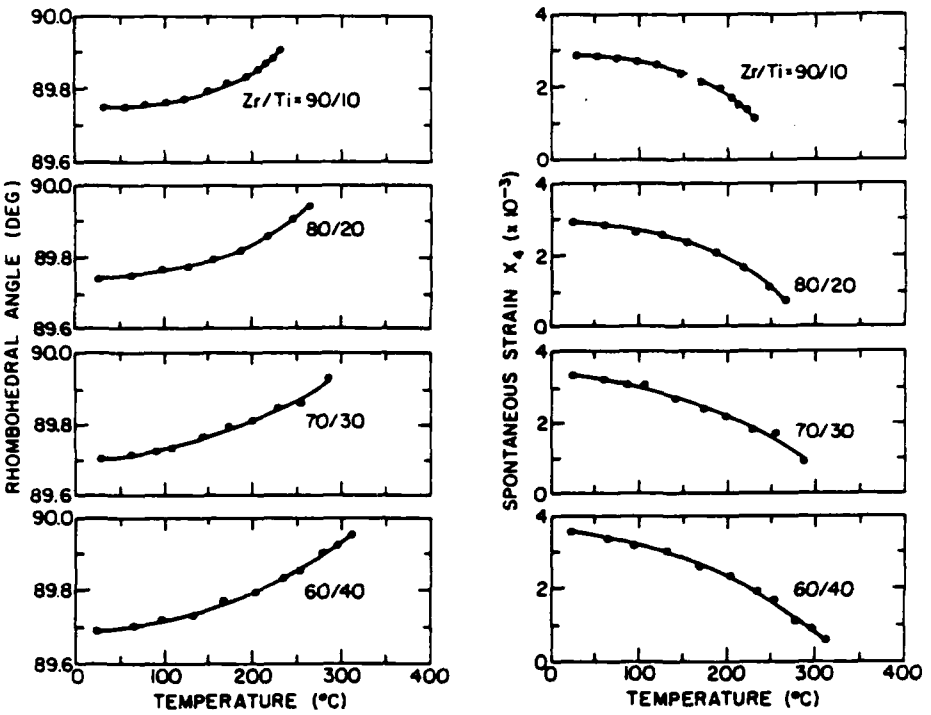

Figure 4. The a) rhombohedral angle and b) spontaneous strain plotted versus temperature for four PZT compositions within the rhombohedral phase field.

The spontaneous polarization was then used to solve for the fourth and sixth order dielectric stiffness constants of an energy function (see Reference 6 for more details of the theoretical calculations).

The fourth order constant was found to be positive, indicating that the transition from cubic to rhombohedral is second order for all four of the compositions. If this constant was negative, the transition would be of first order. The sixth order constant was also positive and decreased with composition from $Pb(Zr_{0.9}Ti_{0.1})O_3$ to $Pb(Zr_{0.6}Ti_{0.4})O_3$, and from a linear extrapolation would become zero near the morphotropic boundary. This indicates that a tricritical point would occur and the transition would change back to first order.

OXYGEN OCTAHEDRAL TILT ANGLE

Spontaneous tilt angle data of the oxygen octahedra in the low temperature rhombohedral phase are needed to determine the tilt angle related coefficients in the energy function for PZT. Unfortunately, the tilt angle has been determined only for $Pb(Zr_{0.9}Ti_{0.1})O_3$ at 25 and 60°C[11,12], and for $Pb(Zr_{0.6}Ti_{0.1})O_3$ at 9k[13] using neutron diffraction.

However, the tilt angle can be calculated from the spontaneous strain data using the following equation derived from the phenomenological theory[6]:

$$x_4 = Q_{44}P_3^2 + R_{44}\theta_3^2 \quad (2)$$

The first term in this equation is an electrostrictive term, and is the same as that used to calculate x_4 in the high temperature state (equation 1). The second term is a rotostrictive term, where R_{44} is a rotostriction constant and θ_3 is a component of the tilt angle.

The high to low temperature rhombohedral transition has been shown to be of first order[2]. The temperature dependence of the rhombohedral angle and spontaneous strain remain similar above and below the transition (see Figure 4), even though the spontaneous polarization and tilt angle change discontinuously at the transition. This happens because the electrostrictive effect causes the structure to expand, while the rotostrictive effect causes it to contract.

The electrostriction Q_{44} and rotostriction R_{44} constants were calculated from experimental spontaneous strain, polarization, and tilt angle data, which are available for the $Pb(Zr_{0.9}Ti_{0.1})O_3$ composition[12]. The tilt angle was then calculated from the spontaneous strain data using the phenomenological theory to determine the spontaneous polarization.

Figure 5 shows the tilt angle of $Pb(Zr_{0.9}Ti_{0.1})O_3$ calculated using this method, along with data that were determined from neutron diffraction. The tilt angle was also calculated for the $Pb(Zr_{0.7}Ti_{0.3})O_3$ and $Pb(Zr_{0.8}Ti_{0.2})O_3$ compositions, and is shown in Figure 6 along with the theoretical calculations (solid curves) of the tilt angle using the phenomenological theory.

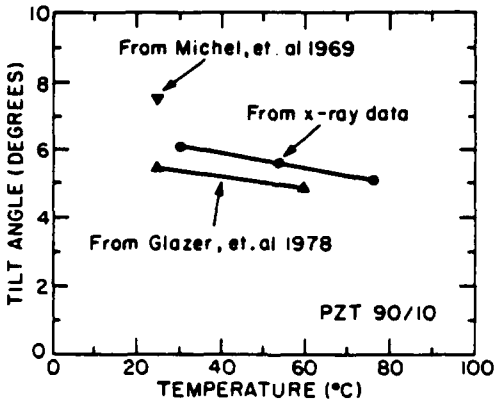

Figure 5. The spontaneous tilt angle plotted versus temperature for the $Pb(Zr_{0.9}Ti_{0.1})O_3$ composition. The circular data points were calculated from x-ray spontaneous strain data, and the triangular data points were determined from neutron diffraction[11,12].

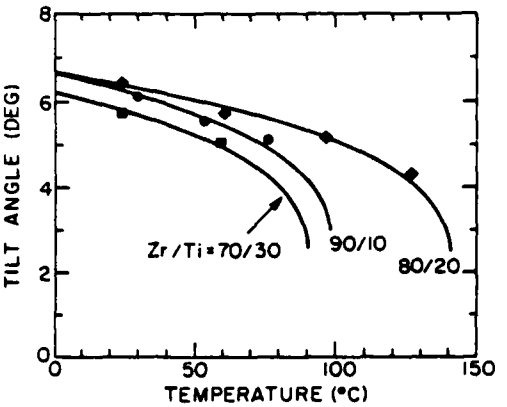

Figure 6. The spontaneous tilt angle plotted versus temperature. The data points were determined from x-ray spontaneous strain data, and the solid curves were calculated from the phenomenological theory[6].

SUMMARY

X-Ray diffraction patterns of sol-gel derived PZT powders were measured as a function of temperature using a microcomputer automated Picker x-ray diffractometer. The angle, intensity, and width of the diffraction peaks were determined from a Cauchy fitting by nonlinear least squares. The cell parameters were calculated from the peak angles using the Cohen least squares refinement method.

The spontaneous strain x_4 was then calculated from the rhombohedral angle and used to determine the spontaneous polarization through the electrostriction constant Q_{44}. The strain data were also used to calculate the oxygen octahedral tilt angle.

A thermodynamic phenomenological theory for the second order region of the PZT solid solution system was developed using this polarization and tilt angle data. A second tricritical point, where the transition changes from first to second order, was found to occur near or possibly at the morphotropic boundary between the tetragonal and rhombohedral phases. Additional spontaneous strain data will be required to precisely determine where this tricritical point occurs.

This second order theory will be combined with a previously developed first order theory, and then extended to include two sublattice polarizations to account for the antiferroelectric region of the phase diagram. A single energy function will then be able to describe the entire PZT system.

REFERENCES

1. B. Jaffe, W. Cook, and H. Jaffe, "Piezoelectric Ceramics," Academic Press, London, p. 135 (1971).
2. R. Clarke, A. M. Glazer, F. W. Ainger, D. Appleby, N. J. Poole, and S. G. Porter, Phase Transitions in Lead Zirconate-Titanate and Their Applications in Thermal Detectors, Ferroelectrics 11:359 (1976).
3. A. Amin, M. J. Haun, B. Badger, H. A. McKinstry, and L.E. Cross, A Phenomenological Gibbs Function for the Single Cell Region of the $PbZrO_3$:$PbTiO_3$ Solid Solution System, Ferroelectrics 65:107 (1985).
4. T. R. Halemane, M. J. Haun, L. E. Cross, and R. E. Newnham, A Phenomenological Theory for Phase Transitions in Perovskite Ferroelectrics with Oxygen Octahedron Tilts, Ferroelectrics 62:149 (1985).
5. M. J. Haun, T. R. Halemane, R. E. Newnham, and L. E. Cross, A Phenomenological Theory for the $PbZrO_3$:$PbTiO_3$ Solid Solution System with the Spontaneous Polarization and Oxygen Octahedral Tilt Angle as Order Parameters, Proceedings of the Sixth International Meeting on Ferroelectricity, Kobe, Japan, Jpn. J. Appl. Phys. 24(2):209 (1985).
6. M. J. Haun, Z. Q. Zhuang, S. J. Jang, H. A. McKinstry, and L. E. Cross, A Phenomenological Theory for the Second Order Transition Region of the PZT Solid Solution System, Proceedings of the 1986 IEEE International Symposium on the Applications of Ferroelectrics in the Transaction of the IEEE Ultrasonics, Ferroelectrics and Frequency Control Society (accepted).
7. G. E. Lenain, H. A. McKinstry, and S. Y. Limaye, Low Thermal Expansion of Alkali Zirconium Phosphates Using a Microcomputer Automated Diffractometer, Advances in X-Ray Analysis 28:345 (1985).
8. H.A. McKinstry, Low Thermal Gradient High Temperature Furnace for X-Ray Diffractometers, J. Appl. Phys. 41(13):5074 (1970).
9. Z.Q. Zhuang, M. J. Haun, S. J. Jang, and L. E. Cross, Low Temperature Dielectric, Piezoelectric, and Elastic Properties of Pure (Undoped) PZT Ceramics, Proceedings of the 1986 IEEE International Symposium on the Applications of Ferroelectrics in the IEEE Ultrasonics, Ferroelectrics and Frequency Control Society (accepted).
10. B. Cullity, "Elements of X-Ray Diffraction Second Edition," Addison-Wesley Publishing Co., Inc., Reading, MA, pp. 350-368 (1978).
11. C. Michel, J. Moreau, G. A. Achenbach, R. Gerson, and W. J. James, Atomic Structure of Two Rhombohedral Ferroelectric Phases in the $Pb(Zr,Ti)O_3$ Solid Solution Series, Solid State Comm., 7:865 (1969).
12. A. M. Glazer, S. A. Mabud, and R. Clarke, Powder Profile Refinement of Lead Zirconate Titanate at Several Temperatures. I. $PbZr_{0.9}Ti_{0.1}O_3$, Acta Cryst. B34:1060 (1978).
13. A. Amin, R. E. Newnham, L. E. Cross and D. E. Cox, Phenomenological and Structural Study of a Low-Temperature Phase Transition in the $PbZrO_3$-$PbTiO_3$ System, J. Solid State Chem. 37:248 (1981).

Associated Programs

TEMPERATURE BEHAVIOR OF THE COMPLEX PIEZOELECTRIC d_{31} COEFFICIENT IN MODIFIED LEAD TITANATE CERAMICS

D. Damjanovic, T.R. Gururaja, S.J. Jang and L.E. Cross

Materials Research Laboratory, The Pennsylvania State University,
University Park, Pennsylvania 16802, USA

ABSTRACT: Piezoelectric properties of modified lead titanate ceramics were investigated in an effort to explain the large electromechanical anisotropy observed in these materials. While the thickness coupling factor is approximately constant with temperature, the planar coupling factor becomes zero near room temperature, probably indicating a change in sign of the piezoelectric d_{31} coefficient . It is shown that for an accurate description of the electromechanical behavior of modified lead titanate ceramics, all material constants relevant for the planar coupling mode (s_{11}, ε_{33}, d_{31}) must be taken as complex. Possible contributions to the complex d_{31} are discussed.

INTRODUCTION:

Modified lead titanate ceramics have recently received a great deal of attention as promising materials for transducer arrays [1,2]. Unlike most piezoelectric ceramics, such as PZT, whose planar coupling factor (k_p) is in excess of 0.50, some of the modified lead titanates show vanishingly small planar coupling factor at room temperature [1-3] . However, the thickness coupling factor (k_t) for both types of materials is approximately 0.50. Among the compositions reported in the literature, the samarium and calcium modified lead titanates have exceptionally high electromechanical anisotropy i.e. high k_t/k_p ratio. The properties of these ceramics have been measured at room temperature and their potential applications described, however little was discussed about the possible mechanisms responsible for the observed electromechanical anisotropy [1,2]. The only data on temperature dependence of the electromechanical properties was reported by Xue et al. [3]. This paper is a report on the preliminary investigations of the temperature behavior of the complex piezoelectric properties of calcium and samarium modified lead titanate ceramics.

MATERIALS PREPARATION AND MEASURMENTS:

Ceramics with compositions $(Pb_{0.85}Sm_{0.10})(Ti_{0.98}Mn_{0.02})O_3$ and $(Pb_{0.76}Ca_{0.24})[(Co_{1/2}W_{1/2})_{0.04}Ti_{0.96}]O_3$ were prepared by conventional processing using mixed oxide powders [2,3]. Sintered ceramics in the form of discs were poled up to 60 kV/cm at 150 °C in silicon oil for 5 minutes. These poling conditions were necessary to obtain a saturation of the thickness coupling coefficient to about 0.45 - 0.50, the piezolectric coefficient d_{33} to about 55-60 pC/N and the planar coupling coefficient k_p of less then 0.01 at room temperature for both compositions. Therefore,

the k_t/k_p was close to 50 at room temperature. The planar coupling coefficient was calculated from the measured frequencies of the series (f_s) and the parallel (f_p) resonance of a thin disk using the equation derived by Mason [4]. The thickness coupling coefficient was calculated from the ratio of the overtone frequency f_2 to the fundamental frequency f_1 of the thickness mode series resonance, f_2/f_1, using Table II in Onoe et al.'s paper [5]. All impedance measurements were performed using an HP 4192A LF Impedance Analyzer interfaced with a computer. The piezoelectric d_{33} coefficient was measured with a Berlincourt piezo d_{33} meter.

RESULTS AND DISCUSSION:

Fig.1 and 2 show planar and thickness coupling factors as a function of temperature for Sm and Ca modified lead titanate ceramics. An interesting behavior was that the thickness coupling factor remains approximately constant with temperature, while the planar coupling factor goes through zero near room temperature. It then increases below and above this temperature reaching a maximum value of approximately 0.04 at the ends of the investigated temperature range. Similar behavior of k_p was reported earlier by Xue et al. [3] for Sm doped lead titanate ceramics.

One could attempt to explain the observed disappearance of the resonance for the planar coupling mode by considering the temperature dependence of relevant material constants. The planar coupling factor is related to the transverse coupling factor k_{31}, which in turn is related to piezoelectric constant d_{31}, elastic compliance s^E_{11} and dielectric permittivity ϵ^T_{33} as given by the relation [6]:

$$k_p = k_{31}\left(\frac{2}{1-\sigma^E}\right)^{1/2} - \frac{d_{31}}{(s^E_{11}\varepsilon^T_{33})^{1/2}}\left(\frac{2}{1-\sigma^E}\right)^{1/2} \qquad (1)$$

where σ^E is the Poisson's ratio. k_{31} and d_{31} could be calculated using a sample in the shape of a thin rectangular bar with the direction of polarization perpendicular to its length. The admittance of such a sample near the fundamental harmonic for the lengthwise vibration is given by [6]:

$$Y = j\frac{\omega lw}{t}(\varepsilon^T_{33} - \frac{d_{31}^2}{s^E_{11}}) + j\frac{2wd_{31}^2}{(\rho s^E_{11})^{1/2} s^E_{11} t}\tan\frac{\omega l}{2}(\rho s^E_{11})^{1/2} \qquad (2)$$

where parameters in Eq. (2) have the usual meaning [6]. From Eqs. (1) and (2) it is seen immidiately that the disappearance of the resonance and the associated coupling factor k_{31} at a certain temperature is possibly due to a zero value of the piezolectric constant d_{31}. Such a possibility could be realized by a change of the sign of d_{31} or by d_{31} going through zero as its extremum point. To measure the material coefficients in the Eqs.(1) and (2) as functions of temperature, an iterative method described by Smits [7] was used. This iterative method enables us to measure the values of the complex material constants s_{11}, ε_{33}, and d_{31}, defined as $m = m' - jm''$, by using the Eq. (2) and the values of the admittance $Y = G + jB$ at three frequencies near the resonance.

A plot of susceptance B vs. conductance G of the transverse mode resonance of a rectangular bar at a temperature close to where $k_p \approx 0$ is shown in Fig.3 for Sm modified lead titanate. Experimental data are represented by full circles. Assuming all matertial coefficients to be complex, the theoretical fit to the experimental data, as in

curve (a) in Fig.3, was obtained by Smits' iterative method. Curve (b) in Fig.3 is obtained by taking the imaginary part of d_{31} equal to zero and using real part for d_{31} and complex values for s_{11} and ε_{33} obtained by the iterative method. From the figure, it is clear that the imaginary part of the piezoelectric constant is necessary for a good fit to the data, especially at temperatures where k_p becomes very small. The analysis was performed to exemplify the effect of imaginary part of d_{31} on the resonance spectrum. The iterative method allows us to calculate only the product $d'_{31}d''_{31}$ and the difference $d'^2_{31} - d''^2_{31}$ from which we evaluate the real and imaginary components of d_{31}, without getting their signs independently. However, as is seen on Fig.4, the product $d'_{31}d''_{31}$ changes its sign indicating that either real or imaginary part of d_{31} changed sign. Analysis of our data, as explained below, suggests that it is more likely to be the real component of d_{31}. Fig.5 shows that the ratio $|d''_{31}/d'_{31}|$ increases rapidly as the temperature of zero k_p is approached. This means that d'_{31} approaches zero at least as fast as d''_{31} i.e. if d''_{31} assumes a value of zero and changes its sign, then d'_{31} should be zero, too. However, according to Eq. (2), if both real and imaginary components of d_{31} are equal to zero, a linear relationship in G vs. frequency is expected. Fig.6 shows plots of conductance G vs. frequency in the temperature range of 60 °C to 80 °C where k_p goes through zero. From the figure, it is clear that the signal at the resonance frequency never disappears completely. Moreover, the conductance vs. frequency curve observed at 70 °C, where it was difficult to perform a fit due to scattering in data, implies that $d''_{31} \neq 0$ and $d'_{31} \approx 0$. Therefore, it follows from the above considerations that the real component of d_{31} is the one that passes through zero and changes sign, somewhere between 65 °C and 75 °C, while the imaginary component d''_{31} remains nonzero throughout the investigated temperature range.

Finally, Fig.7 shows the temperature dependance of d'_{31} and d''_{31} with signs choosen according to analyses above. No anomalies were observed in the temperature behavior of complex ε_{33} and s_{11}, but their imaginary parts are necessary to obtain a good

AD-A194 957 PIEZOELECTRIC AND ELECTROSTRICTIVE MATERIALS FOR TRANSDUCER APPLICATIONS VOLUME 1(U) PENNSYLVANIA STATE UNIV UNIVERSITY PARK MATERIALS RESEARCH LA... 3/3

UNCLASSIFIED L E CROSS ET AL. MAR 88 N00014-82-K-0339 F/G 20/3 NL

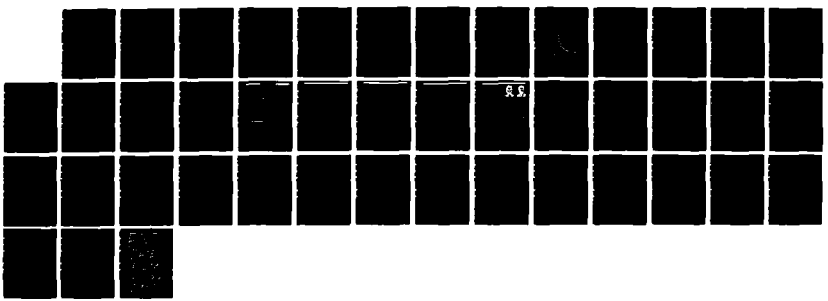

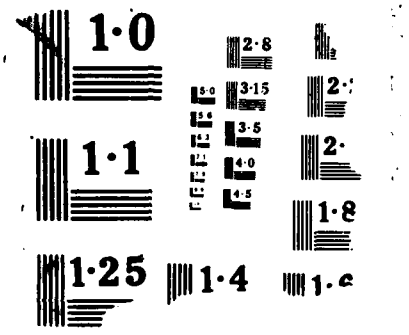
1·0
1·1
1·25
1·4
2·8
3·15
3·5
4·0
4·5
2·
1·8

fit to the resonance data.

The probable change of the sign of d_{31} and the simultaneous presence of the substantial imaginary component of the complex piezoelectric coefficient together with elastic and dielectric losses in these materials, suggest extrinsic contributions to the apparent d_{31} piezoelectric coefficient. Such contributions, if different in sign, could cancel each other giving zero d_{31} or change its sign with temperature. While the origins of the dielectric and elastic losses in the piezoelectric ceramics are well understood, more studies on possible mechanisms of the piezoelectric relaxation have been done only recently. It has been shown [8 - 15] that any defects in a piezoelectric material that are responsive both to the elastic and electric fields (such as certain point defects, 90° domains, second phase in the piezoelectric polymer materials etc.) are a source of piezoelectric relaxation through the coupling of the elastic and dielectric losses. Consequently, it is possible to define the complex material coefficients m^* [8]:

$$
\begin{aligned}
s^*_{11} &= s^{\infty}_{11} + \Delta s'_{11} - j s''_{11} \\
\varepsilon^*_{33} &= \varepsilon^{\infty}_{33} + \Delta \varepsilon'_{33} - j \varepsilon''_{33} \\
d^*_{31} &= d^{\infty}_{31} + \Delta d'_{31} - j d''_{31}
\end{aligned}
\qquad (3)
$$

where m^{∞} represents the value of a coefficient at frequencies far above the relaxation frequency and $\Delta m' - jm''$ is the relaxational contribution of the defects. Using the requirement that the power dissipation in a passive material must be positive, Holland [9] has shown that imaginary parts of diagonal elements of elastic compliance and dielectric permittivity matrices must be positive .There are no similar constraints on the sign of the imaginary part of the piezoelectric coefficients. However, certain relationships, such as $s''_{11}\varepsilon''_{33} \geq d''^2_{31}$, must be satisfied. Therefore, an ideal (a loss free) dielectric or elastic material will also be ideal in its piezoelectric properties. Using symmetry arguments, Nowick and Heller [10] have derived certain selection rules showing that

some but not all the piezoelectric coefficients can undergo the piezoelectric relaxation, depending both on the symmetry of defects and the symmetry of crystal. Furthermore, Arlt and Dederichs [11] have investigated the domain wall contribution to the d_{31} in ferroelectric ceramics assuming no other coupled elastic and electric mechanisms. For the perovskite type ceramics, they have shown this contribution to d_{31} to be negative. In some cases the piezoelectric relaxation can be described by a simple Debye type relaxation. Examples of this type of relaxation in a piezoelectric coefficient are found in $AgNa(NO_2)$ due to relaxational motion of NO_2^- molecules [12], in the epoxy-PZT composite due to d.c. conductivity in the epoxy phase [13], in the ferroelectric ceramics due to 90° domain wall motion [11] etc. In the multiphase materials, such as polymers, the mechanisms of the piezoelectric relaxation are , in general, much more complex [12,14].

Considering the discussion above, it is clear that the existence of the imaginary component of the piezoelectric coefficient indicates the presence of extrinsic contributions to the piezoelectricity in these materials, regardless of the actual mechanisms involved. Knowing that in the perovskite ferroelectric ceramics the intrinsic d_{31} is considered to be negative, the hypothesis of a change of sign of d_{31} with temperature due to a positive contribution, is particularly attractive. A possibility of a change of sign of piezoelectric coefficient with temperature has been demonstrated in organic materials [15] and single crystals such as $AgNa(NO_2)$ [12]. However, it is unknown to us that such piezoelectric behavior has ever been observed in ceramics or oxide single crystals. To resolve this question in the case of the materials investigated in this study it would be sufficient to determine the sign of d_{31} directly, for example by strain vs. electric field measurements, at two temperatures, above and below the temperature where resonance disappears. It should be mentioned here that Xue et al. attempted to measure a change of sign of d_{31} for Sm-modified lead titanate [3]. No change in sign was observed in the limited temperature range were k_p was small . This

could be explained by the fact that the measurements were performed at about 10 Hz of the applied electric field , which was far below the frequency of planar mode resonance at approximately 100 kHz . As we have shown above, modified lead titanate ceramics investigated in this study have significant piezoelectric imaginary component indicating possible piezoelectric relaxation, in which case low frequency properties could be very different from those at higher frequencies.

We point out that although our data strongly suggests that the apparent d_{31} measured at the resonance frequency changed its sign with temperature, it is necessary to perform additional experiments for a full interpretation of the observed phenomena .The mechanisms which lead to piezoelectric relaxation in ceramics are in general poorly understood . With more knowledge, it could be that alternative explanations will become possible.

In summary, the existence of significant piezoelectric imaginary component in modified lead titanate ceramics was shown, indicating extrinsic contributions to the piezoelectric d_{31} coefficient. Disappearance of the resonance for the planar coupling mode is attributed to a probable change in sign of the piezoelectric d_{31} coefficient.

ACKNOWLEDGEMENTS: This work was supported by the North American Philips Co. The authors are grateful to Dr. G. Arlt, Technische Hochschule Aachen, for his suggestions and discussions during his visit to MRL, Penn State University, in February 1986. The authors are also indebted to Dr. W. A. Smith and Dr. R. E. Newnham, for discussions and many useful ideas. The work by Mr. Paul Moses on computer interfacing is highly appreciated.

REFERENCES:

[1] H. Takeuchi, S. Jyomura, E. Yamamoto and Y. Ito, J.Acoust. Soc. Am. 72 (1982) 1114.

[2] Y. Yamashita, S. Yoshida and T. Takahashi, Japan. J. Appl. Phys. ,Suppl. 22-2 (1983) 40.

[3] W.R. Xue, J.N. Kim, S.J. Jang, L.E. Cross and R.E. Newnham, Japan. J. Appl.Phys.,Suppl. 24-2 (1985) 718.

[4] W .P. Mason, Phys.Rev. 74 (1948) 1134 .

[5] M. Onoe, H.F. Tiersten and A.H. Meitzler, J. Acoust. Soc. Am. 35 (1963) 36.

[6] D.A. Berlincourt, D.R. Curran and H. Jaffe, in: Physical Acoustics vol.1, part A, ed. W.P. Mason (Academic Press, New York, 1964) p.225-240.

[7] J.G. Smits, IEEE Transactions on Sonics and Ultrasonics 23 (1976) 393.

[8] G. Arlt, Ferroelectrics 40 (1982) 149.

[9] R. Holland, IEEE Transactions on Sonics and Ultrasonics 14 (1967) 18.

[10] A.S. Nowick and W.R. Heller, Adv. in Phys. 14 (1965) 101.

[11] G. Arlt and H. Dederichs, Ferroelectrics 29 (1980) 47.

[12] K. Hamano T. Yamaguchi, Ferroelectrics 42 (1982) 23.

[13] T. Furukawa and E. Fukada, Japan. J. Appl. Phys. 16 (1977) 453.

[14] R. Hayakawa and Y. Wada, in: Advances in Polymer Science, vol. 11 (Springer-Verlag, Heildelberg, 1973) p.1-55.

[15] E. Fukada, Ferroelectrics 60 (1984) 285.

FIGURE CAPTIONS:

Fig. 1. Planar and thickness coupling factors for Sm-modified lead titanate as a function of temperature.

Fig. 2. Planar and thickness coupling factors for Ca-modified lead titanate as a function of temperature.

Fig. 3. Susceptance,B, vs. conductance , G, loop for Sm-modified lead titanate at 90 °C. Dots represent experimental points. Curve (a) : theoretical fit using Smits' method. Curve (b):theoretical fit assuming $d''_{31}=0$.

Fig. 4. $d'_{31}d''_{31}$ product obtained by the iterative method showing that either d'_{31} or d''_{31}, but not both, changes sign at the temperature of minimum k_p for Sm-modified lead titanate.

Fig. 5. d''_{31}/d'_{31} ratio for Sm-modified lead titanate as a function of temperature

Fig. 6. Plots of conductance G vs. frequency near the temperature where k_p goes through minimum for Sm-modified lead titanate. Dots are experimental points and solid line is a fit to data. Scattering in the data is due to the resolution of the Impedance Analyzer.

Fig.7. Real and imaginary components of the piezoelectric d_{31} coefficient as a function of temperature for Sm-modified lead titanate.

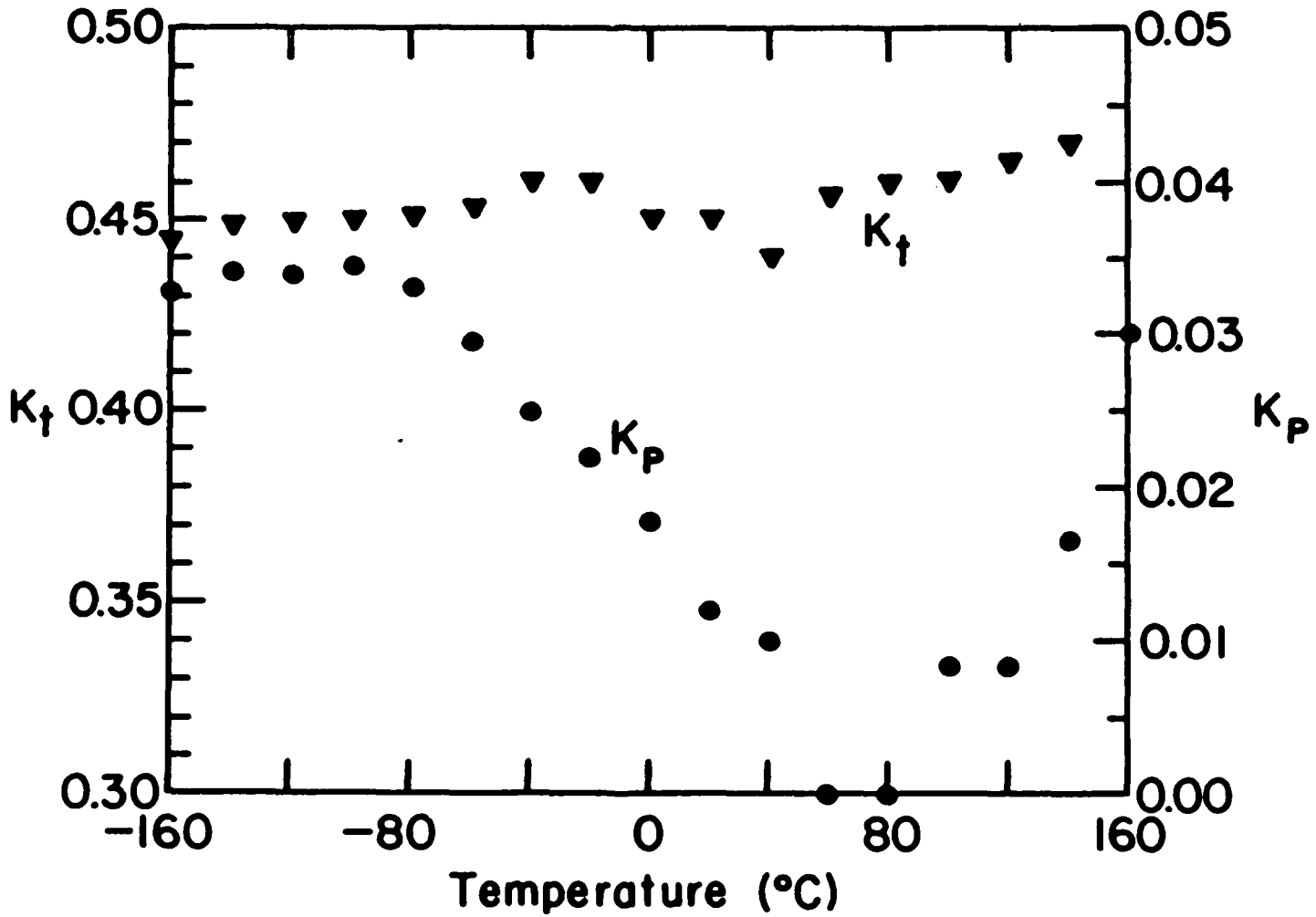
0.50
0.45
0.40
0.35
0.30
K_t
0.05
0.04
0.03
0.02
0.01
0.00
K_P
−160
−80
0
80
160
Temperature (°C)

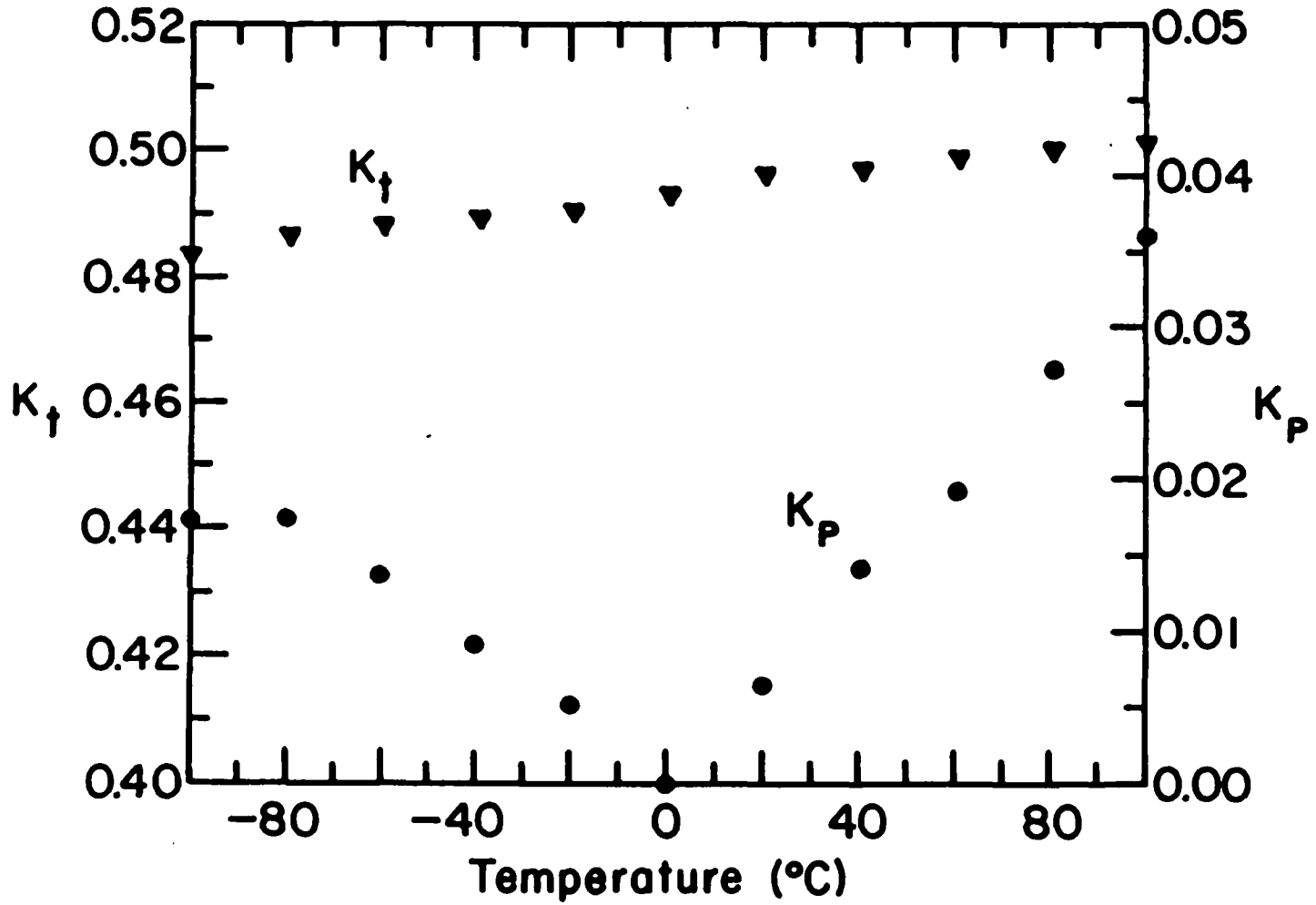
0.52
0.50
0.48
0.46
0.44
0.42
0.40
K_f
0.05
0.04
0.03
0.02
0.01
0.00
K_P
K_f
K_P
−80
−40
0
40
80
Temperature (°C)

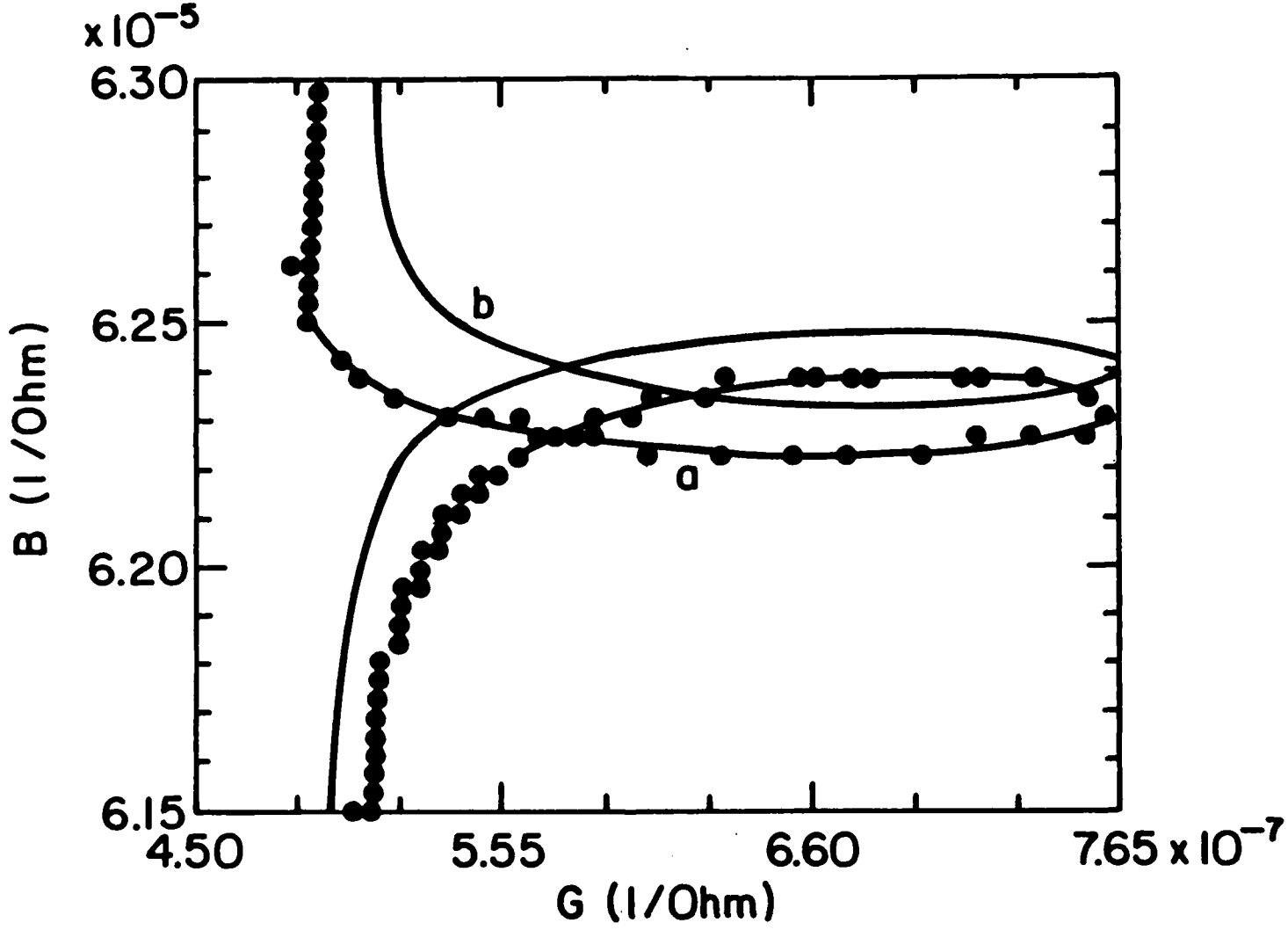
x10⁻⁵
6.30
6.25
6.20
6.15
B (1/Ohm)
b
a
4.50
5.55
6.60
7.65 x 10⁻⁷
G (1/Ohm)

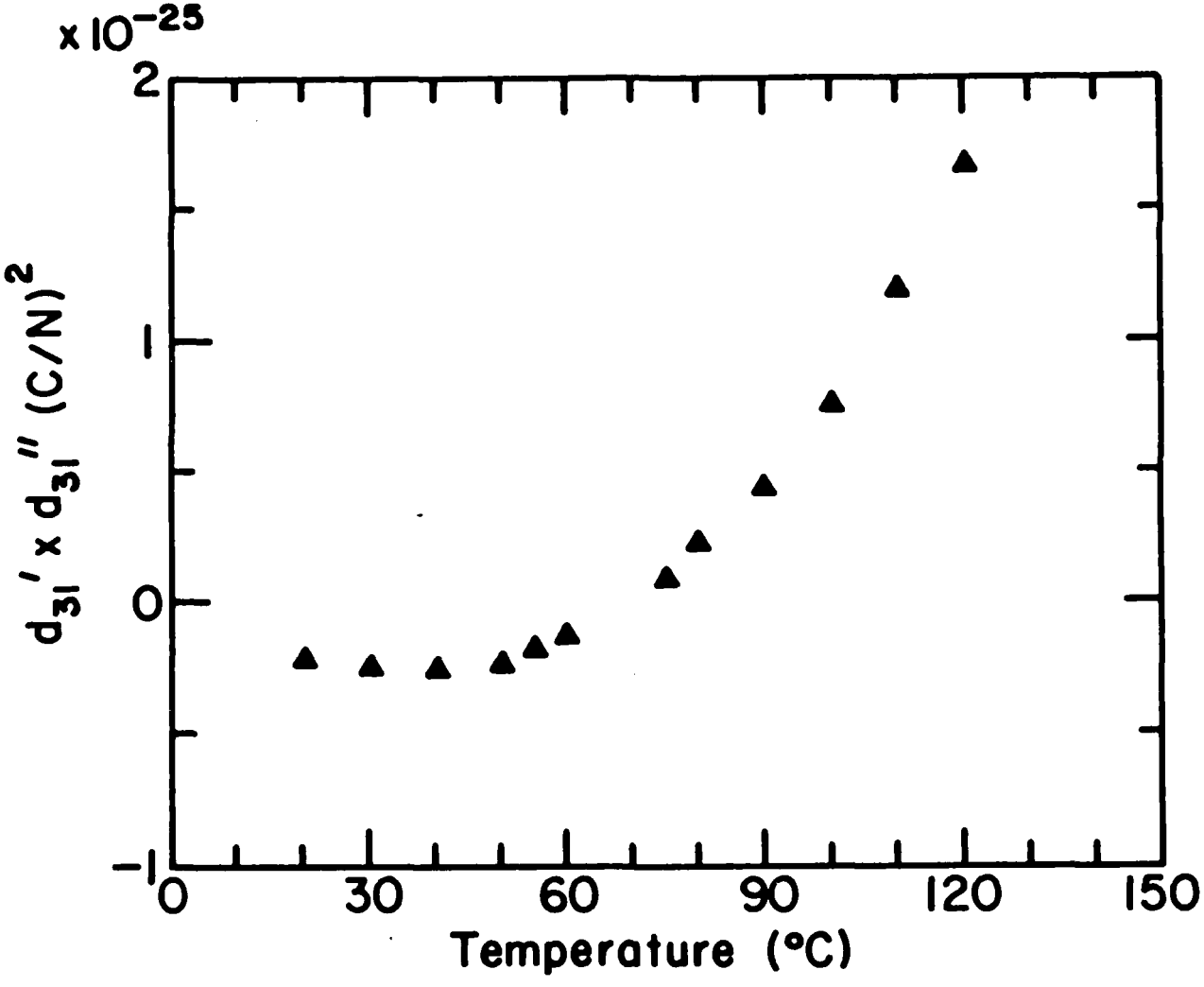
x 10⁻²⁵
2
1
0
−1
$d_{31}' \times d_{31}''$ (C/N)²
0
30
60
90
120
150
Temperature (°C)

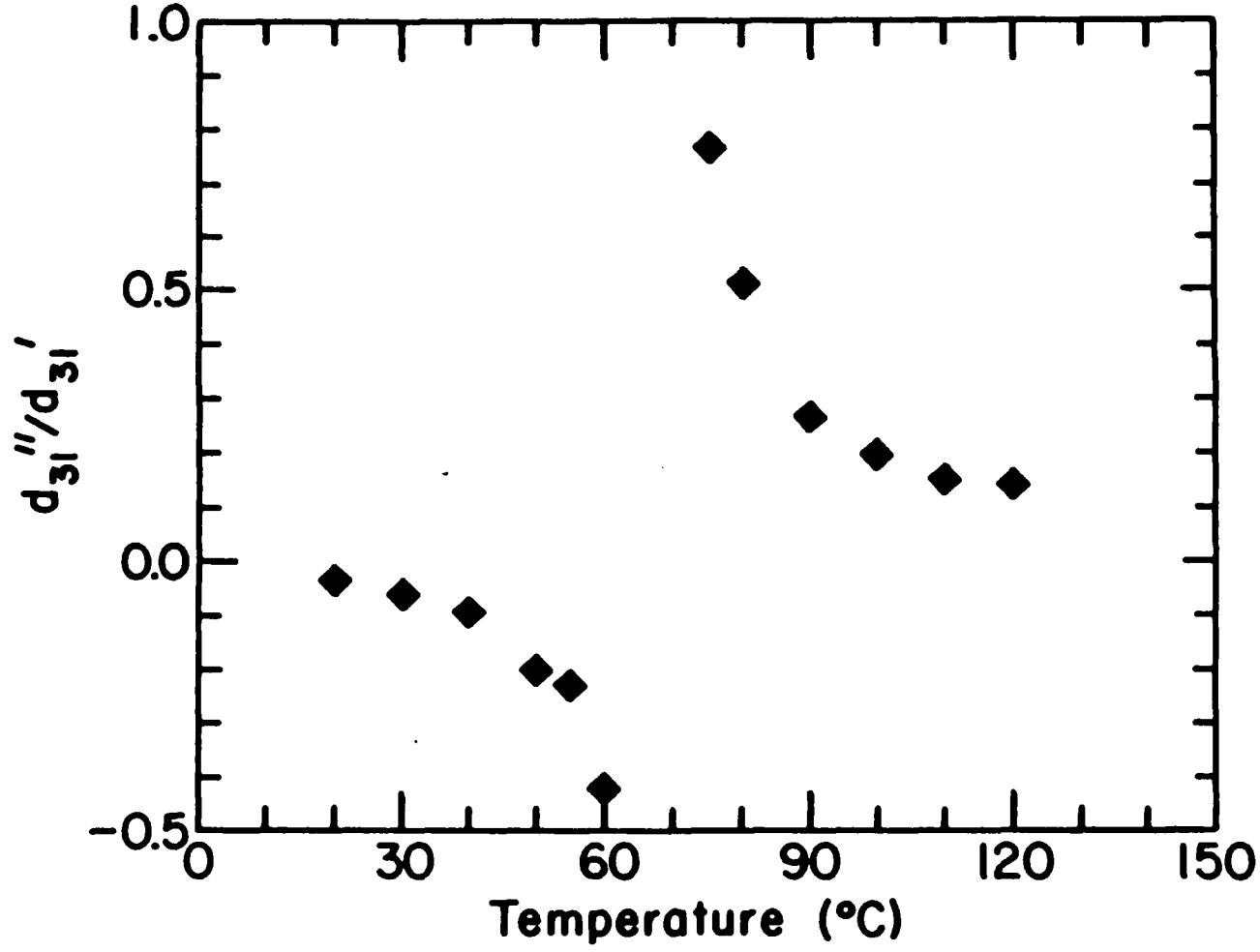
1.0
0.5
0.0
-0.5
0
30
60
90
120
150
d_{31}''/d_{31}'
Temperature (°C)

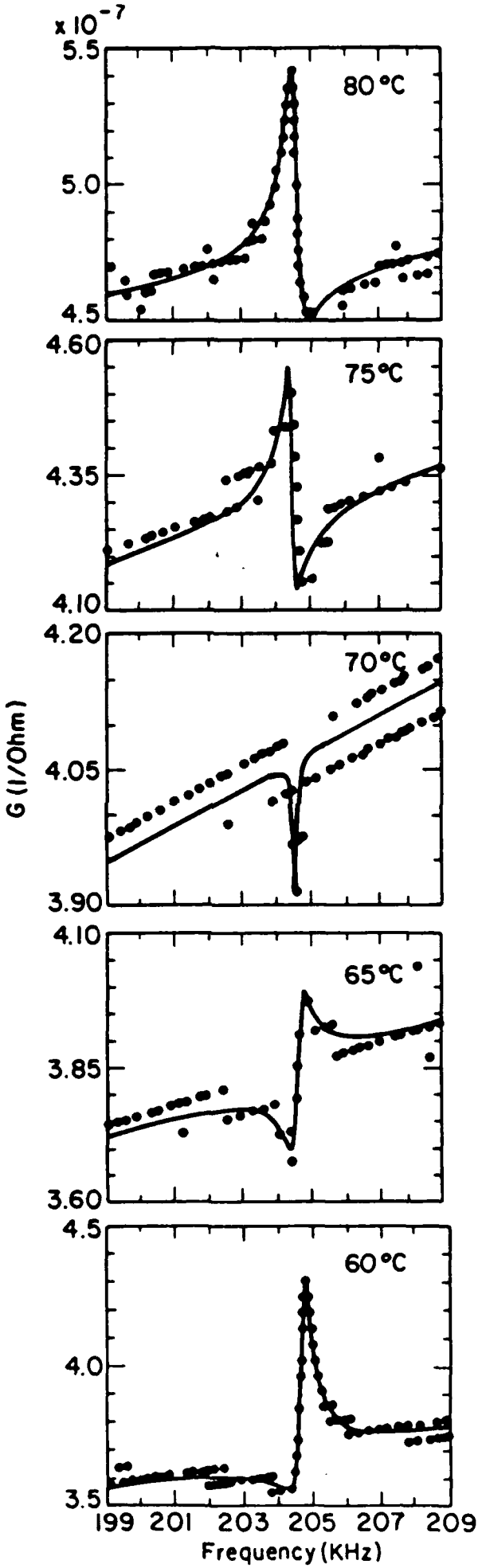
x 10⁻⁷
5.5
5.0
4.5
80 °C
4.60
4.35
4.10
75°C
4.20
4.05
3.90
70°C
4.10
3.85
3.60
65°C
4.5
4.0
3.5
60°C
G (1/Ohm)
199 201 203 205 207 209
Frequency (KHz)

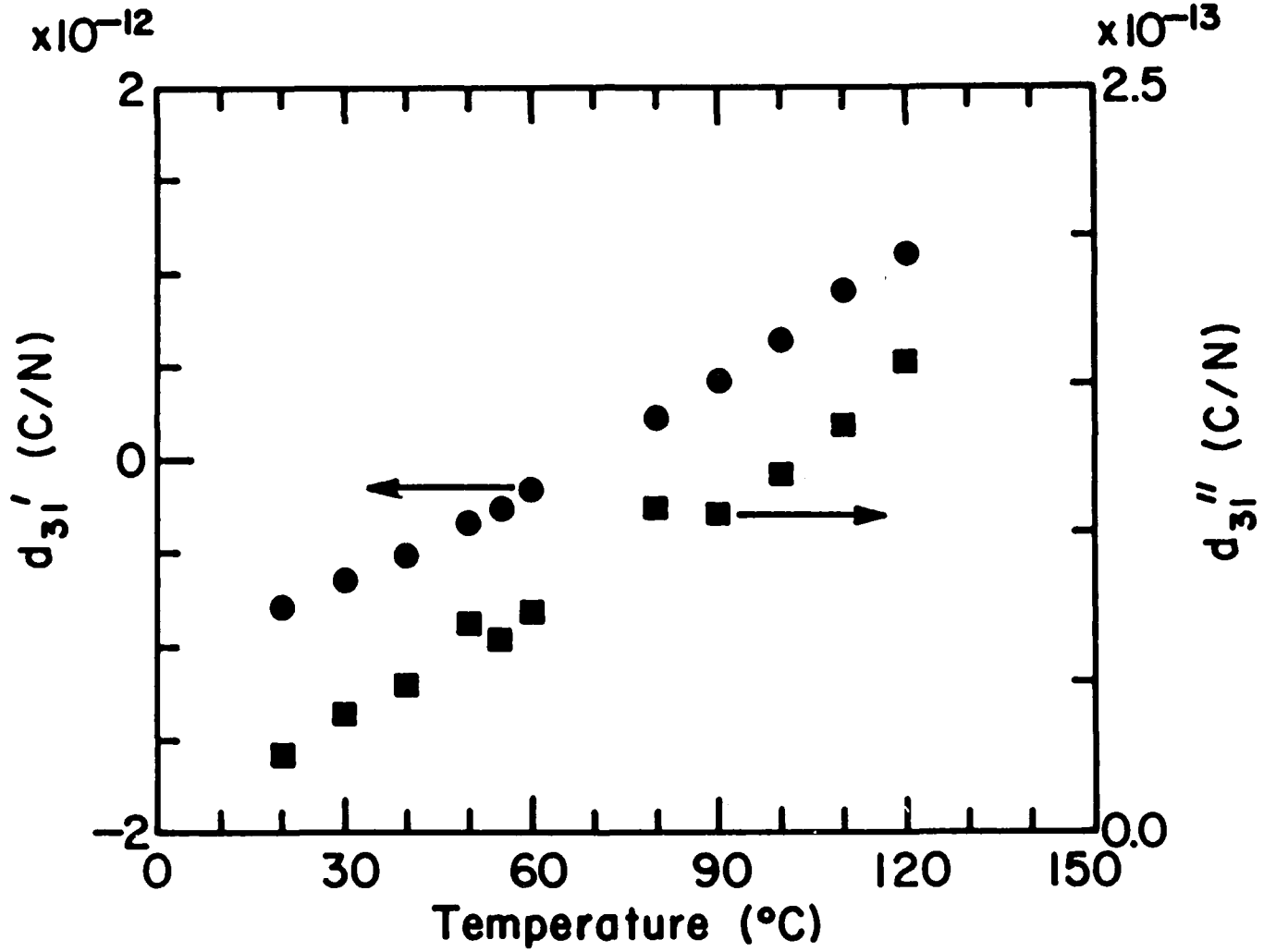
x10⁻¹²
x10⁻¹³
2
0
−2
2.5
0.0
d31′ (C/N)
d31″ (C/N)
0
30
60
90
120
150
Temperature (°C)

ELECTROMECHANICAL ANISOTROPY IN MODIFIED LEAD TITANATE CERAMICS

D.Damjanovic, T.R.Gururaja, S.J.Jang and L.E.Cross

Materials Research Laboratory
The Pennsylvania State University
University Park, PA 16802

ABSTRACT

Lead titanate ceramics modified by Sm and Ca were investigated as materials with exceptionally large electromechanical coupling anisotropy. Both ceramic materials exhibited a minimum of the planar coupling coefficient at certain temperatures whereas the thickness coupling coefficient was essentially a constant over the investigated temperature range. The dielectric, piezoelectric and elastic constants related to the planar coupling mode were all considered to be complex in order to correctly describe the behavior of the ceramics near the resonance. The minimum of the planar coupling coefficient is attributed to a probable change in sign of the d_{31} piezoelectric coefficient with temperature.

1. INTRODUCTION

The conventional piezoelectric ceramics, such as PZT ,with large electromechanical coupling coefficients are desired in many piezoelectric applications. In some cases, however, materials with more directional piezoelectric properties are preferred. In materials for ultrasonic transducer arrays, for example, it is essential to supress the coupling of the thickness to lateral modes, i.e. a small d_{31} and a large d_{33} are desired. Similarly, when a large hydrostatic piezoelectric coefficient, $d_h = d_{33} + 2d_{31}$, is required, it is again necessary to have a large piezoelectric anisotropy (large d_{33}/d_{31}) since the coefficients d_{33} and d_{31} are opposite in sign ($d_{33} > 0$, $d_{31} < 0$). Recently, lead titanate based ceramics have been reported with unusually large ratio of the thickness, k_T, to the planar ,k_p, coupling coefficients, and consequently a large ratio d_{33}/d_{31} [1,2]. The measurements of the electromechanical properties of samarium modified lead titanate showed this ratio to be temperature dependent with k_p becoming zero at certain temperatures [3]. As a possible reason for the high anisotropy in piezoelectric coefficients, the crystal lattice anisotropy [1], and the 90° domain rotation [2] were suggested. No extensive studies on this subject, however, have been yet reported. It was the objective of this work to investigate the electromechanical properties of Ca and Sm modified $PbTiO_3$ ceramics and possibly understand the mechanisms responsible for the anisotropic behavior. It is hoped that a better understanding of the electromechanical anisotropy in the modified lead titanates would provide us with methods of developing other materials with similar properties.

2. MATERIAL PREPARATION AND MEASUREMENTS

Two compositions of the modified lead titanate ceramic were selected for this study, namely $(Pb_{0.85}Sm_{0.10})(Ti_{0.98}Mn_{0.02})O_3$ and $(Pb_{0.76}Ca_{0.24})[(Co_{1/2}W_{1/2})_{0.04}Ti_{0.96}]O_3$. Both compositions have a tetragonal symmetry with the lattice parameters a = 3.902 Å, c = 4.072 Å and a = 3.896 Å, c = 4.041 Å, respectively. The ceramics were prepared by the conventional way from mixed oxide process. The samarium modified composition was calcined at 850 - 900 °C for 6 hours and then pressed disks were fired at 1230 °C for 3 hours. The calcium modified ceramics were calcined at 900 °C for 2 hours and sintered at 1130 °C for approximately 7 hours. The density of the fired ceramics was around 95 % of the theoretical. Electroded ceramics were poled with an electric field up to 60 kV/cm at 150 °C in silicon oil for 5 minutes. These poling conditions were necessary to obtain a saturation of the thickness coupling coefficient k_T to 45 - 50 %, the piezoelectric coefficient d_{33} to about 60 pC/N and the planar coupling coefficient k_p of less than 1 %. Thus, the ratio k_T/k_p was close to 50 at room temperature (Fig. 1). These poled ceramics in the form of thin disks or long thin bars were then used for measurements of the dielectric, elastic and piezoelectric properties of the materials. k_p was calculated from the measured frequencies of the series and parallel resonance frequency of a thin disk using the equation derived by Mason [4]. k_T was calculated from the ratio of the overtone frequency f_2 to the fundamental frequency f_1 of the thickness mode series resonance, f_2/f_1, using Table II in Onoe et al.'s paper [5]. The complex dielectric permittivity ε_{33}, the elastic compliance s_{11} and the piezoelectric coefficient d_{31} at the resonant frequency of the length extensional mode for a bar were calculated using Smits' method [6]. Vector impedance measurments for the above calculations were performed on an HP 4192A LF Impedance Analyzer interfaced with a computer.

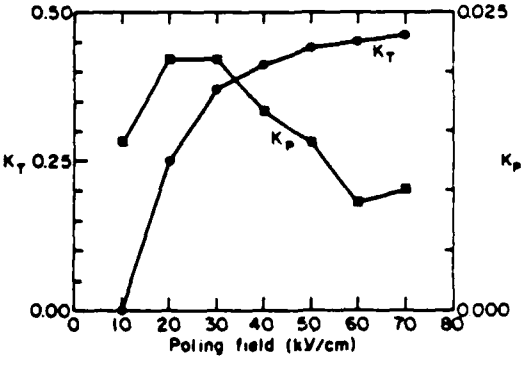

Fig. 1. Thickness, k_T, and planar,k_p, coupling coefficients as functions of poling field for Sm modified lead titanate.

Proc. ISAF '86, Bethlehem, PA. 1986. pp. 344-347

3. RESULTS AND DISCUSSION

The electromechanical coupling coefficients of the samarium and calcium modified lead titanates as a function of poling field exhibit an unusual behavior. The planar coupling factor increases initially and then decreases to a very small value with poling field above 50 kV/cm. However, the thickness coupling coefficient increases to approximately 50 % (Fig.1). As a possible explanation for the anisotropy, Yamashita et al. [2,7] suggested such behavior in calcium modified lead titanate to be caused by the reorentation of 90° domains. Indeed, they showed that a substantial increase in dimensions (up to 0.3 %) of ceramic samples occured as they were poled indicating 90° domain switching. The large stress that accompanies 90° domain switching was considered as a possible reason for the large anisotropy in coupling factors and the small value of the mechanical factor Q_m at poling fields at which k_p became vanishingly small. They also observed that specimens with lower resistivity showed a smaller planar coupling coefficient. Xue et al. showed, however, the k_p to be a strong function of temperature for samarium modified lead titanate [3], becoming zero only at certain temperatures

Fig. (2) and (3) show the thickness and planar coupling coefficients for materials investigated in this study as a function of temperature. Both materials exhibited a minimum in their planar coupling coefficient, reaching –4 % at the ends of the investigated temperature range while their thickness coupling coefficients remained approximately constant over the investigated temperatures. Describing the conversion of electric into elastic energy, and vice versa, the electromechanical coupling coefficients are always defined as positive values. Piezoelectric coefficients in general , however, may be either positive or negative. From the definition of the planar coupling coefficient [8]:

$$k_p = \frac{d_{31}}{(s_{11}^E \varepsilon_{33}^T)^{1/2}} \left(\frac{2}{1-\sigma^E}\right)^{1/2} = k_{31}\left(\frac{2}{1-\sigma^E}\right)^{1/2} \quad (1)$$

(where σ is Poisson's ratio) it is, therefore, seen immediately that resonance can disappear if d_{31} becomes zero , either by changing its sign or by going through zero as an extremum point. For the measurement of material coefficients in Eq.(1) we have used the method described by Smits[6]. This method allows us to calculate the complex material coefficients s_{11}, d_{31}, ε_{33} (i.e. the real parts and their losses) at the resonant frequency of the length extensional coupling mode of a bar. The method consists of measuring the admittance $Y = G + jB$ at three frequencies near the resonance and calculating, in an iterative way, the material coefficients defined as $m = m' - jm''$, using the Equation (2) [8]:

$$Y = j\frac{\omega w l}{t}\left(\varepsilon_{33}^T - \frac{d_{31}^2}{s_{11}^E}\right) + j\frac{2wd_{31}^2}{(\rho s_{11}^E)^{1/2} s_{11}^E t}\tan\frac{\omega l}{2}(\rho s_{11}^E)^{1/2} \quad (2)$$

which describes the resonant behavior of a bar (The notations have their usual meanings). These experiments demonstrated that imaginary components of all three material coefficients are necessary for a good fit to the resonance data, especially at temperatures where planar coupling mode becomes small (Fig. 4.). Furthermore, our data show that even when the resonant signal of admittance Y seems to disappear completely, a weak signal in the conductance G was still observed [9]. Our analysis [9] led to the conclusion that the real part of d_{31} changed its sign near the

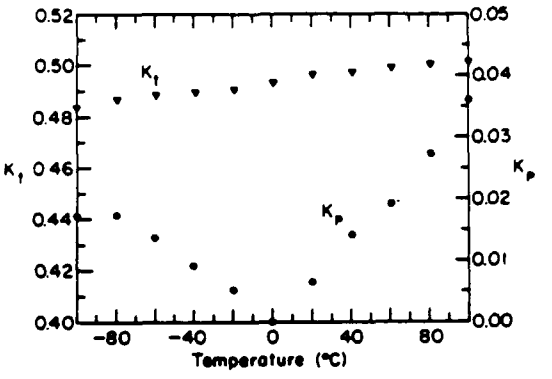

Fig. 2. Planar and thickness coupling coefficients as functions of temperature for Ca modified lead titanate.

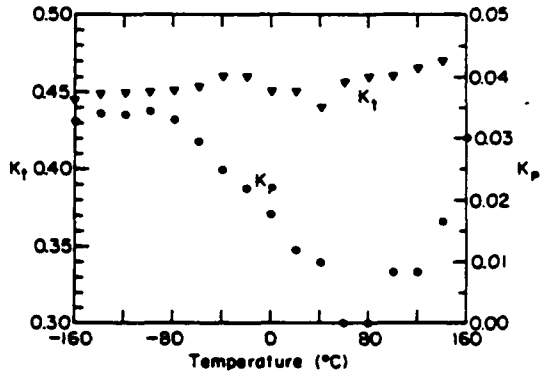

Fig. 3. Planar and thickness coupling coefficients as functions of temperature for Sm modified lead titanate.

temperature where k_p became small but its imaginary component remained nonzero (Fig. 5.). No anomalies were apparent in the behavior of the complex elastic and dielectric coefficients. However, their imaginary components are necessary for a good fit to the data. The mechanical quality Q_m was calculated as the ratio $s_{11}'/s_{11}'' \; (= f_m/2\Delta f)$ [6] of the real and imaginary parts of elastic compliance. Figure 6 shows that the mechanical quality of the samarium modified lead titanate ceramics remained high over the investigated temperatures suggesting that a small k_p is not necessarily accompanied by a decrease in the mechanical quality.

The presence of a significant imaginary component of the piezoelectric coefficient in these modified lead titanates suggests possible piezoelectric relaxation mechanisms which could lead to several contributions to the apparent d_{31}. Such contributions, if different in sign could cancel each other giving zero d_{31} or change its sign with temperature [9,10]. Our experience shows that the temperature where k_p goes through a minimum depends strongly on the poling conditions, the sintering schedule and other processing parameters. Not all of the samples showed the disappearance of the planar coupling mode at investigated temperatures (generally, -180 °C to +150 °C). All samples, however, showed a large

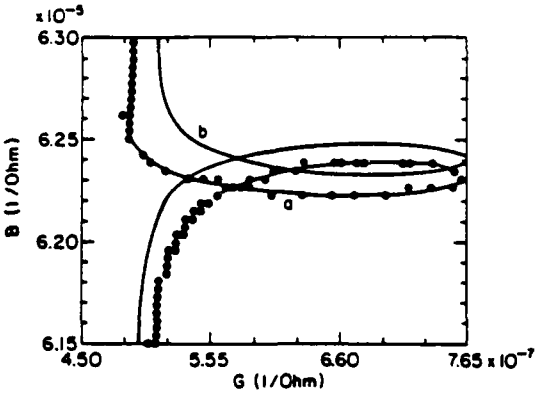

Fig. 4. Susceptance, B, vs. conductance, G, loop for Sm modified lead titanate, at 90 °C; dots represent experimental points.
a) Theoretical fit assuming a nonzero d_{31}" (Smit's method).
b) Theoretical fit assuming d_{31}"=0.

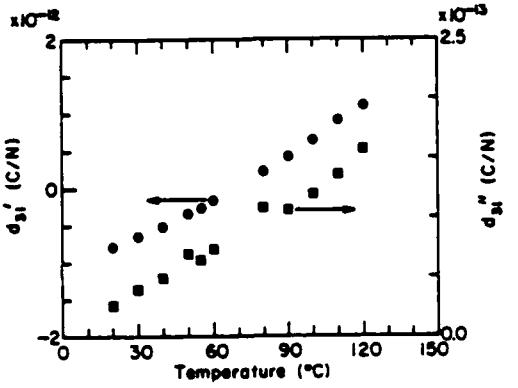

Fig. 5. Real, d_{31}', and imaginary, d_{31}", piezoelectric coefficients as functions of temperature for Sm modified lead titanate.

electromechanical anisotropy, i.e. a large k_T/k_P ratio. This suggests that there are probably two mechanisms responsible for the electromechanical anisotropy in these materials: one mechanism, possibly related to tetragonality, is responsible for the high piezoelectric anisotropy observed in these lead titanate based ceramics. The other mechanism, strongly dependent on processing conditions, seems to be responsible for the temperature dependence of k_P and the change of sign of d_{31}. This latter mechanism could be related to a piezoelectric relaxation through some kind of defects present in these ceramics [10].

It has been proposed that ceramics with high coercive fields, such as modified lead titanates, crack under high poling fields. Such cracks, if oriented parallel to the poling direction, could cause a large difference in the behavior of d_{31} and d_{33}. Measurements are being performed similar to those described above taking poling field as a parameter. Even at 10 kV/cm of applied field we have observed a minimum in the planar coupling coefficient and the disappearance of the resonance signal at low temperatures, appearing again as temperature was further decreased. Assuming that poling field of 10 kV/cm was not sufficient to produce microcracks in a sample, this

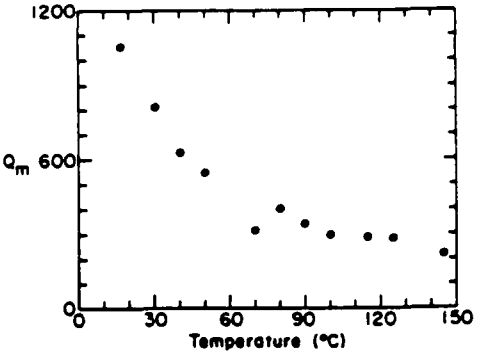

Fig. 6. Mechanical quality Q_m as a function of temperature for Sm modified lead titanate.

experiment shows that (although development of cracks with increased poling field is expected) the cracking of sample by applying poling field is not essential for the observed temperature behavior.

4. CONCLUSIONS

Similarities in the electromechanical coupling behavior between Ca and Sm modified lead titanate ceramics were demonstrated. The temperature behavior of the planar coupling mode is strongly dependent on poling and processing conditions. A zero planar coupling mode at certain temperatures is probably due to a change in the sign of the piezoelectric coefficient. A large electromechanical anisotropy was present in all the samples of the compositions used in this study, regardless of processing conditions. This indicates that more than one mechanism is responsible for the electromechanical coupling properties of these materials.

ACKNOWLEDGEMENTS

This work was supported by the North American Philips Co. The authors are grateful to Dr. G. Arlt, Technische Hochschule Aachen, for his suggestions and discussions during his visit to MRL, Penn State, in February 1986. The authors are also indebted to Dr. W.A. Smith and Dr. R.E. Newnham, for frequent discussions and many useful ideas. The work by Mr. Paul Moses on computer interfacing was highly appreciated.

REFERENCES:

[1] H. Takeuchi, S. Jyomura, E. Yamamoto and Y. Ito, J. Acoust. Soc. Am. 72 (1982) 1114.

[2] Y. Yamashita, S. Yoshida and T. Takahashi, Japan. J. Appl. Phys. 22 (1983) 40, Suppl.22-2.

[3] W.R . Xue, J.N. Kim, S.J. Jang, L.E. Cross and R.E. Newnham, Japan. J. Appl. Phys. 24 (1985) 718, Suppl. 24-2.

[4] W.P. Mason, Phys. Rev. 74 (1948) 1134.

[5] M. Onoe, H.F. Tierstein and A.H. Meitzler, J.Acoust. Soc. Am. 35 (1963) 36.

[6] J.G. Smits, IEEE Transactions SU 23 (1976) 393.

[7] Y. Yamashita, T. Takahashi and S. Yoshida, Ferroelectrics 54 (1984) 131.

[8] D.A. Berlincourt, D.R. Curran and H. Jaffe, in: Physical Acoustics vol. 1,part A, ed. W.P. Mason (Academic Press, New York, 1964) p.225-240.

[9] D. Damjanovic, T.R. Gururaja, S.J. Jang and L.E. Cross, to be published

[10] G. Arlt, Ferroelectrics 40 (1982) 149.

Am Ceram Soc Bull, 66 [4] 699-703 (1987)

Anisotropy in Piezoelectric Properties of Modified Lead Titanate Ceramics

DRAGAN DAMJANOVIC,* TURUVEKERE R. GURURAJA,* and LESLIE E. CROSS*

Pennsylvania State University, Materials Research Lab, University Park, PA 16802

Lead titanate ceramics modified with samarium and calcium exhibit large anisotropy in electromechanical coupling factors. The planar coupling factor in these materials shows a strong temperature dependence passing through a minimum near room temperature, whereas the thickness coupling factor remains practically constant. To explain this behavior, the material coefficients d_{31}, s^E_{11}, and ε^T_{33} characteristic for the planar coupling mode were investigated as a function of temperature (−180° to 100°C) for samples poled at different electric fields (10 to 90 kV/cm). All material coefficients must be considered as complex quantities to describe the piezoelectric resonance in these ceramics. A minimum in the planar coupling factor is explained by a change of sign of the piezoelectric coefficient, d_{31}. The temperature at which the planar coupling factor passes through a minimum depends on the processing conditions and poling field. Possible mechanisms to account for the observed behavior are discussed.

Conventional piezoelectric ceramics, such as lead zirconate titanate (PZT), with large electromechanical coupling coefficients are desired in many piezoelectric applications. In some cases, however, materials with more directional piezoelectric properties are preferred. In materials for ultrasonic transducer arrays, for example, it is essential to suppress the coupling of the thickness to lateral modes, i.e. a small d_{31} and a large d_{33} are desired. Similarly, when a large hydrostatic piezoelectric coefficient, $d_h = d_{33} + 2d_{31}$, is required, it is again necessary to have a large piezoelectric anisotropy (large d_{33}/d_{31}), since the coefficients d_{33} and d_{31} are opposite in sign ($d_{33} > 0$, $d_{31} < 0$).

Recently, lead titanate ($PbTiO_3$) ceramics modified by alkaline and rare earths have been reported to exhibit unusually large anisotropy in piezoelectric properties.[1,2] A zero planar coupling factor, k_p, has been observed in calcium and samarium-modified lead titanate ceramics.[3,4] At the same time, the thickness coupling factor, k_t is comparable to that of PZT ceramics. High frequency (7.5 MHz) linear array transducers fabricated using these modified lead titanate ceramics for ultrasonic diagnostic imaging and NDE applications have much better resolution than their PZT counterparts.[5,6]

It is the objective of the present work to investigate in detail the electromechanical properties of Ca- and Sm-modified $PbTiO_3$ ceramics and possibly understand the mechanisms responsible for the anisotropic behavior. Xue *et al.*[4] have examined the temperature behavior of the coupling factors for Sm-modified $PbTiO_3$. They have found that, with proper processing, practically zero k_p can be achieved near room temperature; k_t, however, remains approximately constant at 0.45 with temperature. As a possible reason for the large anisotropy in coupling factors, the crystal lattice anisotropy,[1] and the 90° domain rotation[2] were suggested. No extensive study on this subject, however, has yet been reported. It is hoped that a better understanding of the electromechanical anisotropy in the modified lead titanates would provide us with methods of developing other materials with similar properties.

Material Preparation

Two compositions of the modified lead titanate ceramic were selected for this study, namely $(Pb_{0.85}Sm_{0.10})(Ti_{0.98}Mn_{0.02})O_3$ and $(Pb_{0.76}Ca_{0.24})[(Co_{1/2}W_{1/2})_{0.04}Ti_{0.97}]O_3$. Both compositions have a tetragonal symmetry with the lattice parameters $a = 0.3902$, $c = 0.4072$ nm and $a = 0.3896$, $c = 0.4041$ nm, respectively. The ceramics were prepared by the conventional mixed-oxide process starting from analytical reagent (AR) grade oxides. The samarium-modified composition was calcined at 850° to 900°C for 6 h and then pressed disks were fired at 1230°C for 3 h. The calcium-modified ceramics were calcined at 900°C for 2 h and sintered at 1130°C for ≈7 h. The density of the fired ceramics was ≈95% of the theoretical. The sintered ceramics were shaped either in the form of thin disks (1.6 cm in diameter and <1 mm thick) or long thin bars (14 by 1.4 by 0.2 mm³) and gold electrodes were sputtered on the major faces. Samples were poled with an electric field up to 90 kV/cm at 150°C in silicon oil for 5 min.

Measurements

All the measurements were performed on the poled samples after 24 h of aging. The capacitance and dissipation factor was measured using an LCR bridge* for estimating the dielectric permittivity. The piezoelectric d_{33} coefficient was measured with a d_{33} meter.† The k_p value was calculated from the measured frequencies of series (f_s) and the parallel (f_p) resonance of a thin disk using the equation derived by Mason.[7] The k_t value was calculated from the ratio of the overtone frequency, f_2, to the fundamental frequency f_1, of the thickness mode series resonance, f_2/f_1, using Table II in the work of Onoe *et al.*[8] The complex dielectric permittivity ε^T_3, the elastic compliance s^E_{11}, and the piezoelectric coefficient d_{31} were calculated using the method developed by Smits.[9] In this method, admittance,

*Member, the American Ceramic Society
*4274A, Hewlett-Packard Co., Palo Alto, CA.
†CPDT 3300 Berlincourt d_{33} meter, Channel Products, Inc., Chagrin Falls, OH.

Received January 16, 1987; approved February 5, 1987.
Supported by the North American Philips Labs.

Peer Reviewed Contribution

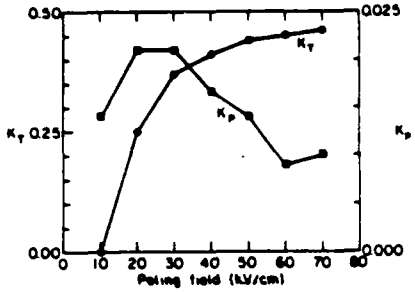

Fig. 1. Thickness (k_t) and planar (k_p) coupling factors as a function of poling field for Sm-modified $PbTiO_3$ ceramics.

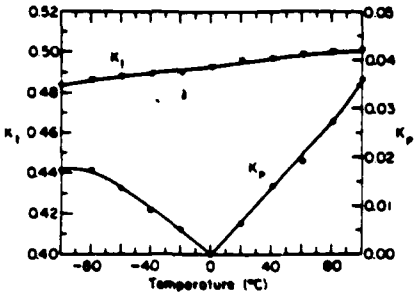

Fig. 2. Thickness and planar coupling factors as a function of temperature for Ca-modified $PbTiO_3$ ceramics poled at 60 kV/cm.

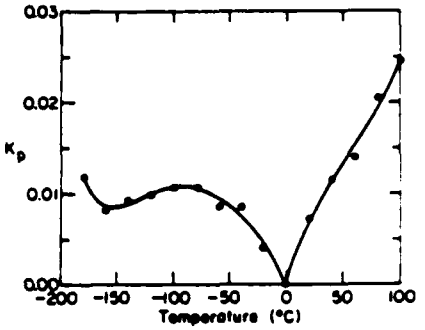

Fig. 3. Planar coupling factor as a function of temperature for Sm-modified $PbTiO_3$ ceramics poled at 60 kV/cm.

$Y=G+iB$, is measured at three frequencies near the resonant frequency of the length extensional mode of a bar, with electric field perpendicular to its length. Material coefficients s^E_{11}, d_{31}, and ϵ^T_{33}, defined as $m=m'-im''$, are then calculated in an iterative way using Eq. (1):

$$Y=i\frac{\omega wl}{t}(\epsilon^T_{33}-\frac{d^2_{31}}{s^E_{11}})+i\frac{2wd^2_{31}}{(\rho s^E_{11})^{1/2}s^E_{11}}\tan\frac{\omega l}{2}(\rho s^E_{11})^{1/2} \quad (1)$$

which describes the resonant behavior of a bar. In Eq. (1), l, t, and w are the length, thickness, and width of the bar, respectively, and ρ its density. The ω is the angular frequency. Vector impedance measurements for these calculations were performed using an LF impedance analyzer[4] interfaced with a computer.

Results and Discussion

The relative dielectric permittivities of both Sm- and Ca-modified $PbTiO_3$ ceramics were in the range 180 to 190 and the dielectric loss tangent was always <1% at room temperature. The electromechanical coupling factors of the Sm-modified $PbTiO_3$ at room temperature as a function of poling field are shown in Fig. 1. It is seen that k_t saturates at high poling fields whereas k_p first increases and then decreases, resulting in a k_t/k_p ratio of ≈50 at a poling field of 70 kV/cm. A similar behavior was observed in Ca-modified $PbTiO_3$ ceramics.

Figures 2 and 3 show k_t and k_p as a function of temperature for Ca- and Sm-modified $PbTiO_3$, respectively. In both materials, k_p goes through zero near room temperature. It then increases gradually below and above this temperature, reaching a maximum value of ≈0.04 at the end of the investigated temperature range. The value k_t, however, remained approximately constant over the investigated temperature range.[10]

We could attempt to explain the observed disappearance of the resonance for the planar coupling mode by considering the temperature dependence of relevant material constants. The k_p is related to the transverse coupling factor k_{31}, which in turn is related to material constants d_{31}, s^E_{11}, and ϵ^T_{33} as given by the Eq. (2):

$$k_p=k_{31}(\frac{2}{1-\sigma^E})^{1/2}=\frac{d_{31}}{(s^E_{11}\,\epsilon^T_{33})^{1/2}}(\frac{2}{1-\sigma^E})^{1/2} \quad (2)$$

where σ^E is the Poisson's ratio. The electromechanical coupling factors, describing the conversion of electric energy into elastic energy or vice versa, are always defined as positive values. Piezoelectric d constants, however, may be either positive or negative. It is, therefore, seen that the disappearance of k_p at a certain temperature is possible if d_{31} becomes zero, either by changing its sign or by going through zero at its extremum point. Real and imaginary parts of the material coefficients d_{31}, s^E_{11}, and ϵ^T_{33} in Eq. (2) were measured as a function of temperature using the Smits[9] iterative method to describe the temperature

[4]4192, Hewlett-Packard Co., Palo Alto, CA.
[4]4194A, Hewlett-Packard Co., Palo Alto, CA.

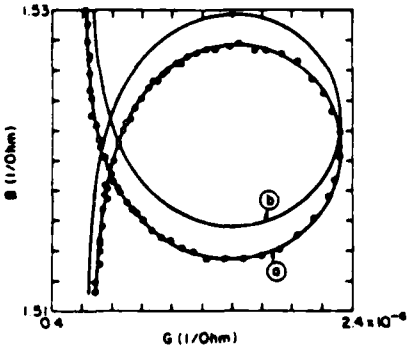

Fig. 4. Susceptance, B, versus conductance, G, loop for Sm-modified lead titanate at 60°C. Dots represent experimental points. Curve (a) is the theoretical fit using Smits' method and curve (b) is the theoretical fit assuming $d''_{31}=0$, sample poled at 90 kV/cm.

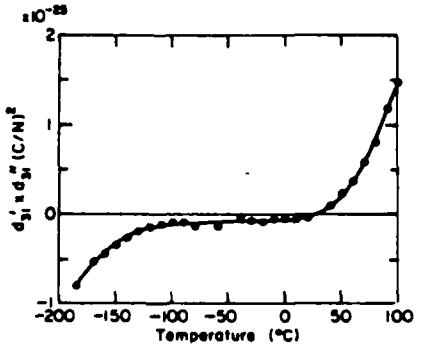

Fig. 5. The $d'_{31}d''_{31}$ product obtained by the iterative method showing that either d'_{31} or d''_{31}, but not both, changes sign at the temperature of minimum k_p for Sm-modified lead titanate, poled at 90 kV/cm.

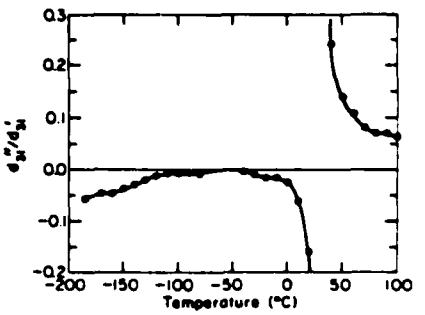

Fig. 6. The d''_{31}/d'_{31} ratio for Sm-modified lead titanate poled at 90 kV/cm as a function of temperature.

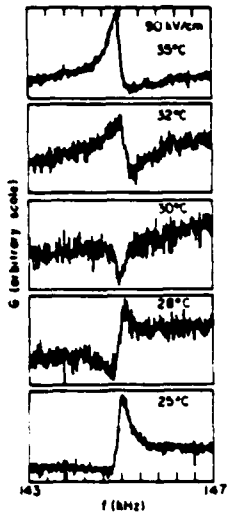

Fig. 7. Plots of conductance G vs frequency near the temperature where k_p goes through minimum for Sm-modified lead titanate, poled at 90 kV/cm.

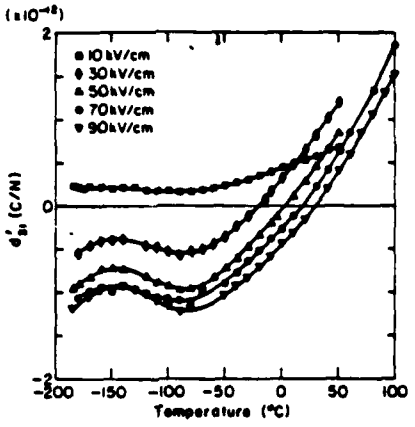

Fig. 8. Real part of the piezoelectric coefficient, d'_{31}, at different poling fields as a function of temperature for Sm-modified $PbTiO_3$ ceramics.

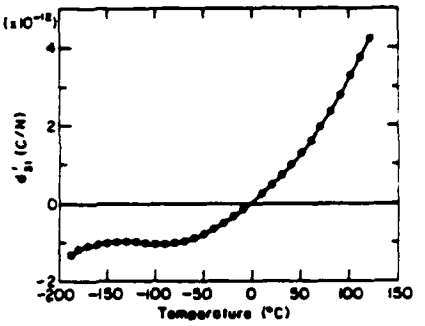

Fig. 9. Real part of the piezoelectric coefficient, d'_{31}, as a function of temperature for Ca-modified $PbTiO_3$ ceramics poled at 60 kV/cm.

dependence of k_p. The data and the discussion presented below show that, for an accurate description of the electromechanical behavior of modified $PbTiO_3$ ceramics, all material constants relevant for the planar coupling mode must be treated as complex.

A plot of susceptance B versus conductance G of the transverse mode resonance of a rectangular bar at a temperature close to where $k_p \approx 0$ is shown in Fig. 4 for Sm-modified lead titanate poled at 90 kV/cm. Experimental data are represented in full circles. Assuming all material coefficients to be complex, the theoretical fit to the experimental data, as in curve (a) in Fig. 4, was obtained by the Smits[9] iterative method. Curve (b) in Fig. 4 is obtained by taking the imaginary part of d_{31} equal to zero and using the real part for d_{31} and complex values for s^E_1 and ε^T_3 obtained by the iterative method. From Fig. 4 it is clear that the imaginary part of the piezoelectric constant is necessary for a good fit to the data, especially at temperatures where k_p becomes very small. The analysis was performed to exemplify the effect of the imaginary part of d_{31} on the resonance spectrum. The iterative method allows us to calculate only the product $d'_{31}d''_{31}$ and the difference $(d'_{31})^2-(d''_{31})^2$ from which we evaluate the real and imaginary components of d_{31}, without obtaining their signs independently. However, as is seen in Fig. 5, the product $d'_{31}d''_{31}$ changes its sign, indicating that either real or imaginary part of d_{31} changed sign. Analysis of our data, as explained below, suggests that it is more likely to be the real component of d_{31}. Figure 6 shows that the ratio $|d''_{31}/d'_{31}|$ increases rapidly as the temperature of zero k_p is approached. This result means that d''_{31} approaches zero at least as fast as d'_{31}, i.e. if d''_{31} assumes a value of zero and changes its sign, then d'_{31} should be zero, too. However, according to Eq. (1), if both real and imaginary components of d_{31} are equal to zero, a linear relation in G versus frequency is expected. Figure 7 shows the plots of conductance G versus frequency in the temperature range from 25° to 35°C, where k_p goes through zero for samples poled at 90 kV/cm. The conductance plots were obtained using an impedance/gain-phase analyzer.[1] From Fig. 7, it is clear that the signal at the resonance frequency never disappears completely. Moreover, the conductance versus frequency curve observed at 30°C implies that $d''_{31} \neq 0$ and $d'_{31} \approx 0$. Therefore, it follows from these considerations that the real component of d_{31} is the one that passes through zero and changes sign, somewhere between 28° and 32°C, whereas the imaginary component d''_{31} remains nonzero throughout the investigated temperature range.

The real part of d_{31} for Sm-modified lead titanate poled at electric fields varying from 10 to 90 kV/cm is plotted as a function of temperature in Fig. 8. As discussed, d'_{31} passes through zero by changing its sign. The temperature corresponding to the zero value of d'_{31} depends on the poling field, increasing from $-30°$ to $+30°$C as the poling field is increased from 30 to 90 kV/cm. For samples poled at 10 kV/cm, d'_{31} remains positive throughout the temperature range investigated. For Ca-modified $PbTiO_3$ ceramics, measurements were performed only on samples poled at 60 kV/cm. A temperature dependence of d'_{31} (Fig. 9) similar to that exhibited by the Sm-modified $PbTiO_3$ was observed. It is expected that the dependence of d'_{31} on the poling field will also be similar to that observed for Sm-modified $PbTiO_3$.

Examples of the temperature dependence of imaginary components of d_{31}, s^E_1, and ε^T_3 are given in Figs. 10, 11, and 12, respectively, for Sm-modified $PbTiO_3$ poled at 30 kV/cm. All

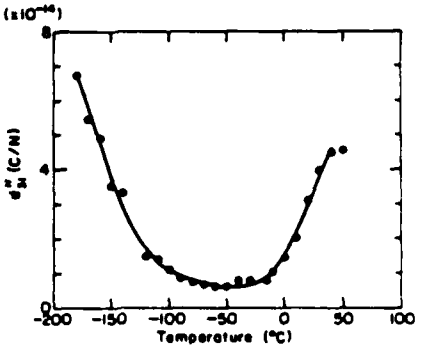

Fig. 10. Imaginary part of the piezoelectric coefficient, d''_{31}, as a function of temperature for Sm-modified $PbTiO_3$ ceramics poled at 30 kV/cm.

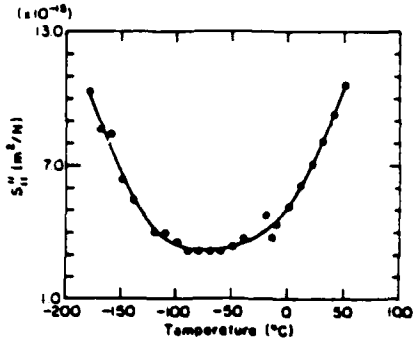

Fig. 11. Imaginary part of the elastic compliance, s_{11}'', as a function of temperature for Sm-modified $PbTiO_3$ ceramics poled at 30 kV/cm.

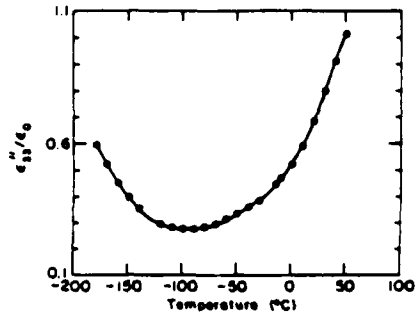

Fig. 12. Imaginary part of the relative dielectric permittivity, $\epsilon_{33}''/\epsilon_0$, as a function of temperature for Sm-modified $PbTiO_3$ ceramics poled at 30 kV/cm.

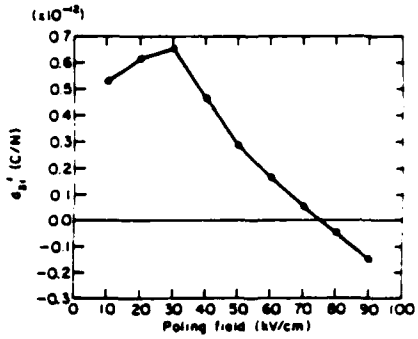

Fig. 13. Real part of the piezoelectric coefficient, d_{31}', as a function of poling field at 20°C for Sm-modified $PbTiO_3$ ceramics.

three imaginary coefficients show a similar temperature behavior, exhibiting a minimum in the temperature range of −50° to −100°C.

From this, we conclude that the zero value of k_p in modified lead titanate ceramics is caused by the change of sign of d_{31}' with temperature. Furthermore, from the plot of d_{31}' versus poling field at 20°C, as in Fig. 13, it is seen that the real part of d_{31} first increases, then decreases with poling field, passes through zero at ≈80kV/cm, and becomes negative near 90 kV/cm. Thus, dependence of k_p on poling field at room temperature, as shown in Fig. 1, is a result of the shift in the zero crossover point of d_{31}' with poling field. It is interesting to note that such a distinct anamalous behavior in k_p versus poling field cannot be observed at temperatures far from room temperature (Fig. 8).

The existence of appreciable imaginary components of the material coefficients and their similar temperature behavior (Figs. 10, 11, and 12) suggests the presence of common extrinsic contributions to the dielectric permittivity, elastic compliance, and piezoelectric coefficient.[11] In such a case, it is possible to express material coefficients in the following form:

$$s_{11} = s_{11}^{\infty} + \Delta s_{11}' - i s_{11}''$$
$$d_{31} = d_{31}^{\infty} + \Delta d_{31}' - i d_{31}''$$
$$\epsilon_{33} = \epsilon_{33}^{\infty} + \Delta \epsilon_{33}' - i \epsilon_{33}'' \qquad (3)$$

where m^{∞} represents the value of a coefficient at frequencies far above the relaxation frequencies and $\Delta m' - i m''$ is due to the relaxational extrinsic contributions.[11]

In the case of ceramic materials, the m^{∞} terms in Eq. (3) are average values of the coefficients, dependent on the level of polarization and the corresponding single-crystal values.[12] Like $BaTiO_3$, lead titanate is a perovskite-type ferroelectric belonging to the tetragonal 4mm point group. However, unlike $BaTiO_3$, lead titanate does not undergo low temperature phase transitions. This behavior is possibly the reason the dielectric permittivity in lead titanate exhibits a low anisotropy as opposed to the high anisotropy in dielectric permittivity of $BaTiO_3$.[13] Turik *et al.*[11] have shown by averaging the single-crystal properties that, in modified lead titanate ceramics, lack of anisotropy in dielectric permittivity results in a large anisotropy of the intrinsic piezoelectric coefficients, with a small value of d_{31} and a relatively large d_{33}.

It was demonstrated in this report that in modified lead titanate ceramics there are extrinsic contributions to the material coefficients. It is then possible that at certain temperatures such contributions to d_{31}, if different in sign from the intrinsic $d_{\overline{31}}$ of the ceramic, cancel with the small value of $d_{\overline{31}}$, giving an apparent d_{31}' of zero. When the extrinsic contributions are larger than the intrinsic value of $d_{\overline{31}}$, a change in the sign of d_{31}' is observed. Such a possibility has been demonstrated in piezoelectric polymers[14] and single crystals.[15]

Only a few studies on piezoelectric relaxation have been done so far in ceramic materials.[16,17] Arlt *et al.*[16] have shown that one such relaxational contribution to the piezoelectric coefficients in PZT ceramics is caused by 90° domain wall motion. The temperature dependence of the imaginary components of the material coefficients, as shown in Figs. 10, 11, and 12, suggests that there are at least two different relaxational mechanisms operating in the modified lead titanate ceramics examined in this study, one mechanism dominant at lower temperatures and the other at higher temperatures. The high-temperature mechanism is apparently responsible for the sign change of d_{31}', since d_{31}' changes its sign as the contribution of this high-temperature mechanism becomes larger.

Following this approach it is possible to qualitatively explain the dependence of the piezoelectric coefficient d_{31}' on the poling field in modified lead titanate ceramics. When the poling field is low, the average intrinsic $d_{\overline{31}}$ for the ceramics is small compared to extrinsic contributions, $\Delta d_{31}'$, and the apparent d_{31}' changes its sign at lower temperatures. As the poling field is increased, $d_{\overline{31}}$ becomes large compared to the extrinsic part, $\Delta d_{31}'$, and the apparent d_{31}' changes sign at higher temperatures. At 10 kV/cm, the average $d_{\overline{31}}$ for the ceramics is small compared to the extrinsic contributions over the whole temperature range investigated and the apparent d_{31}' remains the same in sign.

The choice of sign for d_{31}' and d_{31}'', is represented in Figs. 8, 9, and 10, is justified in the following way. Intrinsic $d_{\overline{31}}$ for ceramics is assumed to be negative; d_{31}' could become zero and then positive only if the extrinsic contributions represented by $\Delta d_{31}'$ are positive. Moreover, near absolute zero, the extrinsic contributions to the material coefficients should be frozen-in, and only the intrinsic contribution to d_{31} will be present. Since there is no experimental evidence that, below −180°C, d_{31}' for the modified lead titanate ceramics investigated in this work changes sign once again, the only choice for the signs of d_{31}' and d_{31}'' are that shown in Figs. 8, 9, and 10. However, it is necessary to determine the sign of d_{31} directly, for example by strain versus field measurements over a wide range of temperature, to confirm the proposed choice.

Thus, in modified lead titanates, we have observed that the temperature behavior of the planar coupling coefficient is dependent on poling conditions and processing parameters, such as the sintering schedule. Some of the samples tested did not show the disappearance of the planar coupling factor within the temperature range investigated (generally, −180° to +150°C).

All samples, however, showed a large electromechanical anisotropy with a k_t/k_p ratio of at least 15 at room temperature. This behavior supports the assumption that there are at least two mechanisms responsible for the observed behavior in modified $PbTiO_3$ ceramics. The first mechanism is related to the anisotropy in piezoelectric coefficients, accounted for by the intrinsic properties of the ceramics such as large tetragonality[1] and low anisotropy in the dielectric permittivity.[13] It has been shown that averaging of single-crystal values in $PbTiO_3$ leads to a large anisotropy in piezoelectric properties.[13] The second mechanism, responsible for the temperature dependence of k_p, may arise from the extrinsic contributions to d_{31}, the origin of which is not presently clear. These extrinsic contributions are common for the three material coefficients, as shown by a similar temperature behavior of their imaginary components. Possible extrinsic contributions include: domain wall motion, electronic and ionic defects, and microstructure-related effects.[10] Clearly, more experiments are required before these extrinsic mechanisms can be identified.

Conclusions

Lead titanate ceramics modified with samarium and calcium show similar temperature dependencies in coupling factors and piezoelectric coefficients. The zero value of the planar coupling factor is caused by a change in sign of the piezoelectric d_{31} coefficient with temperature. Significant imaginary components of the dielectric permittivity, elastic compliance, and piezoelectric coefficient indicate the presence of extrinsic contributions to the material coefficients. These extrinsic contributions seem to be responsible for the change in sign of d_{31}. Another mechanism, possibly related to the structure of these materials is believed to be responsible for the high anisotropy in the piezoelectric coefficients.

Acknowledgments

The authors are grateful to Dr. G. Arlt for his suggestions and discussions during his visit to MRL, Pennsylvania State University, in February 1986. The authors are also indebted to Dr. W. A. Smith and Dr. R. E. Newnham, for frequent discussions and many useful ideas. The work by Mr. Paul Moses on computer interfacing is highly appreciated.

References

[1] H. Takeuchi, S. Jyomura, E. Yamamoto, and Y. Ito, "Electromechanical Properties of (Pb,Ln)(Ti,Mn)O_3 Ceramics (Ln = rare earths)," *J. Acoust. Soc. Am.*, 72 [4] 1114–20 (1982).

[2] Y. Yamashita, K. Yokoyama, H. Honda, and T. Takahashi, "(Pb,Ca)[($Co_{1/2}$ $W_{1/2}$)$_x$Ti]O_3 Piezoelectric Ceramics and Their Applications," *Jpn. J. Appl. Phys.*, 20 [supp. 20–4] 183–87 (1981).

[3] Y. Yamashita, T. Takahashi, and S. Yoshida, "Low Q_m Modified Lead-Calcium Titanate Ceramic," *Ferroelectrics*, 54, 131–34 (1984).

[4] W. R. Xue, J. N. Kim, S. J. Jang, L. E. Cross, and R. E. Newnham, "Temperature Behavior of Dielectric and Electromechanical Coupling Properties of Samarium Modified Lead Titanate Ceramics," *Jpn. J. Appl. Phys.*, 24 [supp. 24–2] 718–20 (1985).

[5] H. Takeuchi, S. Jyomura, Y. Ishikawa, and E. Yamamoto, "A 7.5 MHz Linear Array Ultrasonic Probe Using Modified $PbTiO_3$ Ceramics"; pp. 849–53 in Proceedings of the IEEE Ultrasonics Symposium, San Diego, CA. Institute of Electrical and Electronics Engineers, New York, 1982.

[6] H. Honda, Y. Yamashita, and K. Uchida, "Array Transducer Using New Modified $PbTiO_3$ Ceramics", pp. 845–49 in Ref. 5.

[7] W. P. Mason, "Electrostrictive Effects in Barium Titanate Ceramics," *Phys. Rev.* 41 [A] 1134–47 (1948).

[8] M. Onoe, H. F. Tiersten, and A. H. Meitzler, "Shift in the Location of Resonant Frequencies Caused by Large Electromechanical Coupling in Thickness-Mode Resonators," *J. Acoust. Soc. Am.*, 36 [1] 36–42 (1963).

[9] J. Smits, "Iterative Method for Accurate Determination of the Real and Imaginary Parts of the Materials Coefficients of Piezoelectric Ceramics," *IEEE Trans. Sonics Ultrason.*, SU-23 [6] 393–402 (1976).

[10] D. Damjanovic, T. R. Gururaja, S. J. Jang, and L. E. Cross, "Temperature Behavior of the Complex Piezoelectric d_{31} Coefficient in Modified Lead Titanate Ceramics," *Mater. Lett.*, 4 [10] 414–19 (1986).

[11] G. Arlt, "Piezoelectric Relaxation," Ferroelectrics, 40, 149–57 (1982).

[12] A. G. Luchaninov, A. V. Shil'Nikov, and L. A. Shuvalov, "On the Piezoelectric Effect in Acentric Ferroelectric Ceramics with Zero Polarization," *Ferroelectrics*, 41, 181–87 (1982).

[13] A. V. Turik, E. G. Fesenko, V. G. Gavrilyachenko, and G. I. Khasabova, "Anisotropy of the Dielectric and Piezoelectric Properties of Lead Titanate," *Sov. Phys.*, 19 [5] 677–78 (1975).

[14] E. Fukuda, "Piezoelectricity of Natural Biomaterials," *Ferroelectrics*, 60, 285–96 (1984).

[15] K. Hamano and T. Yamaguchi, "Piezoelectric Relaxation in Ferroelectrics and Polymers," *Ferroelectrics*, 42, 23–33 (1982).

[16] G. Arlt and D. Dederichs, "Complex Elastic Dielectric, and Piezoelectric Constants by Domain Wall Damping in Ferroelectric Ceramics," *Ferroelectrics* 29, 47–50 (1980).

[17] J. G. Smits, "High Accuracy Determination of Real and Imaginary Parts of Elastic, Piezoelectric and Dielectric Constants of Ferroelectric PLZT (11/55/45) Ceramics with Iterative Method," *Ferroelectrics*, 64, 275–91 (1985). ■

Dragan Damjanovic

Turuvekere R. Gururaja

Dragan Damjanovic is a graduate student in ceramic science at Pennsylvania State University, University Park, PA. He is currently working on his Ph.D. thesis on piezoelectric properties of modified lead titanate ceramics. He earned a B.Sc. degree in Physics from the University of Serajevo, Yugoslavia, in 1980.

Turuvekere R. Gururaja is a research associate with the Materials Research Lab, Pennsylvania State University, University Park, PA. He received his B.Sc. and M.Sc. in physics from the University of Mysore, India, in 1974 and 1976, respectively. He earned his M.Tech. in materials science from the Indian Institute of Technology, Kanpur, India, in 1978 and Ph.D. in solid-state science from Pennsylvania State University in 1984.

Leslie E. Cross is professor of electrical engineering and director of the Materials Research Lab at Pennsylvania State University. His photograph and biographical sketch appear on page 676.

Low-temperature dielectric properties of $SrTiO_3$ glass-ceramics

S. L. Swartz,[a] A. S. Bhalla, and L. E. Cross
Materials Research Laboratory, The Pennsylvania State University, University Park, Pennsylvania 16802
C. F. Clark and W. N. Lawless
CeramPhysics, Inc., Westerville, Ohio 43081

(Received 6 December 1985; accepted for publication 16 May 1986)

The low-temperature dielectric properties of strontium titanate aluminosilicate glass-ceramics, in which perovskite $SrTiO_3$ is the primary crystalline phase, have been investigated. These glass-ceramics exhibited dielectric constant peaks at temperatures below 100 K; the magnitude of these peaks, along with their frequency and temperature dependencies, were strongly dependent on the crystallization conditions. In heavily crystallized glass-ceramics, two low-temperature, relaxation-type loss mechanisms were identified, at temperature ranges near 50 and 100 K. The magnitude of the dielectric loss peak increased with increasing frequency for the lower temperature (50 K) mechanism and the magnitude of the loss peak decreased with increasing frequency for the higher temperature (100 K) mechanism. Arrhenius activation energies were calculated to be 0.054 and 0.17 eV for the lower and higher temperature loss mechanisms, respectively. The higher temperature loss mechanism was further analyzed by the Cole–Cole method, and a relaxation strength of 41 was calculated. It was proposed that the dielectric constant and loss peaks were related to ferroic phenomena occurring in the $SrTiO_3$ phase, caused by interactions of the $SrTiO_3$ with the glass-ceramic matrix.

I. INTRODUCTION

Glass-ceramics with ferroelectric perovskite phases, such as $BaTiO_3$,[1,2] $PbTiO_3$,[3,4] and $NaNbO_3$,[5] have been investigated for several dielectric and electro-optic applications. These materials have interesting dielectric properties, resulting from the combination of the high-permittivity ferroelectric crystallites and the low-permittivity glassy matrix. The dielectric properties of glass-ceramics based on perovskite $SrTiO_3$ have also proven to be quite interesting, especially at low temperatures, due to the low-temperature ferroic behavior of $SrTiO_3$.[6]

Strontium titanate glass-ceramics have been utilized for several years as cryogenic capacitive temperature sensors.[7] Their usefulness is based on a peak in the dielectric constant at a temperature near 77 K. However, the nature of this dielectric constant peak has not been clearly defined. Lawless[6] attributed the dielectric constant peaks to an antiferroelectric transition in the $SrTiO_3$ phase, while Siegwarth[8] suggested that the peaks were caused by the relaxation of electret (defect-dipole) states in the $SrTiO_3$. The above researchers only studied a single glass-ceramic sample (the capacitance thermometer), and definitive dielectric loss data were not presented in support of their proposed mechanisms.

The crystallization and dielectric properties of strontium titanate aluminosilicate glass-ceramics, similar to those used in the above studies, have recently been investigated.[9] The crystallization and microstructure of this glass-ceramic system have been reported,[10] along with dielectric properties of glass-ceramics, given a wide range of crystallization conditions, over the temperature range -170 to 200 °C and frequency range 10 kHz–1 MHz.[11] The purpose of this paper is to report some interesting low-temperature dielectric data obtained on these glass-ceramics. Special attention was given to the low-temperature dielectric loss behavior and to gaining a better understanding of possible mechanisms responsible for the dielectric constant peaks.

II. GLASS-CERAMIC PREPARATION AND CHARACTERIZATION

Glass-ceramics were derived from a glass with a nominal composition consisting of 65 wt. % $SrTiO_3$, 23 wt. % SiO_2, and 12 wt. % Al_2O_3. The glass was prepared by melting in platinum crucibles in air at 1650 °C for 2 h, and annealing at 760 °C. Chemical analysis of the glass confirmed that the actual glass composition was close to that which was batched, and no significant amounts of any impurities were detected. Samples for crystallization studies and subsequent dielectric measurements were disks, 9 mm diam and 1 mm thick. The glass disks were heat treated at 700 °C for 100 h prior to crystallization to reoxidize any residual Ti^{3+} which formed during melting. Crystallization conditions employed were isothermal; the glass disks were immersed into a furnace at temperatures between 800 and 1100 °C and removed after times ranging from 15 min to 64 h.

The exact details of the crystalline phase makeup and microstructure of these glass-ceramics given the various crystallization treatments were reported in Refs. 9 and 10. Briefly, perovskite $SrTiO_3$ was the primary crystalline phase of the glass-ceramics, appearing as well-dispersed crystallites. The $SrTiO_3$ crystallite size was less than 100 nm in glass-ceramics crystallized at 1000 °C and below, and slightly less than 1 μm in glass-ceramics crystallized at 1100 °C. Secondary crystalline phases included hexacelsian $SrAl_2Si_2O_8$, which occurred in glass-ceramics crystallized at temperatures of 900 °C and above. At 1100 °C, hexacelsian $SrAl_2Si_2O_8$ appeared in samples crystallized for the shorter times, and transformed to the anorthite polymorph with cry-

[a] Present address: Battelle Columbus Laboratories, 505 King Avenue, Columbus, Ohio 43201.

 0021-8979/86/182069-12$02.40

stallization time; this transformation was complete after 8 h. Also at 1100 °C, anatase TiO_2 appeared, along with a trace of rutile. With crystallization times of greater than 4 h, the titania phase had developed into large acicular crystals of up to 80 μm in length. As will be shown later, the presence of the two matrix phases (hexacelsian and anorthite $SrAl_2Si_2O_8$), and the large acicular anatase crystals, were very important to the dielectric properties.

III. DIELECTRIC PROPERTIES

A. Procedures

Three-terminal dielectric measurements were carried out over the temperature range 10–150 K with a Cryosystems model CT-310 Cryotran system which included a Lake Shore Cryotronics Model DRC-80C temperature controller. Temperature measurements were made with a silicon diode and were accurate to within one Kelvin. Measurements were made over the frequency range of 10 kHz–1 MHz with a Hewlett-Packard model HP-4275A LCR meter. Very precise dielectric measurements were made over the frequency range of 0.1–10 kHz with a general Radio GR-1621 measurement system, consisting of a model 1316 oscillator, a model 1238 detector, and a model 1616 lever-arm capacitance bridge.

B. Dielectric constant versus temperature

Data are presented in Fig. 1, comparing the 100-kHz dielectric constant versus temperature of uncrystallized glass and single-crystal $SrTiO_3$. These data indicated that the temperature coefficient of uncrystallized glass was positive to the lowest temperatures. Conversely, the dielectric constant of $SrTiO_3$ increased dramatically as the temperature was decreased, reaching a value of $> 20\,000$ at 10 K. From these data, peaks in the dielectric constant versus temperature would not be expected in a glass-ceramic with a large amount of $SrTiO_3$, if the dielectric properties of the $SrTiO_3$ in the glass-ceramic were similar to single-crystal data.

Dielectric constant versus temperature curves for glass-ceramics crystallized at 800 °C for 64 h and at 900 °C for 1 h are compared in Fig. 2. Peaks in the dielectric constant occurred at about 80 K in these samples. Dielectric constant peaks at 80 K were also observed in glass-ceramics crystallized at 1000 °C, as shown by plots of dielectric constant versus temperature at frequencies of 10, 100, and 1000 kHz for glass-ceramics crystallized at 1000 °C for 1 and 16 h, presented in Fig. 3. The magnitude of the dielectric constant peaks increased from about 70 to 85 as the crystallization time was increased from 1 to 16 h. A significant dispersion of the dielectric constant was apparent in the vicinity of the dielectric constant peak.

The low-temperature dielectric constant peaks observed in Figs. 2 and 3 were not consistent with dielectric mixing. This was evidenced by two observations: (1) the temperatures of the dielectric constant peaks were relatively independent of crystallization temperature; and (2) the slopes of the dielectric constant versus temperature on the low-temperature side of the dielectric constant peak increased with

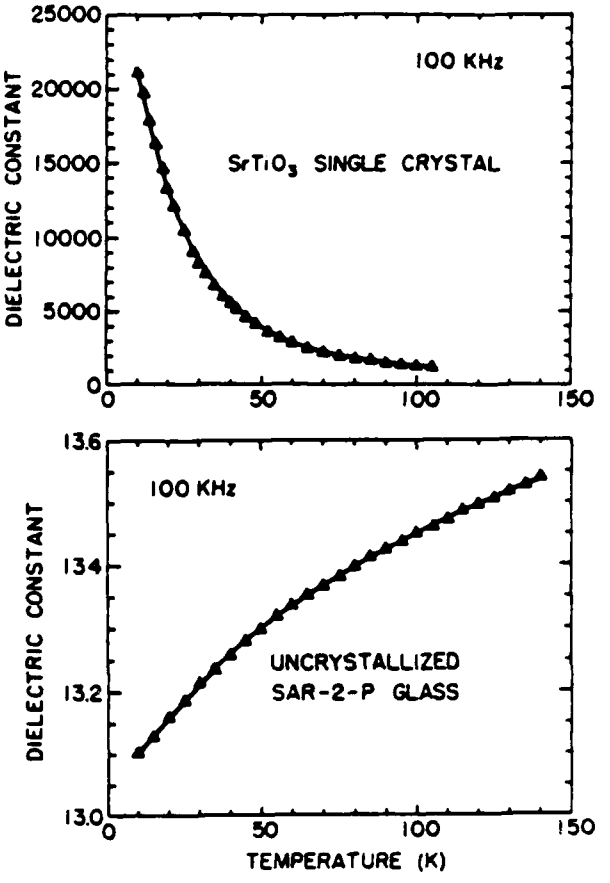

FIG. 1. 100 kHz dielectric constant vs temperature of single-crystal $SrTiO_3$ and uncrystallized glass.

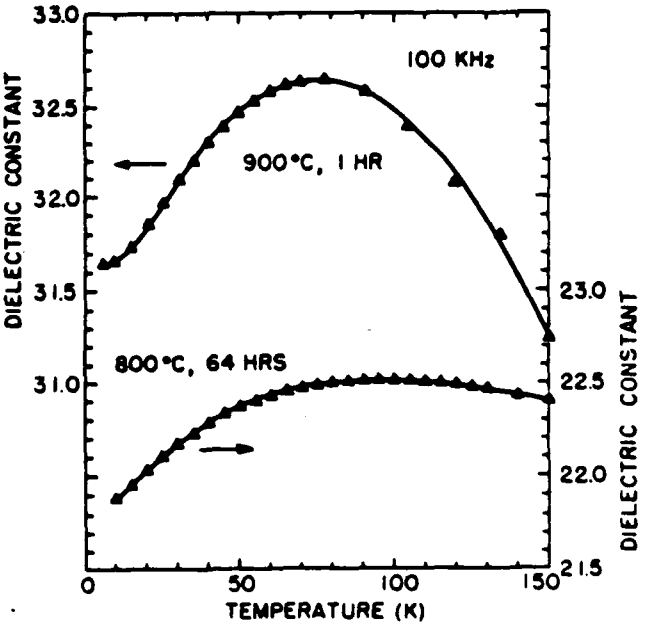

FIG. 2. 100 kHz dielectric constant vs temperature for glass-ceramics crystallized at 800 °C for 64 h and 900 °C for 1 h.

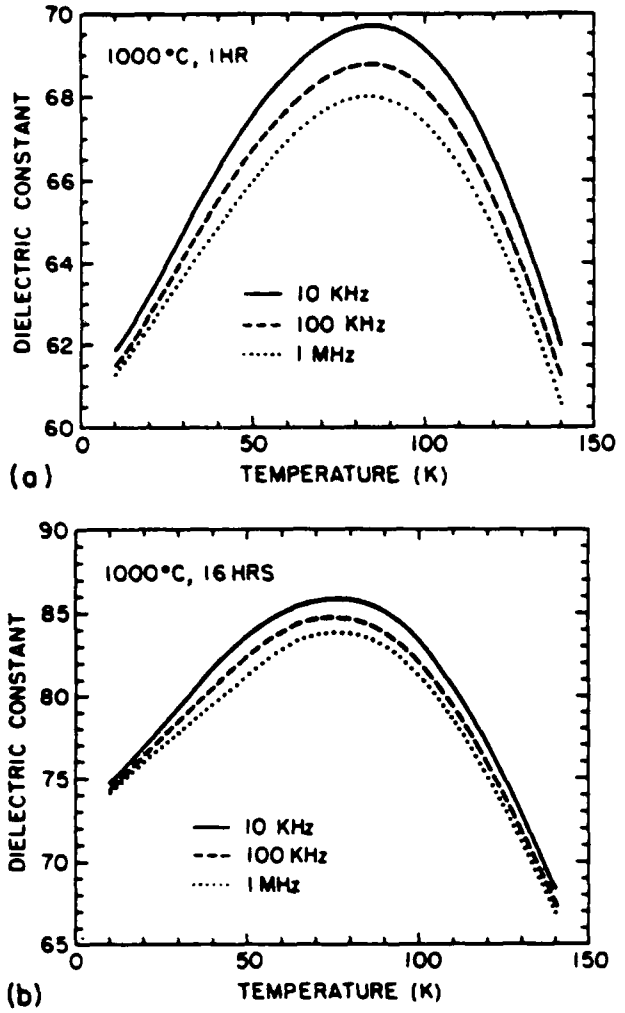

FIG. 3. Dielectric constant at 10, 100, and 1000 kHz vs temperature for glass-ceramics crystallized at 1000 °C for (a) 1 and (b) 16 h.

crystallization temperature (from 800 to 900 and 1000 °C). This increase of slope occurred over a range of crystallization temperature in which the amount of $SrTiO_3$ was increasing. If dielectric mixing were responsible for the dielectric constant peaks, the temperatures of the peaks would have decreased, and the low-temperature slopes of the peaks would not have increased, as the crystallization temperature (or amount of $SrTiO_3$) was increased. These data suggest that the $SrTiO_3$ phase in the glass-ceramic was modified, possibly by an interaction with the matrix, so that the dielectric constant of the $SrTiO_3$ peaked with temperature.

The dielectric behavior of glass-ceramics crystallized at 1100 °C was substantially different from that of glass-ceramics crystallized at lower temperatures. The dielectric constant versus temperature was very dependent on crystallization time with respect to the shape, magnitude, and temperature of the dielectric constant peaks. The observed effect of crystallization time on the low-temperature dielectric constant behavior of these glass-ceramics can be traced to the microstructural changes occurring in the glass-ceramic: (1) the transformation of the major matrix phase from hexacelsian to anorthite $SrAl_2Si_2O_8$; (2) the crystallization of TiO_2 and the development of the large acicular titania crystals; and (3) the increase of the $SrTiO_3$ crystallite size.

The dielectric constant at frequencies of 10, 100, and 1000 kHz are plotted versus temperature for a glass-ceramic crystallized for 1 h at 1100 °C in Fig. 4. This sample displayed a broad, frequency-dependent, two-humped dielectric constant peak over the temperature range 35–55 K. The exact shape of the dielectric constant peak was dependent on the measurement frequency; generally, the double-peaked nature was more apparent for the higher frequency (1 MHz). The temperature of the lower temperature portion of the double peak was independent of frequency; however, the higher temperature portion of the double peak shifted to higher temperatures with increasing frequency. It is likely that the double-peaked nature of the dielectric constant versus temperature was due to the presence of two matrix phases, hexacelsian and anorthite, in glass-ceramics crystallized for less than 8 h at 1100 °C. A complete explanation as

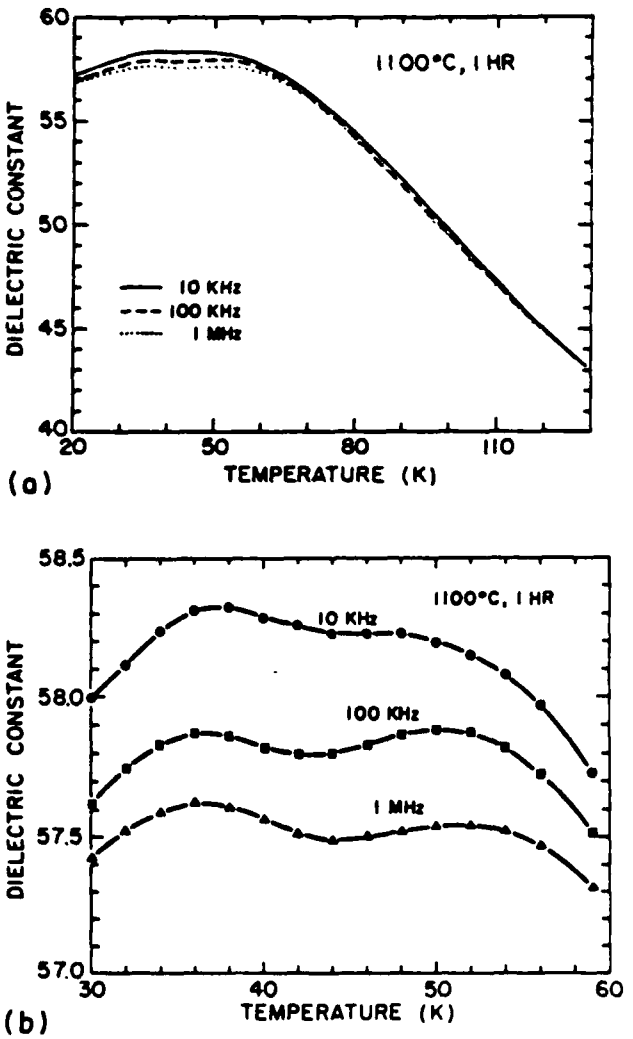

FIG. 4. Dielectric constant at 10, 100, and 1000 kHz vs temperature for the glass-ceramic crystallized at 1100 °C for 1 h, over two temperature ranges: (a) 20–130 K, and (b) 30–60 K.

to how the two matrix phases could cause the double peaks would require more of an understanding as to the actual mechanism responsible for the dielectric constant peaks.

The dielectric constant versus temperature at 10, 100, and 1000 kHz of the glass-ceramic crystallized at 1100 °C for 16 h appears in Fig. 5. The dielectric constant behavior of this sample was substantially different from those of glass-ceramics crystallized for shorter times at 1100 °C. The magnitude of the dielectric constant peak was much larger, the double-peaked nature was not apparent, and the temperature of the peak was much higher than in glass-ceramics crystallized for shorter times. The frequency dependence of the dielectric constant versus temperature of the 16-h sample suggests at least two mechanisms responsible for the dielectric constant peaks. At low frequencies (10–40 kHz), a relaxation mechanism was active resulting in a dispersive dielectric constant peak at about 100 K. The dispersive nature of the dielectric constant peaks suggests anomalies in the dielectric loss which will be described later. At a frequency of 1 MHz, the dielectric constant peaked at a lower temperature (85 K), suggesting that the mechanism responsible for the low-frequency dielectric constant peaks was not as active at higher frequencies.

C. Dielectric loss data

The effect of crystallization conditions on the low-temperature dielectric loss is shown by dielectric loss spectra (plots of dissipation factor at 10, 100, and 1000 kHz versus temperature) of glass-ceramics crystallized at 800 °C for 64 h and 900 °C for 1 h in Fig. 6. The low-temperature dielectric loss levels of the glass-ceramics were larger than those of uncrystallized glass and generally increased with crystallization temperature and time. For uncrystallized glass and glass-ceramics crystallized below 1000 °C, the dielectric loss displayed broad maxima with temperature near 100 K and increased with frequency (from 10 to 1000 kHz). This athermal increase of loss with frequency was observed at higher temperatures, as described in Refs. 9 and 11.

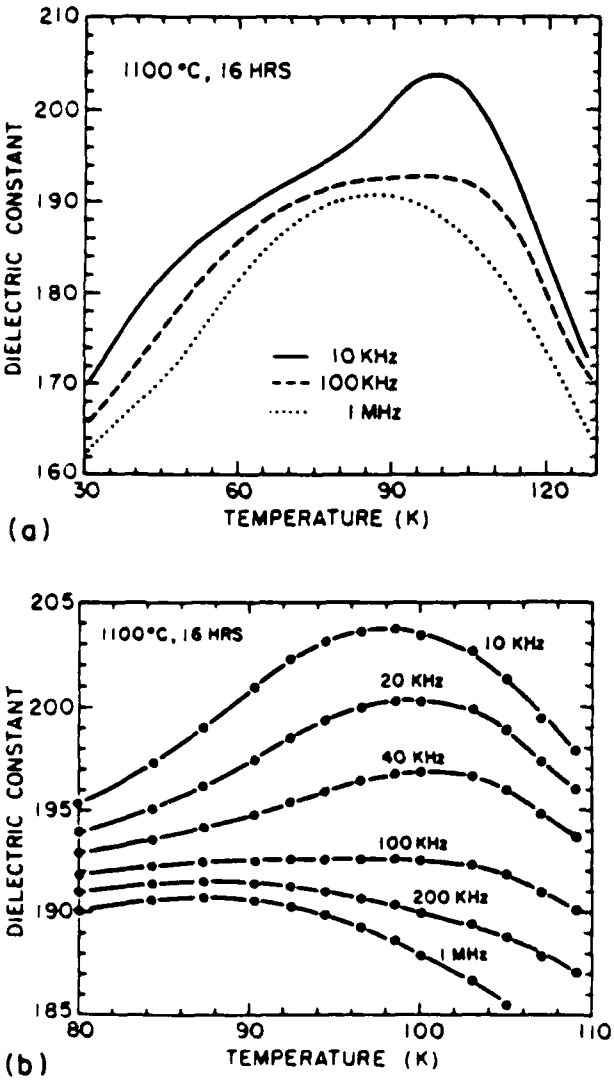

FIG. 5. Dielectric constant at various frequencies between 10 and 1000 kHz vs temperature for the glass-ceramic crystallized at 11000 °C for 16 h, over two temperature ranges. (a) 30–130 K, and (b) 80–110 K.

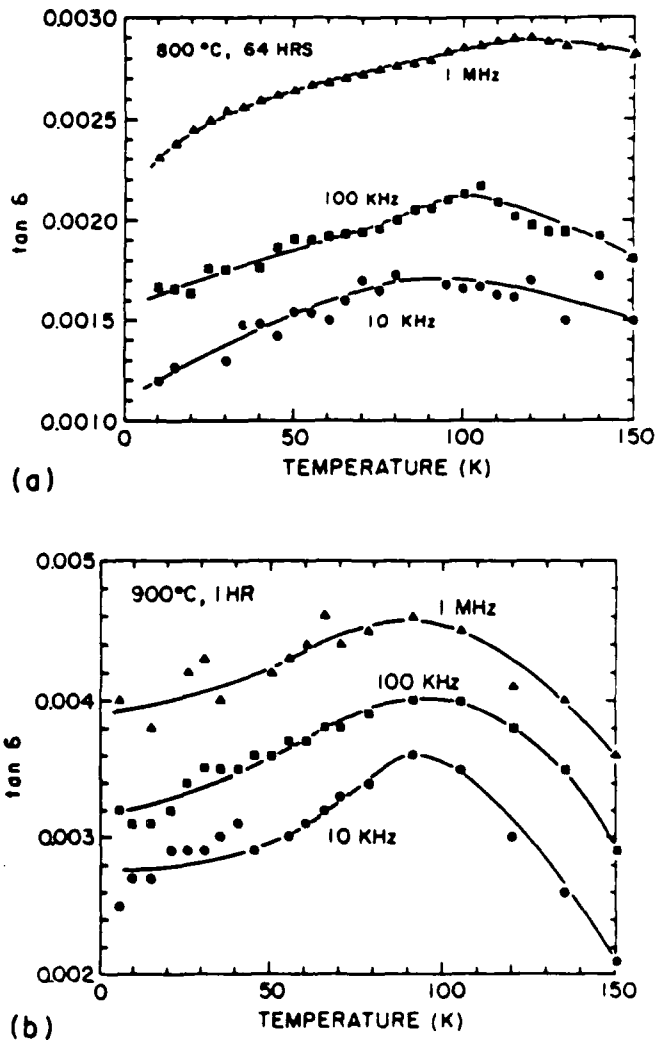

FIG. 6. Dissipation factor at 10, 100, and 1000 kHz vs temperature for glass-ceramics crystallized at (a) 800 °C for 64 h and (b) 900 °C for 1 h.

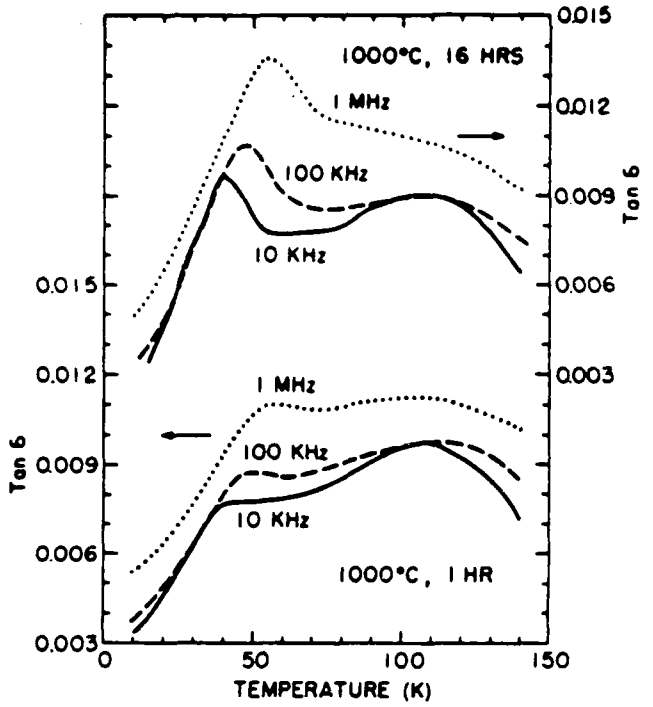

FIG. 7. Dissipation factor at 10, 100, and 1000 kHz vs temperature for glass-ceramics crystallized at 1000 °C for 1 and 16 h.

Dielectric loss spectra of glass-ceramics crystallized at 1000 °C for 1 and 16 h appear in Fig. 7. Dielectric losses of glass-ceramics crystallized at this temperature also increased with frequency; however, two frequency-dependent loss peaks developed at 50 and 100 K, and were superimposed on the athermal loss. The magnitude of the lower temperature (50 K) loss peak increased with crystallization time between 1 and 16 h at 1000 °C, while the higher temperature (100 K) loss peak remained approximately the same. The increase of the lower temperature (50 K) loss peak with crystallization time corresponded to the increased magnitude of the dielectric constant peak. This suggests that the mechanism responsible for this loss peak was related to that of the dielectric constant peak. However, the dielectric constant peak occurred at a temperature of 80 K, closer to the range of the higher temperature loss mechanism.

The dielectric loss behavior of glass-ceramics crystallized at 1100 °C was dominated by the two loss peaks, first observed in glass-ceramics crystallized at lower temperatures. Dielectric loss spectra of glass-ceramics crystallized at 1100 °C for 0.25, 1, 4, and 16 h appear in Fig. 8. The exact nature of the loss peaks could be determined from these data:

(1) For both sets of dielectric loss peaks, the loss peak temperature increased with frequency, from about 38 to 52 K and 85 to 110 K, over the frequency range of 10–1000 kHz; this type of loss peak behavior is typical of relaxation mechanisms.

(2) The magnitude of the higher-temperature (100 K) loss peak decreased and the peak broadened with increasing frequency; the magnitude of the lower temperature (50 K) loss peak increased and the peak sharpened with increasing frequency.

(3) The magnitude of the loss increased steadily as the crystallization time at 1100 °C was increased, corresponding to the increase in magnitude of the dielectric constant peaks.

In the glass-ceramics crystallized for 1 and 4 h, a shoulder was apparent on the low-temperature side of the 50-K loss peak. The shoulders on the loss peaks and the double-peaked nature of the dielectric constant versus temperature of these samples may have been related to the existence of two matrix phases (hexacelsian and anorthite $SrAl_2Si_2O_8$); this suggests that the lower-temperature loss mechanism was responsible for the dielectric constant peaks in these samples and was the result of some kind of interaction between the $SrTiO_3$ and the matrix. With increasing frequency, the low-temperature (50 K) loss peak increased in magnitude. This was consistent with an earlier observation that the two-peaked nature of the dielectric constant versus temperature of the shorter crystallization time samples was more evident at higher frequencies.

The anomalous frequency dependence of the dielectric constant peak of the 16-h sample was caused by the higher-temperature loss mechanism. The magnitude of the higher temperature loss peak increased with decreasing frequency, consistent with the observation that this mechanism affected the dielectric constant curve more at low frequencies (10–40 kHz). Apparently higher temperature loss mechanism contributed a large dispersion of the dielectric constant and caused the low-frequency dielectric constant to peak at higher temperatures.

From the above results, it was obvious that an analysis of the two dielectric loss mechanisms had to be performed before a complete understanding of the low-temperature dielectric properties could be obtained. The frequency and temperature dependences of a relaxation-type loss mechanism can be approximated through the use of Debye formalism. The two loss peaks were most apparent in the glass-ceramic crystallized for 16 h at 1100 °C. Arrhenius plots were constructed from the dielectric loss data in the temperature ranges of the two mechanisms. These plots are presented, along with the dielectric loss spectra, in Figs. 9 and 10. Excellent straight line fits to the Arrhenius data were obtained. Activation energies were calculated to be 0.054 and 0.17 eV for the lower (50 K) and higher (100 K) temperature loss mechanisms, respectively.

D. Low-frequency measurements

Low-frequency dielectric measurements were performed on the glass-ceramic sample crystallized for 16 h at 1100 °C. Dielectric data in the range of the lower temperature loss mechanism are presented as plots of dissipation factor and normalized dielectric constant (capacitance normalized to the value at 200 Hz) versus log frequency at a temperature of 36 K in Fig. 11. At this temperature, the dissipation factor peaked at a frequency of about 800 Hz. The dispersion of the dielectric constant was almost linear over the entire frequency range, with only slight curvature suggesting an inflection point, as predicted by Debye theory. The effect of temperature on the frequency of the dissipation

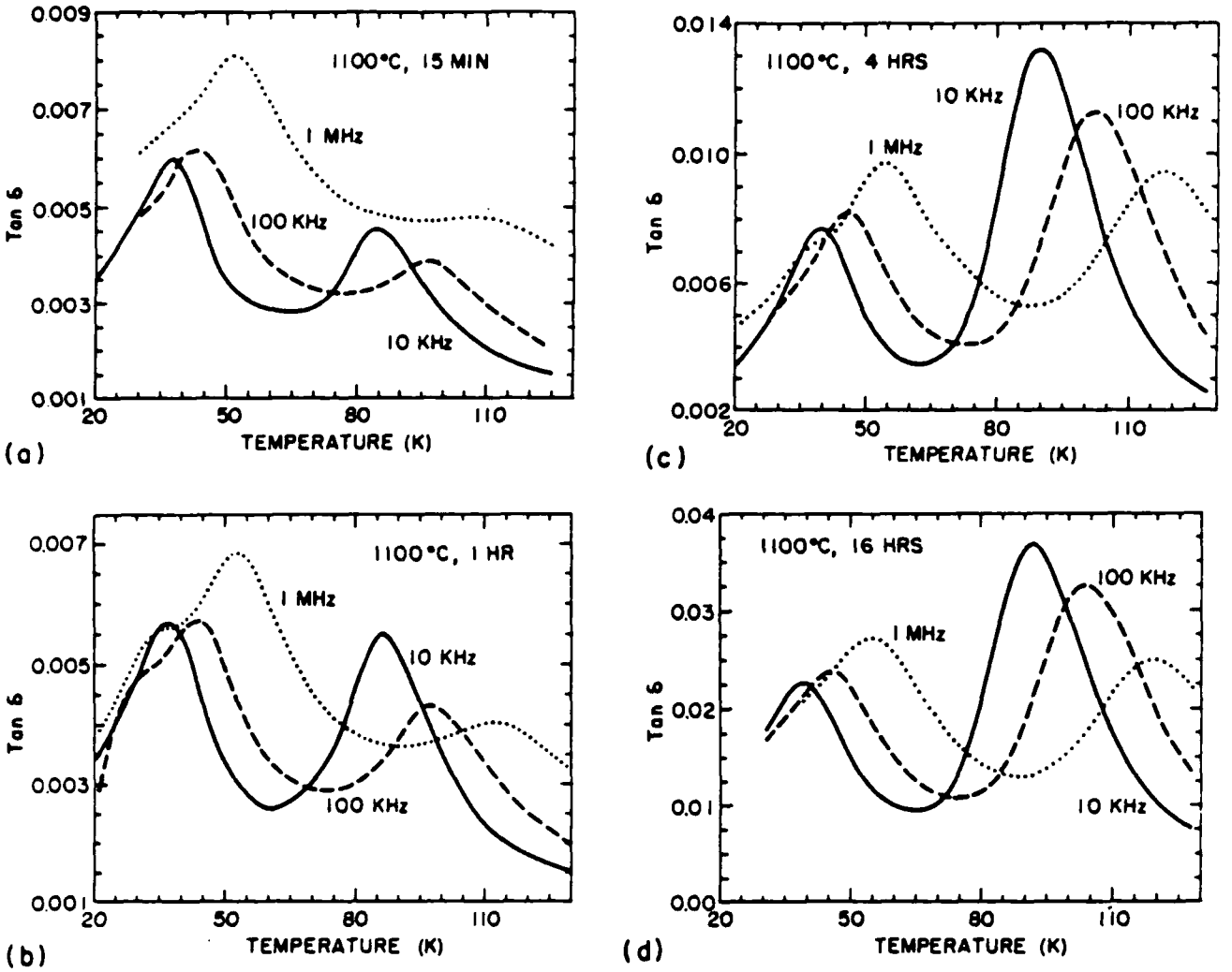

FIG. 8. Dissipation factor at 10, 100, and 1000 kHz vs temperature for glass-ceramics crystallized at 1100 °C for (a) 0.25, (b) 1, (c) 4, and (d) 16 h.

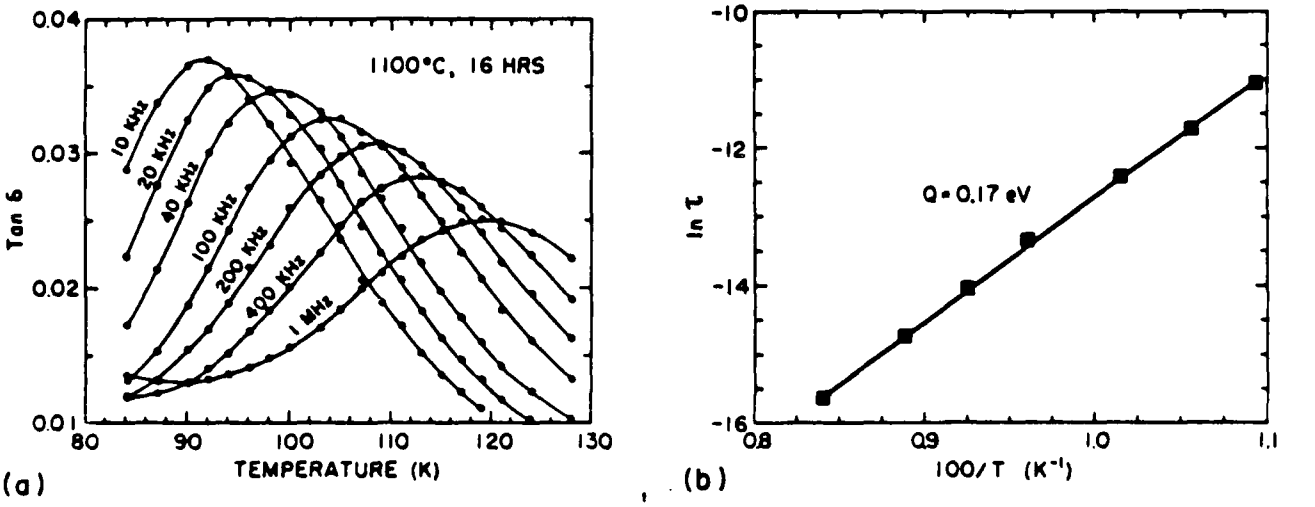

FIG. 9. (a) Dielectric loss spectra corresponding to the lower temperature loss mechanism, and (b) corresponding Arrhenius plot, for the glass-ceramic crystallized at 1100 °C for 16 h.

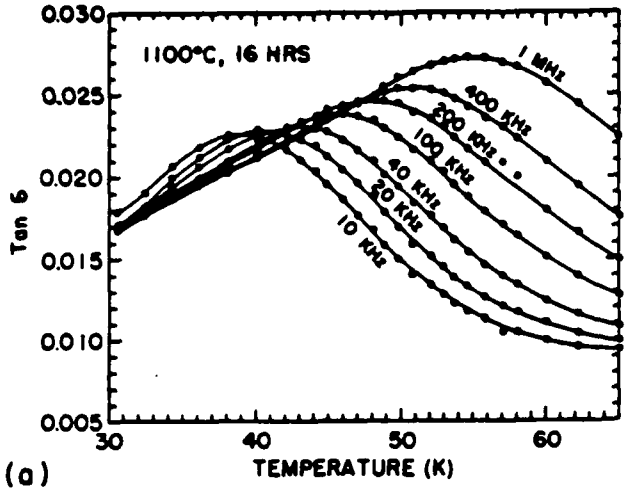

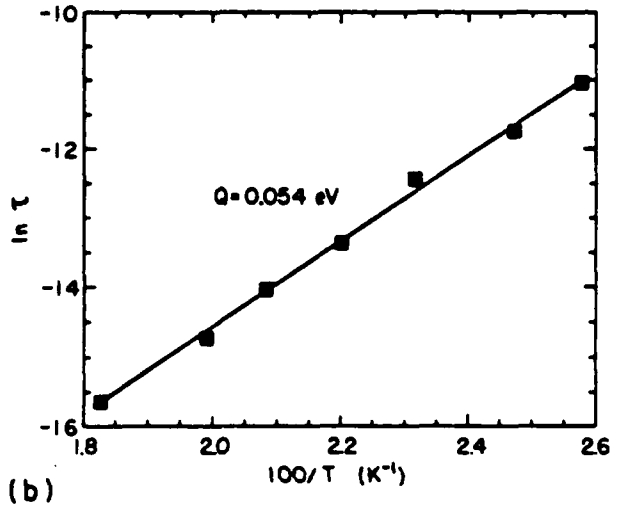

FIG. 10. (a) Dielectric loss spectra corresponding to the higher temperature loss mechanism and (b) corresponding Arrhenius plot, for the glass-ceramic crystallized at 1100 °C for 16 h.

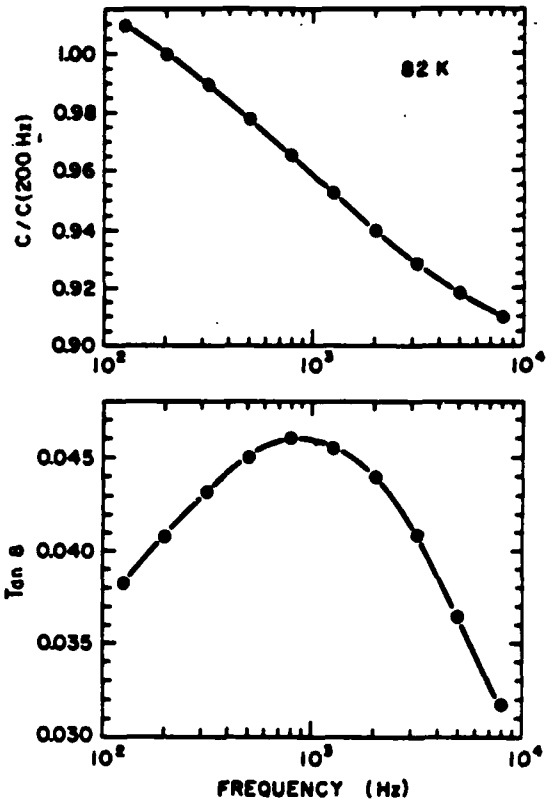

FIG. 11. Capacitance normalized to 200 Hz and dissipation factor vs frequency at 82 K, for the glass-ceramic crystallized at 1100 °C for 16 h.

factor peak is shown in Fig. 12, in which the dissipation factor is plotted versus log frequency at temperatures 33, 36, and 39 K. At temperatures of 33 and 39 K, the loss peaks occurred at the lower and higher extremes of the frequency range. The lower temperature loss mechanism thus resulted in dissipation factor peaks over a relatively small temperature range.

Low-frequency dielectric data in the range of the higher-temperature loss mechanism are presented as plots of normalized dielectric constant and dissipation factor versus log frequency at a temperature of 82 K in Fig. 13. At this temperature, the dissipation factor peaked at a frequency of about 900 Hz, and the dispersion of the dielectric constant was larger than that of the lower temperature mechanism and displayed curvature suggestive of an inflection point near the frequency of the loss maximum. The effect of temperature on the frequency of the dissipation factor peaks of the higher temperature loss mechanism is shown in Fig. 14; the dissipation factor is plotted versus log frequency at temperatures of 78, 80, 82, and 84 K. Dielectric loss peaks with frequency were observed at each of these temperatures, and the frequency of the loss peak increased with temperature, as expected.

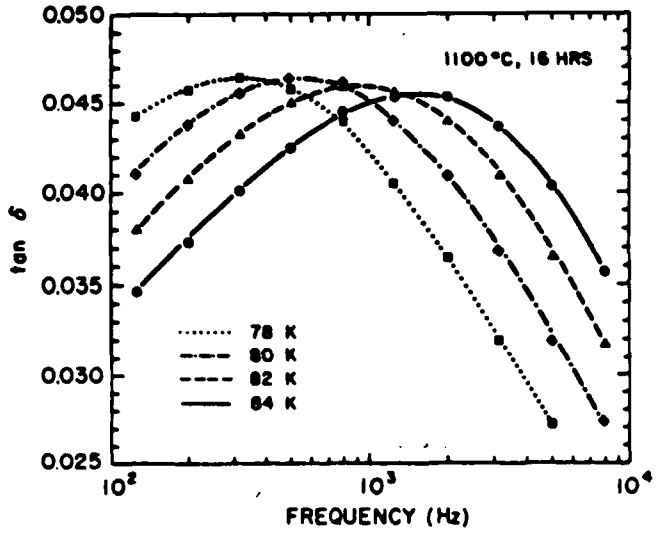

FIG. 12. Dissipation factor vs frequency at various temperatures between 78 and 84 K, for the glass-ceramic crystallized at 1100 °C for 16 h.

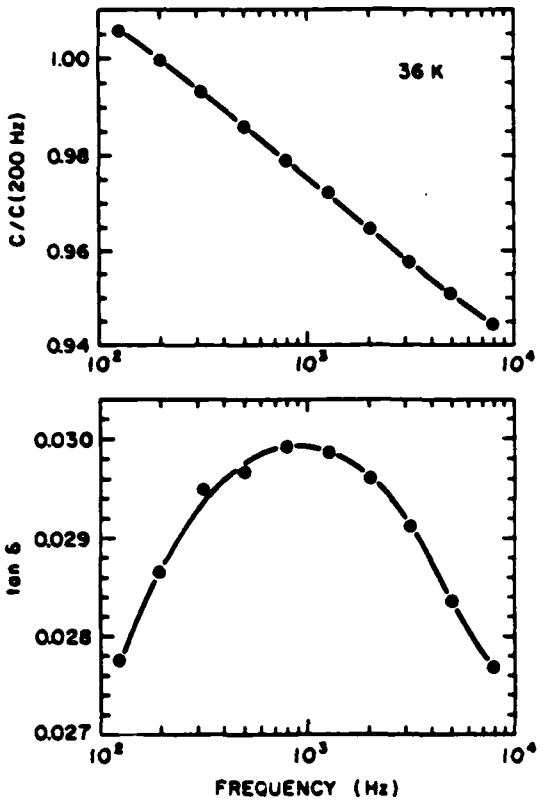

FIG. 13. Capacitance normalized to 200 Hz and dissipation factor vs frequency at 36 K, for the glass-ceramic crystallized at 1100 °C for 16 h.

The Cole–Cole method of analysis was applied to the low-frequency data, relevant to the higher-temperature loss mechanism, so that a better understanding of the observed shapes of the dielectric loss peaks and dielectric constant

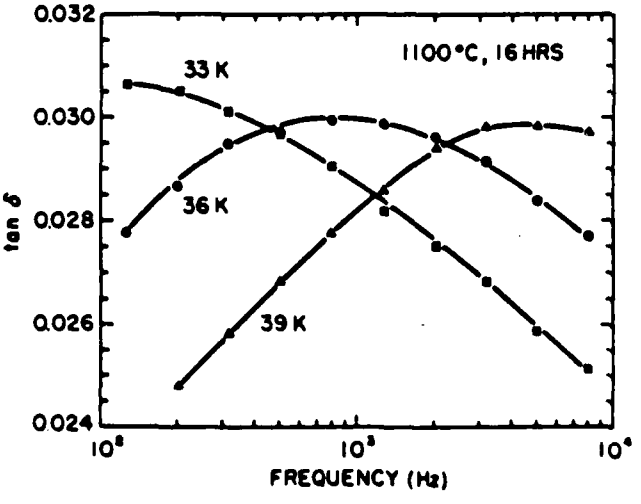

FIG. 14. Dissipation factor vs frequency, at temperatures of 33, 36, and 39 K, for the glass-ceramic crystallized at 1100 °C for 16 h.

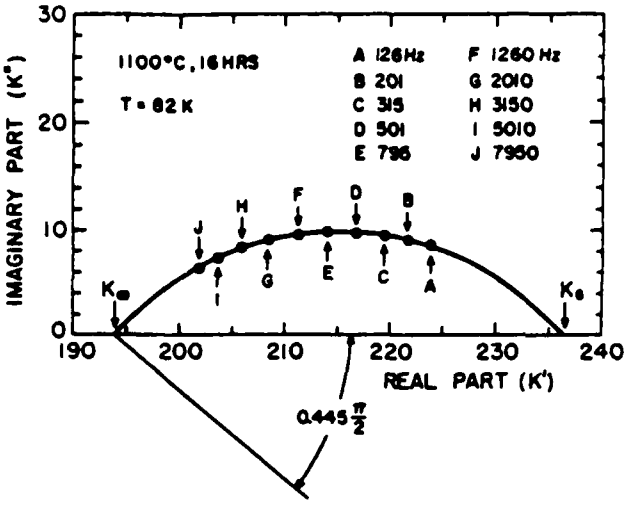

FIG. 15. Cole–Cole plot constructed from the 82 K dielectric data of the glass-ceramic crystallized at 1100 °C for 16 h.

dispersion described above could be obtained. The Cole–Cole analysis was performed with the HP-9816 computer system by fitting K'' vs K' data to a circle with a least-squares technique; the intercepts (K_s and K_∞) and the tilt parameter (α) were then calculated. This computerized analysis also allowed for the calculation of the frequency of maximum loss (for Arrhenius plots) and the maximum values of dielectric loss (for normalized dielectric loss plots).

A Cole–Cole plot, corresponding to dielectric data taken at 82 K, relevant to the higher-temperature loss mechanism, is presented in Fig. 15; the line between the K_∞ intercept and the origin of the circle is shown, defining the tilt angle. An excellent fit of the Cole–Cole arc to the dielectric data was obtained. The effect of temperature on the relaxation process was determined by performing the Cole–Cole analysis on the dielectric data taken at temperatures of 75, 78, 80, 82, and 84 K. Information obtained from the Cole–Cole analyses is summarized in Table I.

The value of K_∞ (the value of the dielectric constant without the contribution of the loss mechanism) decreased with increasing temperature over the range of 75–84 K, even though the measured dielectric constant increased with temperature. This can be explained by the shift in the loci of the data points along the Cole–Cole arc as the temperature was

TABLE I. Dielectric quantities derived from Cole–Cole plots constructed from low-frequency dielectric data.

T(K)	K_s	K_∞	ΔK	α
75	237.56	196.26	41.30	0.423
78	236.80	195.60	41.20	0.420
80	236.62	194.82	41.80	0.431
82	236.25	192.81	42.44	0.445
84	235.54	192.63	42.91	0.459

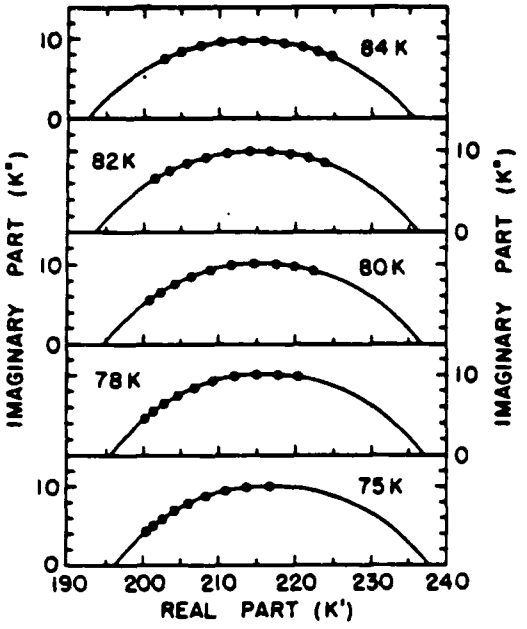

FIG. 16. Comparison of Cole–Cole arcs, constructed from dielectric data taken between 75 and 84 K, for the glass-ceramic crystallized at 1100 °C for 16 h.

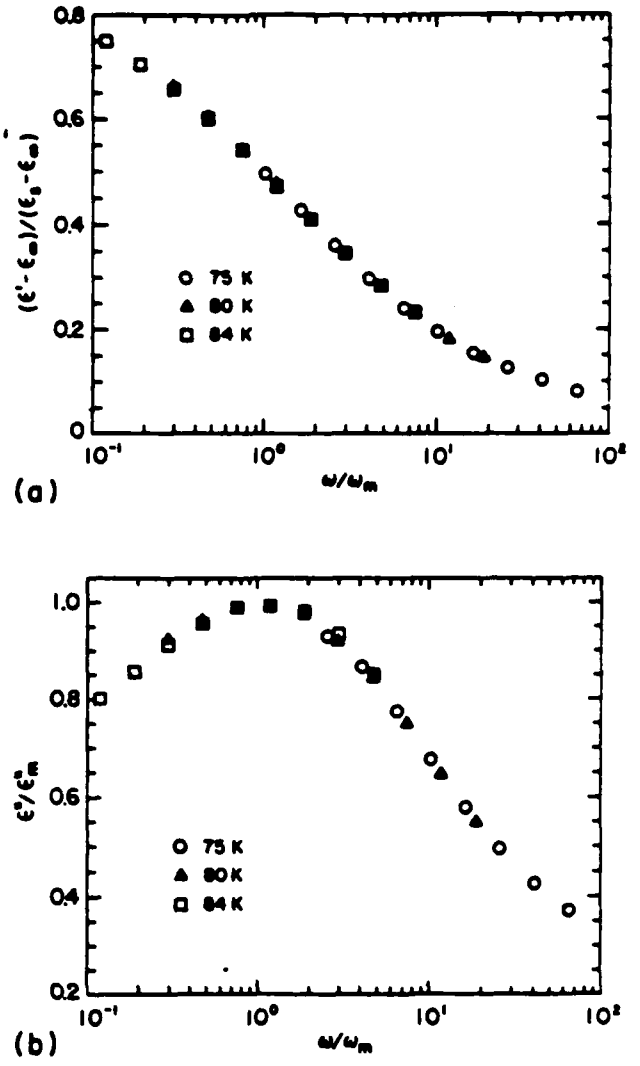

FIG. 17. Normalized plots of (a) permittivity and (b) loss vs frequency, with data taken at 75, 80, and 84 K, for the glass-ceramic crystallized at 1100 °C for 16 h.

increased. This is shown in Fig. 16 for a series of Cole–Cole arcs constructed from dielectric data taken at the five temperatures. At a temperature of 75 K, the dispersion corresponding to this loss mechanism occurred on the high-frequency portion of the arc. As the temperature was increased, the dispersion shifted to lower frequencies, thus increasing the contribution of the loss mechanism to the measured dielectric constant. The increased temperature range of the dielectric constant peak in the 16-h sample was thus caused by the higher temperature (100 K) loss mechanism. Without the contribution of this mechanism, the dielectric constant would have peaked at a lower temperature, consistent with the glass-ceramics crystallized for shorter times at 1100 °C.

The dielectric constant and loss versus frequency were normalized using computer-calculated quantities so that the dielectric data taken at different temperatures could be compared, and the dielectric properties in the range of this loss mechnanism could be studied over an extra decade in frequency. Normalized permittivity and loss are plotted against the log of the normalized frequency in Fig. 17, comparing dielectric data taken at temperatures of 75, 80, and 84 K. The normalized dielectric data at these three temperatures coincided and defined curves with the expected shape for a Debye-like relaxation process. The inflection point which was obvious in the 82 K data presented earlier was more clearly defined by this dielectric constant dispersion curve.

For the higher temperature loss mechanism, a comparison could be made between Arrhenius plots constructed from two types of measurements, constant frequency (10–1000 kHz) with varying temperature, and variable frequency (0.1–10 kHz) at constant temperature. For the high-frequency data, Arrhenius plots were generated from the frequency dependence of the dielectric loss peak temperature; conversely, for the low-frequency data, Arrhenius plots were generated from the temperature dependence of the dielectric loss peak frequency. The comparison of these two Arrhenius plots appears in Fig. 18. The activation energy calculated from the low-frequency data was 0.13 eV, in suitable agreement with the value of 0.17 eV, calculated from the higher frequency data.

E. Electric field dependence

Clues to the nature of the higher-temperature (100 K) dielectric loss mechansim were obtained by a measurement of the electric field dependence of the dielectric constant and loss. These measurements were performed on a glass-ceramic sample crystallized for 32 h at 1100 °C. The measurement system included a GR-1615A capacitance bridge with appropriate protection circuitry to allow from applied voltages of up to 5000 V. The dielectric measurements to be reported

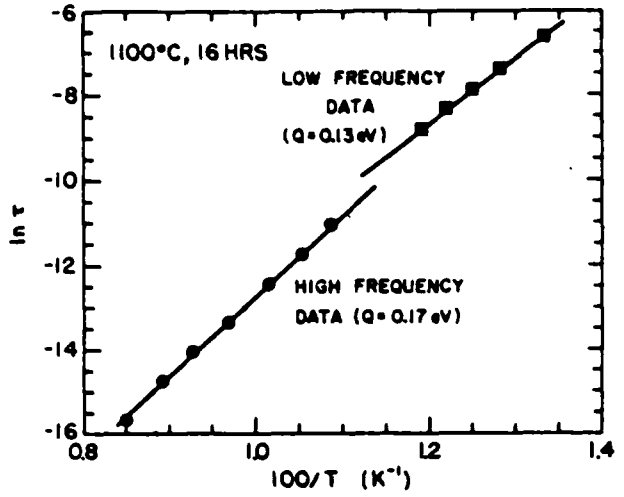

FIG. 18. Comparison of Arrhenius plots constructed from low (0.1–10 kHz) and high (10–1000 kHz) frequency data of the glass-ceramic crystallized at 1100 °C for 16 h.

here were made at a temperature of 77 K; the sample was immersed in liquid nitrogen to prevent temperature fluctuations. Two measurement frequencies were utilized: (1) 126 Hz, the frequency of the dielectric loss maximum at 77 K; and (2) 100 kHz, the highest frequency available with the capacitance bridge used. The dielectric constant and dissipation factor were measured with applied voltages corresponding to electric fields from 0 to 30 kV/cm with increments of 5 kV/cm.

Data are presented as plots of dielectric constant and dissipation factor at frequencies of 126 Hz and 100 kHz versus applied electric field in Fig. 19. With no applied field, the dielectric constant and loss were significantly larger at the lower frequency (126 Hz). This disperison was due to the contribution of the higher temperature loss mechansim which was a maximum at 126 Hz. As the applied electric field was increased, the dielectric constant decreased substantially at both frequencies, but with an applied field of 10 kV/cm, most of the dispersion in the dielectric constant had been removed. With further increase of field, the dielectric constant decayed at the same rate for the two frequencies. A corresponding decrease in dielectric loss to much lower levels with applied electric field was also observed.

From the above data, it was clear that two mechanisms were active in this frequency range and temperature; this was also implied from dielectric measurements presented earlier. The nature of these two mechanisms can be deduced from their electric field dependences. The higher temperature loss mechansim, which dominated the dielectric loss behavior and determined the shape of the dielectric constant peaks in this sample, decayed very rapidly with applied electric field. The second mechanism, which was apparently responsible for the large magnitude of the dielectric constant, decayed more gradually with electric field. Further evidence for the existence of two mechanisms arises from the fact that with an applied field of 30 kV/cm, the decrease in dielectric constant from 211 to 68 was much larger than the relaxation

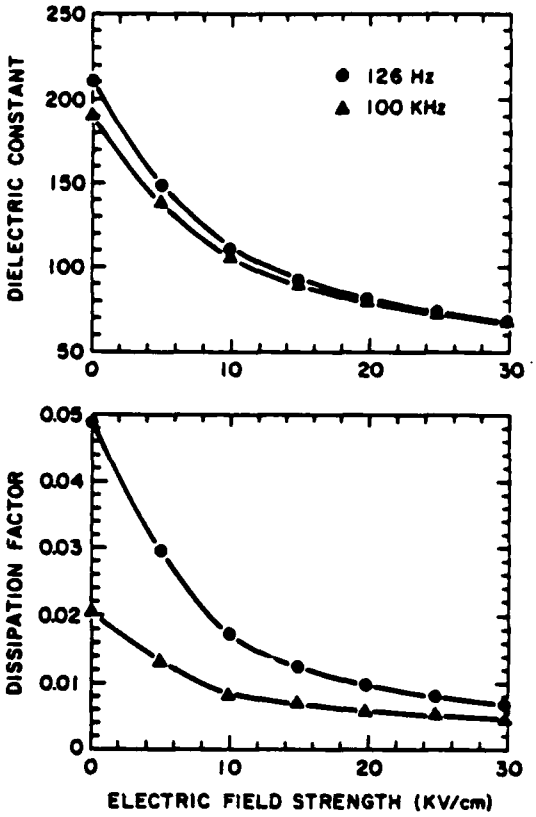

FIG. 19. Dielectric constant and dissipation factor, at 77 K and frequencies of 126 Hz and 100 kHz, vs applied electric field, for the glass-ceramic crystallized at 1100 °C for 32 h.

strength of about 41, calculated for the higher-temperature loss mechanism.

F. Discussion

In this section, the results of low-temperature dielectric measurements have been presented. These measurements have created as many questions as they were intended to answer:

(1) Except for very low loadings of $SrTiO_3$, the peaks in the dielectric constant versus temperature observed in these glass-ceramics could not be attributed to dielectric mixing. Some sort of interaction of $SrTiO_3$ with the matrix was responsible for the dielectric constant peaks.

(2) If an interaction was responsible for the dielectric constant peaks, the nature of this interaction was very sensitive to crystallization conditions. For instance, the magnitude of dielectric constant peaks of glass-ceramics crystallized at 1000 °C increased with crystallization time, without an increased contribution to dielectric loss peaks. Conversely, in glass-ceramics crystallized at 1100 °C, the magnitude of the dielectric constant peaks increased with crystallization time, but with a substantial increase of dielectric loss.

(3) Two low-temperature loss mechanisms were identified in glass-ceramics crystallized at 1100 °C, resulting in frequency-dependent dielectric loss peaks at temperature

ranges near 50 and 100 K. Another mechanism was active in glass-ceramics crystallized for the longer times at 1100 °C, giving rise to a large contribution to the dielectric constant.

As described earlier, low-temperature peaks in the dielectric constant and loss have been observed in similar $SrTiO_3$ glass-ceramics by Lawless[6] and Siegwarth.[8] It was suggested by Siegwarth[8] that the observed dielectric behavior was caused by the relaxation of permanent dipoles, which were present due to electret (defect-dipole) states. He based his conclusion by analogy with similar low-temperature relaxation-type dielectric constant and loss peaks observed in $SrTiO_3$ based ceramics, containing large proportions of vanadium, niobium, or antimony.[12]

Siegwarth[8] proposed that gross defects (or impurities) were incorporated into the $SrTiO_3$, suggesting that interactions of $SrTiO_3$ crystallites with the matrix would not have affected the dielectric properties. In the present study, it does not seem conceivable that enough defects were incorporated into the $SrTiO_3$ crystallites to cause such relaxation behavior. In addition, results of this investigation indicated that interactions of the $SrTiO_3$ with the matrix were important to the dielectric behavior. The double-humped dielectric constant peaks and shoulders on loss peaks observed in glass-ceramics crystallized for the shorter times at 1100 °C were attributed to the presence of two $SrAl_2Si_2O_8$ matrix phases (hexacelsian and anorthite). The magnitude of the decrease of the dielectric constant observed with electric field at 77 K (in the range of the dielectric loss mechanism), in the glass-ceramic crystallized for 32 h at 1100 °C, also rules out a dipolar mechanism. For these reasons, yet another explanation to the observed dielectric properties of the $SrTiO_3$ glass-ceramic is required.

An explanation that would be consistent with the low-temperature dielectric behavior is the possibility that the $SrTiO_3$ was modified by the matrix so that some sort of ferroic phenomenon was induced within the $SrTiO_3$ crystallites. Single-crystal $SrTiO_3$ undergoes a ferroelastic transition from cubic to tetragonal at 110 K, as demonstrated by several workers.[13,14] As the glass-ceramic was cooled through the 110 K transition, the deformation of the tiny $SrTiO_3$ crystallites may have been suppressed by the matrix, causing stresses in addition to those present from differing thermal expansion. The resulting complex stress states existing in the $SrTiO_3$ crystallites may have affected the complicated energy balances between paraelectric, ferroelastic, and ferroelectric states.

It is appealing to consider the possibility that ferroelectricity was induced within the $SrTiO_3$ crystallites in the glass-ceramics. Induced ferroelectricity has been demonstrated in both $SrTiO_3$ (Ref. 15) and $KTaO_3$ (Ref. 16) at low temperatures by the application of uniaxial pressure. If one accepts the premise that ferroelectricity of the $SrTiO_3$ was responsible for the observed dielectric behavior, some of the anomalous low-temperature properties of the glass-ceramics can be explained. Certainly, the peaks in the dielectric constant would be expected at a temperature corresponding to the ferroelectric transition. The increase in magnitude of the dielectric constant peak with crystallization time at 1000 °C suggests that the interaction causing ferroelectricity in the $SrTiO_3$ phase was dependent on the $SrTiO_3$ crystallite size.

For the case of glass-ceramics crystallized at 1100 °C, the situation was complicated by microstructural changes occurring with crystallization time, as discussed earlier. If the $SrTiO_3$ phase in the glass-ceramic was indeed ferroelectric, the increase in magnitude and temperature of the dielectric constant peaks with crystallization time at 1100 °C may be explained by changes in the interactions of $SrTiO_3$ with the matrix caused by the microstructural changes. The development of the acicular titania crystals could have changed the mechanical properties of the matrix, and altered the interaction. Also, the increase of $SrTiO_3$ crystallite size may have allowed for the possibility of domain wall motion.

The higher-temperature (100 K) loss mechanism can be attributed to ferroic domain effects within the $SrTiO_3$ crystallites. The activation energy and frequency dependence (a decrease of the loss peak magnitude with increasing frequency) were consistent with domain wall motion. The temperature range of this loss mechanism also occurred suspiciously close to that of the 110 K transition of $SrTiO_3$. The increase of this loss mechanism with crystallization time at 1100 °C was consistent with the increased domain wall motion possible with the increased $SrTiO_3$ crystallite size. The fact that this loss mechanism did not increase with crystallization time at 1000 °C suggested a lack of domain wall motion in the extremely small $SrTiO_3$ crystallites of glass-ceramics crystallized at this temperature.

The lower-temperature (50 K) loss mechanism was direclty related to the dielectric constant peaks, and was responsible for the increase in magnitude of the dielectric constant peaks with crystallization time in glass-ceramics crystallized at 1000 °C. This mechanism was the result of some kind of interaction of $SrTiO_3$ with the matrix, as evidenced by double-humped dielectric constant peaks and shoulders on the loss peaks in glass-ceramics with the two matrix phases (hexacelsian and anorthite). However, the frequency dependence (an increase of loss peak magnitude with frequency) was not consistent with ferroic domains. The nature of the actual mechanism responsible for the dielectric loss peaks is difficult to speculate upon without further experimentation.

From the above discussion, the difficulty in assigning mechanisms to the observed features in the low-temperature dielectric properties is apparent. Ferroelectricity is only one possible explanation for the low-temperature dielectric constant and loss peaks. Other types of ferroic phenomena and domain structures may have been responsible, although more definitive experiments are required before mechanisms can be assigned to the observed dielectric behavior with absolute certainty.

ACKNOWLEDGMENTS

This work was sponsored by the U.S. Army Research Office under Contract No. DAAG-82-K-0015. The authors are indebted to R. E. Newnham for thoughtful discussions, and to P. Moses for his help with electrical measurements.

[1]A. Herczog, J. Am. Ceram. Soc. Bull. 47, 107 (1964).
[2]T. Kokubo, C. Kung, and M. Tashiro, J. Ceram. Assoc. Jpn. 76, 89 (1968).
[3]T. Kokubo, H. Nagao, and M. Tashiro, J. Ceram. Assoc. Jpn. 77, 293 (1969); T. Kokubo and M. Tashiro, J. Non-Cryst. Solids 13, 328 (1973/1974).
[4]D. G. Grossman and J. O. Isard, J. Am. Ceram. Soc. 52, 230 (1969); J. Phys. D 3, 10(58 (1970).
[5]N. F. Borelli, A. Herczog, and R. D. Maurer, Appl. Phys. Lett. 7, 117 (1965); N. F. Borelli, J. Appl. Phys. 38, 4243 (1967); N. F. Borelli and M. M. Layton, J. Non-Cryst. Solids 6, 197 (1971).
[6]W. N. Lawless, Ferroelectrics 7, 379 (1974).
[7]W. N. Lawless, Rev. Sci. Instrum. 42, 561 (1971); Cryog. Eng. 16, 261 (1961); *A Low Temperature Glass-Ceramic Capacitance Thermometer, Proceedings of the 5th Symposium on Temperature, Washington, D. C., June 1971* (1972); 1143–1151 Capacitive Cryogenic Thermometer, U. S. Patent No. 3 649 891 (1972).
[8]J. D. Siegwarth, J. Appl. Phys. 48, 1 (1976).
[9]S. L. Swartz, Ph.D. thesis, The Pennsylvania State University, University Park, Pennsylvania (1985).
[10]S. L. Swartz, E. Breval, and B. H. Fox, submitted to J. Am. Ceram. Soc.
[11]S. L. Swartz, A. S. Bhalla, L. E. Cross, and W. N. Lawless (unpublished).
[12]J. D. Siegwarth and A. J. Morrow, J. Appl. Phys. 47, 4784 (1976).
[13]F. W. Lytle, J. Appl. Phys. 35, 2212 (1964).
[14]H. Unoki and T. Sakudo, J. Phys. Soc. Jpn. 23, 546 (1967).
[15]W. J. Burke and R. J. Pressely, Solid State Commun. 9, 191 (1971).
[16]H. Uwe, H. Unoki, Y. Fujii, and T. Sakudo, Solid State Commun. 13, 737 (1973); H. Uwe and T. Sakudo, J. Phys. Soc. Jpn. 38, 183 (1975).

Reprinted from the Ceramics and Civilization, Volume III: High Technology Ceramics - Past, Present, and Future

History of Ferroelectrics

L. E. Cross and R. E. Newnham

The Pennsylvania State University
Materials Research Laboratory
University Park, PA 16802

Ferroelectric ceramics are widely used as capacitors, transducers, and thermistors, accounting for about one-half the sales of electroceramic components. The historical roots leading to the discovery of ferroelectricity can be traced back to the last century and the work of the famous crystal physicists Weiss, Pasteur, Pockels, Hooke, Groth, Voigt, and the brothers Curie. Beginning with the pioneering work on Rochelle salt and potassium dihydrogen phosphate, the study of ferroelectrics accelerated rapidly during World War II with the discovery of barium titanate. Then came a period of rapid proliferation with more than 100 new ferroelectrics identified in the next decade, including lead zirconate titanate, the most widely used piezoelectric transducer. In the following decade, the concepts of soft modes and order parameters led to the age of "high science" in the sixties. Neutron experiments authenticated the soft-mode concept and led to the discovery of a number of peculiar improper ferroelectrics such as gadolinium molybdate. In the seventies came the age of diversification in which the electrooptic properties, defect chemistry, and electronic conduction phenomena in ferroelectric ceramics were explored. In the present decade we are witnessing the beginnings of electroceramic integration. Ferroelectric transducers and capacitors are being integrated into multilayer packages along with ceramic substrates, metallic interconnect circuitry, and ceramic resistors. Further integration and miniaturization will take place in the years ahead as electroceramic technology follows the pathways of the semiconductor industry.

Ferroelectricity, involving as it does the complex interplay of dielectric and elastic behavior in highly nonlinear, anisotropic, polarizable, deformable crystals, is perhaps even now almost as much an art as a science. Like both these types of human endeavor, it has passed through a number of well-marked "phases" when specific materials, techniques, or models for study were particularly in vogue. Following the art historian, one might try to identify and name these major periods of activity and our own attempt along these lines is summarized in Table I.

Certainly one of the major "turning points" in ferroelectricity came in the very early 1940s with discovery of the unusual dielectric properties of a number of simple mixed oxides which crystallize with the perovskite structure. In the "preperovskite era," ferroelectricity was something of a scientific curiosity, unique to two rather friable water-soluble crystal families with complex crystal structures. After the 1940 discoveries, the robust, stable ceramic oxides with very simple structures and obviously exploitable properties led to significantly greater involvement with the topic, a steadily broadening base of practical applications, and rapidly deepening fundamental understanding.

To further subdivide about this early period, one may note that, for a long time, from the late 1890s to 1935, a single interesting crystal was the

Table I. Important Events in Ferroelectricity

1920–1930	Rochelle Salt period: discovery of ferroelectricity
1930–1940	KDP age: Thermodynamic and atomistic models of ferroelectricity
1940–1950	Early barium titanate era: High-K capacitors developed
1950–1960	Period of proliferation: Many new ferroelectrics discovered
1960–1970	Age of high science: Soft modes and order parameters
1970–1980	Age of diversification: Ferroics, electrooptics, thermistors
1980–1990	Age of integration: Packages, composites, and integrated optics
1990–2000	Age of miniaturizaion: Size effects, manipulated modes and dipoles

sole object for study. It seems perhaps reasonable to term this the early Rochelle Salt period. In 1935 the agonies of working with this unstable complex crystal were partially relieved by the discovery of ferroelectricity in the potassium dihydrogen phosphate family. These were easier, more symmetric crystals to work with, but with ferroelectricity confined to temperatures below -150°C. We have termed the decade from 1930 to 1940 the intermediate KDP period.

After 1940, in the postperovskite era, it appears that the developments fall rather neatly into four decade-long periods. The barium titanate period, 1940 to 1950, occurred when the major experimental features of this fascinating crystal were first studied, and the capacitor and transducer applications for ceramic $BaTiO_3$ were firmly established. The years 1950 to 1960 were a period of rapid proliferation in the number of known ferroelectrics. Over this period, the number of known ferroelectrics grew from Rochelle Salt, KDP, and three or four ferroelectric perovskites in 1950 to twenty-five firmly established families of ferroelectrics, more than twenty definite perovskite compounds, and innumerable solid solutions in the early 1960s.

Perhaps the most significant theoretical development in ferroelectricity occurred in 1960 with the formulation of the elegant soft-mode description of the ferroelectric transition made almost simultaneously and independently by Cochran and Anderson. This dynamical phenomenological description provided the vital link whereby the static phenomenologies of Mueller and Devonshire could be interconnected with tractable atomistic descriptions through the elementary excitations of the crystal lattice.

Over the 1960 to 1970 period the full weight of the information from inelastic neutron, Raman, Brillouin, and Rayleigh scattering, together with NMR, NQR, and EPR wherever appropriate, was brought to bear in verifying and extending the soft-mode description. Truly an era of "high" scientific endeavor during which ferroelectrics evolved in the solid state physics community from crystallographers' toys to the pivotal prototypes for the description of displacive solid-solid phase transitions.

Subsequent problems associated with central peaks in the Raman and neutron scattering data and the escalating interest in critical phenomena and scaling indices, tempts one flippantly to term the era of the 70s that of "hardening of the modes." This would, however, be a gross injustice to what continues to be a primary tool for studying phase transitions. Rather, we believe that the decade of the 70s may turn out to be a key period of diversification in which the thinking which evolved with considerable refinement for simple proper ferroelectrics was applied to other mimetically twinned ferroic crystals, and the concept of dynamical mode instabilities, which have proved so fruitful in understanding the onset of the static displacement systems in ferroelectric domain structures, were applied to an ever-widening spectrum of solid state phase transitions.

During the age of diversification, a number of interesting practical developments took place as well. Investigations of doped $BaTiO_3$ led to the discovery of a remarkable change in resistance at the Curie point. PTCR thermistors are now used widely as self-regulating heating devices.

At present we are in the midst of the age of integration, in which many electroceramic components are being incorporated into thick-film circuits, thin-film circuits, or multilayer packages. Capacitors, transducers, and electrooptic switches made from ferroelectric ceramics and crystals are among these circuit elements. Looking ahead, it seems obvious that further miniaturization will take place. Many of the techniques developed for semiconductor crystals will be applied to ferroelectrics.

Clearly, in a short paper of this type it is not at all possible to do justice to the many scientists and engineers who contributed to the development of ferroelectrics. Only major highlights can be touched on and, in drawing out these highlights, personal bias is hard to avoid. However, for the basic science, the published record is generally available and the credit already properly apportioned.

The second goal in this presentation is to predict the future of ferroelectric ceramics, and to unravel an evolving technology of this type; an even more difficult task. But, as Lincoln once said, "The world will little note nor long remember what we said here."

The Early Rochelle Salt Period

Some of the more important people and events in this earliest period, which formed the basis for all later ferroelectric activities, are summarized in Table II. The object of this period of study was first separated in 1655 by Elie Seignette, an apothecary in the town of La Rochelle, France. Sodium potassium tartrate tetrahydrate (Rochelle Salt) was used for over 200 years for its mild purgative medicinal properties. Late in the nineteenth century its physical properties began to excite interest. In 1824 Brewster[1] had observed the phenomenon of pyroelectricity in various crystals, among which was Rochelle Salt, but perhaps the first systematic studies were those of the brothers Pierre and Paul-Jacques Curie[2] in 1880. This classic work established unequivocally the existence of the piezoelectric effect and correctly identified Rochelle Salt and a number of other crystals as being piezoelectric.

Table II. Early Rochelle Salt Period $NaKC_4H_4O_6{\cdot}4H_2O$

1655	Elie Seignette	La Rochelle First recorded synthesis of Rochelle Salt
1880	P. Curie, J. Curie	Piezoelectric properties
1894	F. Pockels	Dielectric anomalies Kerr E.O. effect
1917	J. A. Anderson, A. M. Nicolson, W. G. Cady	Piezoelectric effects practical applications
1921 to 1924	J. Valasek W. F. G. Swann	Analogy to magnetism Origin of ferroelectricity
1930	C. B. Sawyer	Rochelle Salt bimorphs "benders" and "twisters"
1937	H. Jaffe	Symmetry change at T_c
1940	H. Mueller	First complete phenomenological theory

It appears that one of the first studies to identify the anomalous dielectric response in Rochelle Salt was by Pockels.[3] Such studies were later to become one of the major diagnostic techniques for finding new ferroelectrics. Unfortunately, some incorrect work by an equally eminent German colleague led Pockels to doubt his original measurements and he did not proceed with the work. Pockels did, however, go on to establish the large quadratic electrooptic Kerr effect in Rochelle Salt.[4]

One of the earliest U.S. involvements with Rochelle Salt appears to have occurred as a response to the urgent demands of submarine warfare in World War I. Sidney Lang,[5] in his dialogue with Walter G. Cady, drew out the importance of a historic meeting in 1917 with French scientists, which became a turning point in Cady's career, leading to the establishment of one of the most important programs on piezoelectricity in this country. Perhaps more than anyone, Walter Cady deserves credit for melding science and technology in the unique way which led to the development of the piezoelectrically stabilized resonator. His massive contribution to the science of piezoelectricity is admirably summarized in his book *Piezoelectricity*, first published in 1946, and still a classic in the field.

Cady's career is a direct negation of the hypothesis by the young and arrogant that a scientist's productive life is over by age thirty. He did not begin work on piezoelectrics until late in his forties and was still a lively experimenter into his 90th year. It was a real sorrow for both piezoelectric and ferroelectric communities that on December 9, 1974, Walter Cady died only one day short of his 100th birthday, and of the many tributes which were being formulated to mark that auspicious occasion. Early

observations on Rochelle Salt by Cady and coworkers included measurements of elastic properties, dielectric constant, piezoelectric effects (including the first observation of the Curie point at 23°C), and the anomalously high d_{14} value in this crystal.

Unfortunately, it is difficult to estimate the full extent of Cady's early work on Rochelle Salt, since much of it was conducted under a U.S. Navy contract for sonar applications and was consequently classified and remained unpublished. Certainly, however, the work must have been rather well known to the small inner circle of workers in this field, and was no doubt most helpful in forwarding understanding of this material.

Another major U.S. contributor to the early Rochelle Salt period was Joseph Valasek. Born in this country, of Czech parents, Valasek studied at the University of Wisconsin from 1921 to 1924. Following a suggestion from his supervisor, W. F. G. Swann, he began a systematic study of the analogy between the magnetic properties of ferromagnetics and the dielectric properties of Rochelle Salt.[6-9] These studies were to lead later to the firm establishment of the term *ferroelectricity* to describe this set of phenonema. His ballistic galvanometer studies of the charge and discharge of carefully prepared *X*-cut Rochelle Salt crystals clearly demonstrated for the first time the hysteritic nature of the polarization and its marked dependence on temperature. Dielectric constant measurements for fields along the *X* axis established the Curie-Weiss form for the permittivity, and the occurrence of two Curie temperatures.

Of very significant practical importance for the whole subject was the origination by C. B. Sawyer[10] of the bimorph configuration for nonresonant transducer applications of Rochelle Salt. With the entrepreneurial skill of Sawyer, and the engineering expertise of Williams, the Rochelle Salt bimorph "benders and twisters" were to evolve into one of the most profitable product lines for the Brush Development Company. By the late 1940s, almost every inexpensive phonograph had a Rochelle Salt bimorph pickup head.

Perhaps an appropriate culmination for the Rochelle Salt period came with a series of four papers by H. Mueller[11-14] of M.I.T. Appearing from 1935 to 1940, they effectively summarized the experimental information of the early period and clearly propounded the static phenomenology which became the basis for Devonshire's later treatment in barium titanate. Mueller for the first time distinguished the three possible origins for proper ferroelectricity in Rochelle Salt, namely the possibility of a dielectric-, an elastic-, or a piezoelectric-dominated instability and, from the experimental information, showed that the driving force in Rochelle Salt was a softening of the clamped dielectric stiffness χ_{11}.

In highlighting the Rochelle Salt era, we have of course emphasized the very important role of studies here in the United States during this formative period. One should also mention the superb work at the Physical-Technical Institute in Leningrad under the direction of Shulvas-Sorokina, and later I. Kurchatov and coworkers.[15] This group was responsible for one of the first realistic microscopic theories for the origin of spontaneous polarization.

Before leaving the early Rochelle Salt work, it would perhaps be as well to review briefly some of the major difficulties which Rochelle Salt presented to these early studies.

First, Rochelle Salt is not stable against dehydration either in vacuum or in dry air. It is thus a difficult material to electrode for reliable electrical measurement. Second, over most of the early period, the crystal symmetry, based on morphological assessments, was incorrectly assigned. The occurrence of spontaneous polarization was a fearsome violation of the by-then sacred Neumann's principle, and it was not until Jaffe's[16] suggestion of the necessary occurrence of phase change at T_c that this seeming conflict was resolved.

Third, we may recognize the very marked structural complexity. With 112 atoms unit cell, it was not until 1941 that Beevers and Hughes in England[17] made the first X-ray structure analysis and it was not until 1954 that the detailed neutron diffraction data of Fraser et al.[18] was finally able to pin down the troublesome water molecules.

Fourth, the strong ferroelastic bias in most small crystals made them almost always unipolar and even the larger samples were often spontaneously biased. It is interesting to note that the domain structure was on a scale entirely unexpected by the original investigators and, though it is quite obvious when the (100) surface is viewed in polarized light, it was not until considerably later, after the methods had been well established for the perovskites, that domain structures were observed optically in Rochelle Salt.

Last, we may note that Rochelle Salt remains one of the few ferroelectric crystals with such a limited ferroelectric range and two clear Curie points. It should therefore not be surprising that the first microscopic theory which even attempted an explanation of this limited range did not evolve until Mason's work in 1950.[19]

In view of these many special problems, one must conclude that the early workers were in many ways highly unlucky in being presented with Rochelle Salt as their only model material, and that under the circumstances their work was truly outstanding.

Intermediate KDP Age

The horizon for workers in ferroelectrics was significantly broadened in 1935 by Busch and Scherer's[20,21] report of the occurrence of ferroelectricity in potassium dihydrogen phosphate and the isostructural dihydrogen arsenate. Here the crystal structure was significantly simpler, the symmetry of the paraelectric phase higher ($\bar{4}2m$), and the basis of the structural arrangement of phosphate or arsenate tetrahedra linked by hydrogen bonding at the corners had already been hypothesized from earlier structural studies by West.[22] It is interesting to note that in the first dielectric studies[20] two Curie points were recorded (this was expected for ferroelectrics) but very quickly the lower "change" was shown to be a domain effect and the polarization P_s to persist down to very low temperatures.

Perhaps the major U.S. contribution to this short KDP period was the brilliant theoretical paper by Slater,[23] which traced the "trigger" for the onset of ferroelectricity to an ordering of the hydrogen bonds (which are almost orthogonal to the X axis) into an antipolar array. This theory was conceived long before the neutron studies of Bacon and Pease,[24] which completely confirmed the basic hypothesis.

It is perhaps interesting to note that, as in Rochelle Salt, the finer points of the kinetics of the changes at T_c remained puzzling for a long period. In KDP, however, Raman and NMR spectra later revealed the fascinating interconnection between the proton ordering and the soft mode in the motion of the potassium and phosphate ions which is the dominant carrier of spontaneous polarization.

The most important applications of the KDP family, which occurred in this preperovskite era (Table III), were not strictly ferroelectric. The strong piezoelectric activity in the paraelectric phase of antiferroelectric ammonium dihydrogen phosphate proved extremely useful for higher power sonar transducers, another activity of the Brush Development Company.[25]

Perovskite Era

Unfortunately, it is impossible to provide a detailed discussion of all the developments since the perovskite families appeared on the scene in the early 1940s. To justify to some extent the categorization used earlier, Tables IV, V, and VI catalog a few of the highlights of the three ten-year periods 1940 to 1950, 1950 to 1960, and 1960 to 1970.

The very important contributions to the field in this country in each of these periods may be noted. The pioneering work at National Lead Company by Wainer, Solomon, and their coworkers firmly established the ceramic perovskite dielectrics in the 1940s. The stimulating competition between Ray Pepinsky and his group at Penn State and Berndt Matthias and his coworkers at Bell Telephone did much to enlarge the number of known ferroelectric families in the 1950s. During the decade the number of ferroelectric families increased from three to twenty-five. The simultaneous but independent realization of the soft-modes description of ferroelectricity in the perovskite by Anderson in the United States and Cochran in the United Kingdom provided the avenue for coupling ferroelectric studies into the mainstream of solid state research and provided just the right framework with which to exploit the full power of the emerging new techniques of laser Raman spectroscopy and neutron inelastic scattering for the study of phonon spectra.

Much more could and should be said about the many important contributions to the exciting developments in ferroelectricity over these times, but the primary task here is to trace a few of the central ideas and applications. References have been inserted in the three tables for a number of the key papers.

Table III. Potassium Dihydrogen Phosphate Group KH_2PO_4

1930	J. West	Crystal structure
1935	G. Busch, P. Scherrer	First report of ferroelectricity
1941	J. C. Slater	Proton ordering theory
1953	G. E. Bacon, R. S. Pease	Neutron diffraction locating hydrogen
1944	B. Zwicker, P. Scherrer	Large longitudinal E.O. effect

Table IV Perovskite Era (Early $BaTiO_3$ Period)

1940 to 1943	Wainer and Salomon (Ref. 26) Ogawa (Ref. 27) Wul and Goldman (Ref. 28)	Discovery of $BaTiO_3$
1945	B. Gray (Ref. 29)	First operating poled $BaTiO_3$ transducer
1945	A. von Hippel (Ref. 30)	Ferroelectricity in $BaTiO_3$
1946	Ginsburg (Ref. 31)	
1946	H. Megaw (Ref. 32)	Crystal structure
1947	Matthias and Merz (Ref. 33)	Single crystals
1948	Matthias, von Hippel, Blattner, (Ref. 34) Kanzig, Merz, Sutter, (Ref. 35) Cross, Dennison, and Nicholson (Ref. 36)	Optical domain structure
1949	A. F. Devonshire (Ref. 37)	Phenomenology
1949	H. F. Kay, P. Vousden (Ref. 38)	Structure changes
1952	W. Merz (Refs. 39–41)	Single crystal
1954		Switching studies
1953	Fraser, Danner, Pepinsky (Ref. 42)	Neutron diffraction study of $BaTiO_3$

Evolution of the Ceramic Piezoelectric Transducer

$BaTiO_3$-Based Transducers

Before discussing the evolution of the technology of piezoelectic ceramics, it is important to reiterate the difficulty of establishing clearly the priorities, and to apologize if someone who had a key but largely "concealed" role because of the proprietary nature of commercial development has been inadvertently omitted from consideration

The difficulty is perhaps rather well illustrated by the considerable legal effort which was required to establish the true patent position in this field. The authors are indeed greatly indebted to Nello Coda, Chief of Engineering of Erie Technological Products, for making available the transcripts of those original proceedings, which now make fascinating reading

On the basis of this evidence, it appears clear that R. B. Gray[29] of Erie should be credited with having the first working piezoelectric ceramic transducer (about 1945) and that it was he who had the first clear understanding of the importance of electrical poling in establishing a remnant polar domain configuration in the ceramic and consequent strong piezo response. It is also clear, however, from the hard-fought legal case that many other scientists and engineers, both in the United States and abroad, were poised on the brink of, or had actually realized but not effectively reported, somewhat similar findings. The dates associated with some of these early studies are summarized in Table VII

It is perhaps difficult now to realize the absolutely revolutionary thinking which was required at that time to accept even the possibility of piezoelectric response in a randomly axed polycrystal, and it is perhaps

Table V Period of Proliferation

1949 to 1960	20 Perovskite compounds	WO_3 to $Pb_3MgNb_2O_9$	Matthias (Refs. 43–45) Smolenskii (Refs. 46–48)
1949	$LiNbO_3$ family		Matthias (Ref. 49)
1951	$LiTiC_4H_4O_6 \cdot H_2O$		Matthias (Ref. 50)
1952	$Cd_2Nb_2O_7$ pyrochlore family		Cook, Jaffe (Ref. 51)
1953	$PbNb_2O_6$ tungsten bronze		Goodman (Ref. 52)
1955	G.A.S.H. family		Holden (Ref. 53)
1956	$Sn(NH_2)_2$ thiourea		Soloman (Ref. 54)
1956	TGS family		Matthias (Ref. 55)
1956	$(NH_4)_2SO_4$ family		Matthias (Ref. 56)
1956	Colemanite		Goldsmith (Ref. 57)
1956	$(NH_4)_2Cd_2(SO_4)_3$ family		Jona, Pepinsky (Ref. 58)
1957	Alums		Jona (Ref. 59)
1957	Dicalcium strontium propionate		Matthias (Ref. 60)
1957	Boracite family		Le Corre (Ref. 61)
1958	$(NH_4)HSO_4$		Pepinsky (Ref. 62)
1958	$NaNO_2$ family		Sawada (Ref. 63)
1958	KNO_3		Sawada (Ref. 64)
1959	$LiH_3(SeO_3)_2$ family		Pepinsky (Ref. 65)
1959	$(NH_4)NaSO_4$		Pepinsky (Ref. 66)
1960	$N(CH_3)_4 \cdot HgCl_3$ family		Fatuzzo, Merz (Ref. 67)
1960	$K_4Fe(CN)_6 \cdot 3H_2O$ family		Waku (Ref. 68)
1962	SbSI family		Fatuzzo (Ref. 69)
1963	$YMnO_3$ family		Bertaut (Ref. 70)

Table VI	The Age of "High" Science	
1959	W. Cochran (Refs. 71,72)	The soft mode
1960	L. Anderson (Ref. 73)	Description of $BaTiO_3$
1962	R. Cowley (Ref. 74)	Confirmation in $SrTiO_3$ by inelastic neutron scattering
1962	Barker, Tinkham, (Ref. 75) Spitzer, Miller, Kleinman, Howarth (Ref. 76)	Confirmation in $BaTiO_3$, $SrTiO_3$ by ir reflectance
1963	R. C. Miller (Ref. 77) Miller, Kleinman, Savage (Ref. 78)	Optical SHG KDP, $BaTiO_3$
1967	Kaminow, Damon (Ref. 79)	Raman spectra in KDP
1967	Fleury, Worlock (Ref. 80)	Raman spectra in $SrTiO_3$, $KTaO_3$
1967	Johnston, Kaminow (Ref. 81)	Raman spectra in $LiNbO_3$, $LiTaO_3$
1968	Fleury (Ref. 82)	Soft modes and 106 K transition in $SrTiO_3$
1968	Cross, Fouskova, Cummins (Ref. 83)	"Peculiar" ferroelectricity in $Gd_2(MoO_4)_3$
1967 to 1969	Aizu (Refs. 84–86) Shuvalov (Ref. 87)	Complete symmetry classification of all ferroelectrics
1970	Pytte (Ref. 88) Sanikov (Ref. 89) Aizu (Refs. 90–91)	Improper ferroelectricity in $Gd_2(MoO_4)_3$
1970	Shirane (Ref. 92)	Inelastic neutron $PbTiO_3$
1971	Nunes (Ref. 93)	Studies of soft $KNbO_3$
1971	Harada (Ref. 94)	Modes in $BaTiO_3$

not surprising that for some time controversy raged as to whether the effect was electrostrictive[96] or piezoelectric.[97,98]

From our present perspective, one can see that there was much merit to both points of view, and that really the phenomena are adequately described either as spontaneous polarization-biased electrostriction of the prototypic phase, or true piezoelectricity of the ferroelectric phase. It was not, however, until the very clear demonstration of pure piezoelectricity in untwinned barium titanate single crystals by Caspari and Merz[99] that the controversy was effectively resolved.

In the earliest studies the ceramics used were largely $BaTiO_3$, processed so as to maintain a rather coarse grain size. Poling was usually

Table VII	Evolution of $BaTiO_3$-Based Transducers	
1945	R. B. Gray	First "working" transducer
1946	Rushman, Strivens	Piezoelectricity in $(Pb,Ba)_{(1-x)}TiO_3$
1947	S. Roberts	Dielectric and piezoelectric properties of barium titanate
1947	W. L. Cherry, R. Adler	Piezoelectric effect in polycrystalline $BaTiO_3$
1948	W. P. Mason	Electrostrictive effect in $BaTiO_3$ ceramics
1949	A. V. Rzhanov	Piezoelectric effect in barium titanate
1950	Caspari, Merz	Demonstration of "pure" piezoelectricity in single-crystal $BaTiO_3$
1952	Berlincourt, Kulesar	$BaTiO_3$ + $CaTiO_3$
1954	W. P. Mason	$BaTiO_3$ + $PbTiO_3$ + $CaTiO_3$

carried out by cooling electroded samples through the Curie temperature at 120°C under a substantial biasing potential, the optimum conditions for individual formulation being established by trial-and-error methods.[100]

By the early 1950s, ceramic piezoelectric transducers based on $BaTiO_3$ were becoming well established in a number of both civil and military applications. There was a real need to improve the stability against depoling which accompanied traversing the 0°C phase transition in pure $BaTiO_3$ and the stability against depoling associated with the low coercivity of the pure titanate ceramics. A number of composition manipulations have been tried to alleviate these problems, and two of the more successful[101,102] still in use are listed in Table VIII.

Evolution of the Lead Zirconate:Lead Titanate and Other Piezoelectric Ceramic Systems

It was rather natural in the early 1950s, following the wide success of the simple $BaTiO_3$-based ceramic transducer, that people should examine other ferroelectric perovskite compounds for potential applicability. Some of the very early basic work on pure $PbTiO_3$ and on the $PbTiO_3$-$PbZrO_3$ solid solution system, which established the useful high Curie temperature of lead zirconate and the outline of the phase diagram for this system, was carried out in Japan by Shirane and Takeda,[103] Shirane et al.,[104] and Sawaguchi.[105] The development of PZT transducers is traced in Table VIII.

The key studies, however, which established the PZT system as exceptionally suitable for the formulation of piezoelectrics in this composition system were carried through by Jaffe and coworkers[106,107] at the National Bureau of Standards. These studies clearly discerned the im-

Table VIII	Evolution of Piezoelectric Ceramic Transducers	
1950	G. Shirane, S. Hoshino, K. Suzuki	$PbTiO_3$
1952	G. Shirane, K. Suzuki	$Pb(Zr,Ti)O_3$ solid solutions
1953	E. Sawaguchi	AF and F in $Pb(Zr,Ti)O_3$
1954	B. Jaffe, R. S. Roth, S. Marzullo	Morphotropic boundary
1955 on	H. Jaffe, B. Jaffe, W. R. Cook, Jr., D. Berlincourt, R. R. Gerson	Evolution of modified PZT formulations
1952	G. Goodman	$PbNb_2O_6$
1959	L. Egerton, D. M. Dillon	$(Na_{0.5}K_{0.5})NbO_3$
1971	H. Jaffe, W. R. Cook, Jr., B. Jaffe	Piezoelectric ceramics

portance of the composition-dependent rhombohedral-tetragonal ferroelectric-ferroelectric phase change near the 52:48 mole fraction composition and initiated a whole new emphasis in piezoceramic research. There was at that time clear realization of the value of proximity to a phase change in facilitating poling.[108] However it was Jaffe's recognition that the temperature-independent morphotropic boundary in PZT allowed one to stay close to the phase change over the whole temperature course of the poling process which was of vital importance.

The earliest measurements show a clear maximum in response for PZT compositions near the morphotropic boundary, and more recent studies have amply confirmed its importance for poling.[109,110] Over the next ten years, the major developmental emphasis was with the lead zirconate-lead titanate solid solution ceramics, and the major center for this activity was certainly the Clevite Company (a development from the old Brush group). Studies associated with the names of H. Jaffe, B. Jaffe, W. R. Cook, Jr., D. Berlincourt, R. R. Gerson, F. Kulcsar, and H. A. Kreuger in that group were at the heart of the development. An excellent account of much of this work has been given in the book *Piezoelectric Ceramics*.[111] This text is essential reading for any serious student of ceramic piezoelectrics.

One interesting facet of the system $PbTiO_3$:$PbZrO_3$ is that the high vapor pressure of PbO at the forming temperature, which was originally believed to be a curse in dealing with these ceramics, has in later studies turned out to be a major blessing. The "fugitive" nature of the PbO provides a measure of autocompensation in the semiconductor properties, and high-resistivity samples can be made with a much wider range of aliovalent dopant ions than would ever be possible in the $BaTiO_3$ family.

It is just this "docility" and flexibility for chemical manipulation to modify the ferroelectric properties which was so effectively exploited at first by the Clevite group, and later by all other transducer manufacturers to tailor the original advantageous properties for specific application

areas. The basis for many of the modifier ion schemes was provided by Jaffe.[112]

Studies by Smolenskii and Agronovskaya[113] in the 1950s provided a large family of lead-containing perovskite compounds of complex composition. It was perhaps natural that a number of these $Pb(X_{\alpha}Y_{1-\alpha})O_3$ materials should be tried as third components to modify the system $PbTiO_3$:$PbZrO_3$. Much recent work in Japan has been concerned with the exploration of such systems. Although some of these new bodies do show practical advantages in specific devices, in general the properties are not markedly different from those of PZT.

Undoubtedly, the PZT family is the most important and versatile composition base for ceramic piezoelectric elements, but two other developments in the materials field are also of major interest. In 1952, studies by Goodman[114] at Globe Union uncovered the interesting and strong ferroelectric properties in the "Goodmanite" phase of $PbNb_2O_6$. Studies by Goodman and by Lewis and coworkers[115-117] at General Electric in Great Britain showed that ceramic lead metaniobate could be poled to a strongly piezoelectric state, and that in the system $PbNb_2O_6$-$BaNb_2O_6$ a morphotropic boundary did occur. Unfortunately, the metaniobate is a tough ceramic to process, and though it has been the subject of considerable research because of its high hydrostatic sensitivity and low mechanical Q, it has found only specialized application.

A later development was the demonstration by Egerton and Dillon at Bell Laboratories of a morphotropic boundary in the $NaNbO_3$-$KNbO_3$ solid solution system and piezoelectrics with compositions near the $(K_{0.5}Na_{0.5})NbO_3$ boundary are still hot-pressed by Bausch and Lomb for specialized applications.

Summary

Ferroelectric ceramics are used in multilayer capacitors, PTC thermistors, piezoelectric transducers, and electrooptic devices. Along with packaging materials and magnetic ferrites, they account for a major portion of the electroceramics market.

The early history of ferroelectrics can be traced to pioneering studies on Rochelle Salt and potassium dihydrogen phosphate, two water-soluble crystals. But the major impetus in ferroelectric ceramics came near the end of World War II, when $BaTiO_3$ and other perovskite-family oxides were discovered.

The number of applications expanded steadily during the next three decades and is now entering an age of integration and miniaturization in which three-dimensional ceramic circuitry is being developed. Multilayer structures on a submillimeter scale incorporate resistors, capacitors, dielectrics, metal interconnects, and piezoelectric transducers. Further advances will undoubtedly occur in the years ahead as the field of electroceramics follows in the footsteps of the semiconductor industry.

References

[1] D. Brewster. Observation of Pyroelectricity of Minerals. *Edinburgh J. Sci.* **1**, 208-14 (1824).

[2] J. Curie and P. Curie. Development by Pressure of Polar Electricity in Hemihedral Crystals with Inclined Faces. *Bull. Soc. Min. de France* **3**, 90-102 (1880).

[3] F. Pockels. On the Effect of an Electrostatic Field on the Optical Behavior of Piezoelectric Crystals. *Abh. Gott.* **39**, 1-7 (1894).

[4]F. Pockels, Lehrbuch der Kristalloptik, B. G. Taubner, Berlin, 1906.
[5]S. L. A. Lang, "Conversation with Professor W. G. Cady," *Ferroelectrics*, **9** [3-4] 141–49 (1975).
[6]J. Valasek, "Piezoelectricity and Allied Phenomena in Rochelle Salt," *Phys. Rev.*, **17** [4] 475–81 (1921).
[7]J. Valasek, "Piezoelectric Activity of Rochelle Salt Under Various Conditions," *Phys. Rev.*, **19** [5] 478–91 (1922).
[8]J. Valasek, "Properties of Rochelle Salt Related to the Piezoelectric Effect," *Phys. Rev.*, **20** [6] 639–64 (1922).
[9]J. Valasek, "Dielectric Anomalies in Rochelle Salt," *Phys. Rev.*, **24** [5] 560-68 (1924).
[10]C. B. Sawyer, "The Use of Rochelle Salt Crystals for Electrical Reproducers and Microphones," *Proc. IRE*, **19**, 2020–24 (1931).
[11]H. Mueller, "Properties of Rochelle Salt," *Phys. Rev.*, **47** [23] 175–91 (1935).
[12]H. Mueller, "Properties of Rochelle Salt II," *Phys. Rev.*, **57** [9] 829–39 (1940).
[13]H. Mueller, "Properties of Rochelle Salt III," *Phys. Rev.*, **58** [6]565–73 (1940).
[14]H. Mueller, "Properties of Rochelle Salt IV," *Phys. Rev.*, **58** [9] 805–11 (1940).
[15]I. V. Kurchhatov, Seignette Electricity, Moscow (1933) (in Russian).
[16]H. Jaffe, "Polymorphism of Rochelle Salt," *Phys. Rev.*, **51** [1] 43–47 (1937).
[17]C. A. Beevers, and W. Hughes, "The Crystal Structure of Rochelle Salt (Sodium Potassium Tartrate Tetrahydrate $NaKC_4H_4O_6 \cdot 4H_2O$)," *Proc. R. Soc. (London)*, **177** [A969] 251–59 (194-).
[18]B. C. Frazer, M. McKeown, and R. Pepinsky, "Neutron Diffraction Studies of Rochelle Salt Single Crystals," *Phys. Rev.*, **94** [5] 1435 (1954).
[19]W. P. Mason, Piezoelectric Crystals and Their Applications in Ultrasonics, Van Nostrand, New York, 1950.
[20]G. Busch, and P. Scherer, "A New Seignette-Electric Substance," *Naturwiss*, **23**, 737-38 (1935).
[21]G. Busch, "New Seignette Electrics," *Helv. Phys. Acta*, **11**, 169 (1939).
[22]J. West, "Crystal Structure of KH_2PO_4," *Z. Krist.*, **74**, 306–308 (1930).
[23]J. C. Slater, "Theory of the Transition in KH_2PO_4," *J. Chem. Phys.*, **9** [1] 16–33 (1941).
[24]G. E. Bacon, and R. S. Pease, "A Neutron Diffraction Study of Dihydrogen Phosphate by Fourier Synthesis," *Proc. R. Soc. (London)*, **220A** [1142] 397–421 (1953).
[25]A. C. Keller, "Submarine Detection by Sonar," *Trans. AIEE*, **66**, 1217–19 (1937).
[26]E. Wainer, and N. Salomon, Electrical Reports Titanium Alloys Manufacturing Division, National Lead Co. Reports No. 8, 9, 10 (1938-1943).
[27]S. Ogawa, "On Polymorphic Change of Barium Titanate," *J. Phys. Soc. Jpn.*, **1** [1] 32–33 (1946).
[28]B. M. Wul, and I. M. Goldman, "Dielectric Constants of Titanates of Metals of the Second Group," *Dokl. Akad. Nauk. SSSR*, **46**, 154 (1945) (in Russian).
[29]B. Gray, "Transducer and Method of Making Same," U.S. Pat. No. 2 486 560, September 20, 1946.
[30]A. Von Hippel, High Dielectric Constant Ceramics. NDRC Div. 14, Rept. 300, PB. 4660 (1944).
[31]V. Ginsburg, "The Dielectric Properties of Ferroelectric (Seignettoelectric) Substances and of Barium Titanate," *J. Exp. Theor. Phys. SSSR*, **15**, 739–43 (1945) (in Russian).
[32]H. Megaw, "Crystal Structure of Barium Titanate," *Nature (London)*, **155** [3938] 484–85 (1945).
[33]H. Blattner, B. Matthias, and W. Merz, "Single Crystals of Barium Titanium Compounds," *Helv. Phys. Acta*, **20**, 225–27 (1947).
[34]B. Matthias, and A. Von Hippel, "Single Crystals of Barium Titanate," *Phys. Rev.*, **73** [11] 1378–84 (1948).
[35]H. Blattner, W. Kaenzig, and W. Merz, "Preparation and Investigation of Barium Titanate Single Crystals," *Helv. Phys. Acta*, **22**, 35–38 (1949).
[36]L. E. Cross, A. T. Dennison, and M. Nicholson, "Optical Studies of Barium Titanate Crystals," *Proc. Leeds Phil. Soc.*, **5**, 199–204 (1949).
[37]A. F. Devonshire, "Theory of Barium Titanate. 1," *Philos. Mag.*, **40** [309] 1040–63 (1949).
[38]H. F. Kay, and P. Vousden, "Barium Titanate Single Crystals," *Philos. Mag.*, **40** [309] 1019–40 (1949).
[39]W. Merz, "Switching Time in Ferroelectric $BaTiO_3$ and Its Dependence on Crystal Thickness," *J. Appl. Phys.*, **27** [8] 938–43 (1956).
[40]W. Merz, "Domain Properties in $BaTiO_3$," *Phys. Rev.*, **88** [2] 421–22 (1952).
[41]W. Merz, "Domain Formation and Domain Wall Motions in Ferroelectric $BaTiO_3$ Single Crystals," *Phys. Rev.*, **95** [6] 690–98 (1954).
[42]B. C. Frazer, H. Danner, and R. Pepinsky, "Single Crystal Neutron Analysis of Tetragonal $BaTiO_3$," *Phys. Rev.*, **100** [2] 745–46 (1955).
[43]B. T. Matthias, "New Ferroelectric Crystals," *Phys. Rev.*, **75** [11] 1771 (1949).
[44]B. T. Matthias, and J. P. Remeika, "Dielectric Properties of Sodium Potassium Niobates," *Phys. Rev.*, **82**, 727-29 (1951).
[45]B. T. Matthias, "Ferroelectric Properties of WO_3," *Phys. Rev.*, **75** [3] 430–31 (1949).

[46]G. A. Somlenskii, and A. I. Agronovskaya, "Dielectric Polarization and Losses of Some Complex Compounds," *Sov. Phys.-Tech. Phys.*, **3** [7] 1380–82 (1958).
[47]G. A. Smolenskii, U. A. Isupov, and A. I. Agronovskaya, "New Ferroelectrics of Complex Composition of the Type $A^{2}_{2}(B^{3}_{2}B^{5}_{1})O_6$. I," *Sov. Phys.-Solid State*, **1** [1] 150–51 (1959).
[48]G. A. Smolenskii, A. I. Agronovskaya, and U. A. Isupov, "New Ferroelectrics of Complex Composition. III. Pb_2MgWO_6, $Pb_2Fe_2WO_6$, and Pb_2FeTaO_6," *Sov. Phys.-Solid State*, **1** [4] 907–908 (1959).
[49]B. T. Matthias, and J. Remeika, "Ferroelectricity in the Ilmenite Structure," *Phys. Rev.*, **76** [12] 1886–87 (1949).
[50]B. T. Matthias, and J. K. Hulm, "New Ferroelectric Tartrates," *Phys. Rev.* **82** [1] 108–109 (1951).
[51]W. R. Cook, Jr. and Hans Jaffe, "Ferroelectricity in Oxides of Fluorite Structure," *Phys. Rev.*, **88** [6] 1426 (1952).
[52]G. Goodman, "Ferroelectric Properties of Lead Metaniobate," *J. Am. Ceram. Soc.*, **36** [11] 368–72 (1953).
[53]A. N. Holden, B. T. Matthias, W. J. Merz, and J. P. Remeika, "New Class of Ferroelectrics," *Phys. Rev.*, **98** [2] 546 (1955).
[54]A. L. Solomon, "Thiourea, A New Ferroelectric," *Phys. Rev.*, **104** [4] 1191 (1956).
[55]B. T. Matthias, C. E. Miller, and J. P. Remeika, "Ferroelectricity of Glycine Sulfate," *Phys. Rev.*, **104** [3] 849–50 (1956).
[56]B. T. Matthias, and P. Remeika, "Ferroelectricity in Ammonium Sulfate," *Phys. Rev.*, **103** [1] 262 (1956).
[57]G. J. Goldsmith, "Ferroelectricity in Colemanite," *Bull. Am. Phys. Soc. Sec. II*, **1** [7] 322 (1956).
[58]F. Jona, and R. Pepinsky, "Ferroelectricity in the Langbeinite System," *Phys. Rev.*, **103** [4] 1126 (1956).
[59]F. Jona, R. Pepinsky, and G. Shirane, "Ferroelectricity in the Alums," *Phys. Rev.*, **102** [4] 1181–82 (1956).
[60]B. T. Matthias, and J. P. Remeika, "Ferroelectricity of Dicalcium Strontium Propionate," *Phys. Rev.*, **107** [6] 1727 (1957).
[61]V. LeCorre, "Etude Optique de Dielectrique de la Boracite," *J. Phys. Radium*, **18**, 629 (1957).
[62]R. Pepinsky, K. Vedam, S. Hoshino, and Y. Okaya, "Ammonium Hydrogen Sulfate: A New Ferroelectric with Low Coercive Field," *Phys. Rev.*, **111** [6] 1508–10 (1958).
[63]S. Sawada, S. Nomura, S. Fuji, and I. Yoshida, "Ferroelectricity in $NaNo_2$," *Phys. Rev. Lett.*, **1** [9] 320–21 (1958).
[64]S. Sawada, S. Nomura, and S. Fuji, "Ferroelectricity in the Phase III of KNO_3," *J. Phys. Soc. Jpn.*, **13** [12] 1549 (1958).
[65]R. Pepinsky, and K. Vedam, "$LiH_3(SeO_3)_2$: New Room Temperature Ferroelectric," *Phys. Rev.*, **114** [5] 1217–18 (1959).
[66]R. Pepinsky, and K. Vedam, "Crystal Structure of the Ferroelectric Phase of $(Glycine)_3H_2SO_4$," *Phys. Rev.*, **115** [2] 323–30 (1959).
[67]E. Fatuzzo, and R. Nitsene, "Ferroelectricity in Tetraethylammonium-Trichloro-Mercurate," *Phys. Rev.*, **117** [4] 936 (1960).
[68]S. Waku, H. Hirabayashi, H. Toyoda, and H. Iwasaki, "Ferroelectricity in Potassium Ferrocyanide Trihydrate," *J. Phys. Soc. Jpn.*, **14** [7] 973–74 (1957).
[69]E. Fatuzzo, W. Harbeke, W. J. Merz, R. Nitche, H. Roetschi, and W. Ruppel, "Ferroelectricity in SbSI," *Phys. Rev.* **127** [6] 2036–37 (1962).
[70]E. F. Bertaut, F. Forrat, and P. H. Fang, "Les Manganites tres rares et d'yttrium une novelle classe de ferroelectriques," *Compt. Rend.*, **256**, 1958–60 (1963).
[71]W. Cochran, "Crystal Stability and the Theory of Ferroelectricity," *Phys. Rev. Lett.*, **3** [8] 412–14 (1959).
[72]W. Cochran, "Crystal Stability and the Theory of Ferroelectricity," *Adv. Phys.*, **9** [4] 387–90 (1960).
[73]P. W. Anderson, paper presented at the Moscow Conferences on Dielectrics, December 1958.
[74]R. A. Cowley, "Temperature Dependence of a Transverse Optic Mode in Strontium Titanate," *Phys. Rev. Lett.*, **9**, 159 (1962).
[75]A. S. Barner, and M. Tinkham, "Far-Infrared Dielectric Measurements on Potassium Dihydrogen Phosphate, Triglycine Sulfate, and Rutile," *J. Chem. Phys.*, **38** [9] 2257–64 (1963).
[76]W. G. Spitzer, R. C. Miller, D. A. Kleinman, and L. E. Howarth, "Far Infrared Dispersion in $BaTiO_3$, $SrTiO_3$, and TiO_2," *Phys. Rev.*, **126** [5] 1710–21 (1962).
[77]R. C. Miller, "Optical Harmonic Generation in Single Crystal $BaTiO_3$," *Phys. Rev.*, **134** [5A] 1313–19 (1964).
[78]R. C. Miller, D. A. Kleinman, and A. Savage, "Quantitative Studies of Optical Harmonic Generation in CdS, $BaTiO_3$, and KH_2PO_4 Type Crystals," *Phys. Rev. Lett.*, **11** [4] 146–52 (1963).
[79]I. P. Kaminow, and T. C. Damon, "Temperature Dependence of the Ferroelectric Mode in KH_2PO_4," *Phys. Rev. Lett.*, **20** [21] 1105–08 (1968).
[80]P. A. Fleury, J. M. Worlock, and R. T. L. Holden, "Electric Field Induced Raman Scatter

ing in $SrTiO_3$ and $KTaO_3$," *Phys. Rev.*, **174** [2] 613–23 (1968)
[81]W. D. Johnson and I. P. Kaminow, "Temperature Dependence of Raman and Rayleigh Scattering in $LiNbO_3$ and $LiTaO_3$," *Phys. Rev.*, **168** [3] 1045–56 (1968)
[82]P. A. Fleury, J. F. Scott, and J. M. Worlock, "Soft Phonon Modes and the 110° Phase Transition in $SrTiO_3$," *Phys. Rev. Lett.*, **21** [1] 16–19 (1968)
[83]L. E. Cross, A. Fouskova, and S. E. Cummins, "Gadolinium Molybdate, A New Type of Ferroelectric Crystal," *Phys. Rev. Lett.*, **21** [12] 812–14 (1968)
[84]K. Aizu, "Ferroelectrics Having an Irreversible But Diverible Spontaneous Polarization Vector," *J. Phys. Soc. Jpn.*, **23** [4] 794–97 (1967)
[85]K. Aizu, "Possible Species of Ferroelastic Crystals and of Simultaneous Ferroelectric and Ferroelastic Crystals," *J. Phys. Soc. Jpn.*, **27** [2] 387–96 (1969)
[86]K. Aizu, "Electrical, Mechanical, and Electromechanical Orders of State Shifts in Non-magnetic Ferroic Crystals," *J. Phys. Soc. Jpn.*, **32** [5] 1287–1301 (1970)
[87]L. A. Shuvalov, "Symmetry Aspects of Ferroelectricity," *J. Phys. Soc. Jpn. (Suppl.)* **28**, 38–47 (1970)
[88]E. Pytte, "Theory of the Structural Transition in NbSn and V_3Si," *Phys. Rev. Lett.*, **25** [17] 1176–80 (1970)
[89]D. G. Sannikov, and A. P. Levanyuk, "Phenomenological Theory of the Ferroelectric Phase in Gadolinium Molybdate," *Sov. Phys.-Solid State*, **12** [10] 2418–21 (1970)
[90]K. Aizu, "Inferred Temperature-Dependence of Electrical, Mechanical and Optical Properties of Ferroelastic-Ferroelectric $Gd_2(MoO_4)3$," *J. Phys. Soc. Jpn.*, **31** [3] 801–11 (1971)
[91]K. Aizu, "Determination of State Parameters and Formulation of Spontaneous Strain for Ferroelastics," *J. Phys. Soc. Jpn.*, **28** [3] 706 (1970)
[92]G. Shirane, J. D. Axe, J. Harada, and J. P. Remeika, "Soft Ferroelectric Modes in Lead Titanate," *Phys. Rev.*, **B2**, 155–59 (1970)
[93]A. C. Nunes, J. D. Axe, and G. Shirane, "Soft Mode Analysis of $KNbO_3$," *Ferroelectrics*, **2**, 291–96 (1971)
[94]J. Harada, J. D. Axe, and G. Shirane, "Neutron-Scattering Study of Soft Modes in Cubic $BaTiO_3$," *Phys. Rev.*, **B4**, 155 (1971)
[95]R. B. Gray, "Transducer and Method of Making Same," U.S. Pat. No. 2,486,560.
[96]W. P. Mason, "Electrostrictive Effect in Barium Titanate," *Phys. Rev.*, **74** [9] 1136–47 (1948)
[97]W. L. Cherry, Jr. and R. Adler, "Piezoelectric Effect in Polycrystalline Barium Titanate," *Phys. Rev.*, **72** [10] 981–82 (1967)
[98]W. P. Mason, p. 290 in Piezoelectric Crystals and Their Application in Ultrasonics. Van Nostrand, New York, 1949.
[99]M. E. Caspari, and W. J. Merz, "The Electromechanical Behavior of $BaTiO_3$ Single Domain Crystals," *Phys. Rev.*, **80** [6] 1082–83 (1950)
[100]D. Berlincourt, "Recent Development in Ferroelectric Transducer Materials," *IRE Trans.*, **PGUE-4**, 53 (1956).
[101]D. Berlincourt, and F. Kulcsar, "Electromechanical Properties of $BaTiO_3$ Compositions Showing Substantial Shifts in Phase Transition Points," *J. Acoust. Soc. Am.* **24** [6] 709–13 (1952).
[102]W. P. Mason, "Use of Temperature- and Time-Stabilized Barium Titanate Ceramics in Transducers, Mechanical Wave Transmission Systems and Force Measurements," *Acustica*, **4**, 200–202 (1954).
[103]G. Shirane, and A. Takeda, "Phase Transitions in Solid Solutions of $PbZrO_3$ and $PbTiO_3$ I. Small Concentrations of $PbTiO_3$," *J. Phys. Soc. Jpn.*, **7** [1] 5–11 (1952)
[104]G. Shirane, K. Suzuki, and A. Takeda, "Phase Transitions in Solid Solutions of $PbZrO_3$ II. X-ray Study," *J. Phys. Soc. Jpn.*, **7** [1] 12-17 (1952)
[105]E. Sawaguchi, "Ferroelectricity vs. Antiferroelectricity in the Solid Solutions of $PbZrO_3$-$PbTiO_3$," *J. Phys. Soc. Jpn.*, **8** [5] 615-29 (1953)
[106]B. Jaffe, R. S. Roth, and S. Marzullo, "Piezoelectric Properties of Lead Zirconate-Lead Titanate Solid Solution Ceramics," *J. Appl. Phys.*, **25** [6] 809–10 (1954)
[107]B. Jaffe, R. S. Roth, and S. Marzullo, "Properties of Piezoelectric Ceramics in the Solid Solution Series Lead Titanate-Lead Zirconate-Lead Oxide-Tin Oxide and Lead Titanate-Lead Hafnate," *J. Res. Natl. Bur. Stand.*, **55**, 239–43 (1955)
[108]H. Jaffe, "Titanate Ceramics for Electro-mechanical Purposes," *Ind. Eng. Chem.*, **2**, 264–68 (1950)
[109]D. Berlincourt, C. Cmolik, and H. Jaffe, "Piezoelectric Properties of Polycrystalline Lead Titanate-Zirconate Compositions," *Proc. IRE*, **48**, 220-23 (1960)
[110]R. Gerson, and H. Jaffe, "Electrical Conductivity in Lead Titanate Zirconate Ceramics," *J. Phys. Chem. Solids*, **24** [7] 979–84 (1963)
[111]B. Jaffe, W. R. Cook, Jr., and H. Jaffe, Piezoelectric Ceramics. Academic Press, London, 1971.
[112]H. Jaffe, "Semiconduction in Ceramics," *Proc. Inst. Elec. Eng. (London)*, **109** [Suppl. No. 22] 351–54 (1962)
[113]G. A. Smolenskii, and A. I. Agronovskaya, "Dielectric Polarization and Losses of Some Complex Compounds," *Sov. Phys.-Tech. Phys.*, **3** [7] 1380–82 (1958)
[114]G. Goodman, "Ferroelectric Properties of Lead Metaniobate," *J. Am. Ceram. Soc.*, **36** [11] 368–72 (1952)
[115]M. H. Francombe, "Polymorphism in Lead Metaniobate," *Acta Crystallogr.*, **9** [8] 683–84 (1956)
[116]M. H. Francombe, and B. Lewis, "Structural, Dielectric and Optical Properties of Ferroelectric Lead Metaniobate," *Acta Crystallogr.*, **11** [10] 696–703 (1958)
[117]B. Lewis, and L. A. Thomas, "Piezoelectric Ceramics Based on $PbNb_2O_6$," *Proc. Intl. Conf. Solid State Physics in Electronics Telecommun., Brussels*, **4**, 883–85 (1958)

END
DATED
FILM
8-88
DTIC